

**Along Margin Variation in Seismic
Stratigraphy and Controls on the evolution of
the Giant Foresets Formation, Taranaki
Basin, New Zealand**

A thesis submitted to The University of Manchester for
the degree of
Doctor of Philosophy

in the Faculty of Science and Engineering

2020

Eoin Dunlevy

Department of Earth and Environmental Sciences

Blank Page

Table of Contents

Table of Contents	3
List of Figures	7
Abstract.....	11
Declaration.....	12
Copyright Statement.....	13
Acknowledgements.....	14
1 Chapter 1.....	15
Introduction.....	15
1.1 Project Rationale.....	15
1.2 Thesis Aims & Objectives.....	17
1.3 Thesis Structure	17
1.4 Clinoform Background.....	18
1.4.1 Delta Scale Clinoforms.....	18
1.4.2 Shelf Edge Clinoforms	20
1.4.3 Continental Margin Clinoforms	22
1.4.4 Compound & Hybrid Clinoforms	23
2 Chapter 2.....	27
2.1.1 Regional Tectonic Evolution.....	29
2.1.2 Basin Structure.....	30
2.1.3 Basin Stratigraphy.....	36
2.1.4 Regional Oceanography	40
2.2 Previous Studies of the Giant Foresets Formation	45
3 Chapter 3.....	53
3.1 Database.....	53
3.1.1 Seismic Data.....	54
3.1.2 Well Data.....	54

3.1.3	Age Data.....	55
3.2	Methods.....	60
3.2.1	Seismic and Sequence Stratigraphy	60
3.2.2	Trajectory Analysis.....	61
3.2.3	Seismic Interpretation Workflow	63
4	Chapter 4.....	65
4.1	Introduction.....	65
4.2	Geological Setting.....	66
4.3	Datasets and Methods.....	68
4.4	Results.....	71
4.4.1	Seismic Stratigraphy of the Giant Foresets Formation	71
4.4.2	Quantitative Characterisation of Progradation.....	98
4.5	Discussion.....	100
4.5.1	Shelf Edge vs. Continental Margin Scale Clinoforms	100
4.5.2	Controls on GFF shelf margin architecture.....	102
4.5.3	Tectonics and lateral variations sediment supply.....	106
4.5.4	Sediment Waves	109
4.5.5	Synthesis.....	113
4.6	Conclusions.....	116
5	Chapter 5.....	119
5.1	Introduction.....	119
5.2	Dataset and Methods.....	120
5.2.1	Data.....	120
5.2.2	Methods.....	121
5.3	Results.....	127
5.3.1	Sequence development.....	127
5.3.2	High amplitude deposits	145
5.4	Discussion.....	150

5.4.1	Age Model.....	150
5.4.2	Origin of the High Amplitude Deposits.....	156
5.4.3	Comparison to other margins	163
5.4.4	Lithology Control and Sediment Delivery.....	165
5.5	Conclusions	172
6	Chapter 6.....	173
6.1	Introduction	173
6.2	Data and Methods.....	174
6.3	Cross Shelf Transport in the Taranaki Basin	179
6.3.1	Highstand	179
6.3.2	Lowstand.....	181
6.4	Deepwater sediment pathways	188
6.4.1	Egmont Terrace/Challenger Plateau Region.....	188
6.4.2	Slope and Basin Floor of the Taranaki Basin.....	192
6.5	Synthesis of shelf, slope and basin floor conduits.....	200
6.6	Taranaki Basin Catchments	202
6.6.1	South Island Catchments	202
6.6.2	North Island Catchments.....	204
6.6.3	Catchment Sizes & Productivity	206
6.7	Sediment Conveyor to the Taranaki Basin.....	211
6.8	Synthesis	213
6.8.1	Highstand	214
6.8.2	Lowstand.....	216
6.9	Conclusions	219
7	Chapter 7.....	221
7.1	Conclusions.....	221
7.2	General Implications.....	227
7.3	Recommendations for Future Research	228

7.3.1	Refinement of Age Model	228
7.3.2	Sediment Provenance Studies	228
7.3.3	Embargoed Seismic Data.....	229
7.3.4	IODP drilling.....	229
8	Bibliography.....	231
9	Appendix 1 – Well Logs	259
10	Appendix 2 – Biostratigraphy	262

Word Count: 46,876

List of Figures

Figure 1.1 Architectural components of a clinoform (from Salazar et al., 2016).	15
Figure 1.2 Clinoform scales and settings	16
Figure 1.3 CHIRP sonar profile of the Gargano subaqueous delta	20
Figure 1.4 Shelf margin clinoform examples.	22
Figure 1.5 Continental Margin clinoform example.	23
Figure 1.6 Compound Clinoforms	25
Figure 2.1 Sedimentary Basins of New Zealand.	27
Figure 2.2 SW Pacific bathymetry and crustal structure of New Zealand.	28
Figure 2.3 Summary stratigraphic and tectonic evolution of the Taranaki Basin	31
Figure 2.4 Taranaki Basin Structure.	32
Figure 2.5 Schematic block rotation model.	34
Figure 2.6 Structural Domains of the Taranaki Basin.	35
Figure 2.7 Challenger Plateau flooding.	37
Figure 2.8 Sediment Pathways to the Taranaki Basin.	40
Figure 2.9 Regional Oceanography of the southwest Pacific region.	43
Figure 2.10 Surface circulation around New Zealand.	44
Figure 2.11 Previous stratigraphic studies of the Giant Foresets Formation.	45
Figure 2.12 Seismic stratigraphy of Salazar et al. (2016).	46
Figure 2.13 Mass transport deposits mapped by Omeru (2016).	47
Figure 2.14 The nine types of clinothem defined by Anell and Mitkandal (2017).	48
Figure 2.15 Idealised clinothem body.	49
Figure 2.16 Slope evolution of the Taranaki Basin.	51
Figure 3.1 Seismic and well database utilised in this study.	53
Figure 3.2 Biostratigraphic correlation to seismic data.	58
Figure 3.3 Late Quaternary ages from Nodder (1994).	59
Figure 3.4 Common seismic reflection configurations and their terminations (after Mitchum et al., 1977).	60
Figure 3.5 Idealised stacking patterns of the Accommodation Succession method of Neal and Abreu (2009) and Neal et al. (2016)	61
Figure 3.6 Shelf edge trajectory classes from Henriksen et al., (2011).	63
Figure 4.1 Basin Location and dataset.	66
Figure 4.2 Basin Structure and Evolution.	68
Figure 4.3 Time-depth relationships for Giant Foresets Formation.	69

Figure 4.4 Measured clinoform geometric parameters.	70
Figure 4.5 Summary of seismic stratigraphy and age model of the Giant Foresets Formation utilised in this study.	72
Figure 4.6 Summary shelf edge map of surfaces T1 to T9 overlain on bathymetry.	73
Figure 4.7 Seismic stratigraphic units in the southern composite line (DTB01-31 & Hector 3D).	74
Figure 4.8 Seismic stratigraphic units on the central composite section (DTB01-23 & SUNZ-91-136).	75
Figure 4.9 Seismic stratigraphic units in the northern composite line (OMV-07-13 and ST03-401).	76
Figure 4.10 Time Structure and Thickness Maps 1.	77
Figure 4.11 Time Structure and Thickness Maps 2.	78
Figure 4.12 Time Structure and Thickness Maps 3.	79
Figure 4.13 Measured and calculated geometric parameters of clinoforms and seismic sequences discussed in this chapter.	81
Figure 4.14 Shelf Edge Trajectories.	82
Figure 4.15 Miocene – Pliocene deep-water channels.	83
Figure 4.16 Shelf and slope geomorphology in Unit B.	85
Figure 4.17 Shelf geomorphology in Unit C.	86
Figure 4.18 Slope failure during Unit E.	89
Figure 4.19 Migration of slope canyons.	92
Figure 4.20 Backstepping shelf margin.	93
Figure 4.21 Slope collapse during unit H.	96
Figure 4.22 Heavily incised corridor.	97
Figure 4.23 Tectonic subsidence curves.	105
Figure 4.24 Tilted stratigraphy in the Southern Taranaki Basin.	108
Figure 4.25 Compression in the Southern Taranaki Basin.	109
Figure 4.26 Plot of sediment wave dimensions separated by unit.	111
Figure 4.27 Sediment Waves in the Taranaki Basin.	112
Figure 4.28 Schematic paleogeography for T1 to T4.	114
Figure 4.29 Schematic paleogeography for T4 to Present.	115
Figure 5.1 Stratigraphic Framework	120
Figure 5.2 Bathymetry of the Southern Taranaki Basin.	122
Figure 5.3 Data utilised in this chapter.	123

Figure 5.4 Egmont Terrace “slug”	123
Figure 5.5 Shelf rollovers mapped in this study.	128
Figure 5.6 Composite dip section of DT08-042, K98-11 & T96-39.	129
Figure 5.7 Dip section DTB01-31.	130
Figure 5.8 Strike section DTB08-132.	131
Figure 5.9 Time Structure Maps for T7 to ET05.	132
Figure 5.10 Time Structure Maps for ET06 to ET11.	133
Figure 5.11 Time Structure Maps for ET12 to ET13	134
Figure 5.12 Time Thickness Maps for T7 to ET06	135
Figure 5.13 Time Thickness Maps for ET06 to ET12.	136
Figure 5.14 Time Thickness Maps from ET12 to Seabed.	137
Figure 5.15 Composite seismic line of DTB08-44 & K98-9	138
Figure 5.16 Change in offlap direction.	139
Figure 5.17 Composite seismic line of DTB08-42 & K98-11.	140
Figure 5.18 Seismic line DTB08-46 showing stratigraphy from ET03 to ET08.	142
Figure 5.19 Seismic line DTB08-42 showing stratigraphy from ET06 to ET10.	142
Figure 5.20 Seismic line DTB08-42 showing stratigraphy from ET09 to ET12.	143
Figure 5.21 Stratigraphy from ET12 to Seabed.	145
Figure 5.22 Distribution of High-Amplitude (HA)Bodies on the Egmont Terrace.	147
Figure 5.23 Variability in slope fan geometries.	148
Figure 5.24 Time thickness maps of slope fans overlying A) ET10 and B) ET11.	148
Figure 5.25 Amplitude extractions along DTB01-31	149
Figure 5.26 Sequence boundaries to sea level correlation.	153
Figure 5.27 Ice extents and vegetation during the LGM.	159
Figure 5.28 Geology northwest South Island.	160
Figure 5.29 Pockmarks on the Egmont Terrace.	161
Figure 5.30 Idealised model of the formation of the high amplitude slope fans.	162
Figure 5.31 Comparison of clinoform lengths and heights from various slope systems from (Hubbard et al., 2010).	163
Figure 5.32 North Slope clinoforms.	165
Figure 5.33 Map of the surficial sediments of the North Island continental shelf.	167
Figure 5.34 Comparison of outcrop and seismic lowstand slope succession.	171
Figure 6.1 Elements of the source to sink system.	173
Figure 6.2 Stratigraphic Framework	176

Figure 6.3 Late Quaternary ages from Nodder (1994).	177
Figure 6.4 Data and bathymetry in the Taranaki Basin.	178
Figure 6.5 Delta scale clinoforms in the Pipeline 3D survey.	180
Figure 6.6 Geomorphology in the Maui 4D seismic survey.	182
Figure 6.7 Seismic geomorphology of the Tui 3D survey.	184
Figure 6.8 Seismic geomorphology of the Karoro 3D survey.	185
Figure 6.9 Embayment in the vicinity of the Hector 3D survey.	186
Figure 6.10 Composite section showing clinoforms downlapping on to Egmont Terrace. See Figure 6.1A for location.	187
Figure 6.11 Sediment pathways from the Egmont Terrace to the Deepwater Taranaki Basin.	190
Figure 6.12 Contourite and moat.	191
Figure 6.13 Seabed slope map from the Vulcan and Romney 3D seismic surveys	195
Figure 6.14 Co-rendered Slope and RMS Amplitude extraction with a sub sea floor window 25 ms on the Vulcan and Romney 3D surveys	196
Figure 6.15 Sediment Waves in the Vulcan and Romney 3D surveys	197
Figure 6.16 Channels, fans and MTDs.	198
Figure 6.17 Composite seismic line DTB01-08 & ATB10-013	199
Figure 6.18 Surficial sand and sediment pathways.	201
Figure 6.19 Celtic–Armorican margin during the Last Glacial Maximum (LGM).	202
Figure 6.20 Generalised geology of New Zealand with exhumation rates and River sediment yields.	205
Figure 6.21 Catchment size vs Sediment Load.	207
Figure 6.22 South Island sediment yield and drainage.	208
Figure 6.23 Highstand vs. Lowstand landmass.	209
Figure 6.24 Sediment yields and surficial sediments.	210
Figure 6.25 Sub Tropical Front variability.	212
Figure 6.26 Sediment routing from land to the deep sea in the Californian Borderlands.	213
Figure 6.27 Highstand compilation	215
Figure 6.28 Lowstand compilation.	218
Figure 7.1 Overview of previous studies undertaken in this thesis.	223
Figure 7.2 Stratigraphic Framework Stratigraphy of the Giant Foresets Formation.	224

Abstract

The Giant Foresets Formation in the Taranaki Basin defines the present-day continental margin of the west coast of New Zealand's North Island. Using regional 2D and 3D seismic datasets calibrated with exploration wells, this thesis presents a new high-resolution seismic stratigraphy that records major changes in basin fill architecture from Late Pliocene to recent. Lateral (across depositional strike) variations in progradational character document a 3-D progradational history more complex than previously recorded. Progradation of the margin took place in two main depocentres on the Western Stable Platform. Initially, sediment was focused mainly into the northern depocentre until approximately 1.2 Ma, resulting in a lobate margin geometry with common mass wasting. From 1.2 Ma, a reconfiguration of sediment pathways is inferred to have switched the focus of progradation to a southern depocentre on the Western Stable Platform. Additional detailed sequence stratigraphic mapping of this southern depocentre (the Egmont Terrace) has characterised 14 unconformity bounded depositional sequences. Within each sequence, highstand deposits are characterised by bland, basinward-dipping seismic reflections with low amplitudes. Lowstand deposits comprise submarine slope fans exhibiting anomalously high seismic amplitudes, an effect attributed to a degree of gas saturation in coarse lowstand material. The scale and frequency of deposits on the Egmont Terrace are tentatively correlated to fluctuations in global eustasy in the Late Pleistocene. Additional insights from 3D geomorphological studies of latest Pleistocene intervals reveal contrasting highstand and lowstand sediment pathways to the Taranaki Basin. Shelf sedimentation during highstands was towards the north and northeast via progradation of delta scale clinoforms carrying sediment from the uplift and erosion products of the Southern Alps. During late Pleistocene sea level lowstands, the Farewell Rise was subaerially exposed and drained by wide fluvial channels to the west and northwest.

The across strike variation in basin fill architecture and contrasting glacial/interglacial provenances highlighted in this thesis show that traditional industry exploration concepts based on single dip lines are insufficient in capturing the complexities in the depositional record.

Declaration

No portion of this work referred to in this thesis has been submitted in support of an application for another degree or qualification of this or any other university or other institute of learning.

Copyright Statement

The author of this thesis (including any appendices and/or schedules to this thesis) owns certain copyright or related rights in it (the “Copyright”) and s/he has given The University of Manchester certain rights to use such Copyright, including for administrative purposes.

Copies of this thesis, either in full or in extracts and whether in hard or electronic copy, may be made only in accordance with the Copyright, Designs and Patents Act 1988 (as amended) and regulations issued under it or, where appropriate, in accordance with licensing agreements which the University has from time to time. This page must form part of any such copies made.

The ownership of certain Copyright, patents, designs, trademarks and other intellectual property (the “Intellectual Property”) and any reproductions of copyright works in the thesis, for example graphs and tables (“Reproductions”), which may be described in this thesis, may not be owned by the author and may be owned by third parties. Such Intellectual Property and Reproductions cannot and must not be made available for use without the prior written permission of the owner(s) of the relevant Intellectual Property and/or Reproductions.

Further information on the conditions under which disclosure, publication and commercialisation of this thesis, the Copyright and any Intellectual Property University IP Policy (see <http://documents.manchester.ac.uk/display.aspx?DocID=24420>), in any relevant Thesis restriction declarations deposited in the University Library, The University Library’s regulations (see <http://www.library.manchester.ac.uk/about/regulations/>) and in The University’s policy on Presentation of Theses.

Acknowledgements

Firstly, thank you to Professors Mads Huuse and Stephen Flint. Your patience and support whilst pulling both myself and this project together have been unerring.

Thanks also to the University of Manchester and the NERC Oil and Gas CDT who generously sponsored this research and provided 20 weeks of additional industry focused training. The large cohort from universities across the UK was a source of fun, friendship and mind opening debates throughout the last 4 years.

Throughout this PhD I have been fortunate to be surrounded by a wonderful and supportive group of people since arriving in Manchester, many of whom have since moved on to bigger and brighter futures. Many lifelong friendships were created, that's a lot to be thankful for.

On a short trip to New Zealand I was fortunate to be warmly welcomed by the research community. This research benefited from the friendly and constructive feedback. Thanks are due to Tim Naish and Lionel Carter at Victoria University of Wellington, Martin Crundwell and Dominic Strogen at GNS, Rochelle Hansen at the University of Waikato and Lorna Strachan and Michael McNaughton at the University of Auckland.

A special thanks are due to my family and friends at home in Ireland who were ever supportive and always on the end of a phone for conversations when I need them. Thanks also to Gina for your love, support and advice through the final months of this thesis.

This PhD has consumed a lot of energy over the last few years and I can say I haven't quite been my cheery self the whole time. Submitting this thesis marks a turning point towards a bright future which I look forward to stepping into with renewed energy and enthusiasm for the people who make this world such a great place to live in.

Chapter 1

Introduction

1.1 Project Rationale

Clinoforms are common building blocks in siliciclastic successions around the world. They consist of topset, foreset and bottomset components (Figure 1.1), are present on different scales, from delta-scale clinoforms to continental margin-scale examples and define a bathymetric break between shallow shelves and basin floors (Figure 1.2) (Helland-Hansen and Gjelberg, 2012; Patruno et al., 2015a; Patruno and Helland-Hansen, 2018; Rich, 1951). The study of basin margin evolution has dominantly been carried out using seismic data where the shelf edge rollover is easily identified (e.g. Paumard et al., 2018; Ryan et al., 2009) and in more detail when coupled with borehole observations (e.g. Cosgrove et al., 2018; Mountain and Proust, 2010).

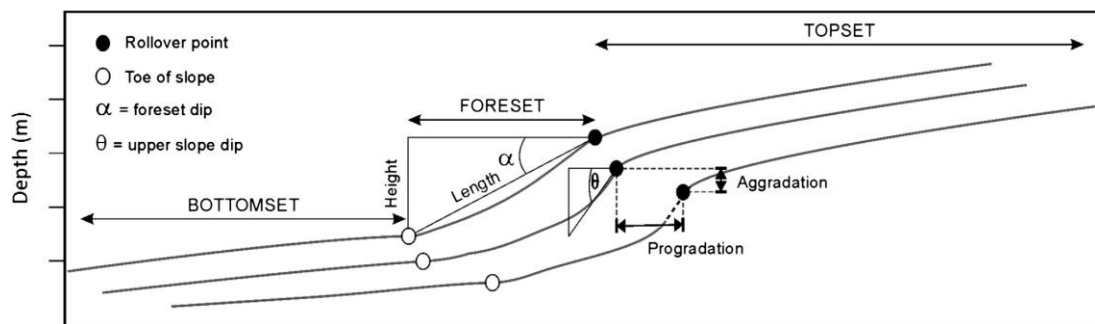


Figure 1.1 Architectural components of a clinoform (from Salazar et al., 2016).

Numerous studies have been undertaken to investigate the links between clinoform geometries, trajectories and sediment distribution along continental margins (Adams and Schlager, 2000; Anell et al., 2014; Anell and Midtkandal, 2017; O’Grady et al., 2000; Patruno et al., 2015b, 2015a, 2014), their sequence stratigraphic context (Houseknecht et al., 2009; Monteverde et al., 2008; Neal and Abreu, 2009) and the trajectory of successive clinoform rollovers (e.g. Gong et al., 2015; Helland-Hansen and Hampson, 2009; Henriksen et al., 2009; Kertznus et al., 2009). Source to sink analysis further integrates data from the complete erosional area (source/catchment) and the complete depositional area (sink) to build a more comprehensive model of basin fill evolution (Figure 1.2; Sømme et al., 2009).

When combined with age data (e.g. biostratigraphy), these methods provide a powerful tool to decipher how a sedimentary basin filled through time and space. To this end, this thesis investigates the Plio – Pleistocene aged Giant Foresets Formation (GFF), in the Taranaki Basin, New Zealand.

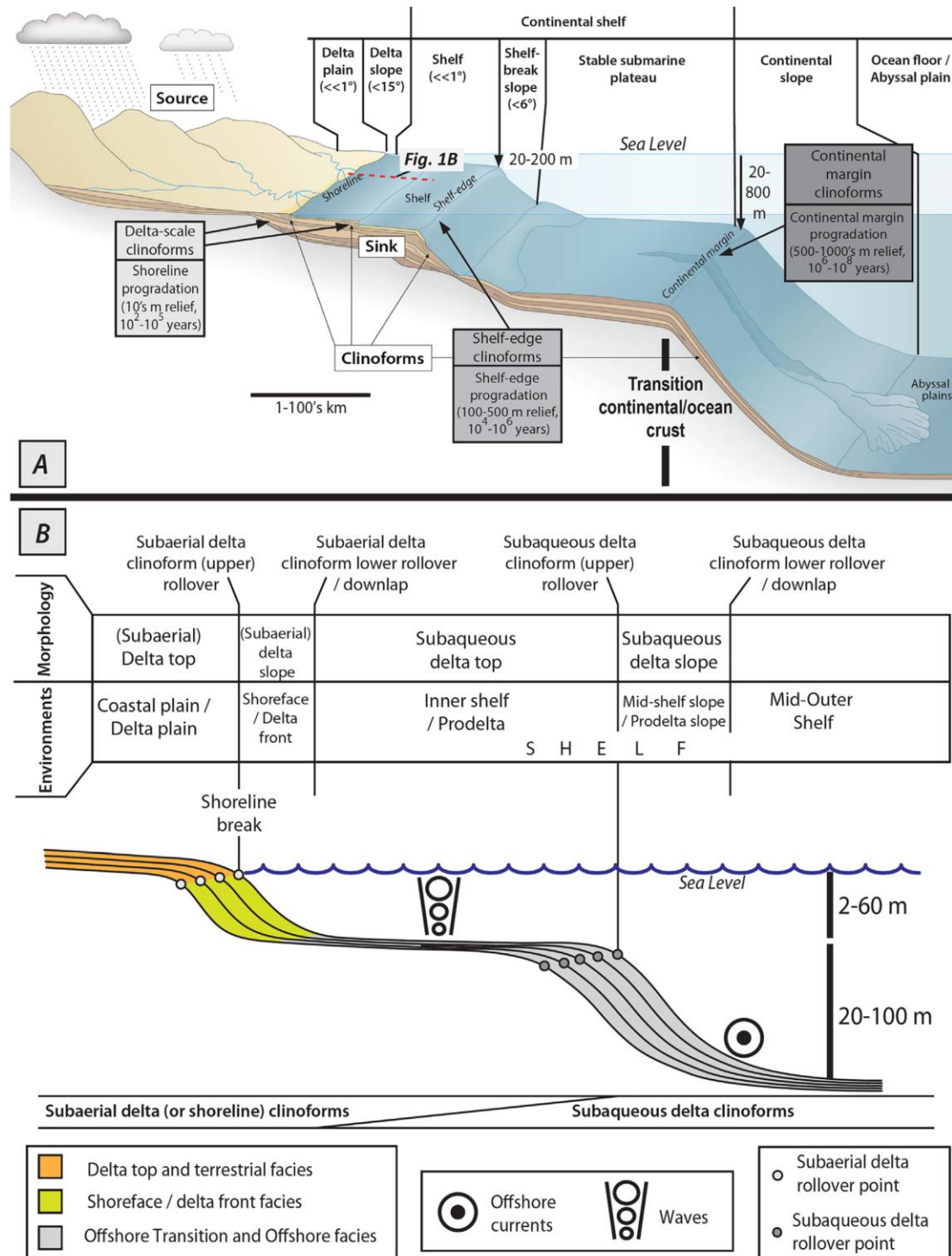


Figure 1.2 Clinoform scales and settings

A) Regional cross-section of an idealised compound clinoform system, highlighting three actively growing clinoforms systems: delta, shelf-edge and continental-margin scale clinoforms. B) Schematic section of the nearshore to inner marine shelf area, showing a shoreline to delta-scale subaqueous clinoform compound system. From Patruno and Helland-Hansen (2018).

1.2 Thesis Aims & Objectives

The principal aim of this thesis is to unravel the controls on the evolution of the Giant Foreset Formation including tectonics, climate, eustasy, hinterland geology and sediment routing processes. The overarching objective is to establish a stratigraphic framework within which the Giant Foresets Formation (GFF) can be examined in a regional and global context. To achieve this objective, several key tasks are set out below:

1. To identify major changes in the stratigraphic architecture of the GFF and map these across the basin.
2. To date these major architectural changes using existing biostratigraphy and, where lacking, investigate other methods of improving age control.
3. To search for and document pathways taken by sediment to the basin in glacial (lowstand) vs. interglacial (highstand) periods.

1.3 Thesis Structure

This thesis comprises seven chapters, Chapters 1 to 3 are introductory in nature, with the bulk of research outlined in Chapters 4 to 7.

Chapter 1 introduces the research topic, project rationale and provides an overview of clinofolds.

Chapter 2 summarises the structural and stratigraphic evolution of New Zealand and the Taranaki basin from the Late Cretaceous to present and outlines the existing body of literature on the Giant Foresets Formation.

Chapter 3 introduces the datasets used by this project and elaborates on the methodologies employed and data limitations.

Chapter 4 utilises the regionally extensive seismic database across the Taranaki Basin to identify major changes in the clinofold packages and establish a regional seismic stratigraphic framework along a 200 km length of the Western Stable Platform for the first time. Within this context, factors controlling the progradation of the margin are explored.

Chapter 5 builds on the regional framework by zooming in on the southwestern limits of the Taranaki Basin (the Egmont Terrace), where a sequence stratigraphic study examines

a portion of the shelf that exhibits remarkably cyclic clinoform geometries. Chapters 4 and 5 evolved symbiotically, each lending context and age information to the other.

Chapter 6 employs seismic geomorphology to investigate sediment pathways taken to the basin in late Pleistocene glacial (lowstand) and interglacial (highstand) times. The results are integrated with information from catchments and advances in the understanding of regional oceanographic patterns to provide a Source to Sink template for the basin.

Chapter 7 synthesises the results of chapters 4 to 6 and discusses their implications, limitations and explores future research questions arising from this study.

1.4 Clinoform Background

Here, clinoforms are discussed on three main scales: delta scale, shelf margin scale and continental margin scale clinoforms. Each clinoform scale has specific geometric, spatial and temporal characteristics (Table 1.1) but may also be observed prograding through the depositional system at different rates as compound or hybrid clinoforms (see section 1.4.4).

Table 1.1 Characteristics of clinoform of different scales

(from Patruno and Helland-Hansen, 2018).

		Delta-scale clinoforms						
		Continental margin clinoforms	Shelf-edge clinoforms	Muddy subaqueous delta clinoforms	Sand-prone subaqueous delta clinoforms		Shoreline clinoforms	
					≤ 20 kyr	> 20 kyr	≤ 20 kyr	> 20 kyr
Rollover water depth (m)	550–1770 It can be as shallow as 0 m in case of shelf-edge and continental margin deltas ^a	60–426	6–59	21–57		0–5		
Foreset	Heights (m)	590–2570	3–46	12–43		5–38		
	Down-dip extent (km)	6.5–82.3	1.0–11.8	0.1–2.6	0.05–1.8		0.1–19.6	
	Slope gradient (°)	1.1–12.5	0.1–0.9	0.6–9.0	0.7–27.0		0.05–6.1 (Coarse grained systems can be as steep as c.30°)	
Time scale (kyr)	10 ³ –10 ⁵ Up to 10 ¹ kyr in case of shelf-edge deltas ^a	10 ² –10 ⁴	10 ⁻¹ –10 ¹	10 ¹	10 ¹ –10 ²		10 ¹ –10 ³	
Progradation rate (m/kyr)	10 ⁻² –10 ¹	10 ⁻¹ –10 ¹ Up to 10 ⁴ m/kyr in case of shelf-edge deltas ^a	10 ² –10 ⁴	10 ¹ –10 ²		10 ³ –10 ⁴		
Clinoform trajectory (°)	+0.9 to +49	-0.4 to +2.4	0 to +0.5	-0.4 to +3.5	-0.5 to +2.0		0 to +0.13 0 to +0.90	
Coarse-grained sediment dispersal	Gravity, large-scale deformation, canyons	Fluvio, wave, tide, gravity, sea-level control	Storm, tide, currents, gravity	Storm, gravity, currents		Fluvio, wave, tide, gravity		
Clinoform reservoir potential	Poor (distal drapes), less than for shelf-edge deltas	Poor (distal drapes)-excellent (shelf-edge delta)	Poor	Minor to Excellent		Poor-Excellent		
Basin floor reservoir potential	Thick, connected	Good potential, possibly disconnected	Minor	Minor, greater if close to the shelf-edge		Few, thin, disconnected		

1.4.1 Delta Scale Clinoforms

Delta scale clinoforms typically occur on scales of tens of metres, form over short time periods of time (< 1000 years) and can be further sub divided into subaerial (shoreline) and subaqueous deltas (Patruno et al., 2015a).

Subaerial/shoreline clinoforms, as suggested in the name, form at the interface between water and land with reliefs typically in the range of 5-40m and have the highest progradation rates ($1-10^2$ km/kyr) of the different types of clinoforms (Patruno and Helland-Hansen, 2018). Their small scale means they are difficult to image on industry standard seismic data but have been successfully studied on ground penetrating radar (e.g. Hampson et al., 2008; Jol et al., 2003), shallow seismic (Hansen and Rasmussen, 2008; Tesson et al., 1990) and outcrops (Enge et al., 2010; Gani and Bhattacharya, 2011). Architecturally, shoreline clinoforms are strongly oblique with an asymmetric morphology, low angle trajectories of $<0.1^\circ$ and inflection points of $0.1 - 1.5^\circ$ in muddy systems and $0.1 - 2.7^\circ$ in sandy systems (Patruno et al., 2015a; Patruno and Helland-Hansen, 2018). Their occurrence in shallow water depths means they can be subject to a variation of wave, tide and fluvial processes are particularly sensitive to allogenic forcing mechanisms such as changes in relative sea level, sediment supply, climate and anthropogenic influence (Ainsworth et al., 2017; Goodbred and Kuehl, 2000; Hampson, 2000; Hampson, 2010).

Subaqueous delta scale clinoforms, on the other hand, typically have foreset heights up to 45 m and rollover in water depths of up to 60m with more regular sigmoidal geometries and trajectories of $0.1 - 2.0^\circ$ (Patruno et al., 2015a; Patruno and Helland-Hansen, 2018). Subaqueous delta scale clinoforms can also be further subdivided on the basis of their relative sand or mud dominance and resulting geometric characteristics (Patruno et al., 2015a).

Mud prone delta scale subaqueous clinoforms are usually found in cratonic or passive margin basins and are typically associated with large river feeder systems, forming at distances of 7.5 – 125km from the shoreline on wide, gently sloping shelves with rollovers in water depth and gentle foreset gradients of $<0.9^\circ$ (Patruno et al., 2015a; Patruno and Helland-Hansen, 2018). Modern examples include the Ganges-Brahmaputra (Goodbred and Kuehl, 2000, 1999; Kuehl et al., 1997), the Amazon (Kuehl et al., 1986) and Mahakam deltas (Roberts and Sydow, 2003). Muddy subaqueous systems without a direct fluvial link have also been documented in the western Adriatic Gargano delta (Figure 3; Cattaneo et al., 2007, 2003), where the delta system is fed by shore parallel currents.

Sand prone subaqueous delta scale clinoforms typically form in extensional or compressional settings capable of delivering coarse sediment to narrow, steep, high energy shelves between fair weather and storm wave bases (Patruno et al., 2015a; Walsh

and Nittrouer, 2003), and are associated with non-deltaic shorelines and strandplains (Fernández-Salas et al., 2009). Modern examples include offshore New Zealand (Dunbar and Barrett, 2005) and the southern Iberian Peninsula (Hernandez-Molina et al., 2000; Lobo et al., 2005).

Although mud and sand prone subaqueous delta scale clinoforms have similar foreset heights, they can be distinguished in seismic data based on geomorphological and architectural measurements and observations compiled by Patruno et al. (2015a) (Table 1.1). Muddy delta scale subaqueous clinoforms are typically associated with large river feeder systems so tend to form larger systems with long strike extents of 100s – 1000s of km and high progradation rates (10^{-1} – 10^1 km/kyr), compared to along strike extents of 10s of km and progradation rates of 10^1 km/kyr for their sand prone counterparts (Patruno et al., 2015a; Patruno and Helland-Hansen, 2018). Foreset slope is perhaps the most useful distinguishing characteristic between these two clinoform sub-types (Table 1.1); muddy subaqueous deltas tend to have gentle slope gradients of 0.1° - 0.9° , whilst sand prone subaqueous delta scale clinoforms tend to be steeper (0.6° – 9°) with limited down dip extents (Patruno et al., 2015a).

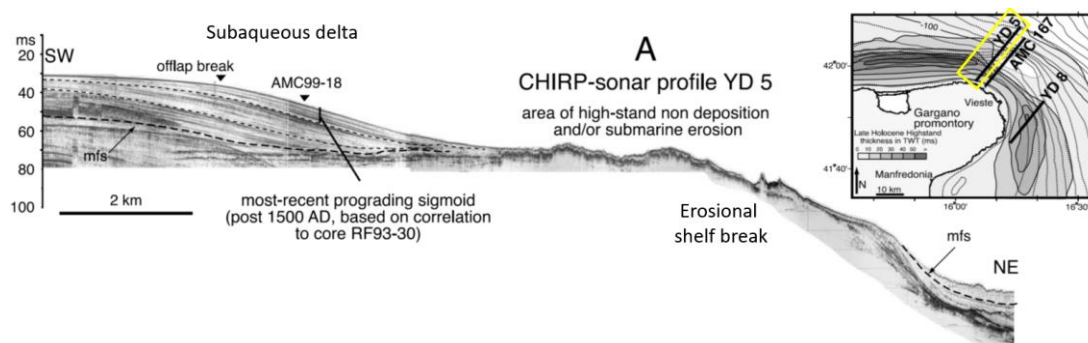


Figure 1.3 CHIRP sonar profile of the Gargano subaqueous delta

(from Cattaneo et al., 2003).

1.4.2 Shelf Edge Clinoforms

Shelf edge clinoforms (previously shelf prism by Patruno et al., 2015a) form in marine or lacustrine environments with minimum water depths of a few hundred metres (Patruno and Helland-Hansen, 2018). A major facies transition occurs across the rollover of shelf margin clinoforms from shallow fluvio-deltaic and offshore transitional facies to deep water bathyal facies dominated by turbiditic processes. Shelf edge clinoforms typically rollover in water depths of 60 – 425 m, have foreset heights typically 100- 300m, slope gradients of 0.6 – 4.8° and progradation rates of 10^{-1} – 10^1 km/kyr (Patruno et al., 2015a; Patruno and Helland-Hansen, 2018). Examples include the Pliocene – Pleistocene Naust

formation (Ottesen et al., 2009), Late Pleistocene Po river (Pellegrini et al., 2018), the Eocene of Spitsbergen (Figure 3A; Steel and Olsen, 2002), Miocene New Jersey margin (Figure 3B; Steckler et al., 1999) and Miocene lacustrine clinoforms of the Dacian basin (Fongngern et al., 2015). Clinoforms of this scale are initiated by the repeated transgressive - regressive cycles of delta scale clinoforms, with the long term stratigraphic climb resulting in progressively steeper and higher clinoforms prograding into deeper frontal waters (Burgess and Hovius, 1998; Helland-Hansen et al., 2012; Johannessen and Steel, 2005; Olariu and Steel, 2009; Steel et al., 2003). This relationship between the progradational dynamics of delta scale and larger shelf margin scale clinoforms is an example of a compound clinoform; a system where more than one type of clinoform is present in a depositional system, although prograding at very different timescales. When a delta scale clinoform reaches the shelf edge (i.e. a shelf edge delta – see section 1.4.4), a significant increases in progradation rate is observed and can be an efficient delivery mechanism of coarse sediment to the deep water (Johannessen and Steel, 2005; Pellegrini et al., 2018; Steel and Olsen, 2002; Uroza and Steel, 2008).

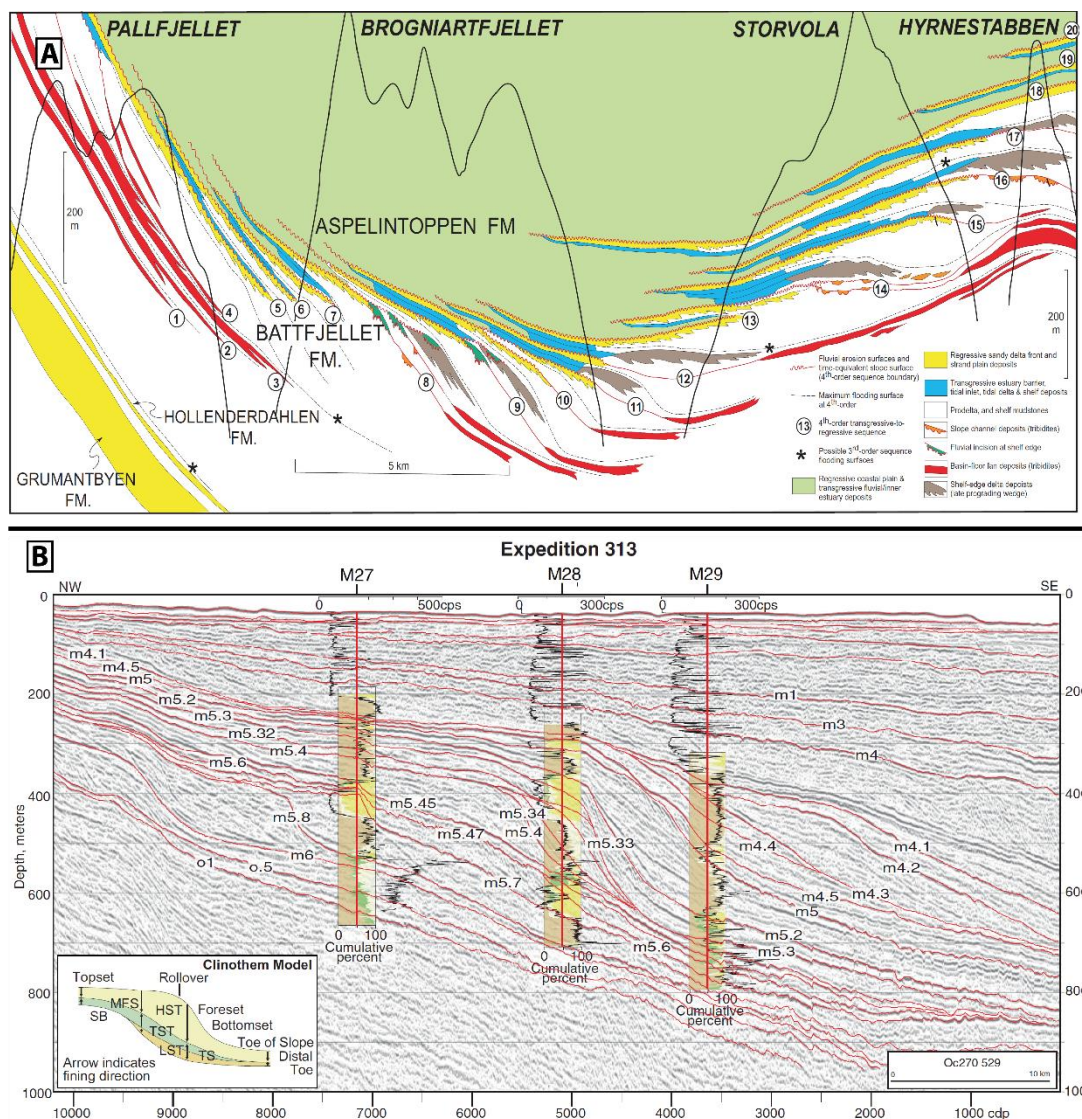


Figure 1.4 Shelf margin clinoform examples.

A) Outcrop example from a Lower Eocene transect across Spitsbergen's Central Basin showing up to 20 mapped clinothem deposited in about 6 Ma (from Steel and Olsen, 2002) B) A seismic example of Miocene shelf margin scale clinoforms from the IODP Expedition 313 on the New Jersey Margin (from Miller et al., 2013).

1.4.3 Continental Margin Clinoforms

Continental margin scale clinoforms represent the largest and deepest in the clinoform size spectrum with rollovers in water depths of 550 – 1770 m, foreset heights ranging from 590 – 2600 m and foreset slopes of 1.1 – 12.5 ° (Table 1.1) (Patrino et al., 2015a; Patrino and Helland-Hansen, 2018). Because of their size, these clinoforms occur over long timescales of 10s to 100s of millions of years with low progradation rates of 10⁻² – 10⁻¹ m/kyr (Table 1.1). Examples of continental margin scale clinoforms include the Jurassic to recent eastern continental margin of the United States (Klitgord et al., 1988; Schlee et al., 1979) and Neogene continental margin of Brazil (Viana et al., 1998) and Cretaceous to recent SW African margin (Figure 3; Austin and Uchupi, 1982).

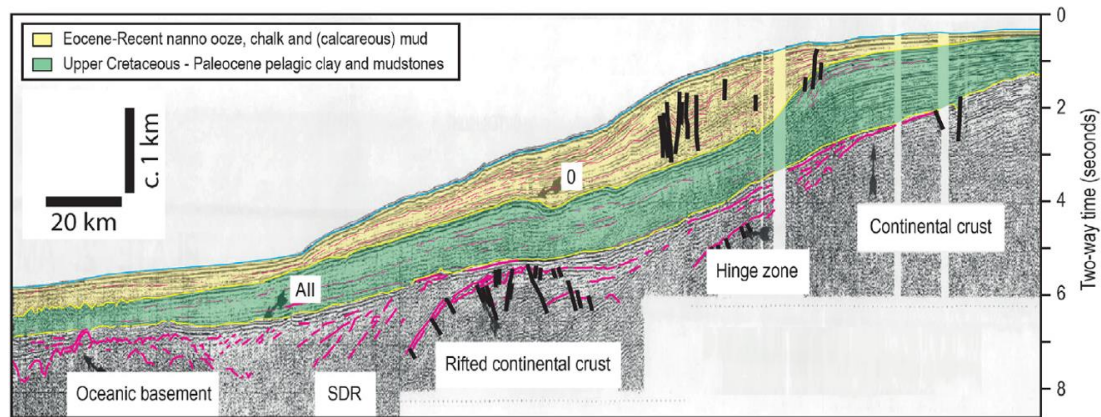


Figure 1.5 Continental Margin clinoform example.

Continental margin off south-west Africa showing a continental margin scale clinoform developed in proximity to the oceanic – continental crust interface (modified by Patruno and Helland-Hansen (2018) after Profile AM56 of Austin and Uchupi, 1982).

The setting of both shelf edge and continental margin clinoforms is on the margins of significant bathymetric depressions. They can, however, be distinguished by their distinct structural styles, bathymetric expressions and clinoform architectures (Henriksen et al., 2011; Patruno et al., 2015a). They are further distinguished from shelf margin clinoforms by the processes governing the initial generation of relief; as detailed above, shelf margin clinoforms are generated by sedimentary processes related to repeated transgressive-regressive cycles of delta scale subaqueous clinoforms. Relief for continental margin clinoforms, however, is generated by geodynamic processes at the boundary between continental and oceanic lithosphere (Steel and Olsen, 2002). Despite this classification, Patruno et al. (2015a) advocate that clinoforms greater than 1000 m can still be classified as continental margin scale clinoforms even if they occur at distance from the boundary between oceanic – continental crust. Also, that shelf margin clinoforms located at the oceanic – continental crust boundary with foreset heights of less than 1000 m can still be classified as shelf margin scale clinoforms.

1.4.4 Compound & Hybrid Clinoforms

Compound clinoforms occur where clinoforms in a proximal position are genetically linked down-dip to a larger clinoforms in that, for example, the bottomset of a subaqueous delta scale clinoform in fact forms the topset/shelf of shelf margin scale clinoform (Figure 1.6A). All four of the clinoform scales discussed above can be present in a depositional system, albeit prograding at very different rates (e.g. the U.S. Atlantic margin). More commonly, however, compound clinoforms are observed as either compound delta scale clinoforms (e.g. Gargano delta, the Yellow Sea and the Ganges-Brahmaputra (Cattaneo et al., 2003; Liu et al., 2004; Michels et al., 1998) or as a compound

subaqueous delta scale and shelf margin clinoform system (e.g. the Ebro delta: Kertznus and Kneller, 2009).

Hybrid clinoforms occur where two or more of the afore mentioned clinoform scales merge together, e.g. when a subaqueous delta scale clinoform progrades to the rollover of a shelf margin scale clinoform, a shelf edge delta is formed, or continental margin delta if the delta reaches the continental margin rollover (Patrino and Helland-Hansen, 2018). Examples include the Eocene of Spitsbergen (Mellere et al., 2002; Steel et al., 2003; Steel and Olsen, 2002), Cretaceous – Paleogene Magallanes Basin (Covault et al., 2009; Hubbard et al., 2010) and the Quaternary Niger Delta (Damuth, 1994; Short and Stauble, 1967). Hybrid Shelf/Continental Margin Deltas can be an efficient mechanism for delivery of coarse clastic material across the shelf rollover to deepwater regions of a basin, forming prolific hydrocarbon provinces in the Mississippi, Niger, Congo and Orinoco deltas. As shelf margin and continental margin scale clinoforms tend to be dominated by mud & silt, these coarse clastic bodies from shelf edge deltas can become encapsulated in low permeability rocks, forming important reservoir intervals for hydrocarbon accumulations (Johannessen and Steel, 2005; Steel and Olsen, 2002; Sydow et al., 2003).

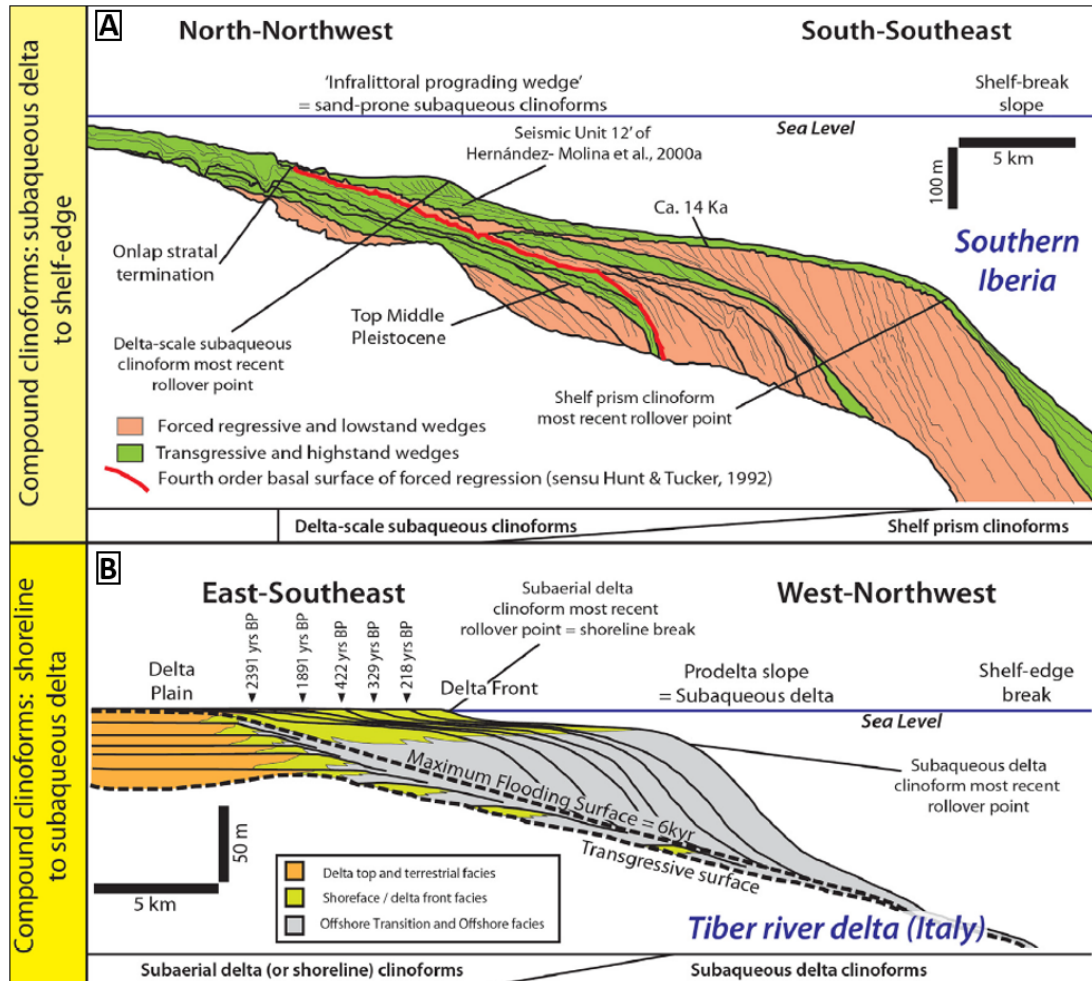


Figure 1.6 Compound Clinoforms

Dip oriented examples of compound clinoform systems at different scales. A) Quaternary delta scale and shelf edge compound clinoforms from the southern Iberian Peninsula (after Hernández-Molina et al., 2000) and B) the Holocene shoreline and subaqueous delta scale compound clinoform system of the Tiber delta (after Amorosi and Milli, 2001). Figure from Patruño and Helland-Hansen (2018)

Blank Page

Chapter 2

Study Area

This thesis investigates the Giant Foresets Formation (GFF) in the Taranaki Basin, located off the west coast of New Zealand's North Island as the dataset for this study of clinoforms (Figure 2.1). The GFF was deposited from the Pliocene to recent and define the modern-day shelf rollover of the basin. In this section, the setting, structure and stratigraphy of the Taranaki Basin is reviewed.

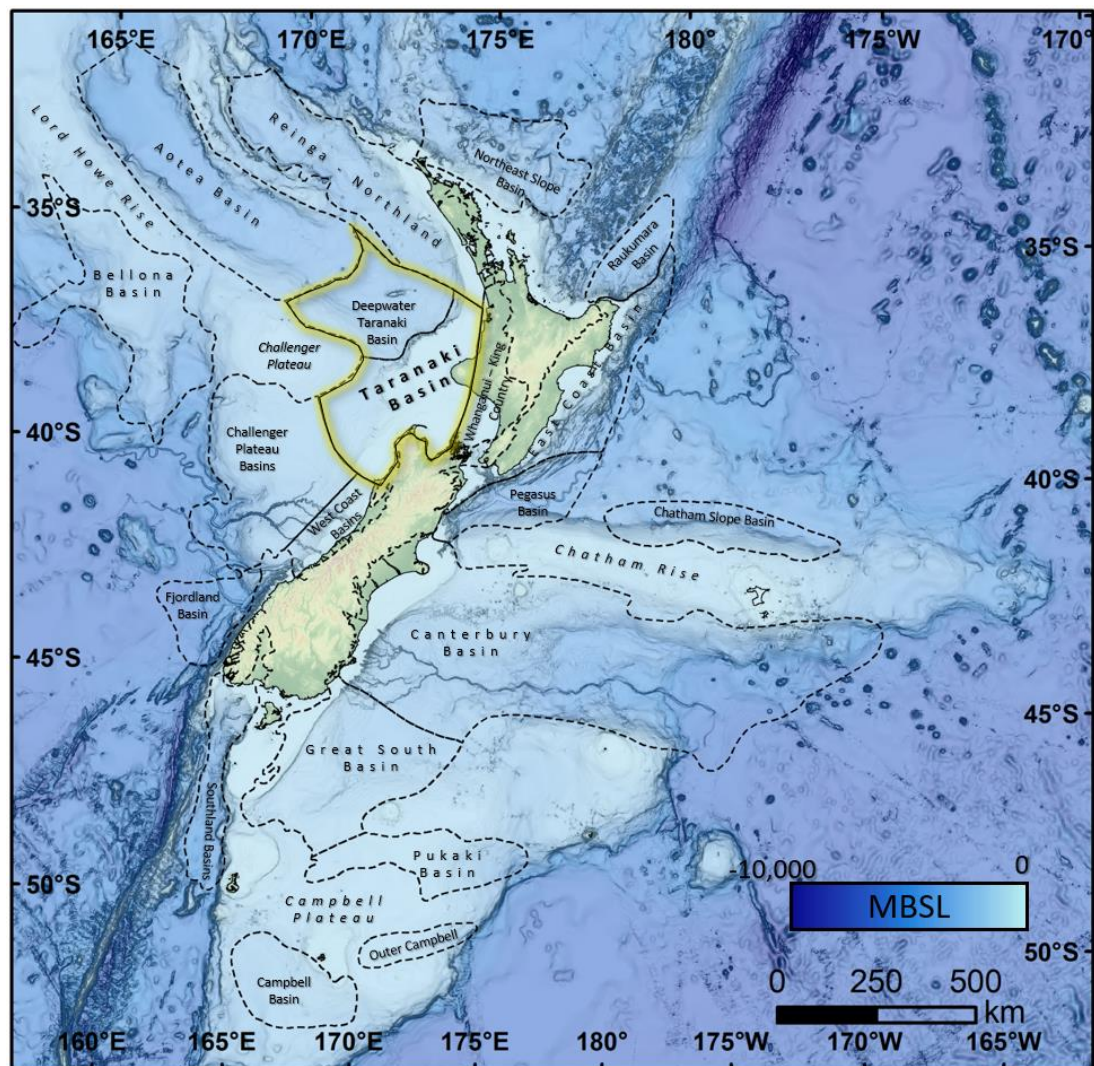


Figure 2.1 Sedimentary Basins of New Zealand.

The Taranaki Basin is highlighted in yellow.

The present-day configuration of New Zealand is dominated by collisional tectonics between the Australian and Pacific tectonic plates (Figure 2.2). This is manifested on the east coast of North Island as the southwest directed Hikurangi Subduction Margin where

the dense oceanic Pacific Plate crust is subducting under the more buoyant continental crust of Australian and Zealandia crust (Giba et al., 2010; Stagpoole and Nicol, 2008). Southwest of South Island the polarity of the collisional margin reverses with the Australian Plate subducting under the Pacific Plate along the Puysegur Margin (Stern et al., 2006). This change in polarity between North and South Island is facilitated by the Alpine Fault system; a large dextral strike slip fault system (Figure 2.2 a-c).

The evolution of the Taranaki Basin is divided into three main phases of development (Figure 2.3); an early rift phase, a middle phase of passive margin activity and finally a recent active margin phase associated with plate convergence (King and Thrasher, 1996).

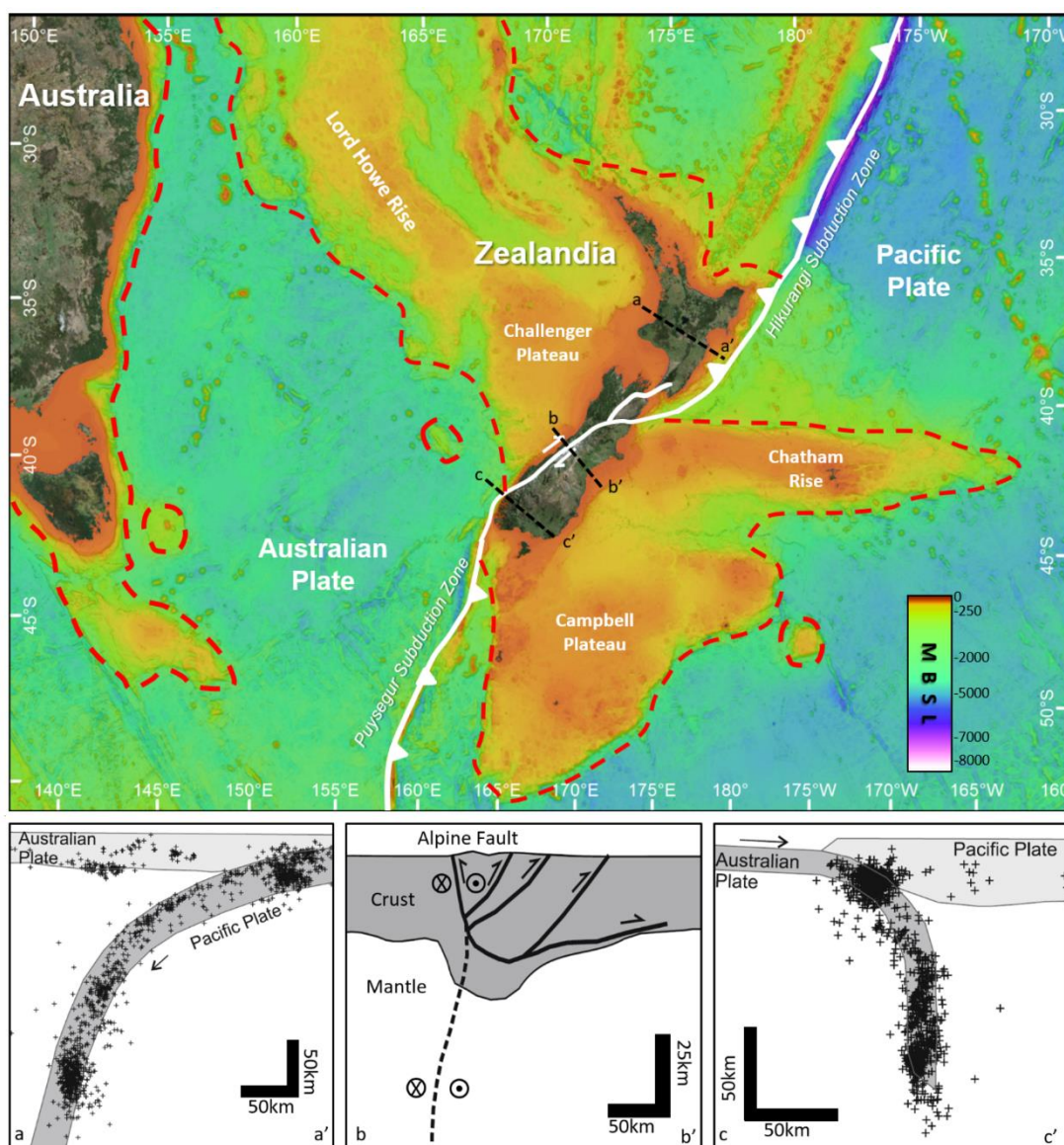


Figure 2.2 SW Pacific bathymetry and crustal structure of New Zealand.

Regional bathymetric map showing tectonic plates and major physiographic features, including continental crust (dashed red) and the submerged continent of Zealandia. Bathymetry sourced from GEBCO. Sections a and c are constructed using earthquake data from GeoNet and are adapted from Nicol et al. (2017).

Section b is adapted from Norris and Toy (2014). Circle with x shows movement into the page, whilst a circle with a dot shows movement out of the page.

2.1.1 Regional Tectonic Evolution

Phase 1 – Cretaceous to Palaeocene Rifting

The early rifting phase is associated with the breakup of Gondwana in the mid-late Cretaceous through to Palaeocene times, resulted in the formation of the Tasman Sea (King and Thrasher, 1992, 1996; Knox, 1982). This extension resulted in the inception of the Taranaki and Aotea/New Caledonia Basins, a 2000 km northwest–southeast trending basin linking New Zealand to New Caledonia (Baur et al., 2014; Tulloch and Kimbrough, 1989; Uruski and Wood, 1991). Early extension in this setting was accommodated along the Taranaki Rift; a series of small elongate sub basins (King and Thrasher, 1996).

Phase 2 – Eocene to Oligocene Passive Margin

From the Palaeocene to Early Oligocene a dominantly transgressive succession records where a passive margin setting was established (King and Thrasher, 1992), with approximately 2.5 km of accommodation created by Cretaceous rifting and subsequent post rift thermal subsidence. (Baur et al., 2014). A second anomalous phase of passive subsidence from approximately 40 Ma is also observed; this second phase exhibits no major structural surface expression, except for creation of accommodation. This is likely linked to a change in mantle convective processes occurred at this time to result in regional long wave crustal down warping (Baur et al., 2014; Baur, 2012; Sutherland et al., 2010).

A link is hypothesised to exist between the behind margin location of this subsided region and the incipient collisional margin of the Australian and Pacific plates that resulted from a change in mantle convective currents (Baur et al., 2014).

Phase 3 – Oligocene to Recent Convergence

Phase three in the development of the Taranaki Basin was dominated by processes associated with the development of a convergent margin between the Australian and Pacific plates. This complex part of the basin history includes the

development of a foreland basin, establishment of major thrusting and shortening within the basin from approximately 40 Ma to present, localised back arc related extension and volcanism from 16 Ma to present (Giba et al., 2010; King and Thrasher, 1992, 1996; Knox, 1982; Uruski and Wood, 1991).

Establishment of a convergent plate boundary at the Hikurangi margin (Figure 2.2) occurred in the Mid Eocene between 40-45 Ma (Stagpoole and Nicol, 2008; Stern and Davey, 1990; Stern and Holt, 1994). In the Taranaki Basin, this convergent margin resulted from the westward movement of dense oceanic Pacific crust subducting under the continental Australian Plate (King and Thrasher, 1992, 1996; Knox, 1982). Loading associated with this area of thickened crust formed a foreland basin along the eastern margin of the Taranaki Basin, with the Taranaki Fault (Figure 2.4) acting as the eastern bounding fault (Stagpoole and Nicol, 2008). Subsidence in the foreland basin affected the entire Taranaki region and was greatest adjacent to the Taranaki Fault (King and Thrasher, 1996).

2.1.2 Basin Structure

Within the Taranaki Basin two distinct structural domains have evolved; the tectonically active Eastern Mobile Belt and the quiescent Western Stable Platform (Figure 2.4B). The boundary between these two domains is the Cape Egmont Fault in the north and the most westerly expression of Miocene thrusting and inversion in the south (King and Thrasher, 1996).

The Eastern Mobile Belt is the behind arc expression of compression, rotation and extension associated with the Hikurangi Subduction Margin and can be further divided into two main structural regimes; 1) extension in the Northern and Central Grabens (Figure 2.4A) and 2) compression in the Southern Inversion Zone (King and Thrasher, 1992, 1996; Knox, 1982). Between approximately 40-12 Ma compression was dominant in the Taranaki Basin (Rait et al., 1991; Stagpoole and Nicol, 2008; Stern et al., 2006). At approximately 12 Ma the North Taranaki region began an extensional phase, forming the Northern Graben. This extension is attributed to the clockwise rotation of the Hikurangi Subduction Zone and slab rollback of the Pacific plate (Ballance, 1976; Nicol et al., 2007; Stern, 1987).

The Northern Graben is a northeast trending structural depression, approximately 200 km in length and 65 km wide at its widest point and is bounded on its western side by the Cape Egmont Fault system and in the East by the Turi Fault System. These fault systems intersect at the southern termination of the graben (King and Thrasher, 1996). Extension in the Northern Graben migrated repeatedly from north to south by 100-150 km, reflecting changes in subduction on the Hikurangi margin (Giba et al., 2010).

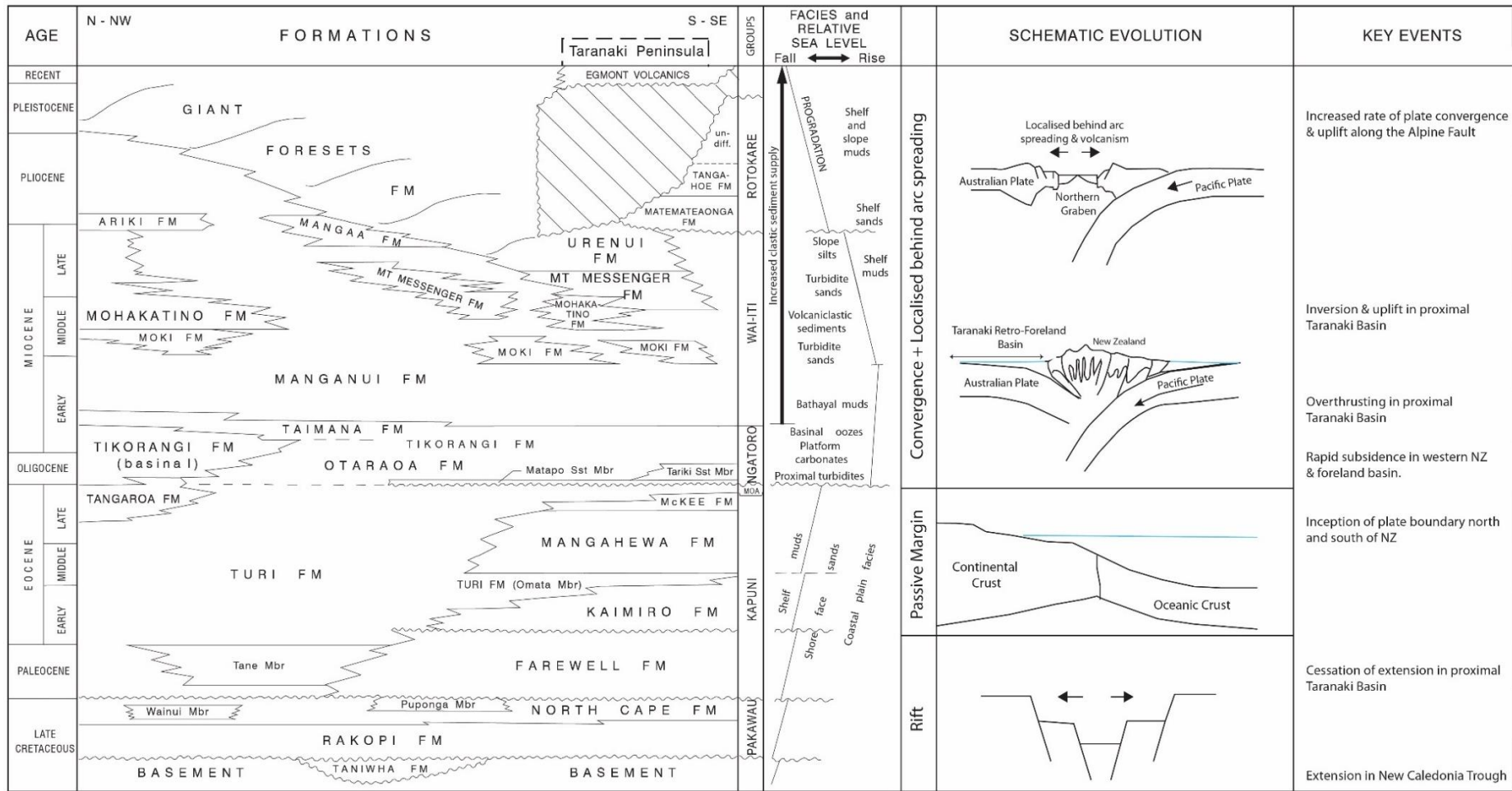


Figure 2.3 Summary stratigraphic and tectonic evolution of the Taranaki Basin (modified from King and Thrasher, 1996).

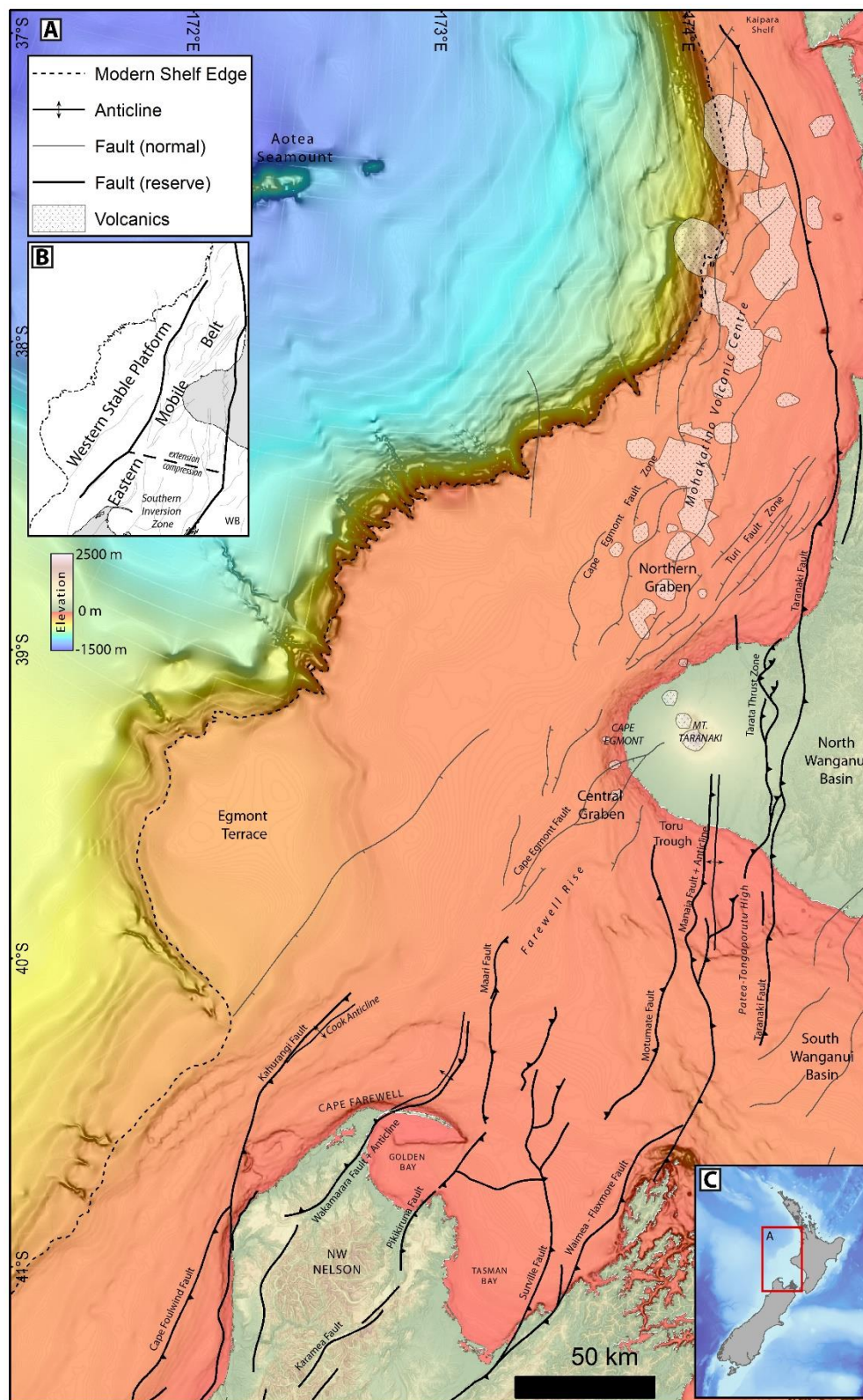


Figure 2.4 Taranaki Basin Structure.

A) Present day seafloor bathymetry annotated with structural features of the Taranaki Basin (after King and Thrasher, 1996). B) Map highlighting structural domains of the Taranaki Basin. C) Regional map showing location of A.

The Mohakatino Volcanic Centre (Figure 2.4) is located along the central axis of the Northern Graben and occupies 15-20% of its total area (King and Thrasher, 1996). Development of this volcanic centre is associated with the Hikurangi Subduction Margin (Ballance, 1976; Kear, 1994) and is composed of pre- and syn-rift andesitic stratovolcanoes, active from 16Ma to present, with most intense activity occurring between 12-4 Ma. Edifices are overlapped and buried by Miocene and Pliocene sediments. Similar to faulting, volcanic activity migrated north to south (Giba et al., 2010), however this occurred over a longer timeframe and was not as geologically instantaneous as fault migration.

The Central Graben lies to the south of the Northern Graben and is also bounded to the west by the Cape Egmont Fault system and on the east by a series of northeast trending faults (Figure 2.4; King and Thrasher, 1992; 1996). This graben is Plio-Pleistocene in age and formed from crustal down-warping and subduction induced flexure (King and Thrasher, 1992; Stern, 1987). The Central Graben represents the southerly limit of extension in the Eastern Mobile Belt. South of this, in the Southern Inversion Zone, a more compressive regime is observed.

The Southern Inversion zone is bounded in the north by the Central Graben, in the west by the Western Stable Platform, and in the east by the Taranaki and Flaxmore Faults (Figure 2.6). The aforementioned extension in the Northern Graben occurred from approximately 12 Ma through clockwise rotation of North Island. This rotation resulted in subsequent compression in the southern Taranaki Basin. Compression was accommodated by inversion of pre-existing structures from Cretaceous – Palaeocene rifting (King and Thrasher, 1996). Inversion and uplift on these structures is noted to increase moving south. This inversion event created anticlines and ridges oriented roughly north-south, which have economic importance as hydrocarbon traps (King and Thrasher, 1996; Reilly et al., 2015).

The concept of extension in the North Taranaki and compression in the South Taranaki is best explained by the block rotation model illustrated in Figure 2.5, where rotation of the North Island around a migrating axis of rotation resulted in compression south of the axis and extension north of the axis (Giba et al., 2010; King and Thrasher, 1996). The axis of rotation and boundary between extension and compression migrated south through the Late Miocene to present. The Western Stable Platform (WSP) has remained predominantly unaffected by the collision of the Australian and Pacific plates that affected

the Eastern Mobile Belt (King and Thrasher, 1992; Knox, 1982). Structures in this region are Cretaceous - Palaeocene half grabens that have subsequently been filled since the Eocene (King and Thrasher, 1996). Stratigraphy on the WSP is the main focus of this project due to its lack of structure directly influencing the Plio-Pleistocene succession.

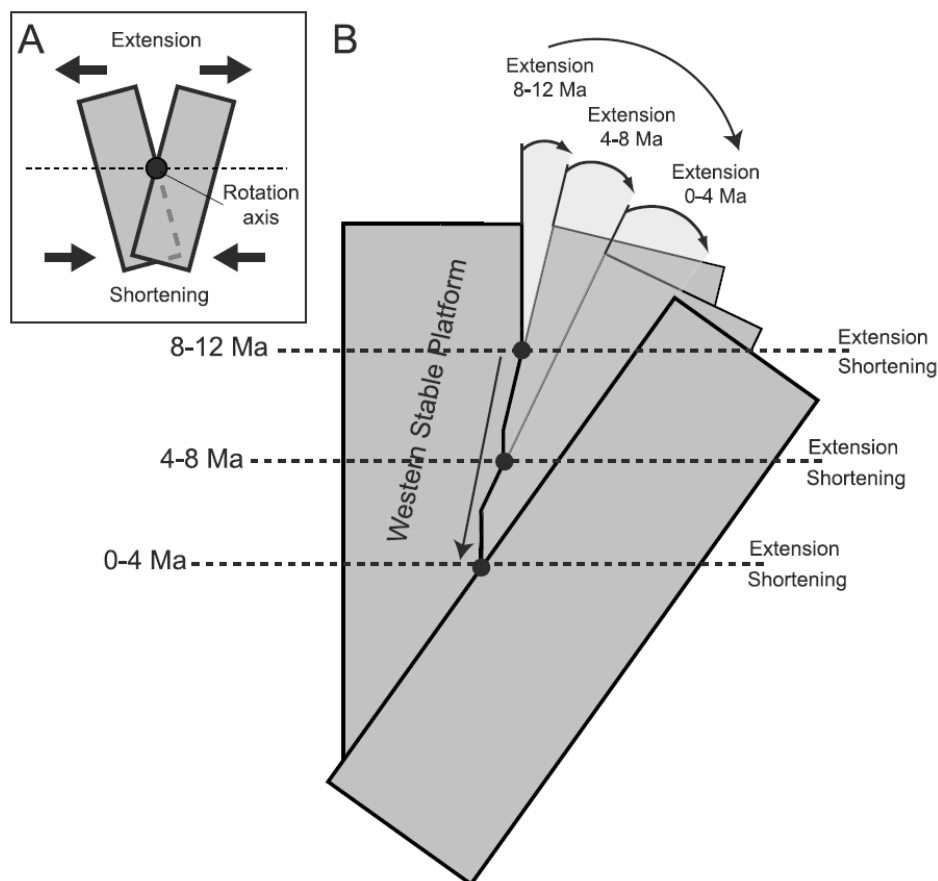


Figure 2.5 Schematic block rotation model.

A) Schematic block rotation model of King and Thrasher (1996) illustrating rotation of crustal blocks giving rise to extension and compressive regimes. B) Modified block rotation model of Giba et al. (2010) showing periodic north to south migration of the axis of rotation.

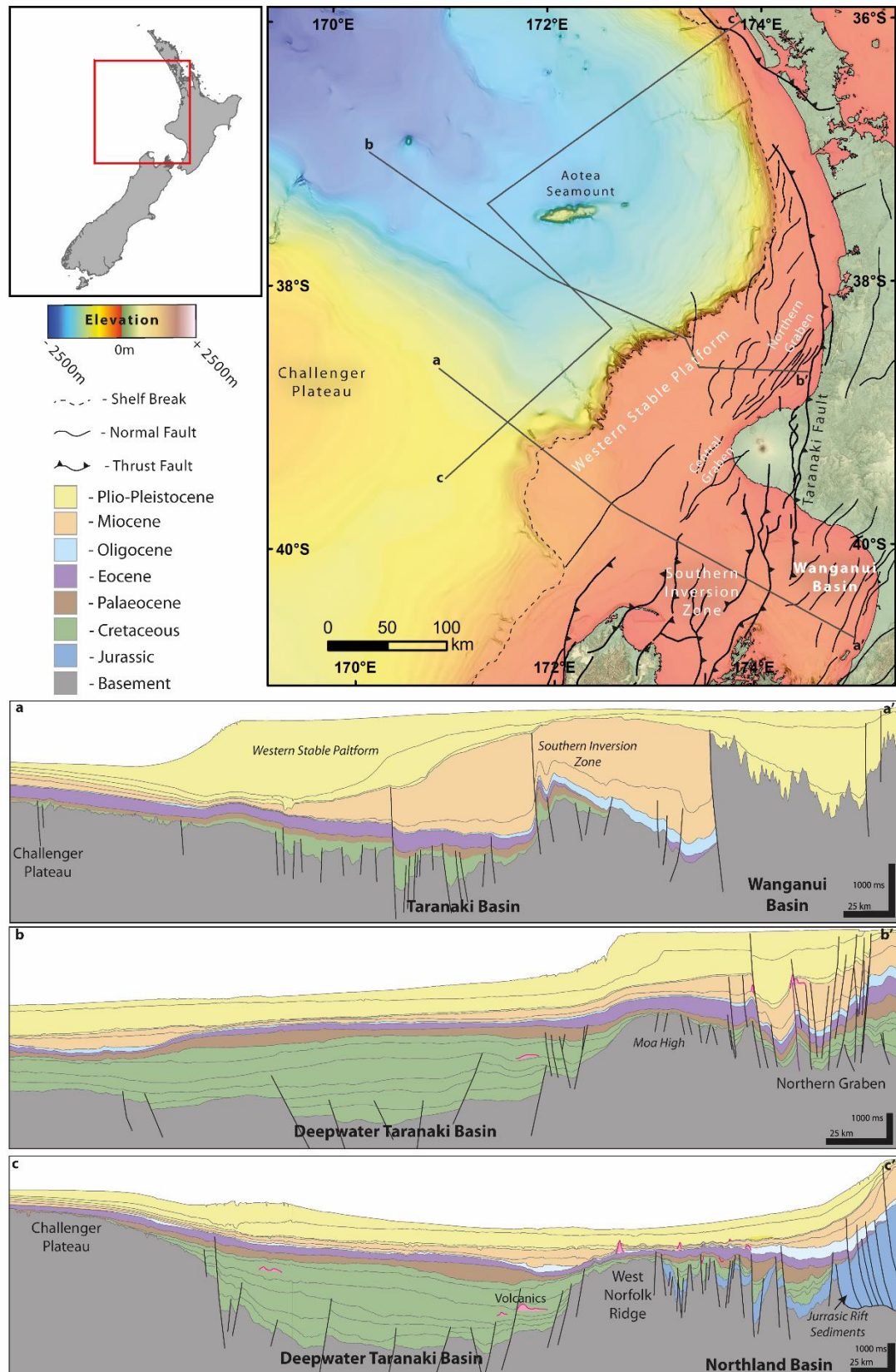


Figure 2.6 Structural Domains of the Taranaki Basin.

Map showing regional structural domains of the Taranaki & Northland Basins on present day seafloor bathymetry. Regional scale sections a to c illustrate the evolution of the region. Two main phases of extension are noted; Cretaceous Gondwana rifting (green) and Mio-Pliocene back arc extension in the Northern Graben. Sections are modified from Strogen et al., 2014.

2.1.3 Basin Stratigraphy

The stratigraphy of the Taranaki Basin, summarised in Figure 2.3, has been well defined by previous authors (King and Thrasher, 1992; 1996; Shell BP Todd Oil Services Ltd., 1986). The stratigraphy can be divided into four main stages of development that reflect the regional tectonic and more localised structural development. The four main stages are outlined below:

1. Late Cretaceous syn-rift succession
2. Palaeocene – Eocene transgressive succession.
3. Oligocene – Early Miocene foredeep and distal starved sedimentation.
4. Miocene – Recent regressive succession.

Cretaceous syn-rift succession

The oldest rocks present in the Taranaki Basin are of Mid-Cretaceous age and belong to the Taniwha Formation (King and Thrasher, 1996). This formation is only present in the northeast part of the Taranaki Basin and is noted to be of marginal marine or terrestrial origin (Shell BP Todd Oil Services Ltd., 1986). The main Late-Cretaceous syn-rift succession is represented by the Pakawau Group, comprising the Rakopi and North Cape Formations with a combined thickness of up to 4200 m (King and Thrasher, 1996). Where the Taniwha Formation is absent, the Pakawau Group unconformably overlies the basement and is the first basin-wide unit. At the time of deposition, the Taranaki comprised a series of rift systems and half grabens which facilitated locally thick accumulations of the Pakawau Group (Wizevich et al., 1992). As the continent flooded, these half graben sub basins became linked and more regionally extensive. Cretaceous coals act as the main source rock for hydrocarbon accumulations in the Taranaki Basin (Sykes, 2001).

The Rakopi Formation is dominated by sands, silts, muds and coal measures (Sherwood et al., 1992) and is interpreted to indicate swamp and floodplain deposits on the margins of the rifting Gondwana continent.

The North Cape Formation records the first marine influence in the Taranaki Basin as the sea began to flood the Gondwanan continent (King and Thrasher, 1996). Lithologically it is comprised of sandstones, siltstones, conglomerates and locally developed coal seams (Puponga Member).

Palaeocene – Eocene Transgressive Phase

A south directed transgression across the flooding Zealandia continent resulted in deposition of two stratigraphic groups; the terrestrial to shallow marine Kapuni Group and its marine equivalent, the Moa Group (King and Thrasher, 1996). As this transgressive event progressed through the Eocene, deposition became more marine dominated, resulting in Moa Group muds deposited basinwide to subsequently onlap and cover the Kapuni sediments, forming a regional seal across Kapuni source and reservoir rocks (Sykes et al., 2014). Regional seismic transects from Bache et al. (2014) across the deep water Taranaki Basin show transgressive ravinement on the Challenger Plateau as the transgression impinges on the basement high (Figure 2.7).

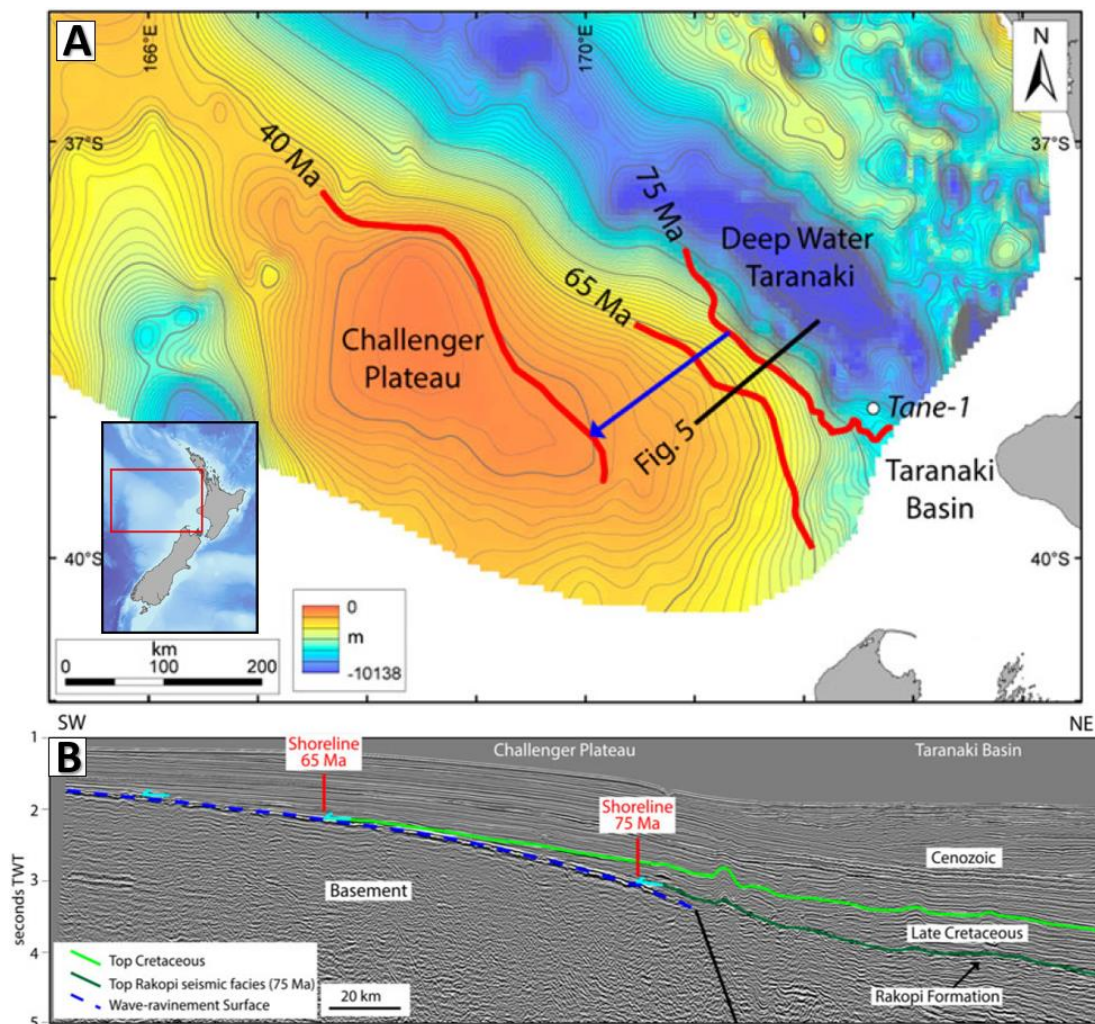


Figure 2.7 Challenger Plateau flooding.

Structure map (A) and seismic profile (B), showing shoreline locations and migrations (blue arrow in A) through the progressive flooding of the Zealandia continent. The blue dashed line in B represents wave ravinement surface as the shoreline transgresses across the Challenger Plateau (from Bache et al., 2014).

The Kapuni Group is composed of a variety of coastal plain and proximal marine strata that represent the nearshore expression of a long-lived marine transgression throughout the Palaeocene and Eocene. The shallow marine clastics, associated with shoreline transgressive – regressive cycles (Higgs et al., 2012; King and Thrasher, 1996), act as the main reservoir for hydrocarbons in the Taranaki region (Farewell and Mangaheva Formations), as well as terrestrial coals providing proven secondary source rock potential (also from the Mangaheva Formation).

The Moa Group comprises an entirely marine succession (King and Thrasher, 1996) and comprises marine mudstones of the Turi Formation, and submarine fans and turbidites of the Tangaroa Formation.

Oligocene – Early Miocene Foredeep

Eocene transgression was followed by additional basin subsidence, associated with establishment of a foredeep. At this time the basin was starved of sediment, resulting in deposition of the carbonate-rich Ngatoro Group (King and Thrasher, 1992, 1996). Evolution of this carbonate rich foredeep is recorded by establishment of outer shelf calcareous sand and silt rich systems of the Otaroa Formation and deep-water calcareous muds of the Tikorangi Formation. This in turn, is overlain by the Taimana Formation, which records the re-establishment of clastic input to the Taranaki Basin, associated with over-thrusting of the Taranaki Fault and associated uplift of the hinterland to the east of the foredeep (King and Thrasher, 1992; 1996).

Miocene – Recent Regressive Succession

From mid Miocene to present, the Taranaki Basin has been dominated by a regressive succession associated with west directed outbuilding of the shelf and infilling of foreland accommodation. This regressive unit is divided into two groups; the Miocene Wai-iti Group and the Plio-Pleistocene Rotokare Group. Combined, this regressive succession volumetrically dominates more proximal areas of the Taranaki Basin (see Figure 2.6). The boundary between the two groups is represented in the south Taranaki Basin by a north-dipping unconformity, resulting from differential uplift and erosion (King and Thrasher, 1996). Moving north, progressively younger sediments downlap onto this surface as the shelf prograded north and west. In central parts of the basin the relationship is conformable. In the Northern Graben the boundary is commonly unconformable, owing to uplift and non-deposition associated with volcanic activity in the area. In the northern segment of the Western Stable Platform the Miocene-Pliocene boundary is present within

the Ariki Formation. This is a condensed carbonate-rich unit arising from sediment starvation on the Western Stable Platform, as sediment was preferentially funnelled into the Northern Graben (Hansen and Kamp, 2006).

Miocene Wai-iti Group

The Miocene Wai-iti Group is a dominantly fine-grained muddy succession that records the infill of the Taranaki Foreland Basin. Earliest Miocene sedimentation was focused in the foredeep adjacent to the Taranaki Fault (King and Thrasher, 1992; 1996), similar to the quiescent Ngatoro Group. In the Mid – Late Miocene a significant increase in sediment supply associated with the evolving collisional margin of the Australian and Pacific Plates is observed (Baur, 2012; Dominic P Strogen et al., 2014). This increase in sediment supply is represented by a series of progradational clinofolds of the mud dominated Manganui and Urenui Formations (King and Thrasher, 1992; 1996).

Two notable submarine fan systems, the Moki (older) and Mount Messenger Formations (younger), delivered sand to the basin floor as northeast-trending turbidites and mass transport deposits (King et al., 2011; King and Thrasher, 1996) and are considered to have good reservoir potential for hydrocarbon exploration. The older Moki Formation is best developed in the south. As the system prograded north, deposition switched to the Mount Messenger fan which is best developed in the northeast (King and Thrasher, 1996). In this northern area, the Mohakatino Volcanic Centre was active at the time of deposition of the Mount Messenger. Consequently the Mount Messenger is interfingered with deposits of Mohakatino volcanoclastic sands, silts, tuffs and muds (King and Thrasher, 1996; Shumaker et al., 2018).

Rotokare Group

The Rotokare Group is the umbrella term for Pliocene to Recent sediments in the Taranaki Basin and is divided into four formations; the Matemateaonga, Tangaho, Mangaa and Giant Foresets Formations (Figure 2.3).

Deposition of the Rotokare Group represents a large increase in sediment supply from approximately 400 m/Myr in the Miocene to >700 m/Myr in the Pliocene (King and Thrasher, 1992). This increase in supply is attributed to uplift and erosion of the Southern Alps (King and Thrasher, 1992; Nodder, 1995). Sediment flux from North Island and the north coast of South Island delivered substantially less sediment to the continental shelf than suspended sediment runoff from the Southern Alps. This runoff was delivered north

to the Taranaki Basin via longshore littoral drift system and the Westland Current (Figure 2.8; Beggs, 1990; Hansen and Kamp, 2006; Nodder, 1995; Payne et al., 2010). The dynamics of this system is discussed further in the proceeding section of this chapter.

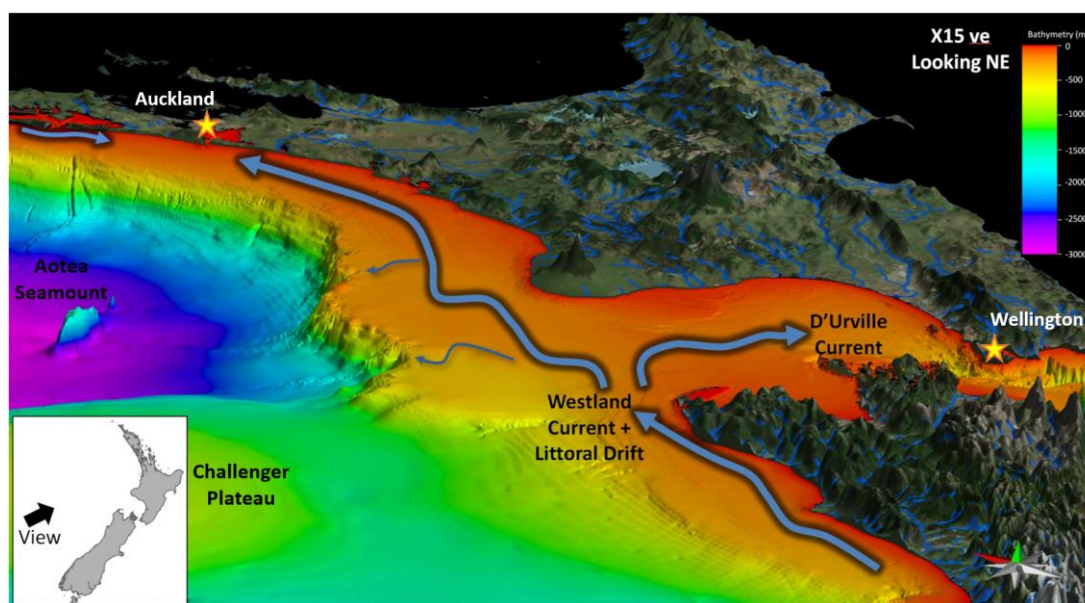


Figure 2.8 Sediment Pathways to the Taranaki Basin.

Perspective view of bathymetry showing modern sediment delivery to the Taranaki Basin via combination of ocean currents and littoral drift system.

In the southeast Taranaki Basin the Matemateaonga and Tangaho Formations represent the initial fills of the Toru Trough (King and Thrasher, 1996). The Mangaa Formation is localised to the Northern Graben and comprises a series of fine-grained sandy turbidites.

The main volume of sediment that constitutes the Rotokare Group is the Giant Foresets Formation (GFF) and is the main focus of this project. The GFF is a strongly progradational set of clinoforms prograding in a west-northwest direction across the Taranaki Basin. The lithology of this clinoform set is dominated by mudstone and siltstone with interspersed sandstones and shell beds (King and Thrasher, 1992; 1996).

The GFF contains foresets up to 1500 m in height, with formation thickness up 2200m (Baur, 2012). In seismic data they appear as large sigmoid shaped bodies with flat topsets, inclined foresets and low angle bottomsets that taper out onto an inclined basin floor.

2.1.4 Regional Oceanography

As described in section above, sediment in the GFF is delivered north to the Taranaki Basin via a longshore littoral drift cell and the Westland Current (Figure 2.8). To better understand and contextualise the proceeding chapters, a brief review of the regional oceanography around New Zealand is provided below.

Ocean circulation in the Taranaki Basin region is dominated by surface currents (top 500m) with no deepwater currents observed in modern datasets. This is due to the topographic barrier of the Challenger Plateau blocking circulation of Antarctic Intermediate Water (AAIW) and other intermediate to deep water currents to the south of New Zealand (Figure 2.9). As such, this review will focus on surface circulation (top 500 m) around New Zealand, particularly along the west coast of South Island.

The primary surface currents observed in the Taranaki Basin are the Westland Current (WC) and D'Urville current (dUC). The WC flows northwards along the west coast of South Island towards the Taranaki Basin, where it bifurcates into the east flowing dUC before it continues north towards Cape Egmont (Brodie, 1960; Heath, 1985; Schofield, 1975). From here, rejuvenated littoral transport continues north along the coastline of the Northland Basin. Sediment dredge samples from the north Kaipara shelf (approx. 100 km NW of Auckland – see Figure 2.8) reveal a mineralogy that identified the northern South Island as source material (Payne et al., 2010). This shows an active along shelf sediment transport system delivering sediment up to 600 km.

The WC itself has a mean flow velocity of to 0.05 m s^{-1} (Heath, 1985), with higher nearshore variability up to 0.3 m s^{-1} (Cahill et al., 1991). The combined actions of the WC and prevailing northeast directed swell generated in the Tasman Sea is enough to create an efficient sediment transport system along the length of New Zealand's west coast (Carter and Heath, 1975; Heath, 1985, 1982).

Zooming out, the Westland Current and related wind and wave systems are an offshoot of the Sub Tropical Front (STF) (Figure 2.10 and Figure 2.9). The STF is a water mass and front system drifting eastward across the Tasman Sea (Chiswell et al., 2015; Hayward et al., 2012). When the STF encounters the New Zealand Landmass it bifurcates into two flows; the WC and the Southland Current (SC). The SC is bathymetrically locked to the shelf and slope as it flows around the southern tip of New Zealand before continuing northwards along the east coast of South Island and subsequently eastward along the Chatham Rise (Brodie, 1960; Carter and Heath, 1975; Heath, 1972; Smith et al., 2013; Sutton, 2003).

Present day, the STF bifurcates at approximately 43°S (Heath, 1982; Smith et al., 2013). Sea surface temperature (SST) proxies indicate that the latitude of the STF in the Tasman Sea periodically shifted towards the equator (Hayward et al., 2012, 2008; McClymont et

al., 2016), influencing the coastal location at which bifurcation into Westland and Southland Currents occurred. Changes in SSTs and fauna from Hayward et al. (2012) suggest that the STF migrated approximately 6° north during Mid Pleistocene Transition glacials (MIS 28-16), but only migrated 3-5° north in post Mid Pleistocene Transition glacials (Figure 2.10). McClymont et al. (2016) also suggest equatorward displacement of the STF between 2.-3.5 Ma.

As sediment delivery has been linked to the Westland Current and a related littoral transport cell, the northward shift in the location of the STF may have the effect of; 1) reduced efficiency of the transport system carrying sediment north and 2) reduction in the size of the catchment area from which sediment is delivered north towards the Taranaki region. The dynamics of this system are explored further in Chapters 6.

Water Masses

- AABW Antarctic Bottom Water
- AAIW Antarctic Intermediate Water
- AASW Antarctic Surface Water
- CDW Circumpolar Deep Water
- EqPIW Equatorial Pacific Intermediate Water
- LCDW Lower Circumpolar Deep Water
- PDW Pacific Deep Water
- SAW Subantarctic Water
- SAMW Subantarctic Mode Water
- SPSTMW South Pacific Subtropical Mode Water
- Water
- STMW Subtropical Mode Water
- STW Subtropical Water
- TSCW Tasman Sea Central Water
- UCDW Upper Circumpolar Deep Water
- WSPCW Western South Pacific Central Water

Currents

- ACC Antarctic Circumpolar Current
- ASF Antarctic Slope Front
- dUC d’Urville Current
- DWBC Deep Western Boundary Current
- EAC East Australian Current
- EACx EAC extension
- EAUC East Auckland Current
- ECC East Cape Current
- SC Southland Current
- WAUC West Auckland Current
- WC Westland Current
- WCC Wairarapa Coastal Current

Fronts

- DSTF Dynamic Subtropical Front
- PF Polar Front
- SACCF Southern ACC Front
- SAF Subantarctic Front
- STF Subtropical Front
- STFZ Subtropical Frontal Zone
- TF Tasman Front

Eddies

- ECE East Cape Eddy
- LHE Lord Howe Eddy
- NCE North Cape Eddy
- NfKE Norfolk Eddy
- RE Rekohu Eddy
- WE Wairarapa Eddy

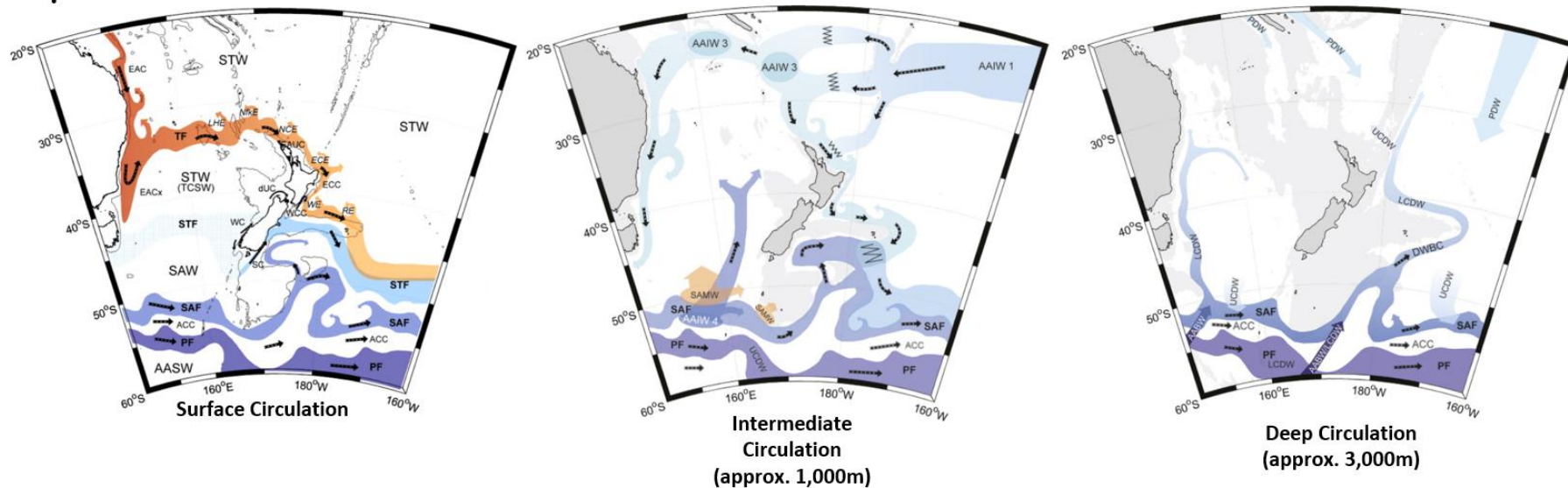


Figure 2.9 Regional Oceanography of the southwest Pacific region.

Grey shading represents the 1,000m and 3,000m contours in respective figures. Relative temperature is shown by red to blue shading. Adapted from Chiswell et al., 2015.

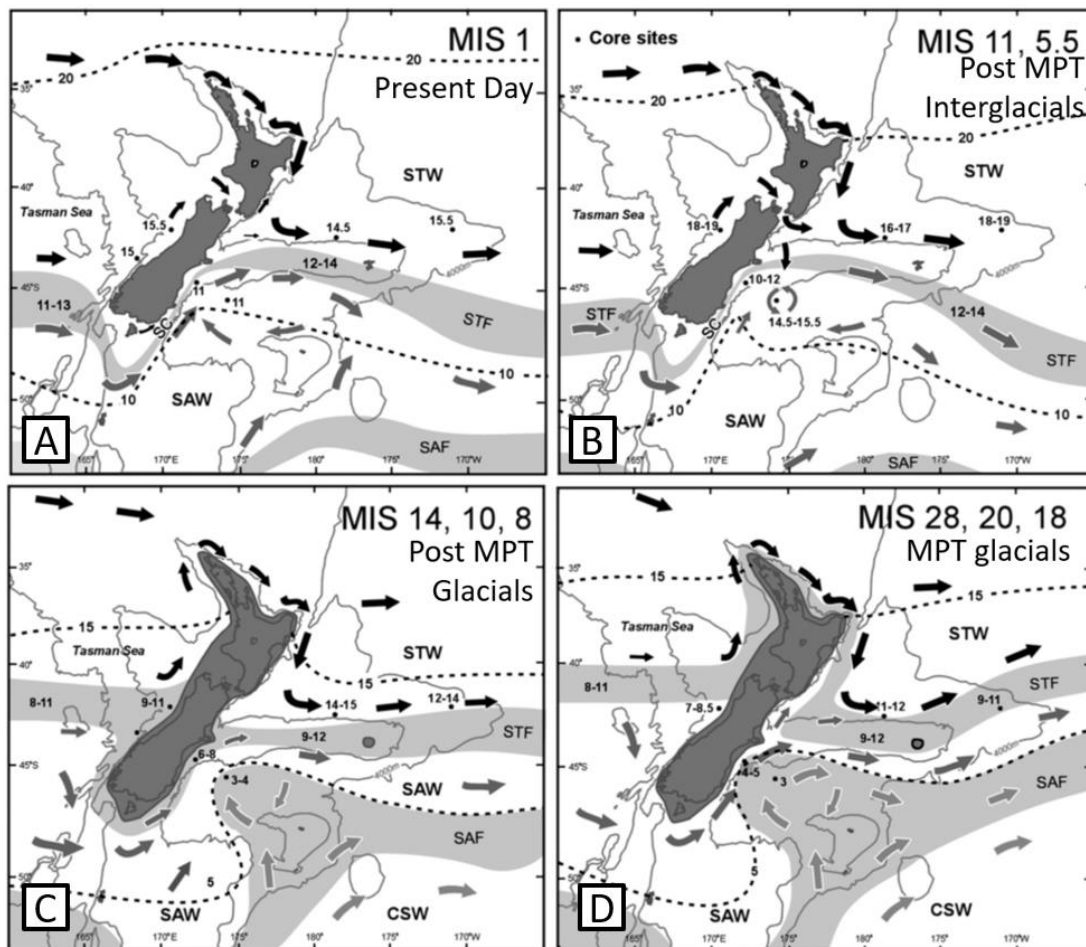


Figure 2.10 Surface circulation around New Zealand.

Palaeoceanographic reconstruction of Sea Surface Temperatures (SSTs) and surface circulation around New Zealand from Hayward et al. (2012). Note in particular the location of the STF on the west coast of New Zealand. Small numerals are the SST estimates in °C for sites and the STF. CSW = Circumpolar Surface Water, SAF = Subantarctic Front, SAW = Subantarctic Surface Water, SC = Southland Current, STF = Subtropical Front, STW = Subtropical Surface Water.

2.2 Previous Studies of the Giant Foresets Formation

Initially described by Beggs (1990), numerous studies of the GFF have since been undertaken to unravel the Plio-Pleistocene evolution of the region. This section will summarise the key stratigraphic studies undertaken on the Giant Foresets Formation (Figure 2.11).

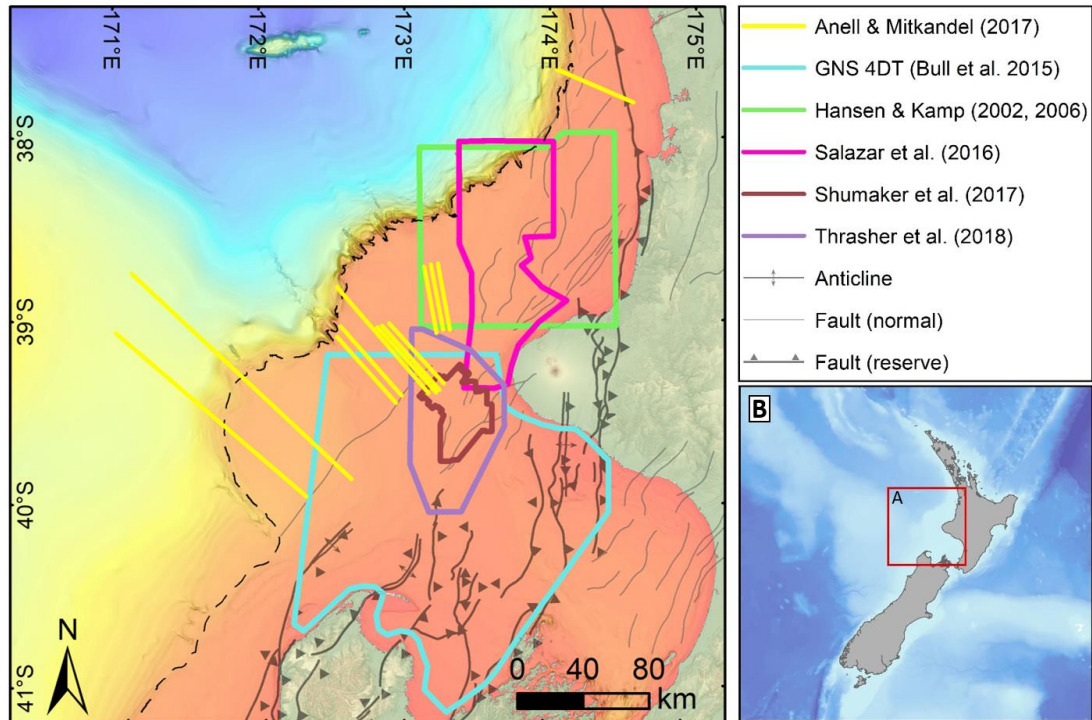


Figure 2.11 Previous stratigraphic studies of the Giant Foresets Formation.

Hansen and Kamp (2002; 2006a; 2006b) investigated the architectural elements and controls on the evolution of the GFF on the WSP. This was carried out in the northern extents of the basin in the Northern Graben & northern portion of the WSP (Figure 2.11) using a widely spaced network of 2D seismic lines and wells in the region. Their study benefited from higher sampling density of wells penetrating the Plio-Pleistocene succession in this part of the basin, allowing construction of a quantitatively weighted biostratigraphic framework tied to seismic data. Within this framework they described the advance of the GFF, showing syn-sedimentary filling of the Northern Graben, likely by a mixed sand & mud rich feeder system. The Northern Graben was subsequently overtopped and the margin prograded onto the Western Stable Platform. This is also associated with a progressively more mud rich system likely sourced from a mud rich line source. In a sequence stratigraphic context, highly asymmetric depositional sequences are described, with slope and basin floor stratigraphy dominated by falling stage and lowstand systems tracts whilst transgressive and highstand deposits are entirely retained on the shelf

in the northern Taranaki Basin. They tentatively identify a 400 ky eustatic signal in their data.

Salazar et al. (2016) utilised a more extensive database, incorporating 2D and 3D seismic data to investigate the drivers of basin margin evolution in a similar part of the northern Taranaki Basin to the studies of Hansen & Kamp (Figure 2.11). Their study split the Plio-Pleistocene GFF into 9 seismic units (SU1-SU9, with SU1 the oldest). By linking clinoform architectures to those of Adams and Schlager (2000), they predicted SU1-SU5 (~5.33 to 2.4 Ma) are mainly composed of muddy lithologies, whilst SU6 – SU9 (2.4 Ma – present) could potentially contain sandier intervals. Clinoform growth patterns were also correlated to uplift events in the Southern Alps. In this northern portion of the WSP from ~2.4 Ma to present, they conclude that most sediment is retained on the outer shelf and upper slope and that sediment delivery to the basin floor was dominated by mass wasting processes, lacking a significant connection to sediment proximal sediment sources and resulting in a tendency toward fine grained sediment delivery to the basin floor.

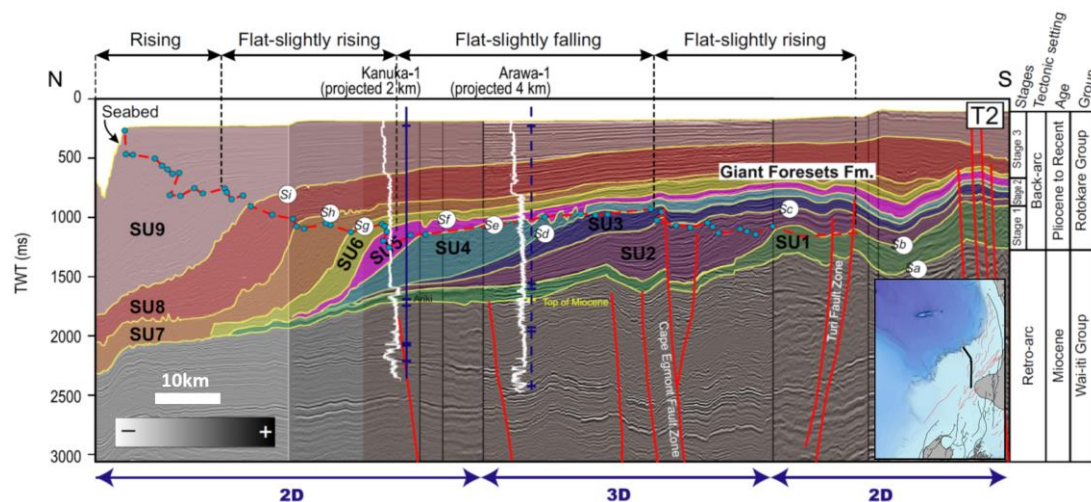


Figure 2.12 Seismic stratigraphy of Salazar et al. (2016).

Interpreted seismic line from Salazar et al. (2016) showing evolution of their seismic units 1-9 across the Northern Graben and shelf break trajectory stippled red. Location of line in inset map.

These mass wasting processes and deposits were further investigated by Omeru et al. (2016), who mapped six mass transport deposits (MTDs) throughout the deepwater regions of the Taranaki and Northland Basins (Figure 2.13), tracing at least two back to headwall scarps in the Giant Foresets Formation. Much of the stratigraphy in the deepwater regions of the Taranaki Basin have been either disturbed or entirely

cannibalised by these MTDs, creating correlation difficulties explored further in Chapter 4.

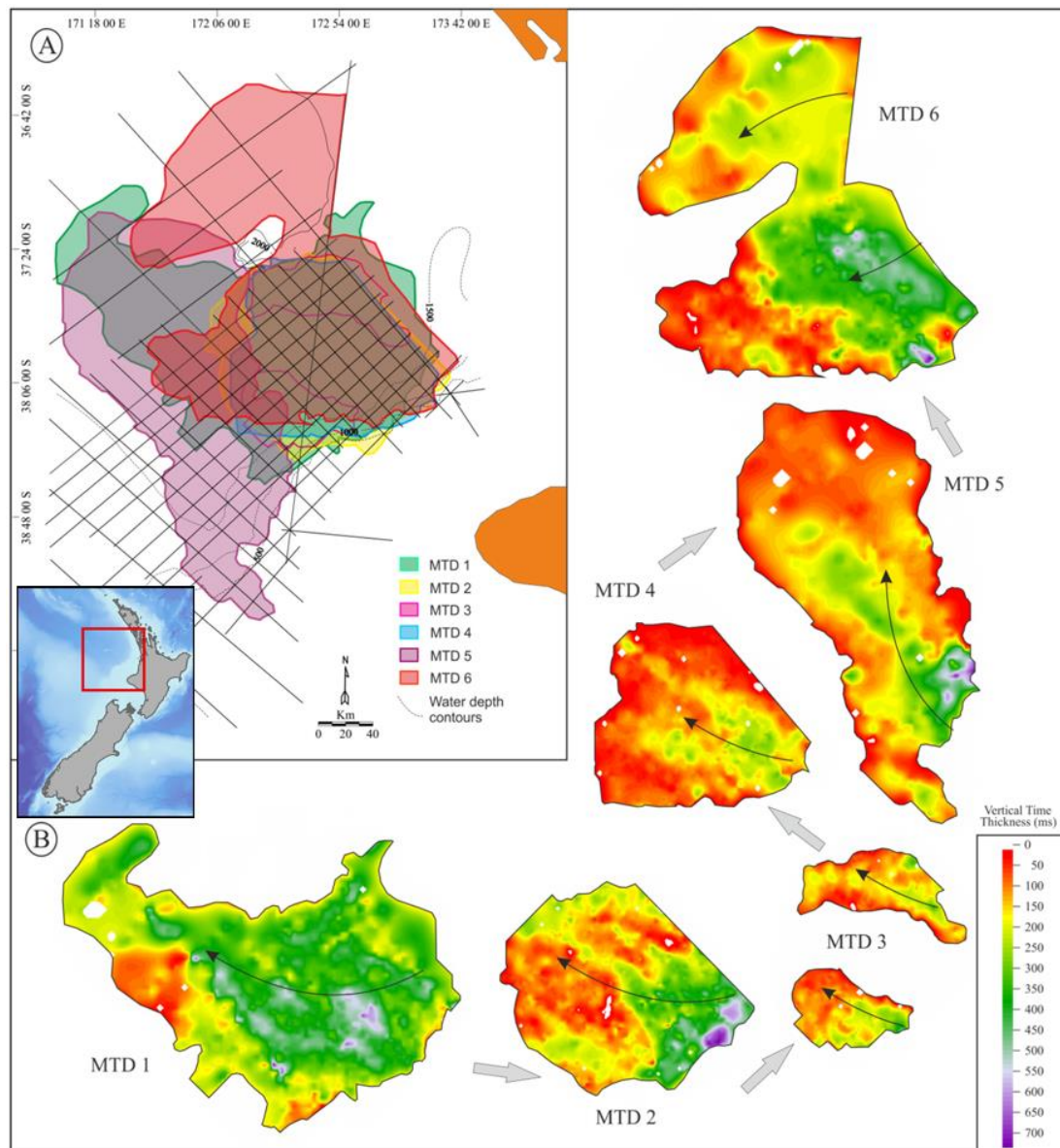


Figure 2.13 Mass transport deposits mapped by Omeru (2016).

A) Outlines of MTDs in the Taranaki and Northland basins. B) Time thickness maps of individual MTDs.

Using the Giant Foresets Formation as a case study, Anell and Midtkandal (2017) assessed relationships between different geometric parameters of clinothem bodies. In doing so they expanded the earlier threefold classification scheme (oblique, tangential and sigmoidal clinoforms) to a more complex 9 fold classification scheme based on slope curvature (linear, exponential or gaussian) and on the internal reflector characteristics of the clinothem (Figure 2.14).

Clinoform geometric parameters were measured and calculated as per Figure 2.15 and included horizontal parameters (Edge to Toe distance, shelf edge advance and toe of slope advance), vertical parameters (slope relief, clinothem maximum vertical thickness and clinoform average vertical thickness) and calculated angles (shelf edge trajectory, toe trajectory, maximum foreset angle, overall slope angle and change in maximum foreset angle compared to the underlying clinoform).

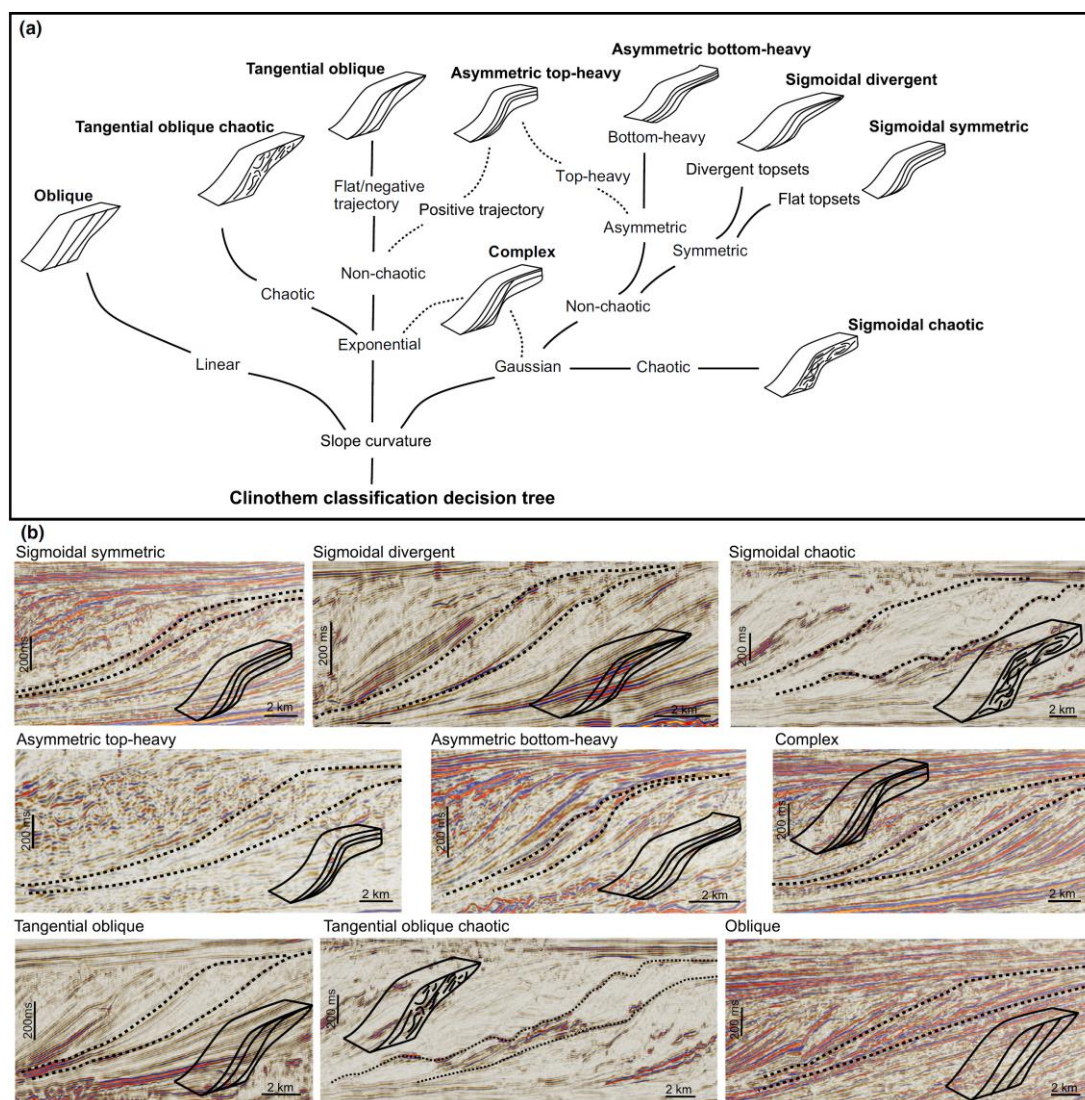


Figure 2.14 The nine types of clinothems defined by Anell and Mitkandal (2017).

A) showing how clinothem types are separated from each other. The first subdivision is based on slope curvature, linear, exponential and Gaussian. The nine types are shown in cartoon form at the end of a branch of the tree. The stippled lines mark the two clinothem types, complex and asymmetrical top-heavy, which can be reached via more than a single path. B) Seismic examples and sketch cartoons of each clinothem type.

Their results show that the dominant control on clinothem shape is accommodation; lowest accommodation settings typically promote development of tangential oblique clinothems (Figure 2.14) which become sigmoidal divergent with increasing

accommodation and later sigmoidal symmetrical clinothem forming in high accommodation settings. Sediment supply is believed to play a role in the degree of symmetry in clinothem; asymmetrical top heavy clinothem are likely caused by low sedimentation rates, giving rise to a short and steep clinoform. In contrast, asymmetric bottom heavy clinothem result from high sedimentation rates, giving rise to a flatter slope and greater accumulation of sediment downslope.

Whilst Anell and Midtkandal (2017) utilise much of the same data as this thesis, their study of relationships between clinoform metrics lacks local context, does not address or map lateral variations and makes limited inferences on factors affecting the evolution of the margin. Additionally, their mapping of two regional surfaces (M1 & M2) is correlated along the margin using two seismic lines in deepwater parts of the basin that this thesis and work by Omeru et al. (2016) show to be disrupted by mass transport processes.

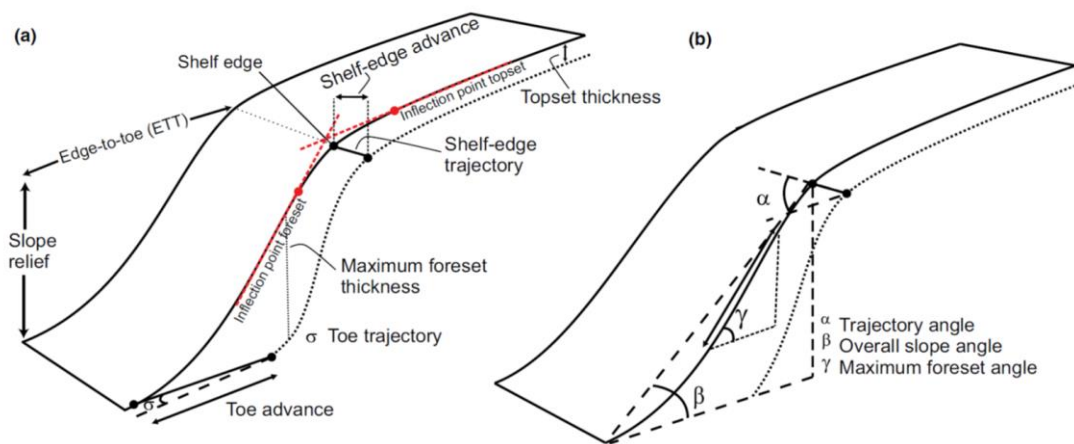


Figure 2.15 Idealised clinothem body.

(a) the various geometric parameters and (b) the angles measured in the studies of Anell and Mitkandal (2017).

Most stratigraphic studies of the GFF have focused on the large scale architectures and unravelling progradational patterns along the basin margin. Shumaker et al. (2017), however, undertook a more detailed 3D geomorphological analysis in a smaller geographic area (Figure 2.11), focusing on documenting submarine gullies and sediment waves developed in Miocene to Pliocene slope deposits of the Taranaki Basin. Gullies ranged from 20-400 m wide, ~10-60 m deep and 2-22 km in length whilst sediment wave amplitudes range from <10 m to 40 m with wavelengths ranging from 287 m to 2150 m. Gullies and sediment waves are noted to be spatially and temporally related but with the resolution of the dataset it was not possible to confidently establish a genetic relationship. By examining sediment wave and gully architectures they conclude that flows on the

continental slope were most likely mud and silt dominated turbidity currents with flow thicknesses up to 40 m (following the criteria of Wynn and Stow, 2002). The large spatial extent of the sediment waves indicated that they were most likely formed by turbidity currents tens of kilometres in wide. This model for sheet like flows is also deemed likely due to the homogenous, fine grained nature of GFF sediments, common mass wasting and fine-grained sediment waves. This type of dilute, muddy flow would have been minimally erosive but widespread.

In addition to published academic studies, GNS (Institute of Geological and Nuclear Sciences) in New Zealand have published a number of studies (Bull et al., 2015; Thrasher et al., 2018) and datasets on the Taranaki Basin that are of use in examining the stratigraphic evolution of the Taranaki Basin. Many of these studies are not academic in nature, but rather consist solely of mapped horizons over a large geographic area, mainly those on the inner shelf where petroleum prospectivity is highest (Figure 2.11). These studies do not elaborate on the evolution of the margin, rather they provide a template for further investigations. The surfaces and wells used in correlation are publicly available and have been a useful reference with which to carry out further studies on the Western Stable Platform.

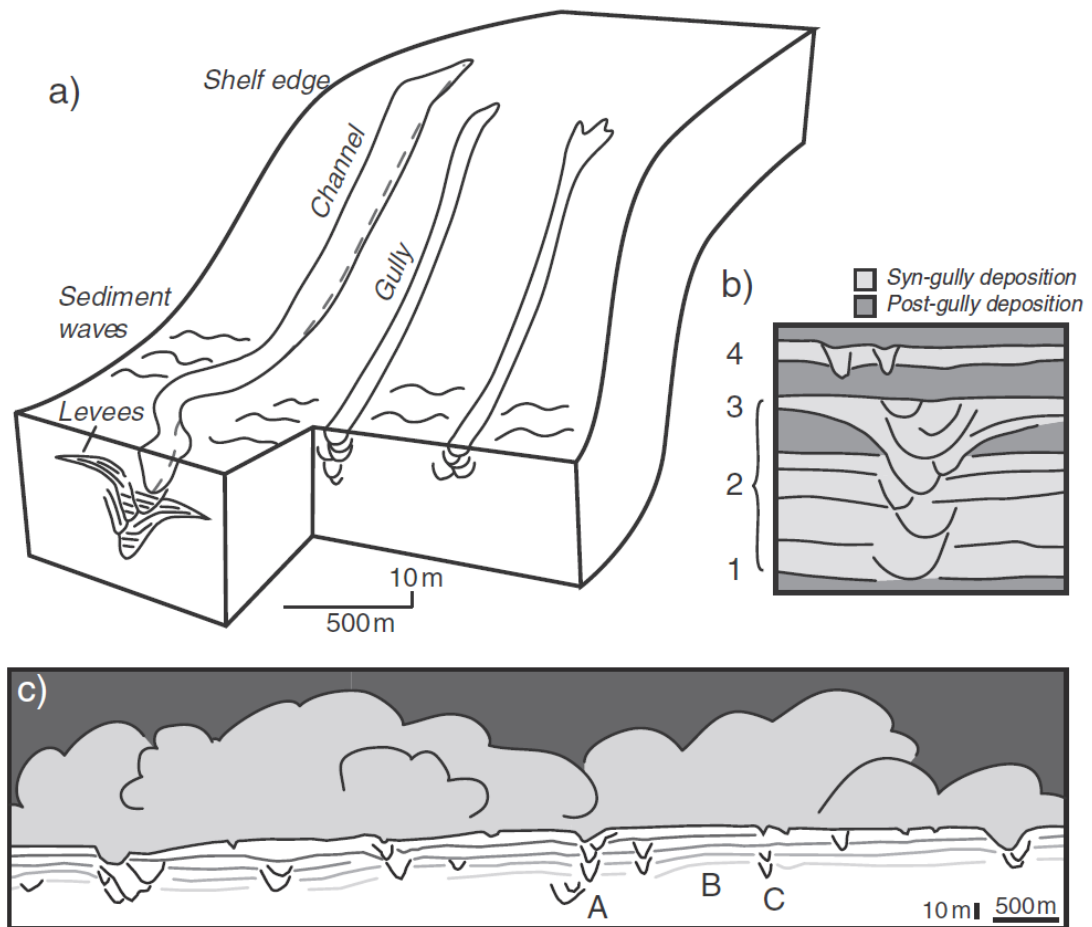


Figure 2.16 Slope evolution of the Taranki Basin.

a) Schematic diagram showing differences in surface and subsurface expression of gullies and channels in the Giant Foresets Formation. (b) Interpretation of a gully complex showing stages of (1) initiation by incision, (2) aggradation and migration, (3) drape along margins, and (4) burial and re-incision. (c) Simplified interpretation of a strike-oriented cross-section showing temporal evolution of gullies and interfluvial aggradation, and schematic representation of a sheet-like turbidity current. A: aggradation and migration. B: self-similar interfluvial aggradation. C: burial and re-incision. From Shumaker et al. (2017)

Blank Page

Chapter 3

Database and Methods

3.1 Database

This study utilised an extensive database of 2D and 3D seismic reflection data, exploration wells with associated biostratigraphy and wireline logs sourced from the New Zealand Petroleum and Minerals (NZP&M) data pack (Figure 3.1). Supplementary information was also accessed through the NZP&M and Geological and Nuclear Sciences (GNS) online databases (data.nzpam.govt.nz and data.gns.cri.nz/pbc, respectively). Subsets of this database are utilised in the individual chapters of this thesis. All maps are projected in New Zealand Transverse Mercator.

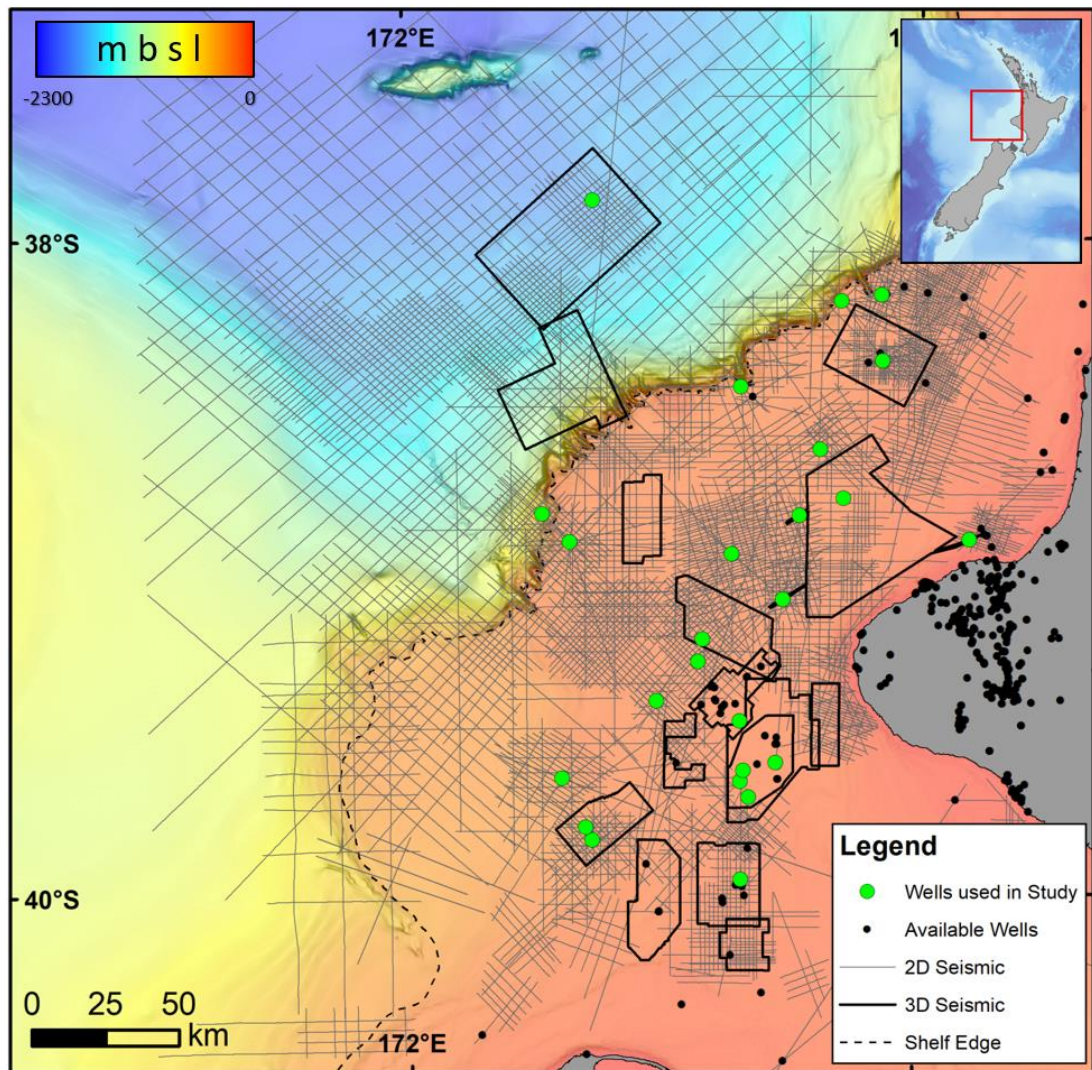


Figure 3.1 Seismic and well database utilised in this study.

3.1.1 Seismic Data

Surveys were acquired by numerous operators between 1973 – 2015 and span a range of acquisition and processing parameters resulting in a database of varying quality, frequency, amplitude and phase. The 2D seismic data base comprises thirty-nine surveys containing over 1,300 lines totalling approximately 51,500 line km. 2D line spacings range from 1.5 km to >10 km and provide sufficient coverage to confidently map horizons on a regional scale. This is accompanied by fifteen 3D surveys covering a total area of approximately 11,500 km². The 3D datasets are concentrated on the inner shelf around existing hydrocarbon discoveries.

In the interval of interest, the dominant frequency of surveys ranges from 7 – 50 Hz, yielding a theoretical maximum resolution of 70-10m respectively. Average vertical resolution is calculated between 20-25m using an averaged interval velocity of 2000 m/s¹.

To ensure consistent interpretation across this diverse database, surveys were mistie corrected to account for phase, amplitude balancing and vertical bulk shift. Where necessary additional manual corrections were implemented. 2D survey DTB01/Astrolabe was selected as the reference survey due to its regional nature and good data quality. Polarity and colour convention is such that a downward increase in acoustic impedance is represented by a positive peak (red reflection).

Seismic interpretation was carried out using a combination of Schlumberger's Petrel 2016.2 software, IHS Kingdom 8.8, Eliis Paleoscan. Some resulting surfaces were imported into ArcMap for more detailed investigation and production of maps.

Time to depth relationships are discussed individually in the proceeding chapters where appropriate time to depth relationships have been established using local well data. Resulting depth measurements remain uncompact; previous studies by Funnell et al. (1996) and Salazar et al. (2016) have demonstrated that a difference of less than 5% between compacted and decompact geometries is calculated for the interval of interest.

3.1.2 Well Data

A large number of wells were available in the database for this study, however due to lack of industrial interest in the nature of the Plio-Pleistocene succession many wells do not record wireline or lithology information until penetration of Miocene strata.

Formation data was provided in the NZP&M data pack and was quality checked against the most up to date re-evaluations (Bland et al., 2014; King et al., 2010; Strogon, 2014).

3.1.3 Age Data

Previous studies in the Taranaki Basin, both industry and academic, have utilised different biostratigraphic markers to assign ages to units. To avoid correlation inconsistencies between wells, the foraminiferal census data (Morgans, 2006; Strong and Wilson, 2002) for key wells were re-evaluated to reflect the most up to date criteria for identifying stage boundaries set out by Raine et al. (2015). Where census data were not available, local New Zealand stage data (Table 3.1) was evaluated from well sheets in King et al. (2010) and well sheets included in the NZPAM petroleum exploration data pack. Further age control was also added to the late Pliocene & early Pleistocene by correlating mapped horizons in this study to GNS studies of Thrasher et al. (2018) (see Figure 2.11).

Absolute ages were assigned to bioevents such as Lowest Occurrence (LO) and Highest Occurrence (HO) of diagnostic microfauna. Two sources were used to define age diagnostic bioevents; the primary, and most recent, being Raine et al. (2015) which incorporates updates to the Global Geochronological Scale of Anthonissen & Ogg (2012). In boreholes where the updated bioevents of Raine et al. (2015) were not present or identified, a secondary, older scheme of (Crundwell et al., 2004b) was adopted to avoid data gaps. A summary chart of bioevents is shown in Table 3.1. Limited additional biostratigraphic information from an ongoing resampling study was also provided by GNS (Crundwell, 2017 pers. comm), however this only contained information for the Pliocene of well Tane-1.

Examination of the biostratigraphy database showed it to be largely of insufficient detail in the Plio-Pleistocene succession to carry out detailed correlations over long distances (Figure 3.2). Several factors contribute to this:

- The strongly progradational nature of the Giant Foresets Formation coupled with sparse well penetrations resulted in a spatially under-sampled succession.
- Lack of age diagnostic fauna, particularly within the Pleistocene (see Table 3.1).
- Many wells do not recover cuttings from the GFF, particularly shallower sections (the GFF is treated as the uneconomic overburden by industry).

In particular, Pleistocene to recent age controls across the Taranaki Basin are poorly defined; as shown in Table 3.1, the two most recent age markers in the Pleistocene are

marked by tephra layers. These tephra layers are not identified in any exploration wells employed in this study.

Poor constraint in the latest Pleistocene is somewhat supplemented by the detailed analysis of Nodder (1995, 1994, 1993), who used a combination of high frequency shallow seismic data (3.5 kHz airgun), piston cores and borehole chippings to identify four late Quaternary “seismic and lithologic couplets” on the Farewell Rise (Figure 3.3). These couplets comprise an acoustically transparent upper unit of silty sediment overlying a strongly reflective sandy unit with an erosive and channelised basal surface. Silty units were interpreted as interglacial/highstand deposits, whilst the sandy, erosive and reflective facies were interpreted to represent glacial/lowstand and possible transgressive erosion and deposition. Chippings recovered from borehole MP-2C, the seismic couplets were dated using a combination of ^{14}C , calcareous nanoplankton and cyclo-stratigraphy of the silt/sand couplets. This portion of the succession (top 150 metres below the seafloor) was interpreted to represent glacial - interglacial cycles from approximately 300 ky to present (Figure 3.3). Whilst this borehole provides high resolution age control, regional correlation was complicated comparatively low resolution of the regional seismic data used in this PhD.

Epoch	NZ Stage Name (abbreviation)	Adopted Age	Primary Criteria (Raine et al., 2015)	Secondary Criteria (Crundwell et al., 2004)
Pleistocene	Base Haweran (Wq)	0.34	Base Rangitawa Tephra	
	Base Castlecliffian (Wq)	1.63	Base Ototoke Tephra	
	Base Nukumaruan (Wn)	2.4	LO Truncorotalia crassula and top upper dextral Truncorotalia oceanica	Top dextral Globorotalia crassaformis
Pliocene	Base Mangapanian (Wm)	3.04	base dextral Truncorotalia crassaformis	FDHA <i>Cibicides molestus</i>
	Base Waipipian (Wp)	3.7	HO Reticulofenestra psuedumbilica (Calcareous Nanoplankton)	
	Base Upper Opoitian (uWo)	4.3	LO Globorotalia inflatata	FDHA Globorotalia pliozea
	Base Opoitian (Top Mio) (lWo)	5.33	LO Globoconella puncticulata	FDHA Globorotalia sphericomiozea
Miocene	Base upper Kapitean	5.6	LO Globoconella sphericomiozea	Top Dextral Globorotalia conomiozea

Table 3.1 Defining bioevents for stage boundaries in New Zealand.

Primary criteria of Raine et al. (2015) and secondary criteria of Crundwell et al. (2004). LO – Lowest Occurrence, HO – Highest Occurrence, FDHA – First Downhole Appearance.

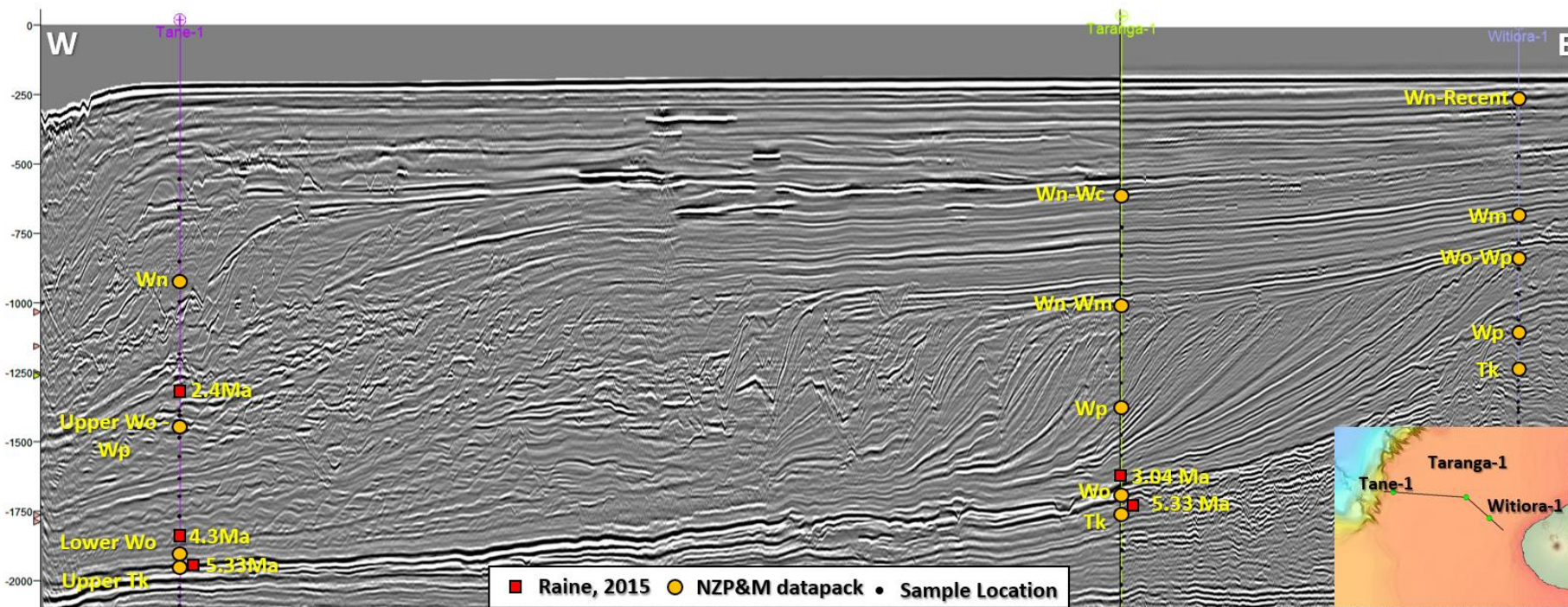


Figure 3.2 Biostratigraphic correlation to seismic data.

Composite section of seismic lines of DTB01-35 & ST03-401 showing biostratigraphic census points (black dots), NZ stage ranges (as in Table 1) from the NZP&M data pack (orange circles) and absolute ages (red squares) when comparing census data to criteria of Raine et al. (2015). Note the inconsistencies when tracing reflectors; for example, if tracing the reflector for 3.04 Ma in Taranga-1 (central well on section) down dip, this is overlain by a sample aged 4.3 Ma in Tane-1.

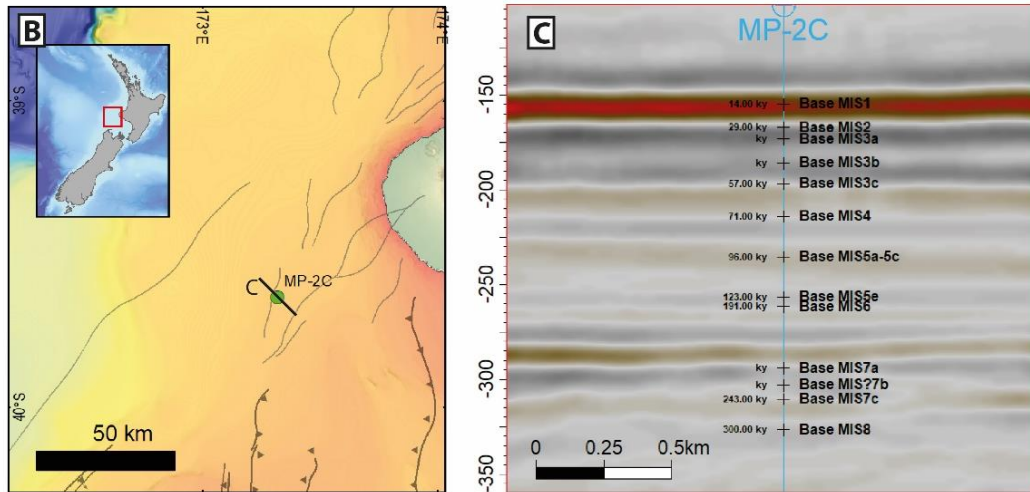
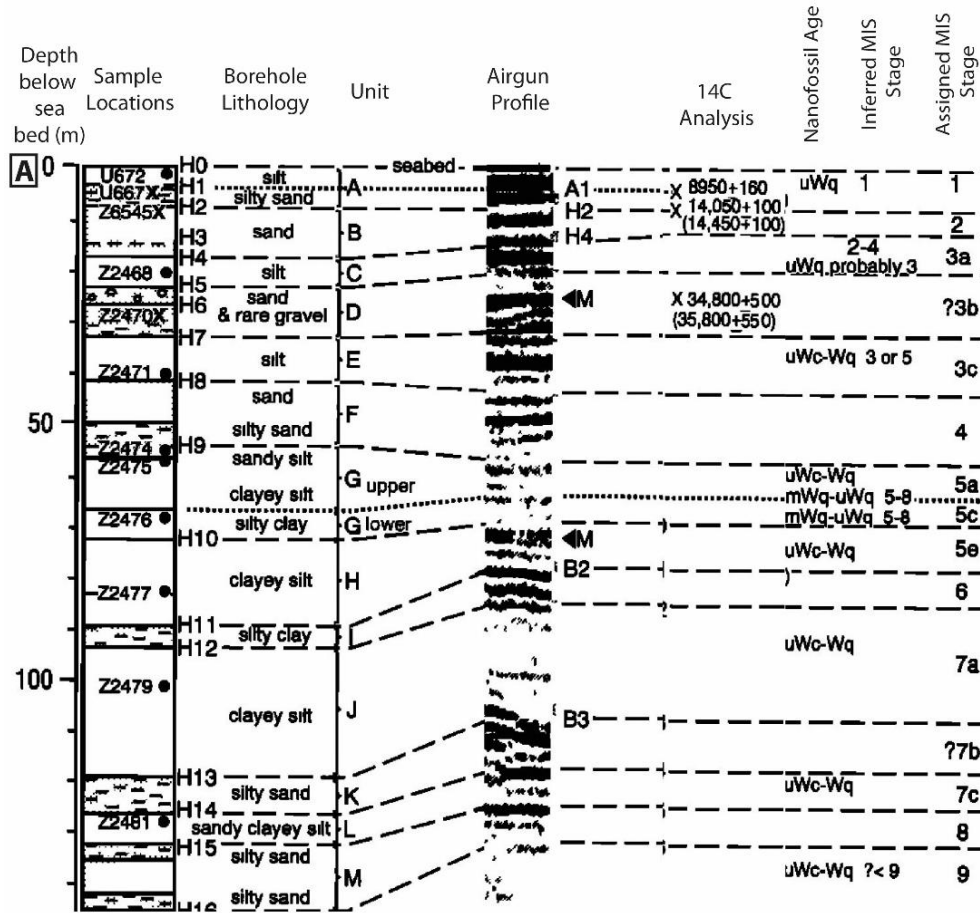


Figure 3.3 Late Quaternary ages from Nodder (1994).

A) Log of borehole MP-2C showing lithology, sample locations, correlation to an airgun profile, shallow carbon 14 ages dates, nanofossil ages and Marine Isotope Stage (MIS) assignments (modified from Nodder, 1994), B) Location of borehole MP-2C and location of seismic line C, C) Inline 296 from the Maui 4D survey showing sample locations from borehole MP-2C. Depth - TWT conversion of sample depths was carried out with a velocity of 1600 m/s for shallow, unconsolidated sediments as in Nodder (1994)

3.2 Methods

3.2.1 Seismic and Sequence Stratigraphy

The advent of seismic reflection surveying revolutionised the understanding of how sedimentary basins fill through time. Key to this understanding was the development of seismic stratigraphy, and subsequently sequence stratigraphy. Mitchum et al. (1977) showed that seismic reflectors and their terminations (Figure 3.4) represented stratigraphic surfaces. This provided a method by which geologists could divide a sedimentary succession into time bound packages, thus understanding how basins filled through time.

Seismic stratigraphy forms the basis for placing interpretations in a sequence stratigraphic framework; this involving the identification of three key surfaces and the stacking patterns of their encapsulated packages (Miller et al. 2013);

1. Sequence Boundary (SB) – a regional unconformity (and correlative conformity) over which an abrupt basinward shift in facies and/or coastal onlap is observed (Van Wagoner et al., 1988).
2. Transgressive Surface (TS) – represents the first major flooding surface in a depositional sequence and the onset of marine transgression (Van Wagoner et al., 1988).
3. Maximum Flooding Surface (MFS) – represents the maximum landward expression of basinal facies and is immediately followed by deposition of a prograding system (Posamentier and Allen, 1999).

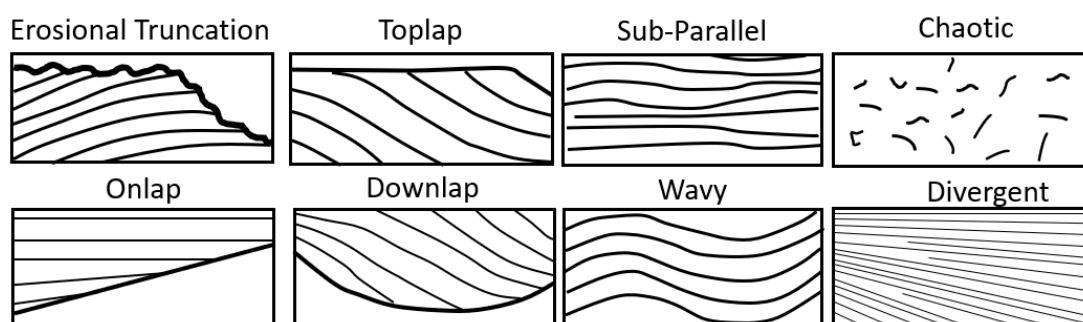


Figure 3.4 Common seismic reflection configurations and their terminations (after Mitchum et al., 1977).

Since its inception, Sequence Stratigraphy has diversified into a series of conflicting classification schemes with much debate as to the exact nature and placement of sequence boundaries. The details, complexity and equivalencies of these schemes are explored in

Catuneanu (2006) and Catuneanu et al., (2011 and 2009). In an effort to overcome the proliferation of controversial and model dependant nomenclature, Neal and Abreu (2009) proposed moving toward a system based on the geometric stacking relationships of strata known as the “Accommodation Succession” method (see Figure 3.5.) in which model independent observations are made before applying a sequence stratigraphic model of choice. The workflow for this method is adapted and presented below from Vail (1987) Neal et al. (2016).

1. Select key regional line along depositional dip.
2. Observe facies and stacking trends.
3. Mark stratal terminations offlap break trajectories.
4. Interpret key sequence stratigraphic surfaces from regionally significant stratal termination surfaces and offlap break trajectories.
5. Define depositional sequences, sequences sets and composite sequences.

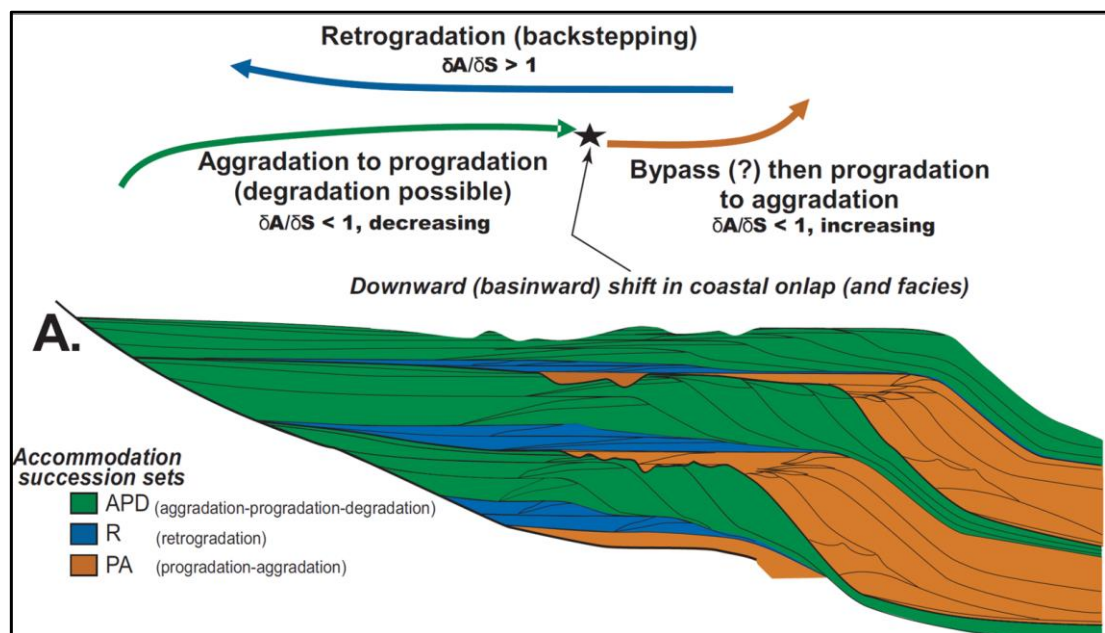


Figure 3.5 Idealised stacking patterns of the Accommodation Succession method of Neal and Abreu (2009) and Neal et al. (2016)

3.2.2 Trajectory Analysis

In studying the development of clinoforms through time the technique of Trajectory Analysis was first developed to study the evolution of shorelines and delta scale clinoforms (Helland-Hansen and Gjelberg, 1994; Helland-Hansen and Martinsen, 1996)

and was later applied to the study of shelf margin scale clinoforms (Houseknecht et al., 2009; Johannessen and Steel, 2005; Kertznus et al., 2009; R. J. Steel and Olsen, 2002). This technique studies the lateral and vertical migration of the clinoform rollover points through time (Henriksen et al., 2009). Migration patterns of the rollover are can be used to contextualise and help predict changes in depositional environment and lithology (Helland-Hansen and Hampson, 2009).

Shelf edges show three main trajectory pathways (Figure 3.6) (Helland-Hansen and Hampson, 2009) however some authors (e.g. Anell et al., 2014; Paumard et al., 2018) have also demonstrated the existence of a fourth backstepping shelf margin trajectory;

1. Positive Trajectory where sediment is retained on the shelf and vertical accretion of the clinoform dominates,
2. Negative Trajectory where sediment is delivered across the clinoform to the basin floor.
3. Flat Trajectory where the shelf is bypassed and sediment is delivered to the basin floor.
4. Retrogradational or Backstepping Trajectory where significant shelf accommodation is generated. This can also occur on over-steepened margins that have undergone collapse followed by continued aggradation.

Shoreline and shelf edge trajectories are genetically linked features (Figure 3.6); sediment from delta clinoforms feeds to shelf edge accretion; consequently, the distance of the shoreline from the shelf edge plays a major role in how much sediment makes it to the shelf edge and onward to the basin floor. Shorelines and associated deltas can migrate seaward and landward (Helland-Hansen and Gjelberg, 1994), when a delta clinoform progrades to the shelf edge to become a shelf edge delta, sediment can be delivered to the deep basin resulting in outbuilding of the shelf margin and delivery of coarse sediment to the basin floor (Johannessen and Steel, 2005; Porebski and Steel, 2006). Conversely, when relative sea level rises this results in landward movement of the delta clinoform and sediment supply to the shelf edge is greatly reduced. In this scenario it should be noted that although the delta clinoform has moved landward, the shelf margin clinoform does not migrate landward.

As with most techniques, care must be taken not to oversimplify interpretations; for example in a rising shelf edge trajectory more sediment is retained on the shelf instead of

being delivered to the basin, however as noted by previous authors sediment may be delivered over the shelf edge in a rising trajectory if sediment supply is sufficient (Burgess and Hovius, 1998; Carvajal and Steel, 2009; Jones et al., 2013).

The trajectory method has also been incorporated into the afore mentioned Accommodation-Succession method of Neal and Abreu (2009).

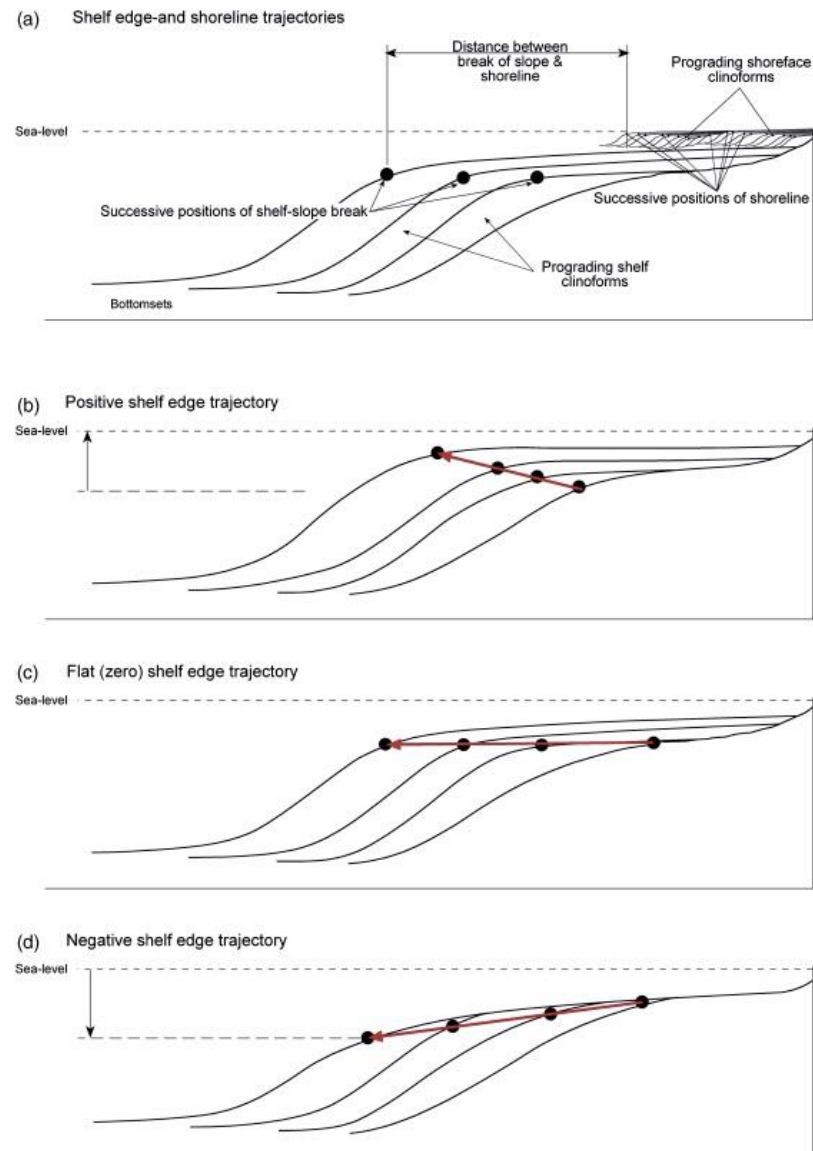


Figure 3.6 Shelf edge trajectory classes from Henriksen et al., (2011).

3.2.3 Seismic Interpretation Workflow

Using the seismic and sequence stratigraphic methods outlined above, seismic data was interpreted in Petrel 2016.2 using a combination of manual, semi-guided and guided auto-tracking to trace horizons of interest across the seismic database. In this way, a regional

seismic stratigraphic framework was established (Chapter 4) with more detailed sequence stratigraphic interpretations were undertaken in Chapter 5.

Regional 2D seismic data is supplemented in some areas of the basin by 3D seismic surveys (Figure 3.1) and allowed for localised 3D seismic geomorphological studies of the Giant Foresets Formation.

Seismic geomorphology allows detailed identification and mapping of depositional features in a 3D seismic volume (Posamentier, 2004; Posamentier et al., 2007), allowing improved understanding of depositional environments.

Continuous time-amplitude data allows for continuous mapping of a horizon throughout a 3D cube. Using this mapped horizon, it is then possible to extract seismic attributes (e.g. RMS amplitude and variance) at specified windows above, below or on the mapped horizon.

Eliis PaleoScan 2016.1 was used in a semi-automated manner to extract maximum value from the large number of available surveys. This software uses an algorithm to automatically track all possible horizons within a 3D seismic cube to create a “Model Grid” of horizons (Daynac et al., 2016; Pauget et al., 2009). The model grid was then quality-controlled and edited where necessary to ensure automatic interpretations are representative of the data. Using this quality-controlled model grid, a 3D geomodel of the seismic cube was generated. From this geomodel, a horizon stack consisting of a user selected number of chronostratigraphically correct horizons, allowing the user to scroll through the data in a similar manner to scrolling through time slice data. Key surfaces were exported to Petrel 2016.2 and integrated with a manually interpreted horizons. Generation of this horizon stack proved an efficient way to extract geomorphological information from a large number of surveys through a dipping clinoform succession like the Giant Foresets Formation.

Chapter 4

Along margin variability in sequence architecture in the Taranaki Basin, New Zealand.

4.1 Introduction

Since the late 1970s, seismic stratigraphy has revolutionised the study of sedimentary basins and how they fill through time. Following the observation that seismic reflectors follow time lines and their terminations may define stratigraphic surfaces (Mitchum et al., 1977b), geologists were provided with a tool for systematically subdividing genetically related sedimentary packages within a chronostratigraphic framework.

Trajectory Analysis was developed as an additional approach to understand the stacking patterns of clinoforms and their sedimentary facies successions by tracking the clinoform rollover position in shelf margin clinoforms and can be used to aid in unravelling changes in palaeoenvironment and lithology distribution (Helland-Hansen and Gjelberg, 1994; Helland-Hansen and Hampson, 2009; Helland-Hansen and Martinsen, 1996; Henriksen et al., 2009). This method provides an objective analysis of a stacked clinoform succession without the assumptions of the physical controls on sequence generation.

Both sequence stratigraphy and trajectory analysis are typically studied by interpretation of regional dip sections; owing to the 3D nature of sedimentary systems this can lead to misleading and incorrect interpretations of key bounding surfaces and stacking patterns (Martinsen and Helland-Hansen, 1995; Wehr, 1993). It has been shown by many authors that significant lateral variations exist in terms of subsidence, physiography, sediment supply and process regime (e.g. Fulthorpe and Austin, 2008; Helland-Hansen and Hampson, 2009; Henriksen et al., 2011; Jones et al., 2015; Madof et al., 2016; Marin et al., 2017; Monteverde et al., 2008; Sanchez et al., 2012). These factors have significant implications on how coarse clastic sediment is distributed along a basin margin and how it is partitioned into deep water; this has become an increasingly important topic to understand as hydrocarbon exploration moves toward deep-water targets and has applications to the subsurface storage of CO₂ in regional aquifers.

This study presents a seismic stratigraphic framework supported by trajectory analysis for the Giant Foresets Formation along 300 km of the basin margin. Lateral variations in

sequence architecture, 3D seismic geomorphology, aggradation and progradation rates are documented with the aim of unravelling factors that controlled the evolution of the basin margin.

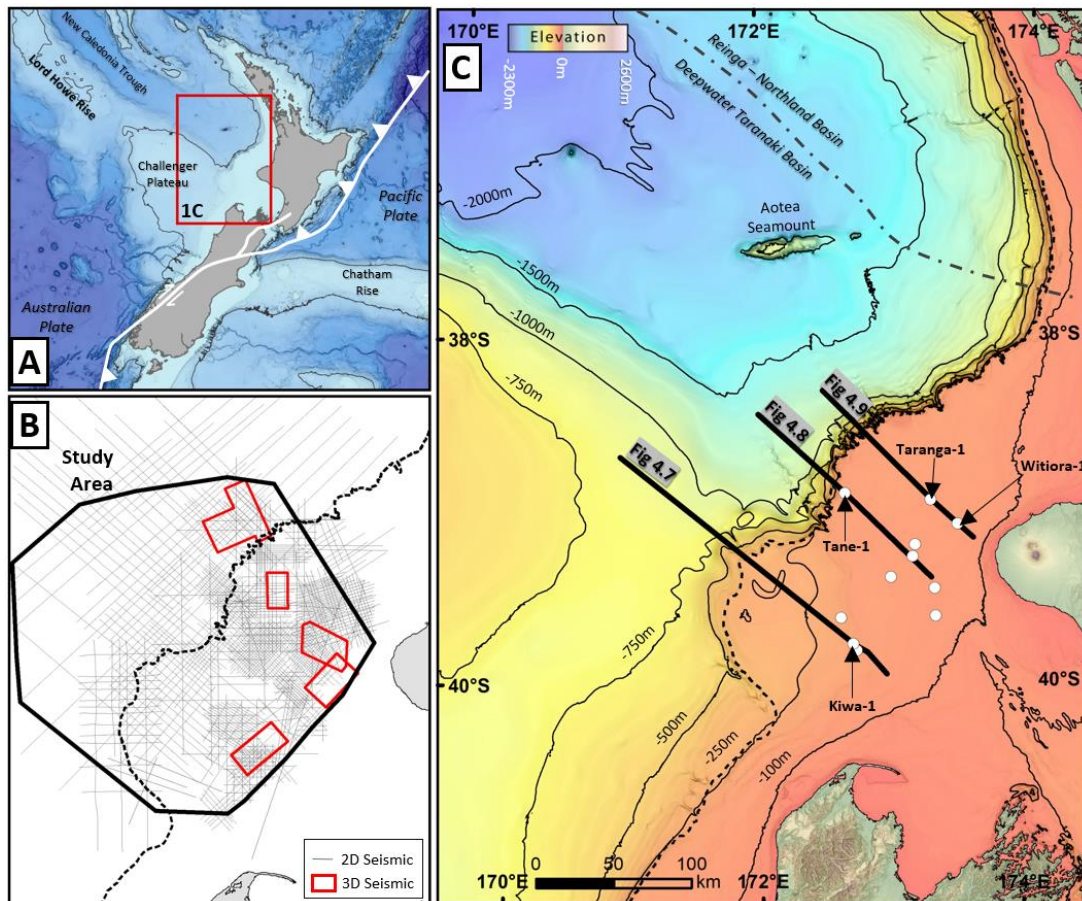


Figure 4.1 Basin Location and dataset.

A) Regional bathymetric data and physiographic features of New Zealand with 1000m contour. B) Outline of study area with 2D & 3D data utilised in this project. C) Seafloor map of the Taranaki Basin with locations of key seismic sections and wells utilised in this study. Bathymetric data sourced from NIWA.

4.2 Geological Setting

The present-day Taranaki Basin is located offshore to the west of New Zealand's North Island in a retro-arc setting to the Kermadec–Hikurangi subduction margin (King and Thrasher, 1992). Up to 9 km of sediments record the multiphase history of the basin from Late Cretaceous rifting, through Palaeocene transgression and establishment of a passive margin in the Eocene (King and Thrasher, 1992, 1996). This transgression continued through the Eocene and also saw establishment of a proto-plate boundary as the Pacific and Australian plates collided. Rapid subsidence through the Oligocene was driven by orogenic loading and flexure as foreland subsidence dominated the region. Ongoing

collision related uplift through the Miocene – Recent has resulted in an overall regressive succession infilling existing foreland accommodation.

As discussed in Chapter 2, the Taranaki Basin can be split into two distinct structural domains, the Eastern Mobile Belt and Western Stable Platform (WSP) (King and Thrasher, 1996). The Eastern Mobile Belt is a structurally complex zone where extension and andesitic volcanism in the Northern and Central Grabens (16Ma – 2Ma) was coupled with compression in the Southern Inversion Zone (Figure 4.2) (Giba et al., 2010; King and Thrasher, 1996). Compression in the Southern Inversion Zone has been mostly accommodated by inversion of pre-existing Late Cretaceous rift structures. The doming of overlying strata formed economically important hydrocarbon traps (Figure 4.2) (King and Thrasher, 1996; Reilly et al., 2015).

The Western Stable Platform is separated from the tectonically active Eastern Mobile Belt in the north by the east dipping Cape Egmont Fault System and in the south by the Kahurangi Fault System (King and Thrasher, 1996; Reilly et al., 2015).

We focus on the Pliocene to recent succession, dominated by the Giant Foresets Formation (GFF), a set of strongly progradational shelf margin scale clinoforms up to 1500 m high. This wedge of sediment prograded from SE to NW, infilling the Northern and Central Grabens (Figure 4.2) before overtopping these depocentres in the Late Pliocene (Hansen and Kamp, 2004; 2006; Salazar et al., 2016) and prograding in a north-westerly direction across the Western Stable Platform to form the modern day shelf break. Sediments were dominantly sourced from the rapid uplift and erosion of the Southern Alps (Nodder, 1995), and delivered north to the Taranaki Basin via a combination of ocean currents and littoral drift (Hansen and Kamp, 2006; Payne et al., 2010).

The structural stability of the Western Stable Platform and exquisite clinoform geometries make the Giant Foresets Formation an ideal natural laboratory to test sequence stratigraphic models and to investigate lateral variability within a rapidly prograding margin.

Anell and Midtkandal (2017) also studied the same succession as this study, focusing on defining and quantifying geometric relationships of clinoforms. Their work did not attempt to address local factors or lateral variability of the succession and made limited comments on the temporal evolution of the margin. Comparison is made to their work throughout the results section of this chapter where overlap is apparent.

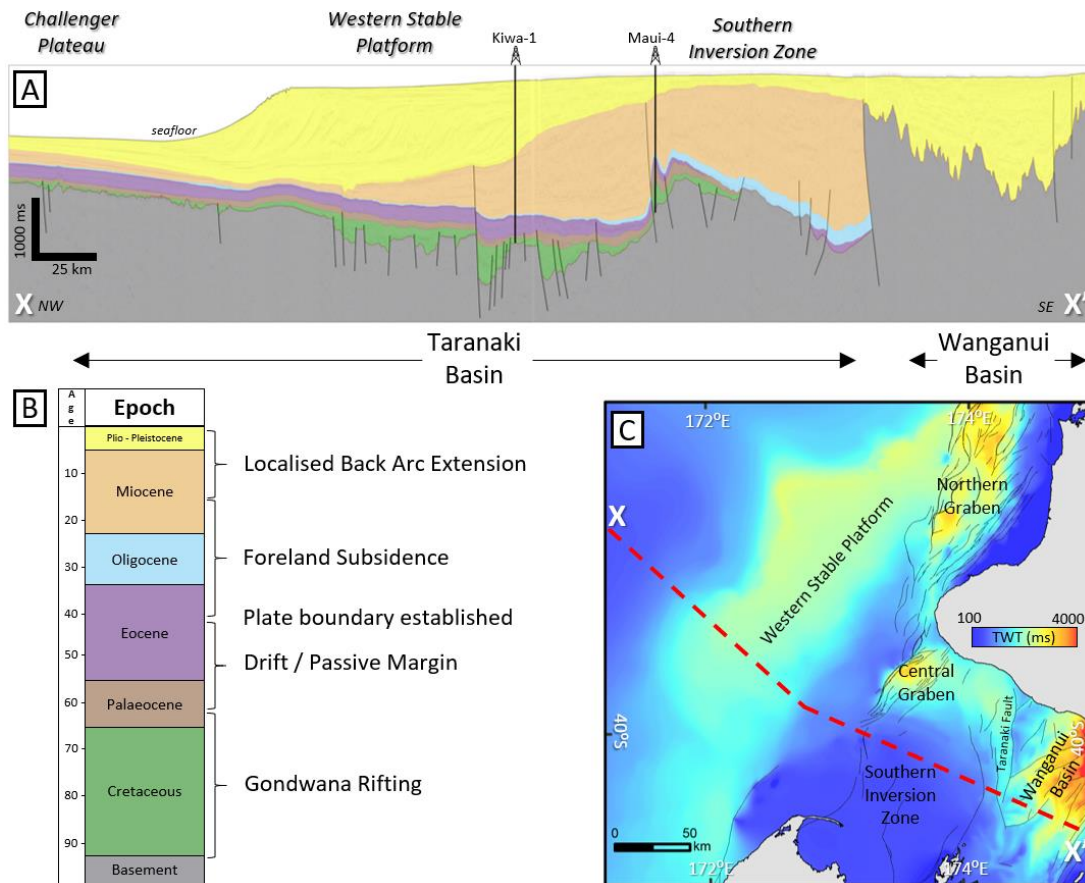


Figure 4.2 Basin Structure and Evolution.

A) Regional seismic section showing main stratigraphic units encountered in the Taranaki Basin (Adapted from Strogon et al. 2014). Note inverted anticline structure drilled by borehole Maui-4. B) Stratigraphic chart highlighting major events within the Taranaki Basin. C) Time thickness map of the Plio-Pleistocene succession showing main structural domains in the Taranaki Basin. Also shown are Plio-Pleistocene faulting – note the Western Stable Platform is unaffected by faulting. Compiled with data from Thrasher et al. (1995).

4.3 Datasets and Methods

This project utilises industry 2D and 3D seismic and well data made available through New Zealand Petroleum and Minerals (NZPAM). The dataset covers an area of approximately 70,000 km² (Figure 4.1). Data were collected from the 1970s to 2015; as such there is a large range in the quality of seismic data. The dominant frequency of surveys ranges between 7 and 50 Hz in the interval of interest (low frequencies are from the oldest surveys), yielding maximum vertical resolutions from 70m to 10m respectively; average resolution is calculated at approximately 19m using a velocity of 2 km/s. Surveys have been corrected for amplitude and time offsets and have been phase matched to display in zero phase with a European polarity (i.e. where an increase in acoustic impedance is displayed as a red peak). Seismic interpretation was carried out using a combination of Schlumberger Petrel 2016, IHS Kingdom 8.8 and Eliis PaleoScan

software. A seismic stratigraphic approach was used to define and map regionally extensive packages along the margin of the WSP.

The seismic data are calibrated by hydrocarbon exploration wells along the margin of the Taranaki Basin. Some 16 wells were used that penetrate the Pleistocene succession of the Western Stable Platform and contain partial wireline logs through the GFF. Velocity information was obtained from checkshots and, where available, further constrained with sonic velocity logs, yielding an averaged interval velocity of 2 km/s for the GFF. +/- 20-25%. Within this uncertainty, time structure and thickness maps (Figure 4.10 to Figure 4.12) in ms are broadly equivalent to thickness in metres. The time depth relationship in Figure 4.3 was further used to estimate clinoform geometries and trajectories, however a full time depth conversion of surfaces and thickness maps was not carried out.

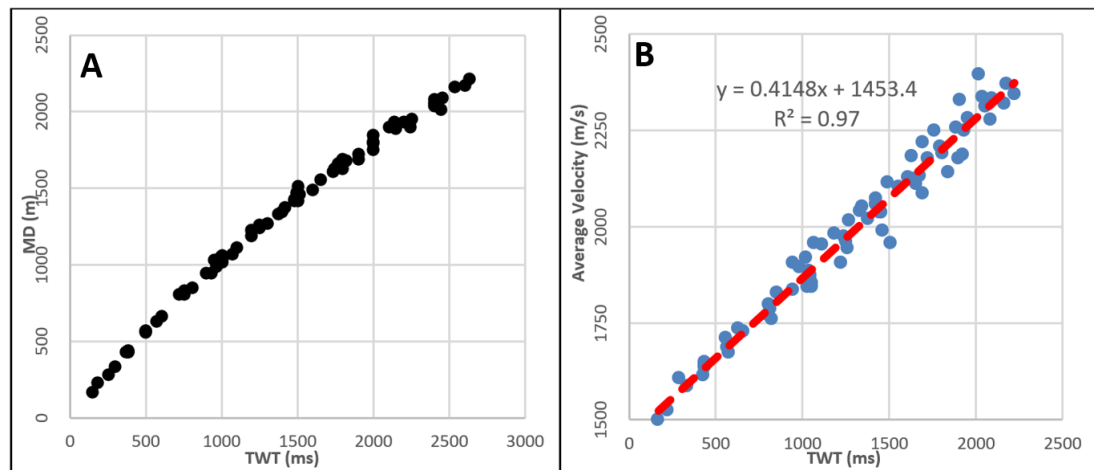


Figure 4.3 Time-depth relationships for Giant Foresets Formation.

A) Recorded checkshot data for wells across the Western Stable Platform. B) Average velocity equation derived from checkshot data.

Age estimates were obtained from a compilation of biostratigraphic data and correlation to existing GNS studies (Chapter 3). To supplement a lack of age diagnostic fauna in the Pleistocene succession, age estimates were derived from a detailed sequence stratigraphic study carried out in Chapter 5, in which depositional cyclicity is correlated to global eustatic fluctuations of known age and magnitude. In using this method two testable assumptions were carried: 1) global eustasy exerted a strong control on sequence formation in the Pleistocene section of the Taranaki Basin because 2) negligible tectonic subsidence occurred on the WSP during the Pleistocene.

Clinoform geometries (height, foreset length and foreset angle) were measured for the bounding surface of each seismic sequence and are presented in Table 4.1. In the Plio-

Pleistocene succession, compaction was negligible (Funnell et al., 1996), with a study in the Northern Graben reporting less than 5% difference between compacted and decompacted geometries in the Giant Foresets Formation (Salazar et al., 2016). As such, measurements were made on undecompressed two way time dip sections and later converted to depth (Figure 4.3). The shelf and bottomset rollovers (sensu Patruno et al., 2015) were used to define foreset height, slope length and foreset dip (Figure 4.4).

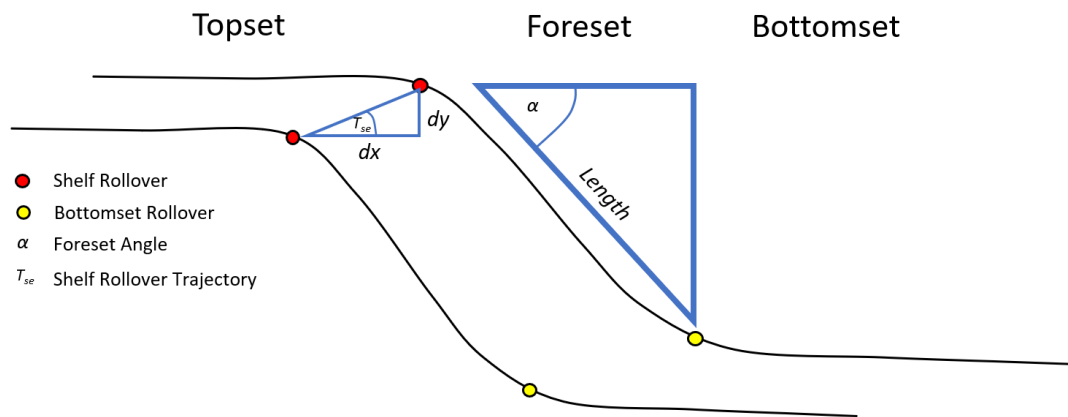


Figure 4.4 Measured clinoform geometric parameters.

Trajectory Analysis was also carried out on a number of dip sections along the margin of the basin to reveal and quantify along-margin variability in stratigraphic character. This was carried out by flattening dip sections of interest on topset flooding surfaces (these are considered to be near horizontal at time of deposition) and quantifying clinoform progradation (dx), aggradation (dy), trajectory angles ($T_{se} = \tan^{-1} [dy/dx]$) between two points (Gong et al., 2016, 2015). Using biostratigraphic ages and relative ages derived from our sequence stratigraphic model the progradation rate (Rp) was also calculated for each seismic sequence, where $Rp = dx/t$ (t represents the age spans of the sequence in question).

The Giant Foresets Formation is dominated by mudstones and siltstones with occasional sandstones, marls and shell beds (Hansen and Kamp, 2008, 2002; Hansen and Kamp, 2006; King and Thrasher, 1996). An overall coarsening upward trend is interpreted in gamma ray logs through the succession (Appendix 1; Hansen and Kamp, 2002). Due to sparse data collection in well penetrations through the GFF on the Western Stable Platform, limited lithological information was available to this study. Data from three wells (Kiwa-1, Tane-1 and Taranga-1) are used to add lithological information to seismic interpretations (Figure 4.1; Appendix 1).

4.4 Results

4.4.1 Seismic Stratigraphy of the Giant Foresets Formation

In this study nine regional surfaces were mapped along approximately 200 km of the Western Stable Platform. Interpretations are presented on three key dip lines (Figure 4.7 to Figure 4.9). Mapped horizons are named, from oldest to youngest, T1 to T9 and are presented as time structure maps. The stratigraphic units between these horizons are named, oldest to youngest, Unit A to Unit I (Figure 4.5).

Time structure and thickness maps showing the evolution of the margin are presented in Figure 4.10 to Figure 4.12 and summarised in Figure 4.6. Much of the stratigraphy in the deep-water Taranaki Basin has been disturbed and remobilised by mass transport processes (partly described by Omeru, 2014; Omeru et al., 2016) resulting in limited continuity of horizons mapped in deep-water regions of the basin.

A summary of the nomenclature used to describe the seismic stratigraphy in this study is presented in Figure 4.5 alongside an age model incorporating multiple sources discussed above. Poorly defined biostratigraphy is supplemented by correlation to nearby studies (Thrasher et al., 2018) and re-evaluation of planktic foraminifera (pers. comm Crundwell, 2017) from well Tane-1.

When carried out on multiple transects along a basin margin, shelf edge trajectories can help to capture the along margin variation in basin architecture (e.g. Sanchez et al., 2012), and hence act as a starting point to further discuss the controls on accommodation and sediment supply (A/S).

The trajectory between the shelf edge rollovers of each seismic sequence was measured and is used to describe the architectural changes observed between each regional surface (Table 4.1 and Figure 4.14). Modifying the classification of Paumard et al. (2018), this is coupled with the ratio of progradation to aggradation (P/A) to further constrain changes in progradation style of the Giant Foresets Formation (Table 4.1). In combination, these measures are used to define four main categories of shelf margin growth and associate them with relative values of A/S:

1. *Flat shelf edge trajectory*: these are clinoforms with a P/A ratio of greater than 100 and a trajectory of $0^\circ < 0.5^\circ$. The interpretation of this trajectory is that sediment supply outpaced creation of shelf accommodation ($A/S \ll 1$) leading to strongly progradational clinoforms.

2. *Slightly rising shelf edge trajectory*: displays a combination of strongly progradational clinoforms with a slightly aggradational element. Trajectories range from 0.5° to 1°, with a P/A ratio of 50 to 100. In these settings the interpretation is that $A/S < 1$.
3. *Moderately rising shelf edge trajectory*: have trajectories of 1° to 2° with P/A ratios of 30 to 50. These clinoforms developed in environments with moderate amounts of shelf accommodation where sediment supply rates were still sufficient to outpace the rate of accommodation generation ($A/S < 1$).
4. *Steeply rising shelf edge trajectory*: these clinoforms show a strongly aggradational nature with steep trajectories of greater than 2° and P/A ratios of 0 to 30. In these settings, it is inferred that $A/S \sim 1$, and that sediment supply rates balanced the rate of accommodation generation.

The following section contains a description of the basal surface and overlying stratigraphy of each unit. Additionally, it summarises key geometric parameters and trajectory of the shelf rollover between the unit's bounding surfaces.

Epoch	NZ Stage	Seismic Stratigraphy (This Study)	Assigned Age	Age Source	
Pleistocene		Seabed	0 Ma	Seabed	
	Wq	Unit I	0.191 Ma	Chapter 5	
	Wc	Unit H	0.621 Ma	Chapter 5	
		Unit G	1.2 Ma	Chapter 5	
		Unit F	1.5 Ma	GNS N85 (Thrasher et al. 2018)	
		Unit E	2.0 Ma	GNS N82 (Thrasher et al. 2018)	
	Wn	Unit D	2.4 Ma	GNS N80 (Thrasher et al. 2018)	
	Pliocene	Wm	Unit C	3.0 Ma	Biostratigraphy (Crundwell, 2017 pers. comm)
		Wp	Unit B	4.3 Ma	Biostratigraphy (Kiwa-1)
		uWo			
IWo		Unit A	5.33 Ma	Biostratigraphy (All Wells)	
		T1			

Figure 4.5 Summary of seismic stratigraphy and age model of the Giant Foresets Formation utilised in this study.

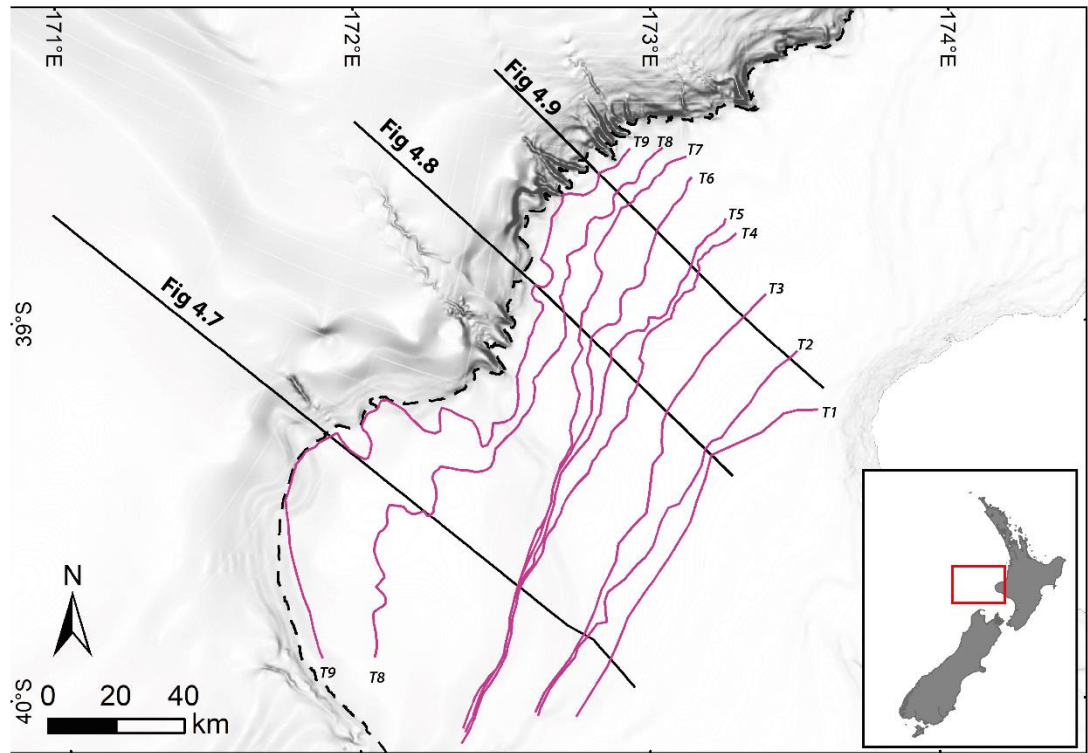


Figure 4.6 Summary shelf edge map of surfaces T1 to T9 overlain on bathymetry.

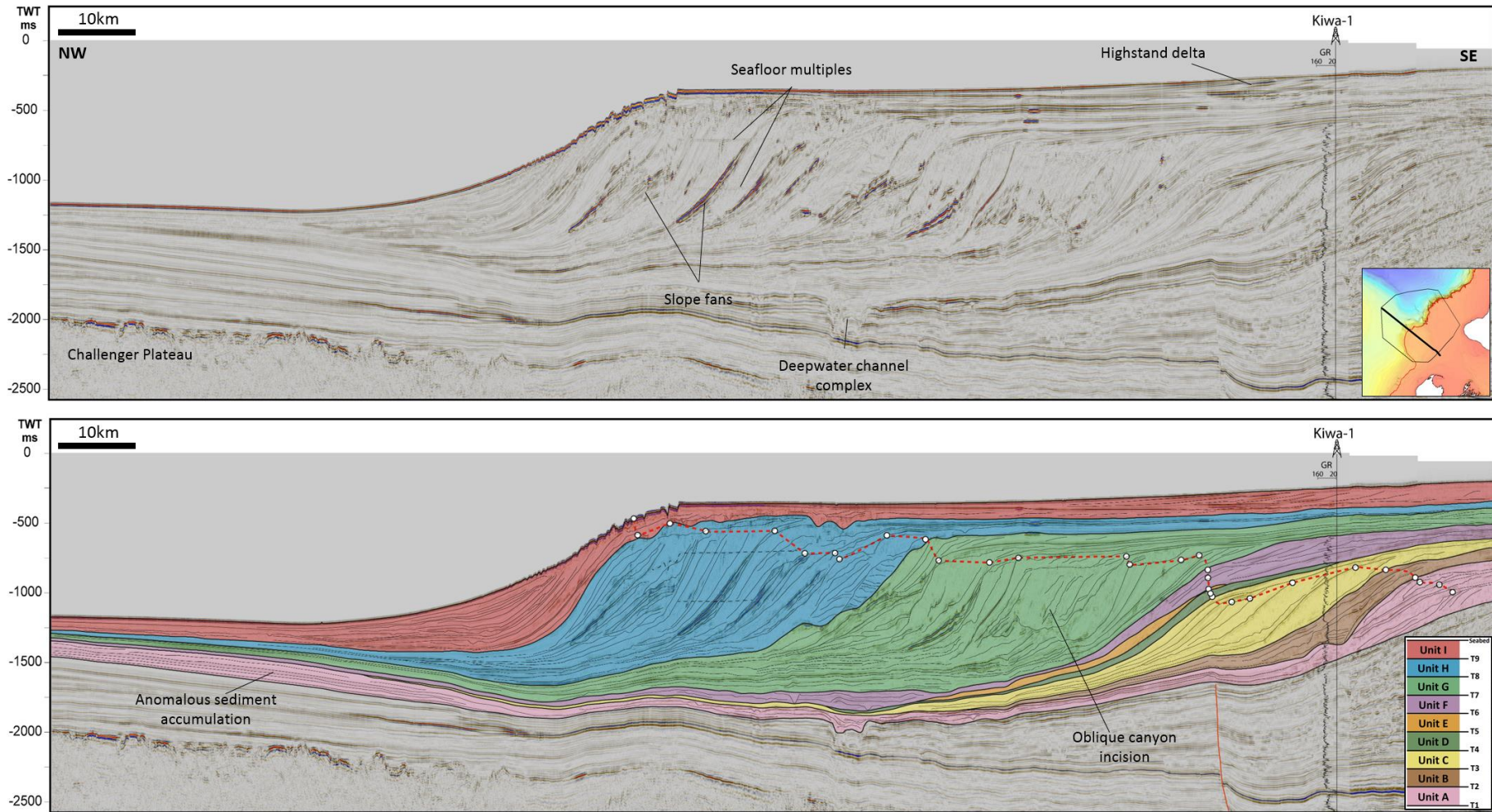


Figure 4.7 Seismic stratigraphic units in the southern composite line (DTB01-31 & Hector 3D).
 See inset and Figure 4.1 for location. Shelf break trajectory is given by red stipple and white dots.

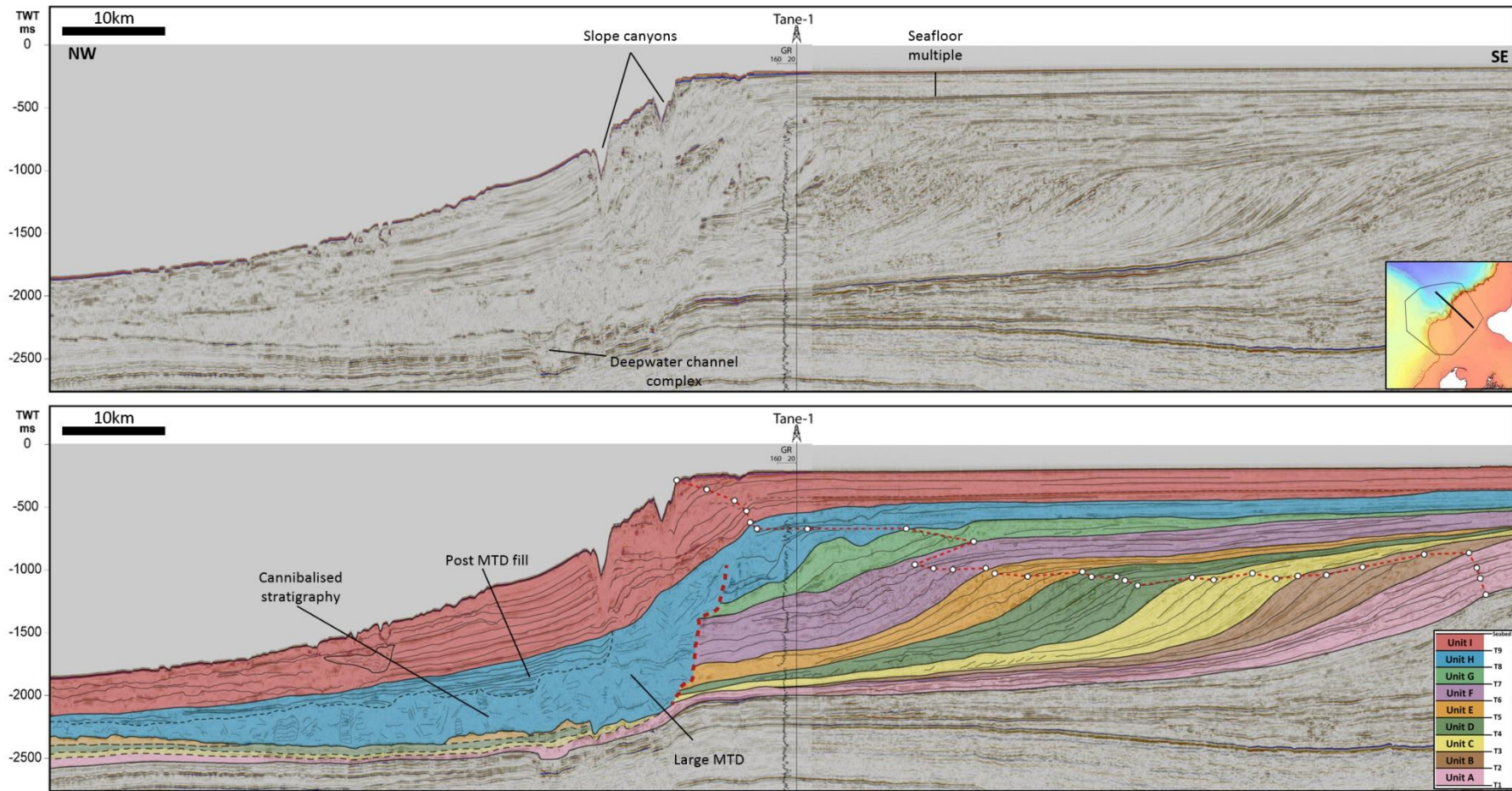


Figure 4.8 Seismic stratigraphic units on the central composite section (DTB01-23 & SUNZ-91-136). See inset and Figure 4.1 for location. Shelf break trajectory is given by red stipple and white dots.

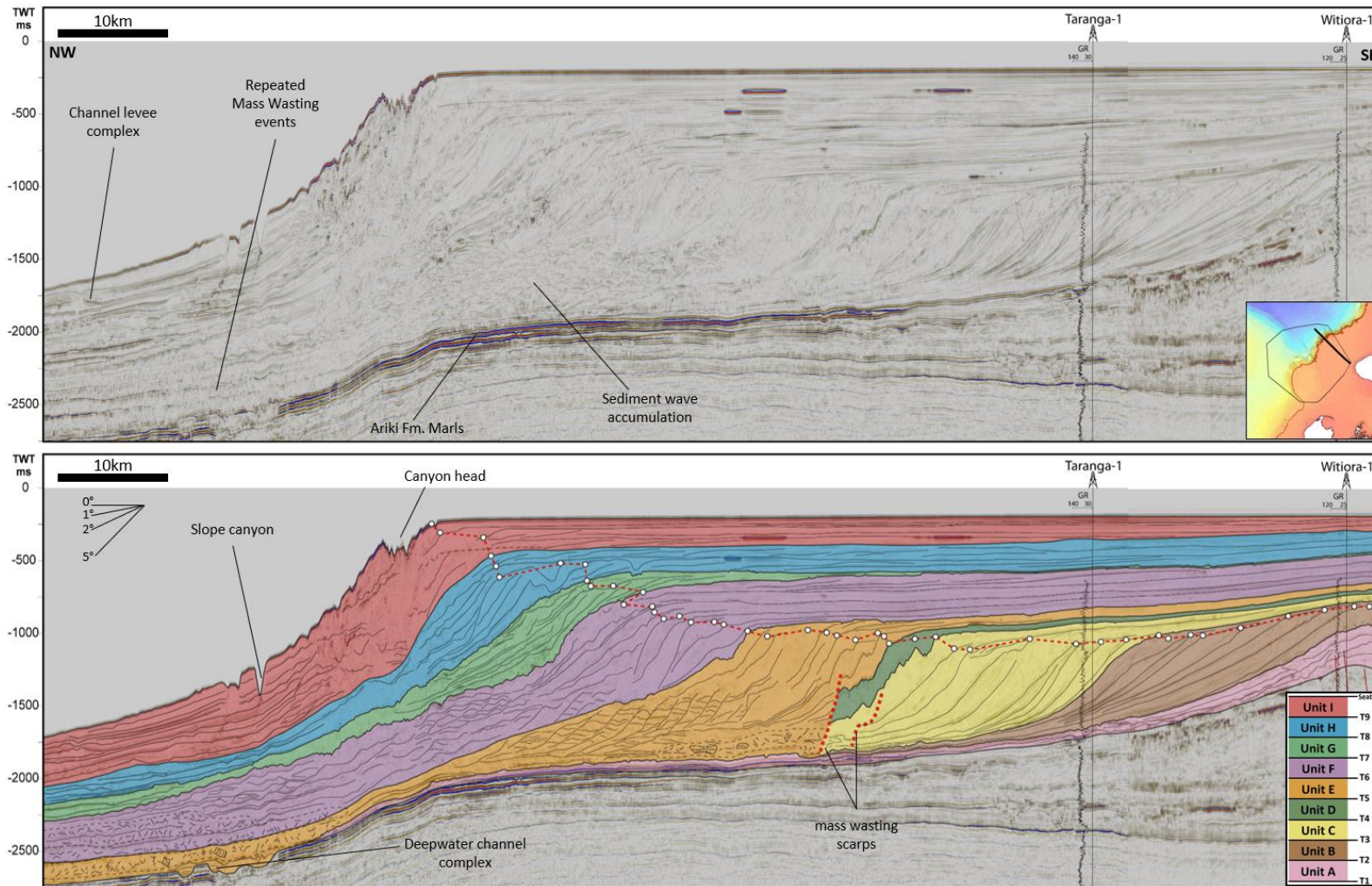


Figure 4.9 Seismic stratigraphic units in the northern composite line (OMV-07-13 and ST03-401). See inset and Figure 4.1 for location. Shelf break trajectory is given by red stipple and white dots.

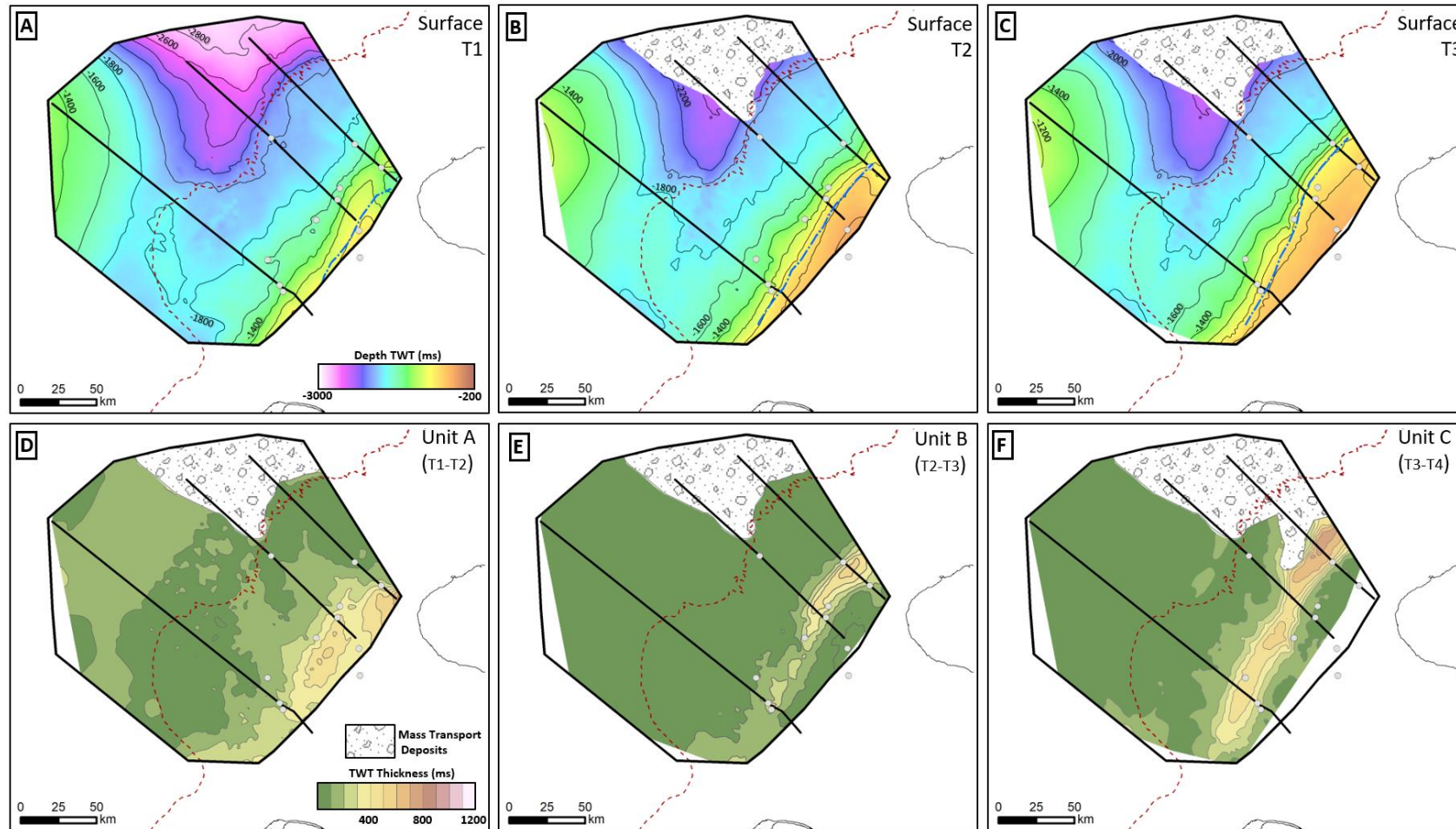


Figure 4.10 Time Structure and Thickness Maps 1.

A to C Time structure maps for surfaces T1 to T3. D to F show time thickness maps for units A to C. Contour intervals at 200 ms. Modern shelf edge rollover is represented as a red stipple, ancient shelf rollover is shown as a blue stippled line. Maps are clipped to the extent of Mass Transport Deposits (MTDs) affecting the stratigraphy.

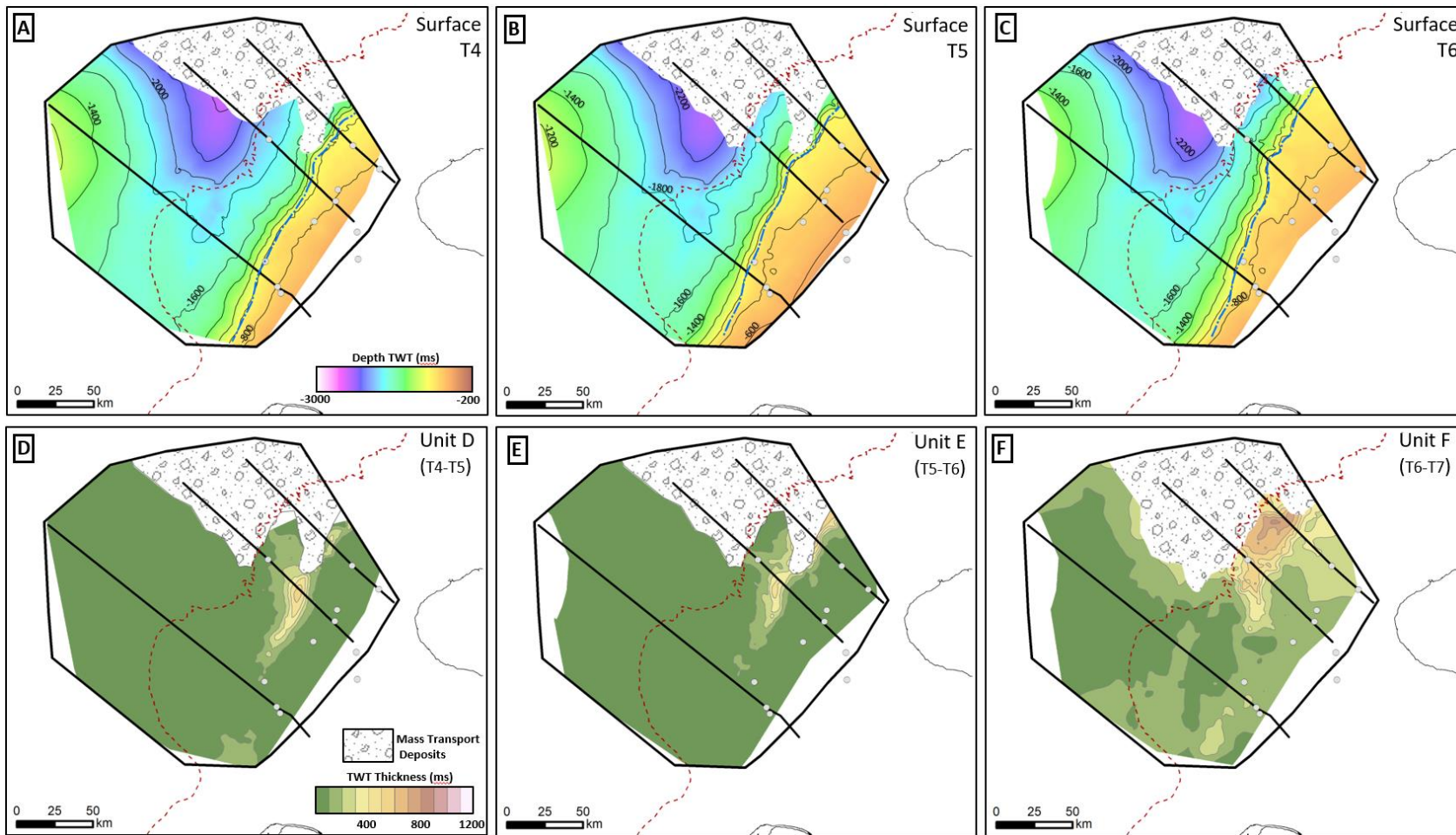


Figure 4.11 Time Structure and Thickness Maps 2.

A to C Time structure maps for surfaces T4 to T6. D to F show time thickness maps for units D to F. Contour intervals at 200 ms. Modern shelf edge rollover is represented as a red stipple, ancient shelf rollover is shown as a blue stippled line. Maps are clipped to the extent of MTDs affecting the stratigraphy.

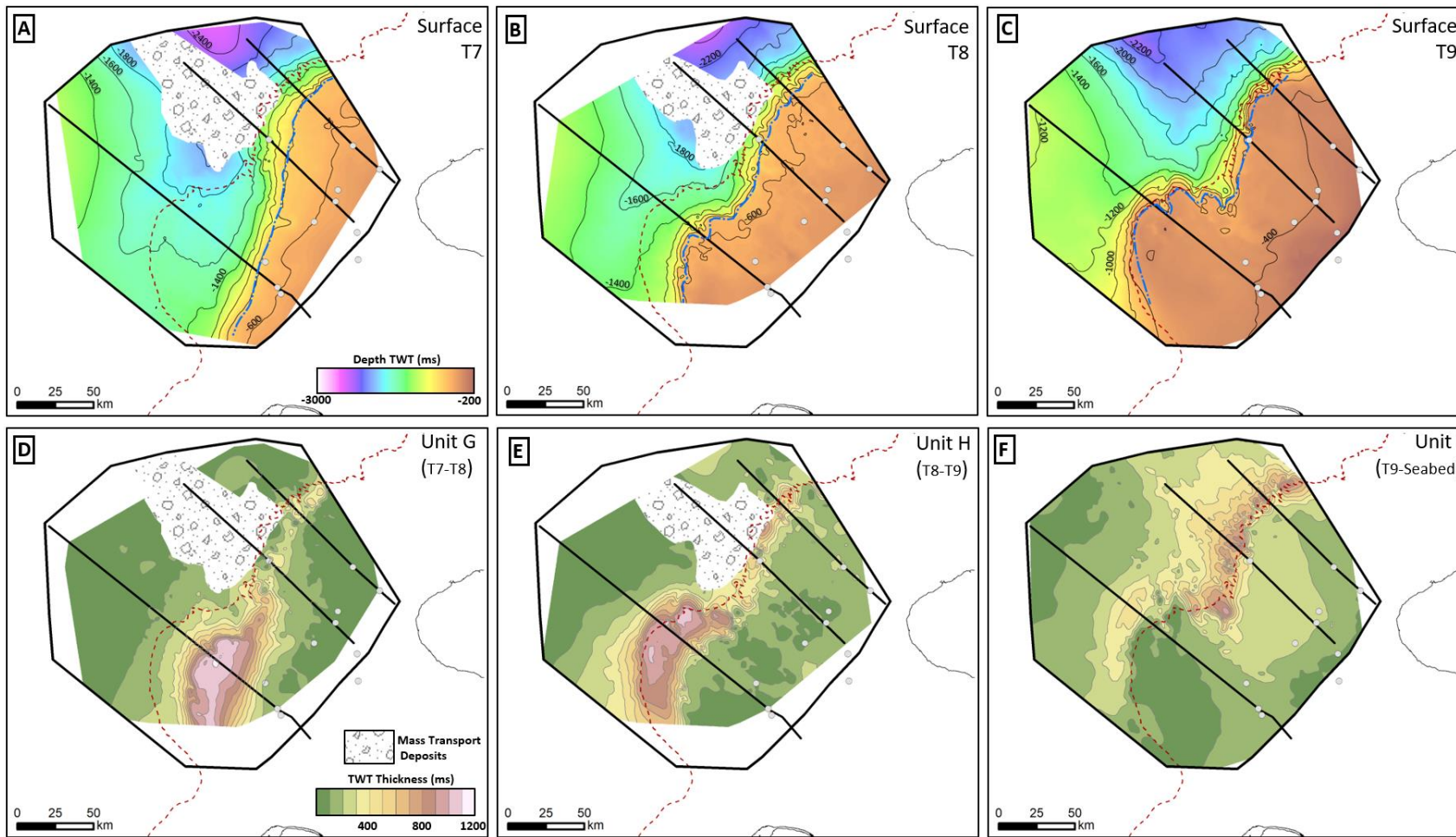


Figure 4.12 Time Structure and Thickness Maps 3.

A to C Time structure maps for surfaces T7 to T9. D to F show time thickness maps for units G to I. Contour intervals at 200 ms. Modern shelf edge rollover is represented as a red stipple, ancient shelf rollover is shown as a blue stippled line. Maps are clipped to the extent of MTDs affecting the stratigraphy.

Table 4.1 Summary of measured and calculated parameters of key horizons used to describe clinoform geometries and evolution of the Giant Foresets Formation. Clinoform dimensions (height, slope length & gradient) are quoted on the basal surface. Aggradation, progradation and T_{SE} are measured between the base and top surface of the unit.

Seismic Sequence (base surface)	Composite line	Unit Thickness (ms)	Clinoform Height (m)	Slope Length (km)	Slope Gradient (Degrees)	Aggradation Dy (m)	Progradation Dx (m)	P/A	Shelf Edge Trajectory (T_{SE} °)	Trajectory Style	Progradation Rate (R_p) (m/kyr)	Aggradation Rate (R_A) (m/Myr)
Unit I (T9 Rollover)	North	470	1328	21.5	3.5	189	5485	29	2.0	Steeply rising	28.7	991.2
	Central	950	1116	22.1	2.9	329	7830	24	2.4	Steeply rising	41.0	1724.6
	South	880	829	17.6	2.7	23	4675	207	0.3	Flat	24.5	118.1
Unit H (T8 Rollover)	North	600	870	16.5	3.0	142	8731	62	0.9	Slightly Rising	20.3	329.9
	Central	610	MTD	MTD	MTD	52	15450	299	0.2	Flat	35.9	120.0
	South	1050	699	14.5	2.8	98	33177	340	0.2	Flat	77.2	226.8
Unit G (T7 Rollover)	North	420	750	17.2	2.5	123	4604	37	1.5	Moderately Rising	8.0	212.9
	Central	410	MTD	MTD	MTD	94	6775	72	0.8	Slightly Rising	11.7	162.0
	South	1120	725	30.7	1.4	191	36627	191	0.3	Flat	63.3	330.4
Unit F (T6 Rollover)	North	850	826	24.5	1.9	245	10465	43	1.3	Moderately Rising	34.9	815.8
	Central	560	670	18.6	2.1	199	1250	6	9.1	Steeply Rising	4.2	665.0
	South	230	715	27.3	1.5	126	120	1	46.3	Steeply Rising	0.4	419.0
Unit E (T5 Rollover)	North	600	MTD	MTD	MTD	116	13130	113	0.5	Slightly Rising	26.3	231.8
	Central	440	750	26.8	1.6	54	9630	178	0.3	Flat	19.3	108.2
	South	20	715	27.3	1.5	-	-	-	-	Stationary	-	-
Unit D (T4 Rollover)	North	340 (more removed by MTD)	MTD	MTD	MTD	5	3950	790	0.1	Flat	9.9	12.5
	Central	530	666	22.8	1.7	71	10850	153	0.4	Flat	27.1	177.8
	South	80	693	27.3	1.5	126	120	1	46.3	Steeply Rising	0.4	419.0
Unit C (T3 Rollover)	North	760	802	28.6	1.6	92	19845	217	0.3	Flat	33.1	152.6
	Central	460	648	19.7	1.9	69	10400	151	0.4	Flat	17.3	114.5
	South	470	590	19.2	1.8	134	22500	167	0.3	Flat	37.5	224.0
	North	530	861	43.2	0.9	140	19695	140	0.4	Flat	15.2	107.9

Chapter 4 - Regional Progradation

Unit B (T2 Rollover)	Central	450	835	28.8	1.7	17	16850	1003	0.1	Flat	13.0	12.9
	South	300	525	22.1	1.4	86	3853	45	1.3	Mod. Rising	3.0	66.1
Unit A (T1 Rollover)	North	700	not observed	not observed	not observed	-	-	-	-	-	-	-
	Central	450	690	30.1	1.3	323	1730	5	10.6	Steeply Rising	1.7	313.9
	South	320	626	31.6	1.1	161	15270	95	0.6	Slightly Rising	14.8	156.7

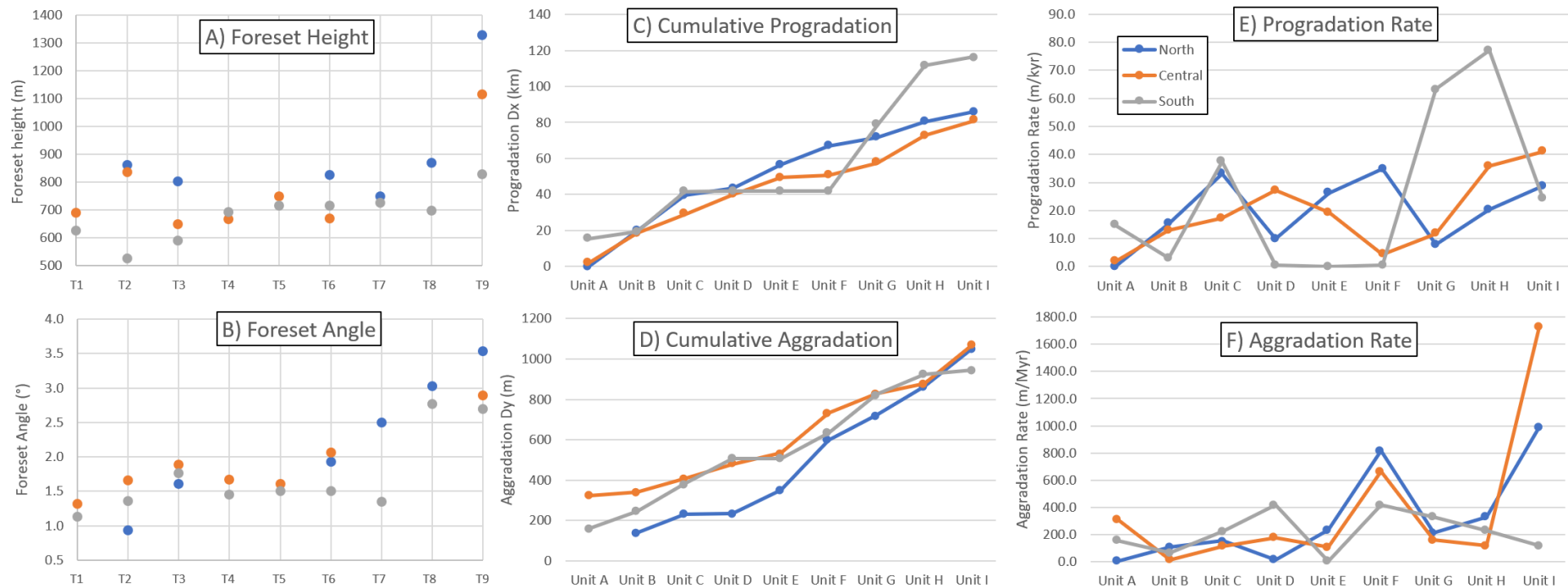


Figure 4.13 Measured and calculated geometric parameters of clinoforms and seismic sequences discussed in this chapter.

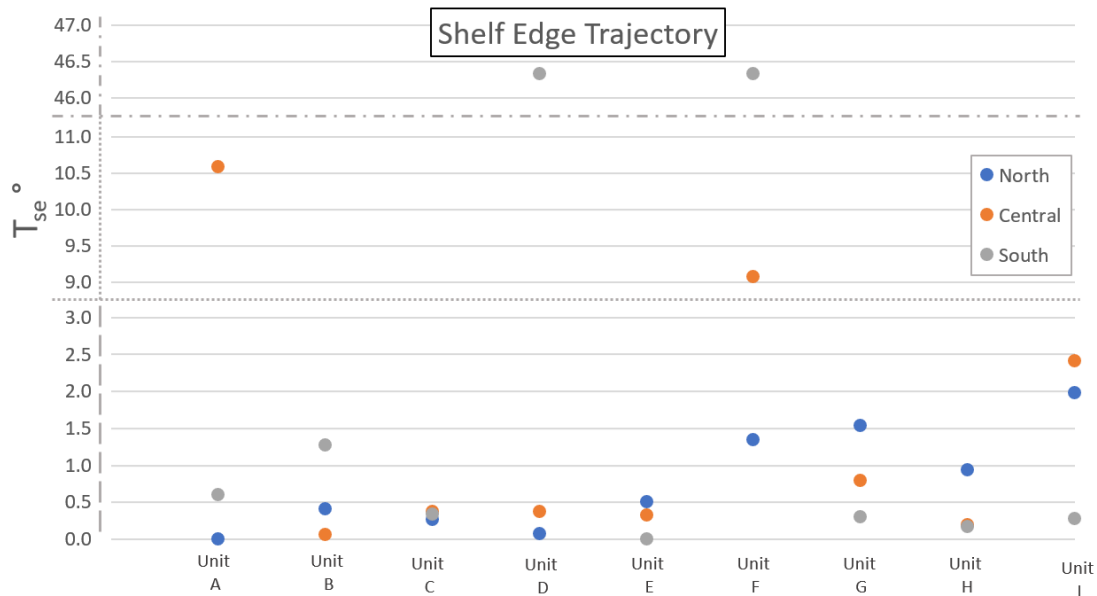


Figure 4.14 Shelf Edge Trajectories.

Shelf edge trajectories of the seismic stratigraphy taken along north, central and composite lines. Note changes in intervals along the y-axis.

4.4.1.1 Unit A - T1 to T2

Unit A is bounded at its base by T1 and top by T2 and spans approximately 1.03 million years. T1 represents the boundary between Miocene – Pliocene strata, is well constrained throughout the Taranaki Basin. Within the study area, Unit A varies in maximum thickness from 320 ms in the southern depocentre to 700 ms in the northern depocentre. Outside the study area to the northeast, Unit A thickens into the Northern Graben. In the south, a mounded sediment accumulation up to 200 ms thick is observed on the Challenger plateau (Figure 4.7).

In the deep-water regions of the Taranaki Basin, surface T1 is truncated by a chaotic seismic facies as the unit is cannibalized by younger Mass Transport Complexes (Figure 4.8, Figure 4.9, Figure 4.18 & Figure 4.21). These mass transport deposits cover large areas of the deepwater succession and complicate correlations. Omeru et al. (2016) mapped a number of these deposits, which are traceable to scarps in both the Taranaki and Reinga – Northland Basin.

In the south of the Western Stable Platform sediment was bypassed from the uplifting Southern Alps via a large deepwater channel network (Figure 4.15) to the basin floor. In northern areas sediment was diverted into the actively subsiding Northern Graben and Toru Trough (Figure 4.2) (Giba et al., 2010; Hansen and Kamp, 2006a; Hansen and Kamp, 2006c; Salazar et al., 2015). This resulted in sediment starvation across the WSP

and deep-water regions, and deposition of the Ariki Formation, a condensed marly unit (Hansen and Kamp, 2004, 2008). In seismic data, this unit forms a prominent high amplitude seismic facies at the base of the GFF on the Western Stable Platform (Figure 4.8 and Figure 4.9). In well penetrations it is characterised by low gamma ray values and marl rich mud log (wells Tane -1 & Taranga 1 in Appendix 1).

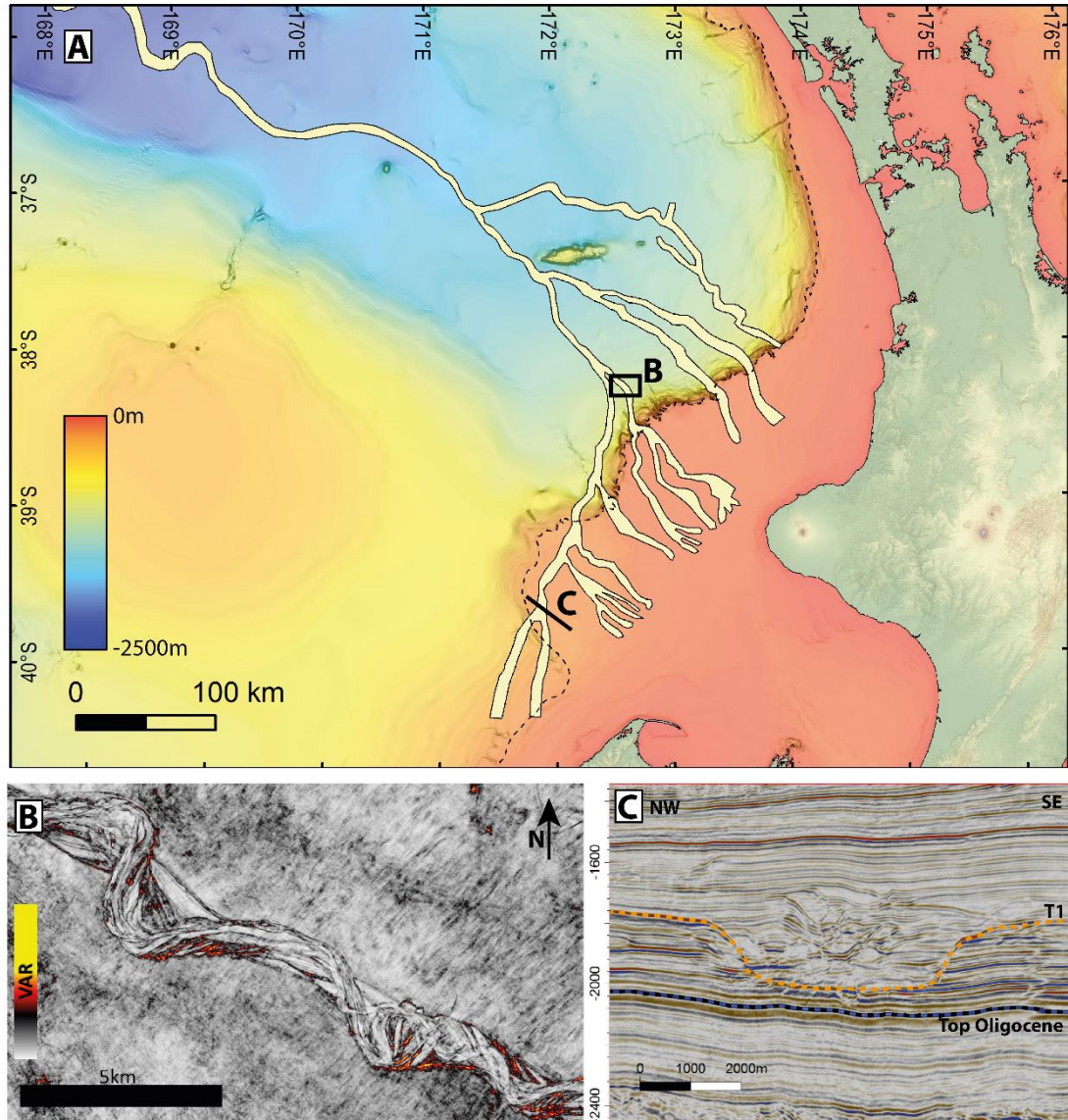


Figure 4.15 Miocene – Pliocene deep-water channels.

A) Distribution of Late Miocene - early Pliocene deepwater channel network from Grahame (2015) shown on present day seafloor bathymetry. B) variance time slice at -3600ms through the Romney 3D survey showing sinuous migration of the deepwater channel system. C) Large drainage system bypassing sediment from the Southern alps to the deepwater Taranaki Basin.

4.4.1.2 Unit B – T2 to T3

Unit B is bounded at its base by T2 and top by T3, and spans approximately 1.3 million years (4.3 – 3.0 Ma). In this time interval, the margin prograded up to 20 km in the north

but only ~3.8 km in the south (Figure 4.13), with corresponding accumulations up to 530 ms and thinner accumulations up to 300 ms in the south (Figure 4.10E; Table 4.1).

In the south of the study area progradation rate was lower, although with continued evidence for bypass to the deep-water Taranaki Basin observed on the slope and basin floor (Figure 4.16). A large slope canyon system on the T2 surface (1.7 km wide and 180 ms thick) fed by numerous slope gullies is observed in Figure 4.7 at the base of unit B. This canyon shows a lower gamma response and increased sand content in logs for well Kiwa-1 (Appendix-1). This large drainage system links to a larger axial drainage system bypassing sediment to the deep water Taranaki Basin shown in Figure 4.15. In the central region of the WSP, a 2 km wide by 200m deep NE trending incised valley is observed cutting through the mid – outer shelf late in Unit B (Figure 4.16A &B). Bypass in this area is reflected in the low aggradation values in Figure 4.13.

The slope succession in the vicinity of well Taranga-1 is characterized by mudstone showing a serrate shallowing upward gamma ray profile with minor sands recorded in the upper 100 m of the unit (Taranga-1 in Appendix-1). On the outer WSP, there was limited siliciclastic input during this time period, as evidenced by continued high amplitude seismic facies and low gamma ray values associated with Ariki marls (Tane-1 in Appendix 1).

The overall T_{SE} between the T2-T3 rollovers in this period was flat on northern and central lines with a moderately rising trajectory on the southern composite line (Figure 4.14; Table 4.1), suggesting that sediment supply rates outpaced accommodation generation in the north ($A/S \ll 1$), whilst in the south the A/S was slightly higher.

4.4.1.3 Unit C – T3 to T4

Unit C is bounded at its base by T3 and top by T4 and spans approximately 0.6 Ma (3.0 – 2.4 Ma). Maximum thicknesses of 760 ms are observed in the northern depocentre (Figure 4.10F). However, the highest amounts of progradation (up to 22.5 km) were recorded in the south (Figure 4.13; Table 4.1). Throughout unit C the shelf margin trended progressively toward a more linear northeast-southwest orientation as the southern depocentre advanced (Figure 4.10). Small amounts of mass wasting are observed in the northern depocentre (Figure 4.9).

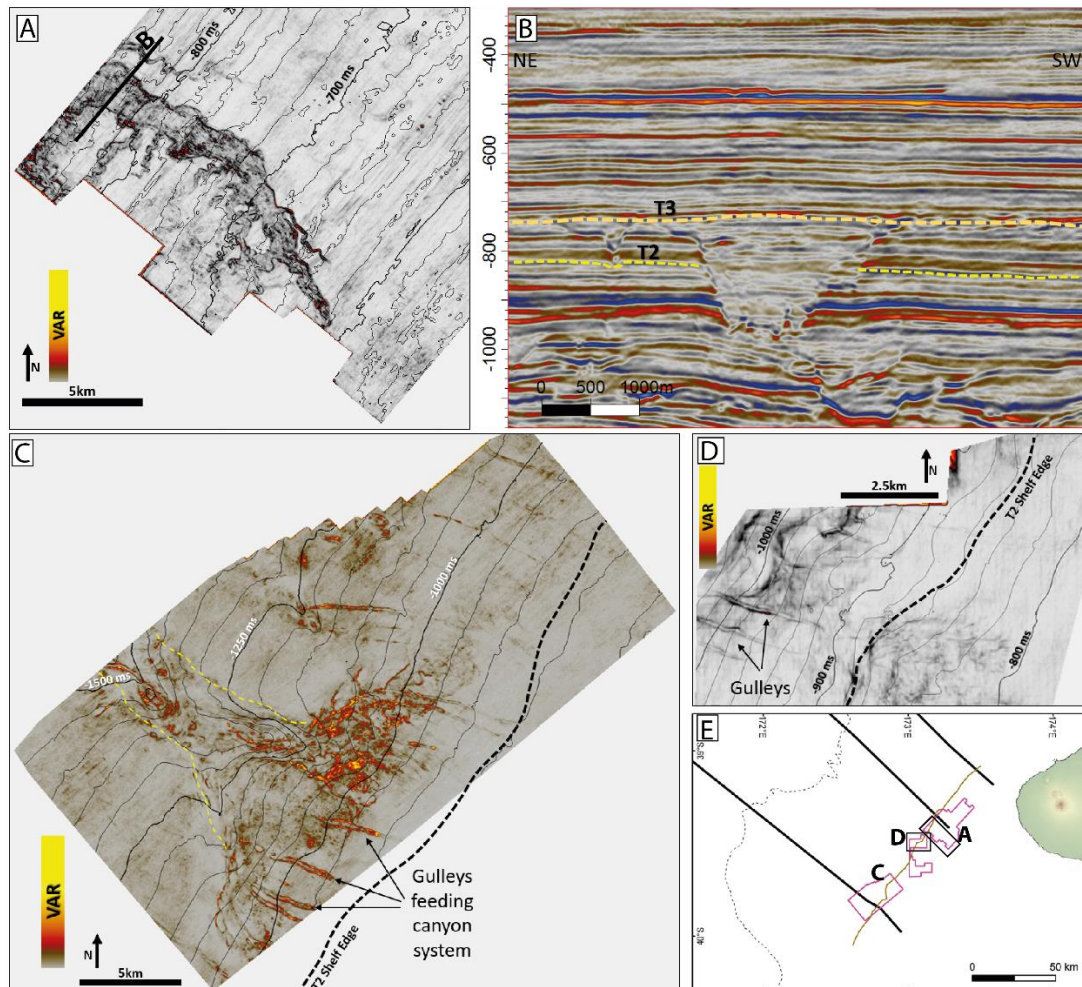


Figure 4.16 Shelf and slope geomorphology in Unit B.

A) and B) Variance extraction displayed on surface T3 between T2-T3 in the Tui 3D survey showing an incised valley, 2 km wide and 200 ms deep, cutting across the shelf; C) Variance extraction from Hector 3D showing gulleys feeding into a larger canyon system (dashed yellow lines) on surface T2; D) Matuku 3D slope gulleys; E) Location of surveys with regional context to hero lines and T2 shelf edge rollover.

Stratigraphy in the south has been tilted, giving the appearance of a descending trajectory throughout Unit C. When flattened to a palaeo-horizontal datum, however, minor aggradation and a flat to rising trajectory are apparent. The events causing the tilted stratigraphy are discussed further in section 4.5.1. Flat trajectories are also observed along the margin throughout this interval (Figure 4.14; Table 4.1), suggesting that sediment supply outpaced accommodation generation ($A/S \ll 1$).

Lithology information from well Kiwa-1 (Appendix-1) shows slope facies with a serrate gamma ray motif and overall coarsening upward profile, with mud logs showing an increasing % of sand toward the top of the unit in an outer shelf setting. This is also coincident with increased content of bioclastic limestones and minor amounts of coal. Further north in well Taranga-1 (Appendix-1), a coarsening upward gamma ray profile

up to mid-Unit C (~1,100 MDkb) is followed by a sharp increase in gamma ray, decrease in sand % in the mudlog and a serrate shallowing upward gamma trend to the top of the unit. In well Tane-1 (Appendix-1) show a serrate fining upward trend with a corresponding decreasing marl content interpreted to represent increased siliciclastic input to the outer shelf. Further north, between the central and northern composite lines, a north directed drainage network is evident in the Kokako 3D survey (Figure 4.17). This drainage network is set approximately 6 km shoreward of the T4 shelf rollover and is oriented parallel to the rollover.

Additionally, from T3 to T7, a gradual change from the large network of deep-water channels in Units A and B, to a smaller network of channels is observed.

Several step-like bedforms are observed in the bottomsets of the Central Composite section. These bedforms occur in a base of slope position and extend approximately 25 km across the basin floor. They have been interpreted as sediment waves and resemble features mapped by Shumaker et al. (2017) in late Miocene clinoforms of the Taranaki Basin and other locations such as the Var ridge (Migeon et al., 2001) and the Selvage field in the NE Atlantic ocean (Wynn et al., 2000). Wavelengths range from 340 m – 1,100 m with heights of <10 m to 19 m (although resolution of the seismic data biases measurements to waves with heights of 10 m or more). Wave crests are aligned parallel to the margin (as confidently as can be confirmed from 2D seismic) suggesting formation by downslope currents. These features are observed primarily between the central and northern composite lines (although in the north they have been disturbed by later mass wasting processes). No waves were observed in the region of the southern composite line. The significance of these waves is discussed further below.

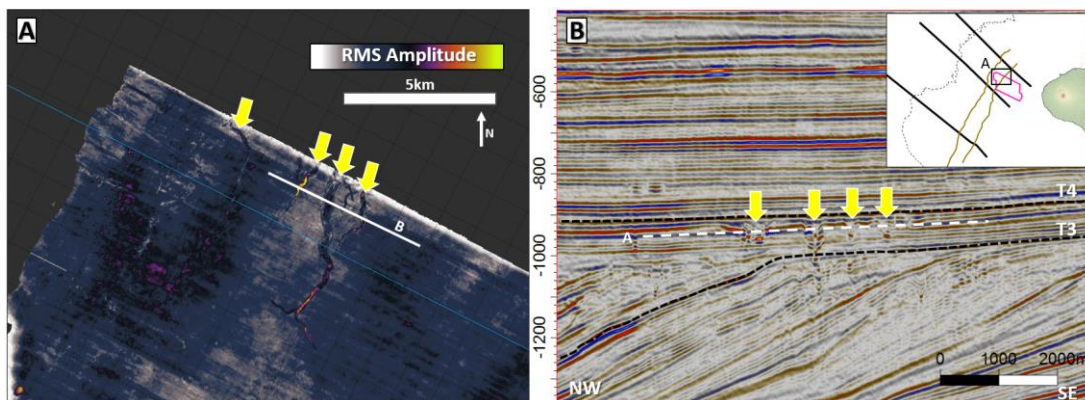


Figure 4.17 Shelf geomorphology in Unit C.

A) RMS amplitude extracted along horizon between T3-T4 showing north directed drainage in Kokako 3D and B) Inline 1052 showing with inset showing bero lines and T3 and 4 shelf margins. Channels annotated by yellow arrows in A & B.

4.4.1.4 Unit D – T4 to T5

Unit D is bounded at its base by T4 and top by T5 and spans approximately 0.4 Ma (2.4 to 2.0 Ma). Surface T4 represents the Pliocene – Pleistocene boundary and represents a significant change in the progradational nature of the GFF across the Western Stable Platform. Unit D shows virtually no progradation in the south but up to 11 km of progradation is observed on the central composite line along with maximum thicknesses of up to 530 ms (Figure 4.13; Table 4.1; Figure 4.11D). Much of the stratigraphy in the north has been removed by mass wasting during deposition of Unit E (Figure 4.18). Flat shelf edge trajectories and strongly progradational nature of the clinofolds on the northern and central composite sections suggest that sediment supply strongly outpaced accommodation generation ($A/S \ll 1$), whilst in the south a steeply rising trajectory is apparent (Figure 4.14; Table 4.1). This unit marks a significant change along the basin margin as progradation became almost entirely focused in the north of the Western Stable Platform whilst the south was starved of sediment. On the outer WSP in a basin floor setting, well Tane-1 shows a fining upward serrate gamma trend entirely of mudstone. Well Taranga-1 penetrates Unit D in a mid-shelf position and shows a serrate gamma profile dominated by mud with up to 10% sand.

Further occurrences of sediment waves are observed in a lower slope to basin floor environment with wavelengths of 650 m to 1190 m and wave heights of 10m to 17 m. As in Unit C, no waves were observed in the vicinity of the southern composite line.

4.4.1.5 Unit E – T5 to T6

Unit E is bounded at its base by T5 and top by T6 and spans approximately 0.5 Ma (2 – 1.5 Ma). This unit shows continued progradation on northern and central composite lines (up to 13 km), with little to no progradation in the south. Maximum thicknesses up to 600 ms are observed in the northern depocentre with little to no accumulation in the south (Figure 4.11E).

The shelf rollover remained essentially stationary in the south, whilst on the central and northern composite lines a flat to slightly rising shelf edge trajectory is recorded (Figure 4.14; Table 4.1), suggesting sediment supply was sufficient to outpace accommodation generation.

On the central composite line, Anell and Midtkandal (2017) also studied the succession between Units B to E (their clinoforms B1 to 14), recognising the same trends in accommodation and sediment supply based on the shelf edge trajectory.

The northern focus of progradation led to a more lobate orientation of the shelf margin. Accompanying the rapid progradation was a significant increase in the amount of slope incision with slope canyon systems observed along the length of the northern depocentre of the WSP (Figure 4.18 & Figure 4.19). Rapid progradation and aggradation gave rise to an unstable shelf margin, resulting in mass wasting (Figure 4.18).

Failure of the slope was to the north (Figure 4.18 & Figure 4.11E), which transported blocks of slope material up to 10 km in length. Figure 4.18 shows the MTD is comprised of sediment waves. Subsequent healing of the accommodation generated by this mass wasting is also dominated by an extensive sediment wave field with crests oriented parallel to the shelf margin, wavelengths of 1390 m to 2430 m and heights of 15 m to 32 m. Prior to the mass wasting event, sediment waves occurred in comparably thin sheets in the base of slope and proximal basin floor. Following this event however, sediment waves become prominent features on the mid slope to basin floor environments throughout Unit E and F (Figure 4.8, Figure 4.9 and Figure 4.21F).

Well Taranga-1 (Appendix-1) penetrates a shelf succession with an overall shallowing upward trend into Unit F where the logs end. Mud logs show a succession dominated by mudstone with occasional sandy and carbonate rich intervals. A serrate fining upward gamma ray trend, with a sharp drop in gamma approaching the T6 surface is interpreted to represent a deepening of the shelf, consistent with seismic interpretations for Unit E.

4.4.1.6 Unit F – T6 to T7

Unit F is bounded at its base by T6 and top by T7 and spans approximately 0.3Ma (1.5 – 1.2 Ma). Progradation remained focused in the northern portion of the study area where the margin prograded approximately 10.5 km in this time interval with only minor progradation in the south (< 1 km). This resulted in a progressively more N-S oriented shelf margin (Figure 4.6). Maximum thicknesses of up to 850 ms are recorded in the north, whilst resumption of sedimentation in the southern of the WSP resulted in accumulations up to 230ms (Figure 4.11F).

Despite an increase in aggradation, sedimentation in the north of the WSP was sufficiently high to drive progradation and sustained bypass throughout Unit F (Figure 4.19). From

T6 to T7, slope stratigraphy in the vicinity of the northern and central composite lines is dominated by sediment wave accumulations (Figure 4.8, Figure 4.9 and Figure 4.21F), with wavelengths of 830 m to 2400 m and heights of 13 m to 32 m. Further downslope, much of the stratigraphy was removed by subsequent collapse of the slope during Unit H (Figure 4.21F).

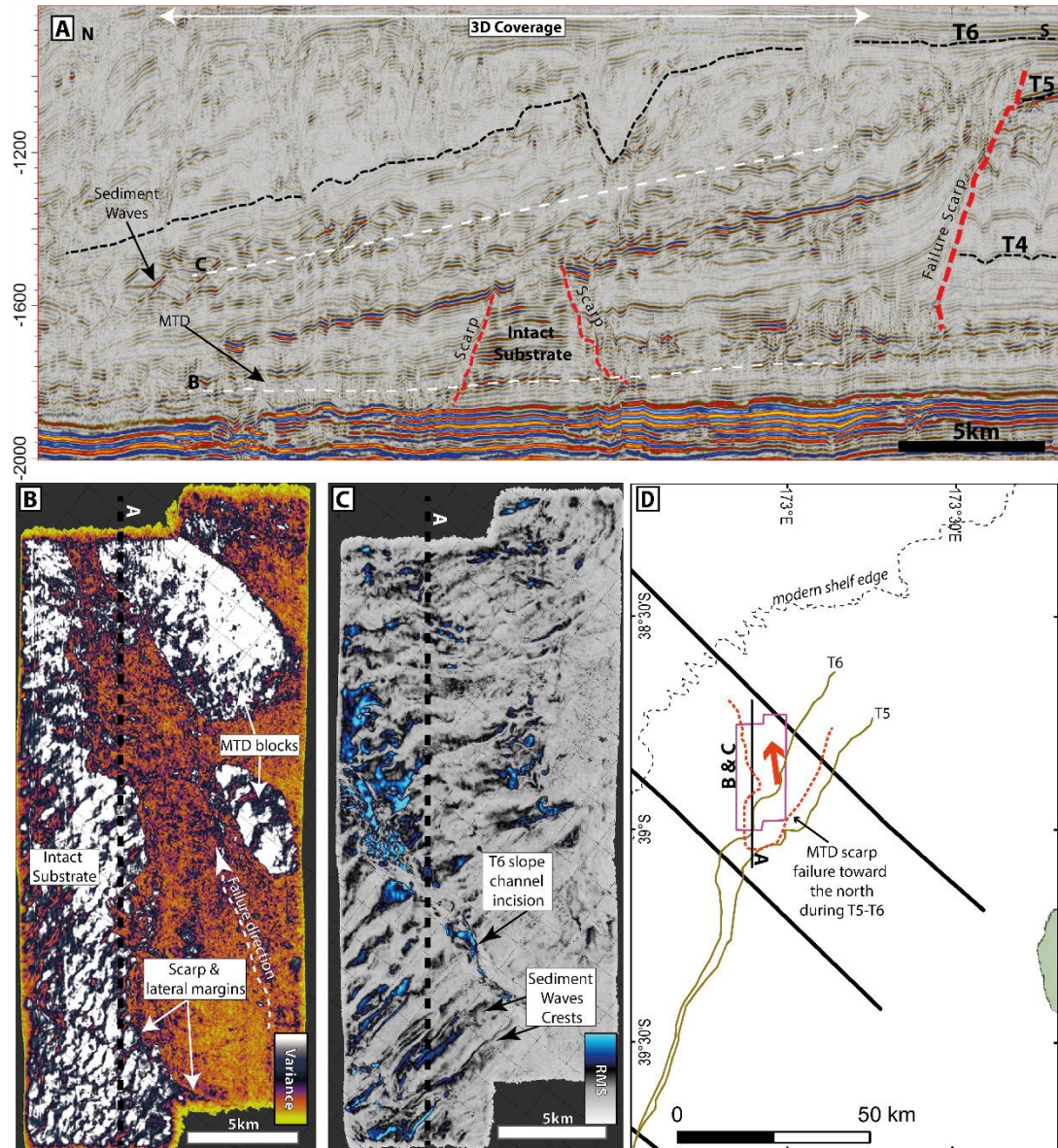


Figure 4.18 Slope failure during Unit E.

A) 2D seismic line showing MTD failure during T5 - T6 and subsequent infill of slope accommodation.
 B) Variance extraction through MTD in Karoro 3D showing north directed failure of the slope; C) RMS amplitude extraction showing sediment wave crests forming parallel to the shelf break and later incision by a T6 slope canyon.

Canyon systems became nested in the slope stratigraphy during Unit F in the north of the study area and persist to the present day (Figure 4.19). Moving up stratigraphy, these canyon systems show a dominant migration from southwest to northeast. Similar

migration of canyon systems has also been observed offshore Brazil (Viana et al., 2002, 1999), the South China Sea (Zhu et al., 2010), in the Otway Basin in Australia (Leach and Wallace, 2001) and offshore Gabon (Rasmussen, 1994). In all these examples, migration is attributed to the action of bottom currents sweeping sediment into canyon margins from a consistent direction resulting in canyon migration in the same direction as current flow. Consequently, a current sweeping from southwest to northeast can be inferred as the likely cause of canyon migration along the Western Stable Platform. The Westland Current is a surface current flowing from southeast to northwest (Carter and Heath, 1975; Chiswell et al., 2015; Heath, 1985), however little has been reported about the offshore extents, stratification, velocity and depths to which it is in effect.

The inference that a northeast directed bottom current is in action along the margin of the Western Stable Platform is at odds with the observed direction of sediment wave crests, which are oriented parallel to the shelf margin, suggests downslope processes are dominant (Figure 4.18; Shumaker et al. (2017)). In a scenario where along slope and downslope processes are interacting, wave crests would be expected to be oblique to the margin. Given the limited coverage of 3D seismic data and paucity of dip oriented 2D lines in this part of the WSP, it is plausible that waves are at an oblique angle to the margin, but we cannot image them optimally.

The shelf rollover trajectory between T6 to T7 is moderate to steeply rising along the basin margin (Figure 4.14; Table 4.1). On northern and central composite lines, this can be split into an early progradation to aggradation event, followed by backstepping of the shelf margin by up to 3 km (Figure 4.8 & Figure 4.9 & Figure 4.20). This event is also recognised by Anell and Midtkandal (2017), with T7 of this study approximately equivalent to their M2 surface. In the south of the WSP a sharply rising trajectory reflects the same event without a shoreward shift in the position of the shelf (Figure 4.7). The bulk aggradational nature across Unit F suggests a period where the A/S ratio shifted in favour of accommodation with and $A/S \sim 1$.

4.4.1.7 Unit G – T7 to T8

Unit G is bounded at its base by T7 and top by T8 and spans approximately 0.58 Ma (1.2 – 0.68 Ma). As detailed above, T7 is interpreted to represent a maximum flooding surface across the basin. On the central composite line, T7 is approximately equivalent to M2 of Anell and Midtkandal (2017). Following this event, we see a significant change in the focus of progradation across the Western Stable Platform, whereby progradation was

concentrated in the south of the study area where the margin prograded ~37 km in this time period, with limited progradation on the central and northern lines of 4-6 km (Figure 4.13; Table 4.1). This significant change in the focus of progradation resulted in accumulations up to 1120 ms thick in the southern depocentre (Figure 4.12D). Additionally, delta scale clinoforms are observed prograding from east to west across the flooded T7 shelf of the northern WSP (Figure 4.20).

The shelf rollover of surface T7 strikes approximately north-northeast, with a slight prominence in the northern depocentre (Figure 4.6). By T8, however, the significant increase in progradation in the south led to the development of a shelf margin with two distinct “lobes”/prominences across the Western Stable Platform (Figure 4.12A&B, Figure 4.6). Accompanying the major change in the focus of progradation, sediment waves are no prominent in the slope stratigraphy throughout Unit G along the WSP. It is worth noting, however that much of the slope stratigraphy has been removed by collapse of the margin during Unit H. The change in progradation is also observed in the significant along margin variations in shelf rollover trajectories; with flat trajectories in the south becoming steeper on central and northern composite lines. This suggests an increasing A/S ratio from south to north, with progressively higher shelf accommodation.

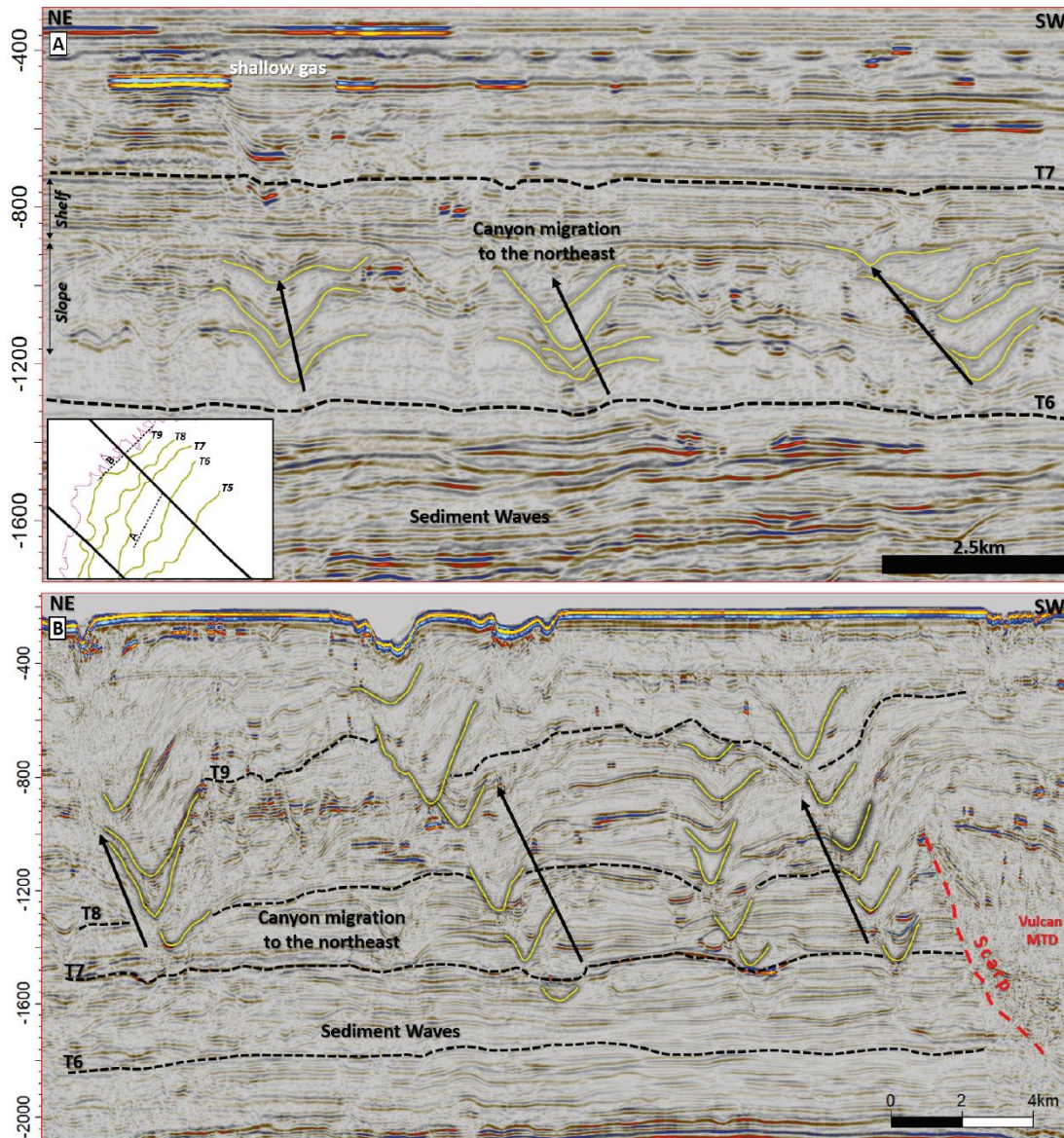


Figure 4.19 Migration of slope canyons.

A) Arbitrary line through the Karoro 3D survey parallel to the shelf margin showing north-eastward migration of the shelf margin through unit F. B) Strike section through the slope stratigraphy showing a dominantly north-eastward migration of nested slope canyons.

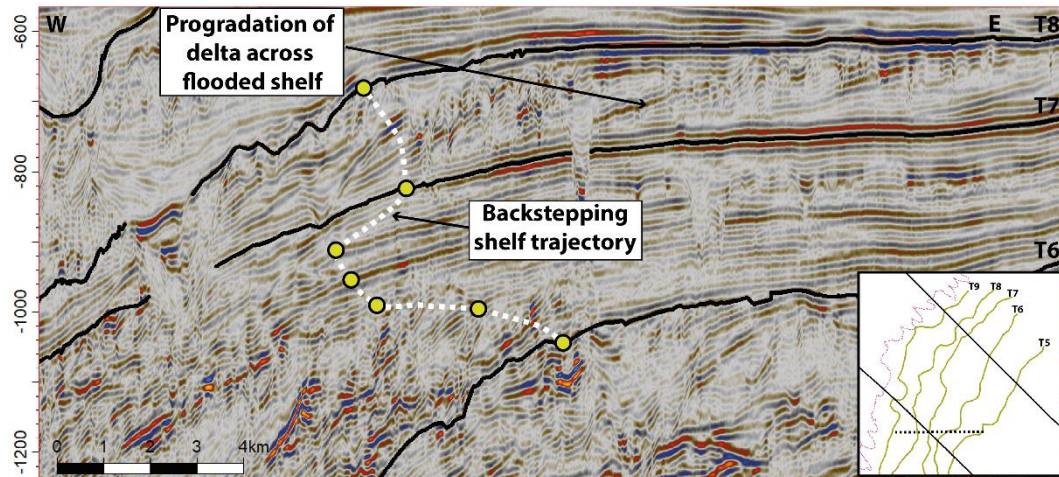


Figure 4.20 Backstepping shelf margin.

Backstepping of the shelf margin in late T7 inferred to represent a maximum flooding surface. This is subsequently overlain by delta clinoforms prograding across the shelf in Unit G. Section location dashed as line in inset map relative to central and northern composite sections.

In the southern depocentre, we no longer see evidence of sediment bypassing the Western Stable Platform (as described earlier in Unit A), with no significant basin floor channels observed in post T7 stratigraphy. Rather than bypassing to deepwater regions of the basin, sediment prograded rapidly to the northwest, infilling basin floor accommodation between the Challenger Plateau and the New Zealand landmass (Figure 4.7). Clinoforms deposited in the south of the basin during Unit G show degraded character and show a curious high amplitude seismic facies deposited in an apparently cyclical fashion (Figure 4.7); a pattern not observed further north in the basin. These features are explored in greater detail in Chapter 5. Anell and Midtkandal (2017) carried out a quantitative analysis of clinoform geometries in the south of the basin, mapping 10 clinoform surfaces (C1 to C10) equivalent to Unit G and H of this study. Their results agree with this study that suggests units in the south formed in a setting with limited shelf accommodation and high sediment supply.

4.4.1.8 Unit H – T8 to T9

Unit H is bounded at its base by T8 and top by T9 and spans approximately 0.43 Ma (0.621 – 0.191Ma). Progradation remained focused in the south, where the margin prograded approximately 33 km in this interval with thicknesses up to 1050 ms (Figure 4.12, Figure 4.13 & Table 4.1). Deposition in the south was dominated by cyclical sets of alternating high and low amplitude clinoforms (Figure 4.7), these are discussed in greater detail in Chapter 5. The shelf edge trajectory between T8 to T9 is flat on both south and central lines, with a slightly rising trajectory in the north (Figure 4.14; Table 4.1), suggesting increasing A/S ratio to the north. Anell and Midtkandal (2017) carried out a

quantitative analysis of clinoform geometries in the south of the basin, mapping 10 clinoform surfaces (C1 to C10) equivalent to Unit G and H of this study. Their results agree with this study that suggests units in the south formed in a setting with limited shelf accommodation and high sediment supply.

In the northern depocentre, much of the stratigraphy was removed by a large slope failure (MTD 1 of Omeru et al. (2016), named here as the Vulcan MTD. The resulting mass transport deposit was exported to the deepwater Taranaki Basin 225 km from the headwall scarp (Figure 4.8 and Figure 4.21A), cannibalising older stratigraphy as it moved basinward. The flow of this MTD was partially confined on its western flank by the Challenger Plateau and to the north by the Aotea seamount (Figure 4.21) and has a volume of approximately 2,600 km³ (Omeru et al., 2016a). The headwall scarp of the Vulcan MTD trends NE, parallel to the shelf margin, extends for 80 km and is up to 1200 ms in height (Figure 4.21F). As the shelf collapsed and the MTD flowed to the north, significant accommodation was generated on the slope and basin floor in the immediate vicinity of the scarp. The Vulcan 3D survey (Figure 4.21 C & D) reveals that although MTD transport was dominantly to the northwest, local collapse also occurred in a southerly direction, likely due to the destabilising effect of the removal of buttressing sediments and generation of significant accommodation.

Following the extensive collapse of the shelf margin late in Unit H, sediment was funnelled into the newly generated accommodation via canyon systems between the north and south depocentres (Figure 4.22) throughout late Unit H and into Unit I. These canyon systems are deeply incised into the margin by up to 550 ms, making correlation between north and south depocentres difficult. Omeru et al. (2016) attributed the collapse of margin to over-steepened clinoforms (Figure 4.8 and Figure 4.21F), however Kroeger et al. (2017) suggest that fluid flow (hydrate or microbial gas) and overpressure in the slope succession of the Giant Foresets Formation may also have contributed to collapse of the margin. This is in line with observations by Wolinsky and Pratson (2007), who calculated that overpressure in the shallow subsurface along fine grained continental margins is a common contributor to submarine mass failures. Similar processes have been attributed to slope failures on New Zealand's east coast (Mountjoy et al., 2014) and offshore Gabon (Sultan et al., 2004), offshore US Atlantic margin (Hill et al., 2004) and offshore Vancouver Island (López et al., 2010).

No occurrences of sediment waves were observed in the northern portion of the WSP, however, waves of wavelength 1000 m to 1900 m with heights of 13 m to 22 m are evident on in the southern region of the study area.

4.4.1.9 Unit I – T9 to Seabed

Unit I is bounded at its base by T9 and top by the seabed and spans approximately 191 kyr (0.191 – 0 Ma). In this time period, the highest amount of progradation was recorded on the central composite line (~ 8 km), with lowest values on the southern line (Table 4.1). Thicknesses up to 950 ms are also focused in the central portion of the WSP (Figure 4.12F). Shelf rollover trajectories are flat in the south but steeply rising in the north (Figure 4.14; Table 4.1), highlighting a stark lateral contrast in accommodation at the shelf edge.

In this interval, sedimentation was focused on the central and northern portions of the Western Stable Platform, which is interpreted to reflect infill of the significant amount of accommodation generated by slope collapse described in Unit H. The heavily incised corridor separating north and south depocentres continues through this interval and is expressed in the present-day seafloor bathymetry (Figure 4.22). Additionally, lower progradation rates in the south may reflect the effects of the challenger plateau, whereby the progradation is gradually deflected to the northeast into areas of higher accommodation (Chapter 5).

Sediment waves are once again prominent in the vicinity of the northern and central composite lines where wavelengths of 930 m to 1475 m and heights of 15 m to 25 m are recorded. Work in Chapter 6 suggests sediment waves in this interval are related to overspill of turbidity currents from submarine canyons on the slope.

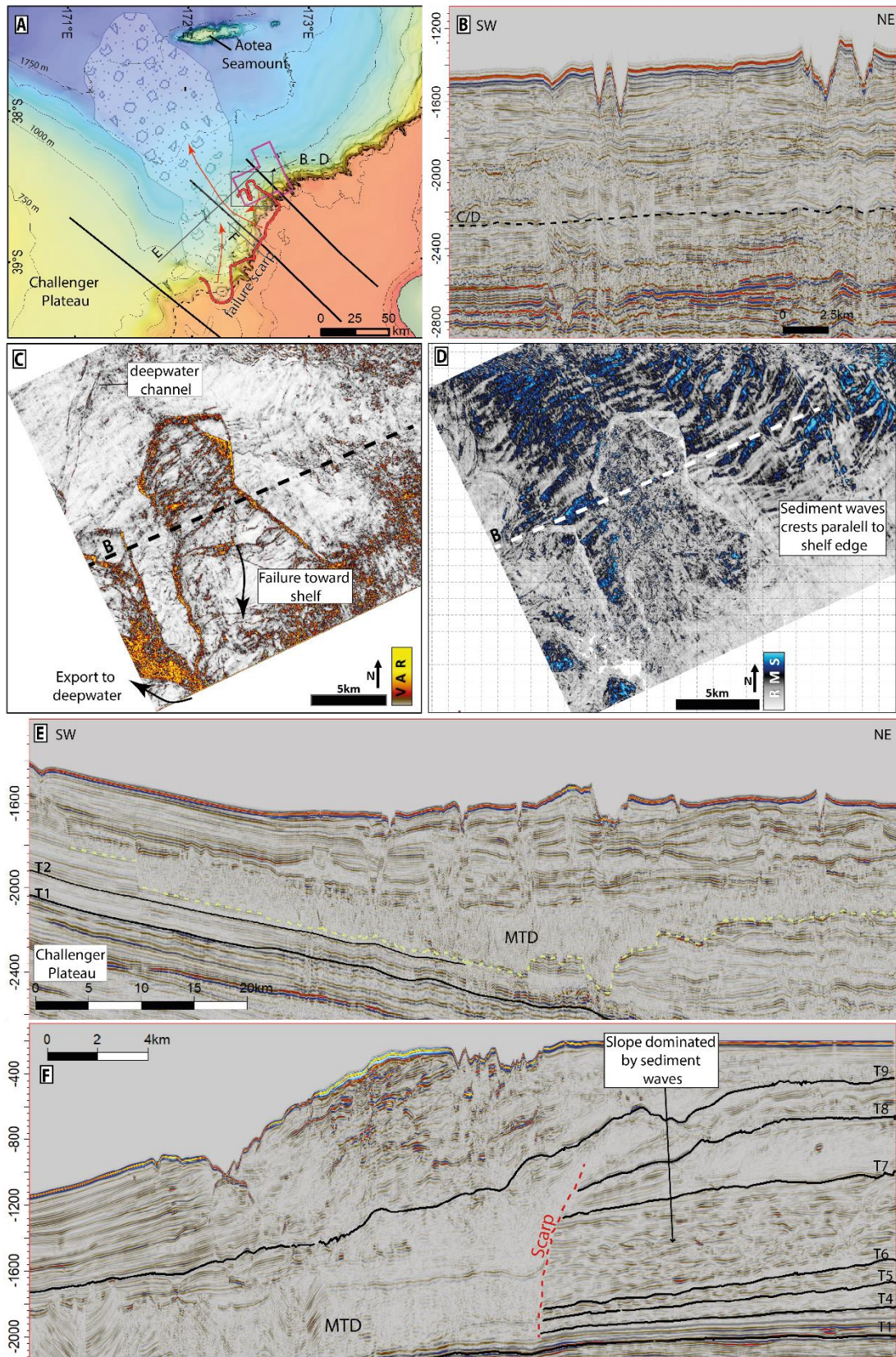


Figure 4.21 Slope collapse during unit H.

A) Mass transport deposit created by slope collapse during T8- T9. B) Crossline through the Vulcan 3D survey showing incipient collapse of slope. C) Variance extraction along horizon shown in B showing outline of failure. D) RMS amplitude extraction along surface highlighted in B showing sediment wave crests oriented parallel to the shelf margin. E) Regional 2D seismic line DTB01-24 showing the MTD

cannibalising underlying stratigraphy and abutting against the Challenger Plateau. F) Dip section showing Vulcan scarp, MTD and initial substrate slope dominated by sediment waves.

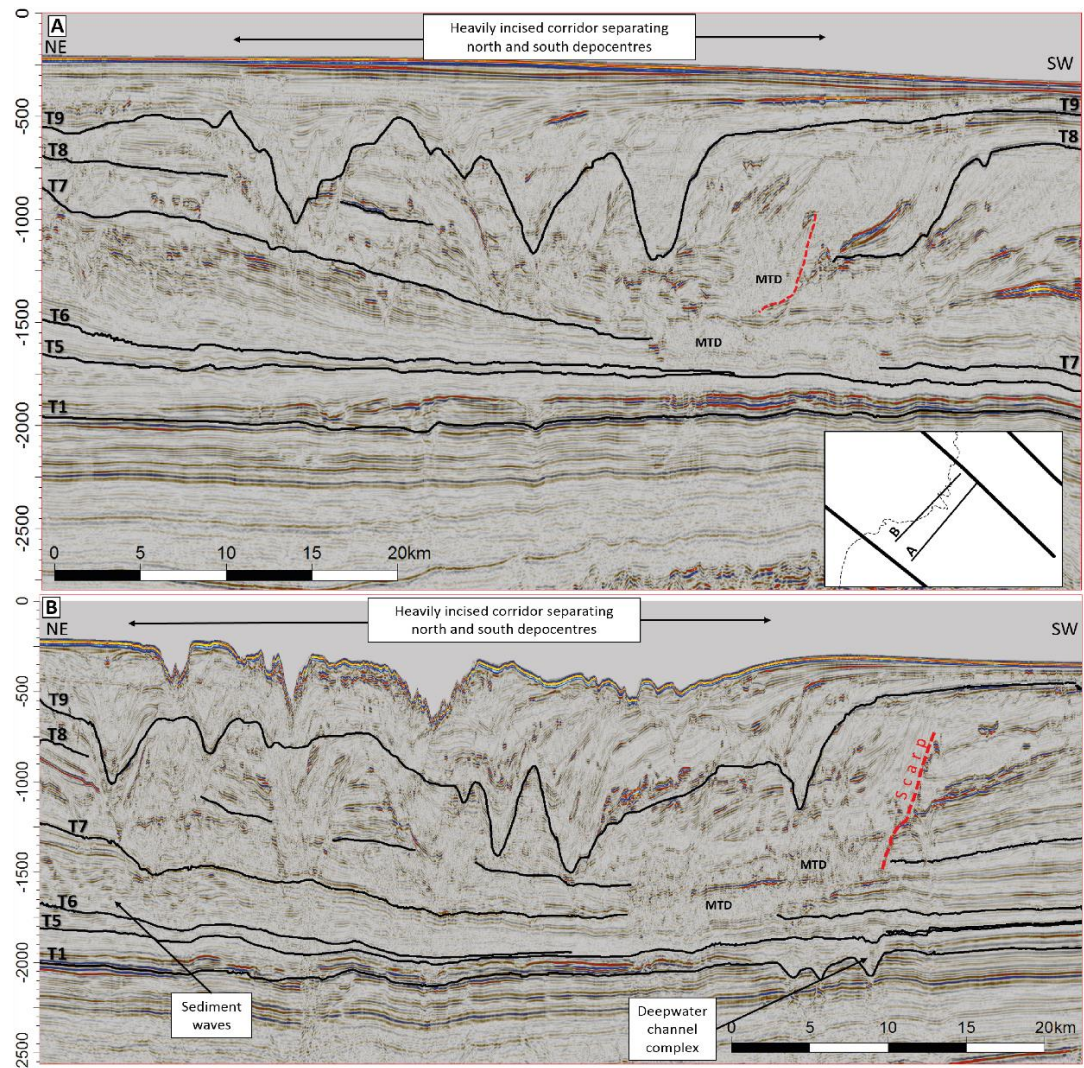


Figure 4.22 Heavily incised corridor.

Strike section DTB01-38 (A) & DTB01-32 (B) showing a heavily incised corridor separating north and south depocentres, correlations of regional surfaces across this corridor are tenuous due to mass transport deposits and deeply incisive slope canyons.

4.4.2 Quantitative Characterisation of Progradation

Measurements of clinoform geometries were made on the bounding surfaces of the seismic sequences in order to characterise and compare the Giant Foresets Formation to other examples. This section focuses on characterising trends evident in the dataset presented in Table 4.1 and graphically in Figure 4.13. In some cases, it was not possible to measure the clinoform heights due to modification by mass transport deposits (e.g. T4/T5 on the northern section).

Foreset Heights

Measurements of foreset heights along the margin (Figure 4.13; Table 4.1) range from 525 m to 1328 m, with the highest values consistently measured on the Northern Composite section (Figure 4.9). With the exception of T6, clinoforms on the southern composite section were the smallest. This suggests that there was less accommodation in the south than in the north and is interpreted to be a result of the shallower bathymetry of the Challenger Plateau, upon which the clinoforms in the south prograded. The overall trend of increasing foreset heights with time observed in the dataset match the trend reported by Baur (2012).

The highest clinoforms are associated with the T9 surface on the northern composite line, which may indicate that this surface has undergone less compaction than older measured clinoforms. However, this effect may be minimal as previous studies in the Giant Foresets Formation suggested a difference of less than 5% between decompacted and undecompacked geometries (Salazar et al., 2016).

Foreset Gradient

Foreset gradients range from 0.9° to 3.5°, with clinoforms on the southern composite line generally having the shallowest gradient (with the exception of T3 and T4). A general steepening from T1-T3 can be observed across all lines (Figure 4.13; Table 4.1), followed by a decreasing trend until T5 (or T7 in the southern depocentre), followed by a general increasing gradient to the modern day.

Progradation & Aggradation

In the studied Pliocene to recent interval, the margin prograded between 85 km and 116 km to the modern day shelf edge (Figure 4.13; Table 4.1), with the highest amounts of progradation recorded in the southern regions of the WSP. In this part of the basin, progradation effectively halted between T4 and T7 (units D-F). Throughout this southern

hiatus, progradation was focused further north on the WSP. Following the southern hiatus, a general increasing trend in progradation is observed in the south (Figure 4.13).

The total amount of aggradation along the margin ranges from 944 to 1068 m (Figure 4.13; Table 4.1), with highest values of cumulative aggradation on the southern and central composite lines.

Measured progradation and aggradation values were also converted to progradation and aggradation rates. In the studied Pliocene to recent interval, average progradation rates of 16 to 22 m/kyr are calculated, with average aggradation rates of 177 to 200 m/Myr. Using the age model proposed in Figure 4.5, more detailed progradation and aggradation rates can also be calculated (Figure 4.13 & Table 4.1), although these may contain inaccuracies inherited from the unverified age model. Nonetheless, conversion to progradation and aggradation rates is beneficial to further classify the nature of the Giant Foresets Formation and highlight along margin variations. It can also provide indications on the factors controlling this lateral variability (sediment supply, eustasy, tectonics, etc).

Highest progradation rates of up to 77 m/kyr are recorded in the south of the WSP but high lateral and temporal variability exists in the dataset (Figure 4.13 & Table 4.1). Aggradation rates show similar variability with rates exceeding 1,000 m/Myr. The higher amount of progradation in the south is attributed to clinoforms prograding into a shallower bathymetry (the Challenger Plateau), when compared clinoforms further north.

A reduction in progradation rate is observed in Unit I and is accompanied by an increase in clinoform height. Both are attributed to clinoforms in the southern WSP being gradually deflected north as they impinged on the Challenger Plateau. This effect resulted in the margin prograding into deeper waters, thus resulting in increased clinoform heights and a corresponding reduction in progradation rate as sediment must fill more accommodation in order to prograde. A more detailed study of clinoforms in the southern WSP shows the same process where clinoform progradation is deflected incrementally toward the deepwater Taranaki Basin (Chapter 5).

4.5 Discussion

4.5.1 Shelf Edge vs. Continental Margin Scale Clinoforms

As detailed in Chapter 1, clinoforms occur at different scales and settings throughout a basin and can be classified based on a numerous geometric parameters such as foreset height, slope gradient, rollover trajectory and progradation rates (Patruno and Helland-Hansen, 2018).

Shelf edge clinoforms typically rollover at water depth of 60 m to 426 m, have foreset heights of 97 m – 300 m, average slope gradients of 0.6° to 4.8° , rollover trajectories of -0.4° to $+2.4^{\circ}$ and progradation rates of tens of m/kyr. Continental margin scale clinoforms, however, typically rollover at water depths of between 550 m – 1770 m, have foreset heights of 590 m – 2600 m, average slope gradients of 1.1° - 12.5° , rollover trajectories of $+0.9^{\circ}$ - $+49^{\circ}$ and low progradation rates of less than 10 m/kyr (Patruno et al., 2015a; Patruno and Helland-Hansen, 2018). An additional criterion for differentiating these two classes of clinoform is the tectonic setting, whereby the relief of continental margin scale clinoforms is formed by geodynamic processes on major structural elements such as ocean – continent boundaries (Patruno and Helland-Hansen, 2018; R. Steel and Olsen, 2002).

Alternatively, Carvajal et al., (2009) recognised two broad classes of clinoforms found at moderately deep and very deep-water margins. Moderately deep-water margins have clinoforms <1000 m high with progradation rates of < 60m/kyr and aggradation rates of <270 m/Myr. Such clinoforms fill their basins rapidly and display more progradational architectures. Very deep-water margins have clinoforms >1000m in height and have progradation rates of <40 km/kyr and aggradation rates of < 2500 m/Myr. Clinoforms along very deep-water margins infill their basins more slowly.

Pliocene to recent clinoforms on the Western Stable Platform measured in this study have relief of 525 m to 1328 m, average foreset gradients of 0.9° to 3.5° , rollover trajectories of $+0.1^{\circ}$ to $+46^{\circ}$, progradation rates of <1 to 77 m/kyr and aggradation rates of 12 to 1725 m/Myr (Table 4.2) or time averaged values for the Pliocene to recent succession of 16 to 22 m/kyr and 177 to 200 m/Myr. Clinoforms in this study span classification criteria in both classification schemes (Table 4.2), sharing characteristics of both continental and shelf margin scale clinoforms (sensu Patruno and Helland-Hansen (2018) or moderately deep and very deep water clinoforms (sensu Carvajal et al., 2009).

Table 4.2 Comparison of clinoform classification characteristics to this study.

	<i>Patruño and Helland-Hansen (2018)</i>		<i>Carvajal et al. (2009)</i>		This study
	Continental Margin	Shelf Edge	Mod. Deep Water	Very Deep Water	
Foreset Height (m)	590 to 2570 m	97 to 300 m	< 1000 m	> 1000 m	525 to 1328 m
Foreset Gradient (°)	1.1 to 12.5°	0.6 to 4.8°	-	-	0.9 to 3.5°
Rollover Trajectory (°)	+0.9 to +49°	-0.4 to +2.4°	-	-	+0.1 to +46 °
Progradation Rate (m/kyr)	< 10	< 100	< 60	< 40	Up to 77

Based on forest height and rollover trajectory, the GFF could be classified as continental margin scale clinoforms, whilst the average foreset gradient and progradation rate promotes classification as a shelf edge clinoform system.

Patruño and Helland-Hansen (2018), stipulate that in order for a clinoform to be classified as continental margin in scale it should be associated with large scale geodynamic processes such as, for example, those found at the boundary between continental and oceanic crust.

In terms of basin setting, the GFF was deposited in a retro-arc foreland setting; accommodation was associated with convergence of the Australian and Pacific plates during the late Oligocene and Miocene (Baur et al., 2014; Holt and Stern, 1991, 1994; King and Thrasher, 1992; Pilaar and Wakefield, 1978; Stern and Davey, 1990; Stern and Holt, 1994). Rapid tectonic subsidence of 1.2 to 2.0 km occurred between approximately 35 to 25 Ma (Figure 4.23), and is suggested to be associated with upper mantle processes coincident with inception of the nearby Australia-Pacific plate boundary (Baur et al., 2014; Baur, 2012). This event occurred on a regional scale, affecting an area of up to 500 km along strike and over 2000 km in length, extending into the Taranaki Basin and beyond to the New Caledonia Trough (Figure 4.1).

Additional tectonic subsidence also occurred along the eastern margin of the Taranaki Basin, where compression along large crustal faults resulted in creation of foredeep accommodation. Subsidence associated with this event was, however, localised to within ~150 km of the thrust front and caused limited tectonic subsidence on the WSP (King and Thrasher, 1992; Stagpoole and Nicol, 2008). Foreland accommodation was filled by a prograding wedge of sediment sourced from hinterland uplift and erosion (King and Thrasher, 1996) and by the end of the Miocene (i.e. base of the GFF), paleobathymetry on the basin floor was in the region of 0.8 to 1.4 km (Baur, 2012; Holt and Stern, 1991). The GFF represents the ongoing filling of this accommodation as the margin prograded

beyond the foredeep and into regional accommodation generated along the margin between ~35-25 Ma.

Hence, we can propose that whilst the GFF did not form directly at a continental – oceanic interface, the regional scale geodynamic processes responsible for generating the accommodation into which the GFF has prograded, are associated with plate boundary processes and thus could satisfy the criteria for classification as continental margin scale clinoforms, albeit with much shallower rollover depths than stipulated by Patruno and Helland-Hansen (2018). This suggests the criteria for differentiating shelf edge and continental margin scale clinoforms may require further refinement.

4.5.2 Controls on GFF shelf margin architecture

Results detailed in Figure 4.13 and Table 4.1 indicate along strike variations in the shelf margin architecture and progradational history of the GFF. Such along strike variability has been documented in other systems (e.g. Fulthorpe and Austin, 2008; Madof et al., 2016; Martinsen and Helland-Hansen, 1995) and can be explored in the context of variations in the ratio of accommodation generation rate to sediment supply rate (A/S). This section discusses factors affecting sediment supply to the basin and those governing accommodation generation such as eustasy, tectonic subsidence, sediment loading and compaction.

4.5.2.1 Accommodation

In a marine basin, accommodation is primarily controlled by the interplay of eustasy and subsidence (Jervey, 1988; Posamentier et al., 1981; Posamentier and Vail, 1988). Subsidence is generated primarily by tectonic processes, with contributions from sediment loading, compaction and mass wasting. Each of these factors is discussed below in the context of their significance in controlling the along margin variations observed in the Giant Foresets Formation.

Seismic sequences identified in this study span ~0.2 to 1.2 Ma, consequently, any factors responsible for causing observed along strike variability in the seismic stratigraphy should take place over a similar time scale.

Eustasy

Global eustatic fluctuations in the Pliocene and Pleistocene have been well studied (Lisiecki and Raymo, 2005; Miller, 2005; Miller et al., 2011) and can be correlated to progradational patterns (e.g. Kertznus and Kneller, 2009). In the neighbouring Wanganui

Basin (Figure 4.2) integrated outcrop, seismic and borehole data have been used to describe a dominant 41 ky cyclicity in shelf deposits until approximately 1 Ma, after when an apparent 100 ky cyclicity became dominant (Abbott et al., 2005; Carter and Naish, 1998; Naish and Kamp, 1997; Naish et al., 2005; Saul et al., 1999).

Whilst higher order depositional cyclicity is apparent in seismic data in the Taranaki Basin and may be attributable to global eustasy (Chapter 5), it does not explain lateral variations in margin architecture described in this study as eustasy would have affected the margin as a whole. Additionally, the broad changes in margin architecture on the WSP occur on a longer timescale than those attributable to global eustatic fluctuations in the Pliocene and Pleistocene.

Sediment loading and compaction

Accommodation can be generated locally by emplacement of a body of sediment on the crust (e.g. Mississippi delta; Kuchar et al., 2018). The Giant Foresets Formation was deposited across the Western Stable Platform over approximately the last 5 million years and exhibits a positive free air gravity anomaly (Wood and Woodward, 2002). Studies by Holt and Stern (1991) have shown that this sedimentary load is regionally compensated by the crust and has induced little subsidence across the region. Subsidence plots in Figure 4.23 show an apparent uplift in the Plio-Pleistocene section; this is considered an artefact of the backstripping process which underestimates the regional flexural support for the rapidly deposited load and assumes that sediment compaction is complete (Baur et al., 2014). Compaction in the Taranaki Basin has been deemed insignificant in the interval of interest (Funnell et al., 1996), with as little as 5% difference between decompacted and undecompressed clinoform geometries (Salazar et al., 2016).

As sediment loading and compaction generate accommodation over a longer time period than the duration of the seismic sequences mapped in this study, they do not explain variations in along margin variations in A/S on the scale observed.

Tectonic Activity

The Taranaki Basin is located on active margin in a retro-arc foreland setting which has undergone localised back arc extension in the Northern and Central Grabens (Giba et al., 2012, 2010; Holt and Stern, 1991; King and Thrasher, 1992, 1996; Pilaar and Wakefield, 1978; Salazar et al., 2016; Stern and Holt, 1994). Seismic and well data for the Western Stable Platform show that this part of the basin has not undergone any back-arc extension but has remained tectonically quiescent since cessation of rifting in the early Palaeocene.

Accommodation on the WSP was not controlled by localised faulting, but rather larger-scale tectonic processes acting on the entire margin; as discussed above, the GFF prograded into accommodation generated between ~ 35 to 25 Ma by upper mantle geodynamic processes associated with the establishment of the Australia – Pacific plate boundary (Figure 4.23; Baur et al., 2014). By approximately 5 Ma, along margin variation in tectonic subsidence of ~ 1.15 km is evident between wells Kiwa-1 in the south and 96 km further north in Tane-1 (Figure 4.23). This is attributed to less subsidence having occurred on the fringes of the basement in proximity to the Challenger Plateau; whilst this provides a useful indication of where more accommodation was generated, it does not explain the lateral variations in how this accommodation was subsequently filled by the GFF.

Through the Plio-Pleistocene, aggradation values at the shelf rollover show that the Western Stable Platform has aggraded between 944 m and 1068 m throughout the Plio-Pleistocene, with an average aggradation rate of 177 to 200 m/Myr, with high variability in shorter term rates along the basin margin (Figure 4.13; Table 4.1).

In addition to active margin tectonics, lateral variability in aggradation rates along high relief margins can also be linked to accommodation generated in areas underlain by mobile substrates such as salt or shale (Carvajal et al., 2009). In these settings high volumes of sediment can be accommodated in localised depocentres, thus decreasing the sediment budget available to prograde the margin. In the case of the Taranaki Basin, there is no such underlying mobile substrate that created localised depocentres on the WSP.

4.5.2.2 Sediment Supply

Sediment supply has been postulated to be the main driver of shelf margin growth and can be related directly to the progradation rates (Carvajal et al., 2009; Gong et al., 2016). As detailed above, averaged Pliocene to recent aggradation rates of 16 to 22 m/kyr and up to 177 to 200 m/Myr are measured for the Giant Foresets Formation (Figure 4.13; Table 4.1); these values are consistent with those of a high supply margin (*sensu* Gong et al., 2016) detailed in Table 4.3.

In the Taranaki Basin, sediment was dominantly sourced from erosion of the uplifted Southern Alps (Hansen and Kamp, 2002; Kamp et al., 2004), with the highest exhumation rates exceeding 5 km/Myr along the west coast of South Island (Herman et al., 2013; Jiao et al., 2017; Koppes and Montgomery, 2009). The onset of Quaternary glaciations is likely

to have increased erosion rates in the Southern Alps (Jiao et al., 2017), however uplift, exhumation and erosion rates have been in steady state throughout glacial and interglacial cycles since approximately 1Ma (Batt et al., 2000; Herman et al., 2010). Sediment was interpreted to be delivered from the Southern Alps to the Taranaki Basin via a longshore drift cell (Beggs, 1990; King and Thrasher, 1996), although little work has been undertaken to investigate this further (see Chapter 6). Additionally, much of the stratigraphy that could be used to highlight sediment pathways has been removed by uplift and erosion in proximal locations in the Taranaki Basin.

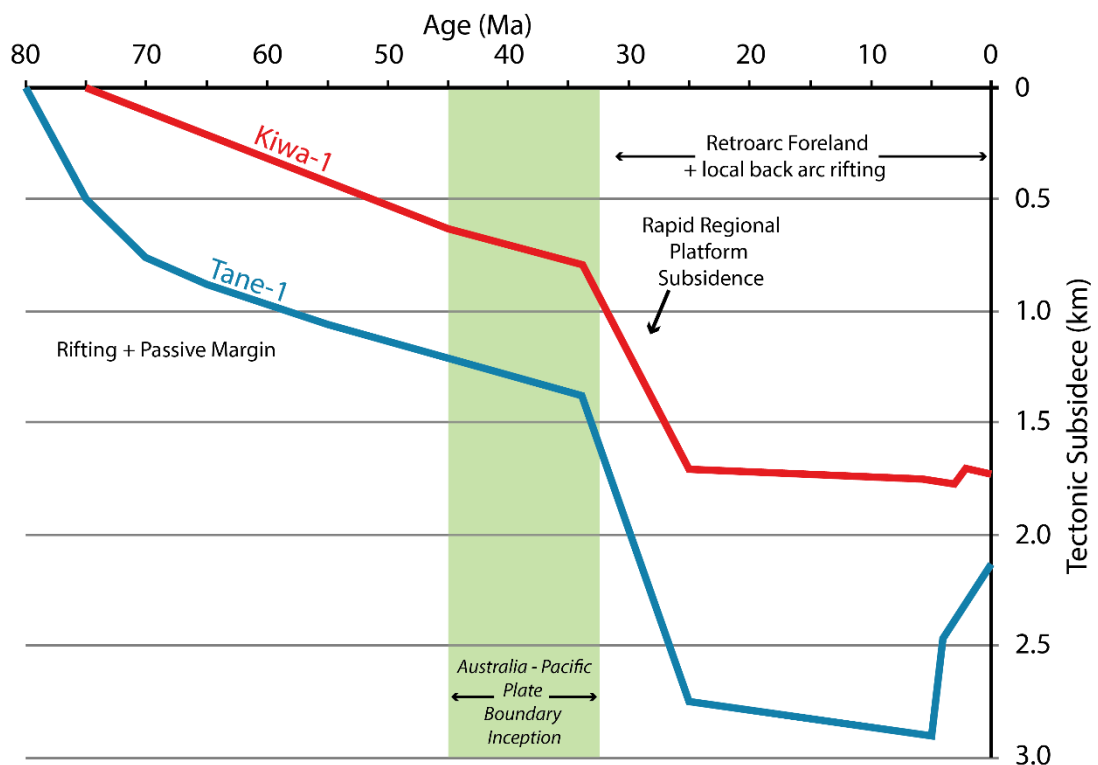


Figure 4.23 Tectonic subsidence curves.

Back-stripped tectonic subsidence curves for Western Stable Platform wells Kiwa-1 and Tane-1. Initial rapid subsidence in Tane-1 related to late stage rifting. This is followed by passive margin subsidence and accelerated subsidence from ~35 to 25 Ma. Late Miocene to recent uplift is likely an artefact due to rapid sedimentation of the Giant Foresets Formation. Figure modified from Baur et al., (2014) and Baur, 2012).

Whilst increases in sediment supply would undoubtedly result in increased progradation along the margin, it does not explain the lateral variability we see in the margin, particularly as the sediment was likely not sourced from a singular point source.

As discussed above, accommodation on the WSP was generated by a regionally extensive geodynamic subsidence event between ~35-25 Ma associated with the collision of the Pacific and Australian plates and does not explain the lateral variations in progradational history highlighted by this study. The following section highlights how later compression

along this plate boundary throughout the deposition of the Giant Foresets Formation may have influenced sediment pathways to the WSP and explain lateral variations in margin architecture highlighted by this study.

Table 4.3 Aggradation and Progradation rates for different margins (modified from Carvajal et al., 2009)

Shelf Margin	Age	Agg. Rate (m/Myr)	Prog Rate (m/kyr)	Reference
Taranaki Basin	Pliocene – Recent	177 to 200	16 to 22	This Study
New Jersey	Mid Miocene	43	17	Steckler et al. (1999)
Lewis-Fox Hills	Maastrichtian	267	48	Carvajal and Steel (2006)
West Siberia	Valanginian– Hauterivian	111	61	Pinous et al. (2001)
North Slope of Alaska	Albian	100	16	Houseknecht et al. (2009)
Columbus Basin	Pleistocene to present	2450	16	Sydow et al. (2003)
Borneo	Pliocene	460 to 540	3 to 11	Saller and Blake (2003)

4.5.3 Tectonics and lateral variations sediment supply

Globally, clinoform topsets typically have a basinward dip of much less than 1 degree (Patruno and Helland-Hansen, 2018); however, topsets of older units of the GFF dip up to 1.3 degrees to the northwest (Figure 4.24). Tilting affects progressively younger strata moving south.

The tilting of these strata is related to inversion along the pre-existing Cretaceous – Paleocene rift structure, resulting in doming of overlying sediments (Figure 4.24; King and Thrasher, 1996; Reilly et al., 2016). The doming has created several north to northeast trending anticlines throughout the Southern Inversion Zone of the Taranaki Basin, many of which are economically exploited by the hydrocarbon industry as traps (Figure 4.24). The western limbs of these anticlines form the topsets of the GFF on the Western Stable

Platform, hence an understanding of these structures is important to unravelling controls on the evolution of the GFF.

On the northern composite line, tilting ceased late in Unit B/early Unit C. On the central composite line, tilting ceased late in Unit C and is related to the inverted Whitiki Fault (Figure 4.24). On the southern composite line, tilting initiated late in Unit C and ceased by T7 and is related to a combination of inversion along the Kahurangi Fault and associated Cook Anticline, Wakamarara Fault and Anticline with possible influence from the Manaia structures (see Figure 4.7 to Figure 4.9 and Figure 4.24). The Kahurangi and Cook faults represent the western boundary between the compressive eastern mobile belt and tectonically stable WSP.

Figure 4.24A & B shows the evolution of the Cook Anticline however many of the stratal and structural relationships adjacent to the Kahurangi fault underwent wave base erosion as they were uplifted and exposed on the seabed (King and Thrasher, 1996). Truncation of topset strata in Unit C, however, provides a proxy for a period of activity along the Kahurangi Fault. Truncation of foreset reflectors is interpreted to have occurred by tilting of the palaeo-shelf, inducing erosion. This tilted topography was gradually healed by Units D and E, restoring the shelf to a grade of less than 1 degree.

Compression in the Southern Inversion Zone was a consequence of the clockwise rotation of New Zealand, which resulted in back arc extension in the north, and compression in the south along previously extensional structures (Figure 4.25). The axis between northern extension and southern compression migrated periodically south through the late Miocene to present (Giba et al., 2010; Reilly et al., 2016). This southward transit of the extensional-compressive front records changing subduction processes along the Hikurangi subduction zone, with extension reflecting slab rollback (Ballance, 1976; Giba et al., 2010; Kamp, 1986; Seebeck et al., 2014) and compression reflecting plate convergence (Stagpoole and Nicol, 2008).

The timing of tilting in this part of the basin is co-incident with a period of virtually no progradation of the GFF in the southern area of the basin but high progradation rates focused further north on the northern and central composite sections (Figure 4.7, Figure 4.8, Figure 4.13 & Table 4.1). It is suggested here that whilst Plio-Pleistocene tectonics did not play a role in generation of accommodation on the Western Stable Platform, compression and uplift along pre-existing structures may have altered the sediment

pathways in the hinterland to cause focusing of sediment toward northern parts of the WSP, thus explaining the along strike difference in progradation history.

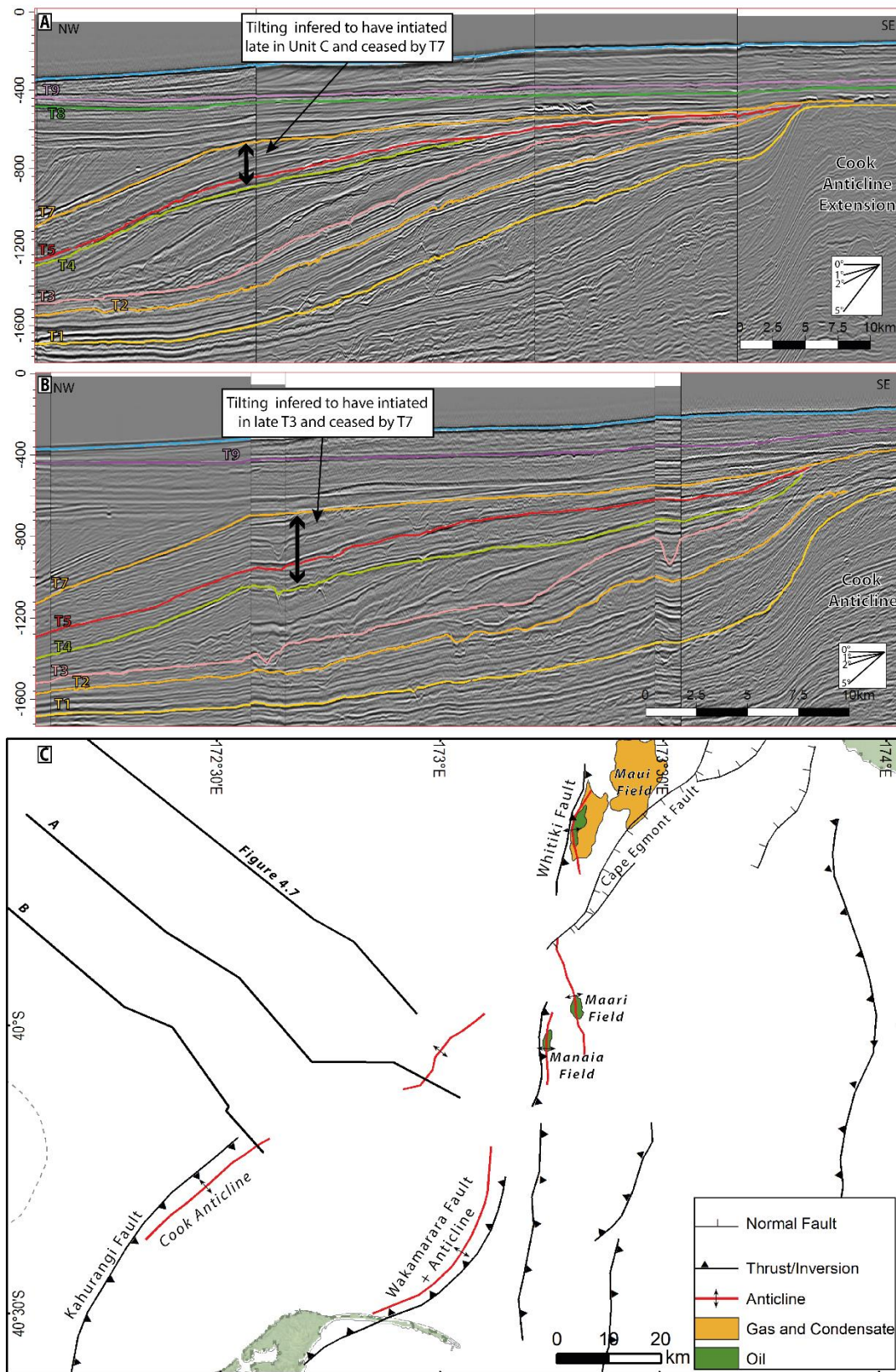


Figure 4.24 Tilted stratigraphy in the Southern Taranaki Basin.

A & B) Sections showing the timing of tilting of Miocene and Pliocene stratigraphy associated with formation of the Cook Anticline. Topsets of clinoforms T3-T4 are inferred to have initially been flat surfaces. Tilting of stratigraphy by up to 1.3 degrees towards the northwest is inferred to have initiated late in unit C, truncating topset rollovers. Topset strata between T4-T7 are also tilted, post T7 topset are relatively flat. C) Structure map of the southern Taranaki Basin. Oil and gas accumulations (NZP&M, 2014) are also annotated to highlight spatial association with inversion related anticlines. Structure map modified from King and Thrasher (1996).

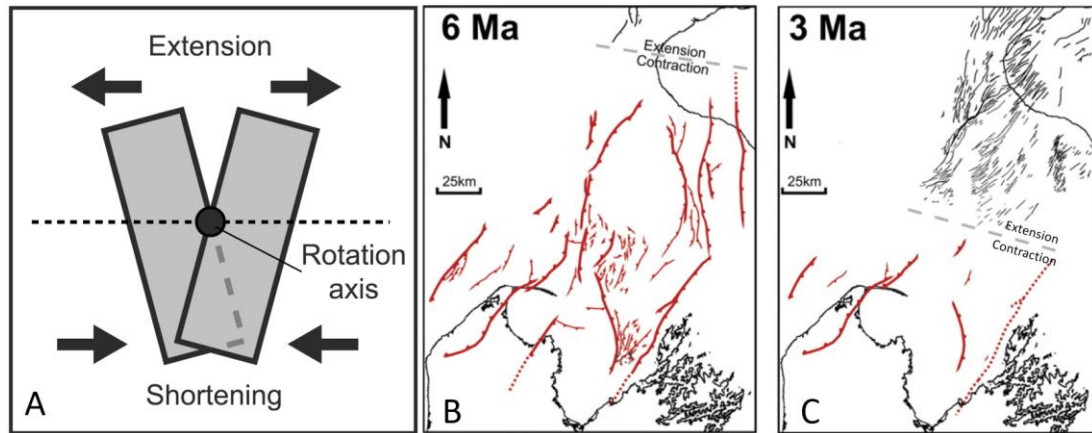


Figure 4.25 Compression in the Southern Taranaki Basin.

A) Schematic model representing northern extension and southern compression from Giba et al., (2010); B) & C) Paleo-Structure maps from Reilly et al. (2016) showing southward migration of the boundary between extension & compression in the southern Taranaki Basin.

4.5.4 Sediment Waves

Sediment waves are prominent features throughout the progradation of the Giant Foresets Formation and occur over a large geographic area along the margin, cumulatively covering over 6,700 km² of the basin (this figure would be larger if stratigraphy had not been removed by mass wasting). They occur in unconfined settings on the basin floor to mid slope environments and are mainly concentrated along the northern margin of the Western Stable Platform (Figure 4.27A) where progradation was focused until T7. One field of sediment waves, however, was observed in the south of the WSP, associated with the rapid progradation of Unit H (T7 to T8) (Figure 4.27B).

Analysis of sediment wave morphologies can provide insight into the types of flows and processes that were occurring on the slope of the Giant Foresets Formation. Measurements of 63 waves from throughout the succession (Figure 4.26) show wavelengths ranging from 350 m – 2500 m and wave heights of up to 32 m (smallest observable waves within seismic resolution is approximately 10 m). Dimensions are consistent with parameters for fine grained sediment waves of turbidity current origin (Symons et al., 2016; R B Wynn and Stow, 2002). This is in agreement with the mud log for well Tane-1 on the Western Stable Platform (Appendix-1) and observation of a similar wave field in the basin by Shumaker et al. (2017). When observed in 3D seismic data,

wave crests are oriented parallel to the shelf margin, suggesting downslope processes were responsible for the formation of the waves, in agreement with a turbidity current origin suggested by wave dimensions.

To account for the widespread occurrences of sediment waves along the margin of the Taranaki Basin, Shumaker et al. (2017) suggested that sediment waves were formed by sheet like turbidity currents tens of kilometres across and up to 40 m thick (based on sediment wave dimensions) cascading over the shelf margin. While this hypothesis may account for some of the GFF sediment waves, the larger dataset used in this study suggests many of the sediment waves in the basin form from overbank processes as turbidites over run their container walls at bends in canyons or channels (Figure 4.27B). Similar examples have been described from offshore eastern Borneo (Posamentier and Kolla, 2003) and on the Shepard Meander of the Monterey Canyon, offshore California (Fildani et al., 2006). Within the youngest GFF unit (Unit I), sediment waves can also be observed nucleating on pre-existing bathymetry from an underlying MTD (Figure 4.27C).

While the regional 2D seismic data have delineated large fields of sediment waves, the quality, orientation and data density in many cases preclude confidently attributing modes of formation to all sediment waves bodies. For example, contrasting the interpretation of down slope processes by Shumaker et al. (2017) and this study, the northward migration of slope canyon systems along the margin (Figure 4.19) may suggest the presence of a north directed along slope current. Other processes such as internal waves (e.g. Ribó et al., 2016; Shepard et al., 1974; Stride and Tucker, 1960), seafloor creep (e.g. Li et al., 2016; Rebesco et al., 2009; Shillington et al., 2012) or a combination of factors (e.g. Li et al., 2019) may have given rise to regionally extensive wave fields along the margin of the Western Stable Platform.

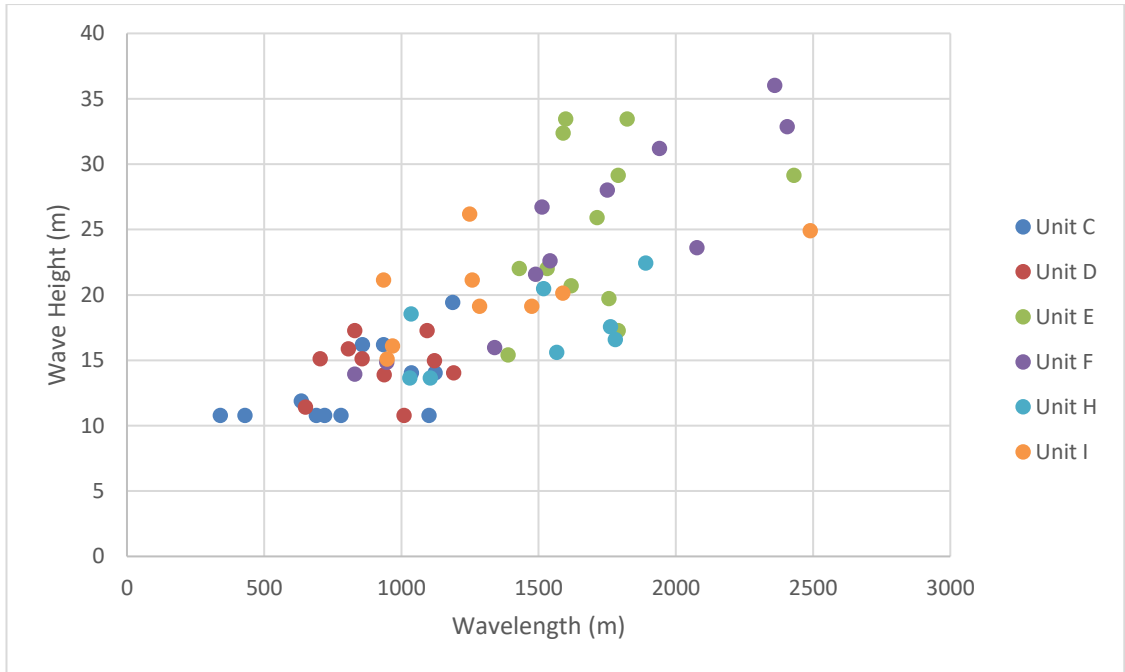


Figure 4.26 Plot of sediment wave dimensions separated by unit.

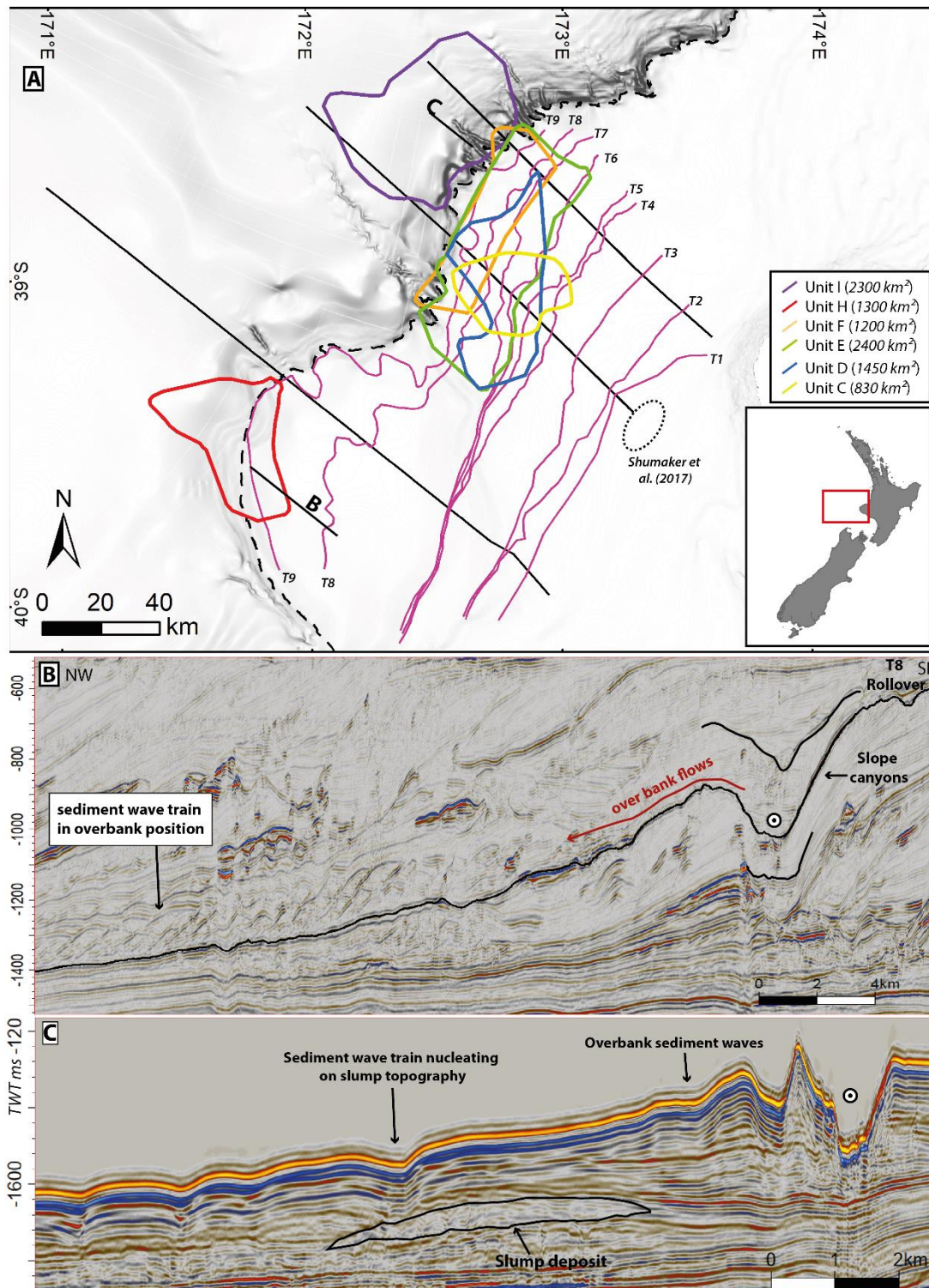


Figure 4.27 Sediment Waves in the Taranaki Basin.

A) Distribution of sediment waves fields along the Western Stable Platform, B) Dip section from the southern extent of the WSP showing upslope migration of sediment waves in an overbank environment and C) Example of an overbank wave and wave train nucleating on existing bathymetric irregularities in the northern portion of the WSP. See A for section locations. Circles with dots in B & C denote flow a direction out of the page.

4.5.5 Synthesis.

Although the Western Stable Platform remained tectonically stable throughout the collision of the Pacific and Australian plates, it is apparent that structures accommodating the collision played a role in controlling sediment pathways to the WSP.

This chapter combines observations from the progradational history of the GFF and inferences on the timing of movements on structures to synthesize the controls on the evolution of the GFF across the Western Stable Platform and in particular the along strike variability of the system. These observations are integrated with paleogeographic syntheses of Baur (2012), King and Thrasher, (1996) and Strogon (2011) and are presented in Figures Figure 4.28 and Figure 4.29.

From T1 (5.33 Ma) to T3 (~3.0 Ma), progradation was focused in the northern portion of the study area, producing a lobate margin geometry. Sediment from the uplifting Southern Alps bypassed the southern portion of the basin to the deep-water Taranaki and Aotea Basins. Consequently, minimal progradation occurred in the south of the WSP. In addition to progradation on the Western Stable Platform, sediment was also funnelled into depocentres of the Northern Graben, Toru Trough and Wanganui Basin (Baur, 2012; Kamp et al., 2004, 2002). Sediment was sourced from the uplifting South Island and delivered to the Taranaki Basin by longshore drift (Beggs, 1990; Hansen and Kamp, 2002; Hansen and Kamp, 2006).

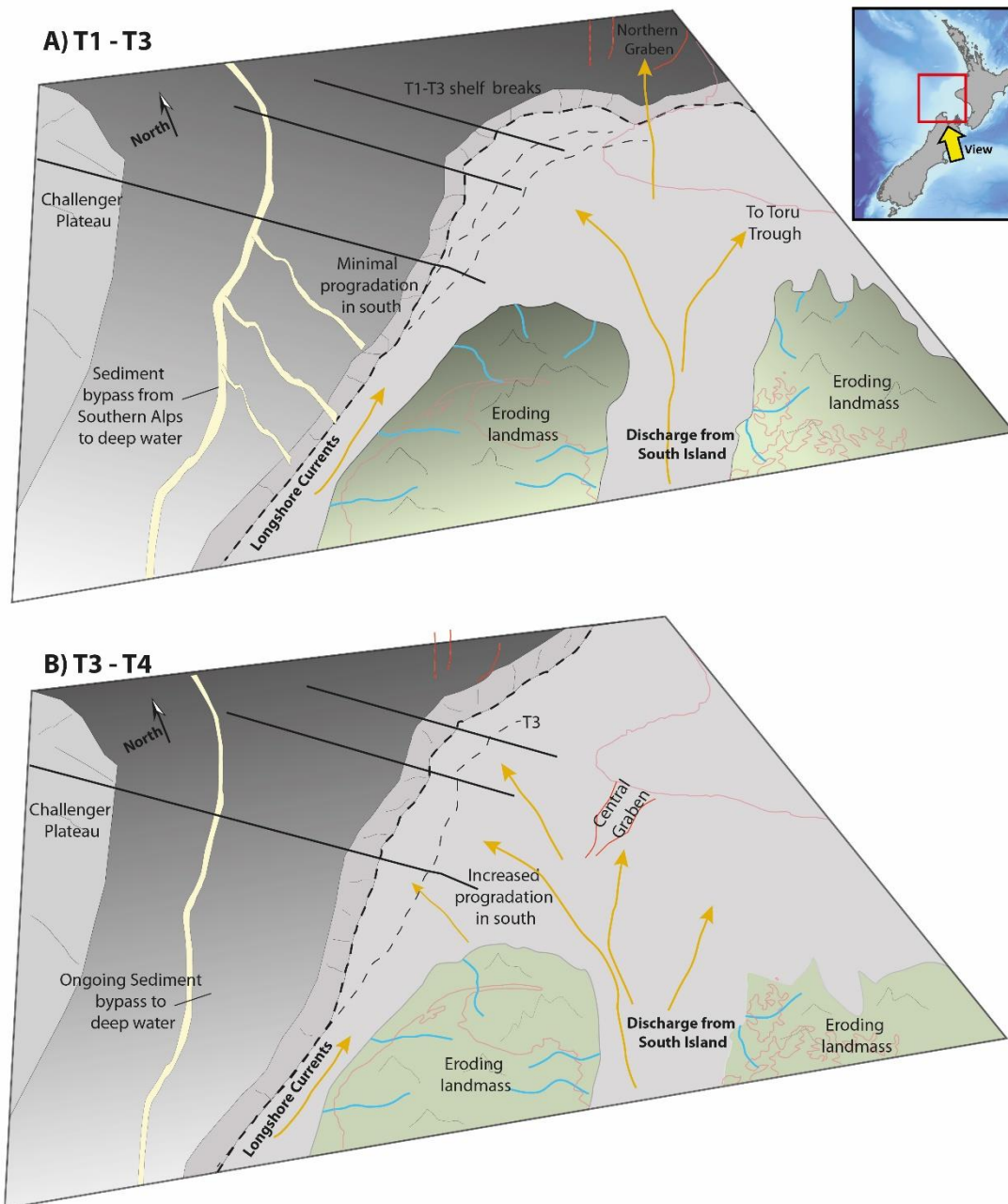


Figure 4.28 Schematic paleogeography for T1 to T4.

Perspective view looking northeast towards the Taranaki Basin showing the schematic evolution of the Western Stable Platform from T1 to T4. Adapted from (Strogen, 2011).

From T3 to T4 (approximately 3 – 2.4 Ma) sediment continued to bypass the southern depocentre of the WSP. Despite this, there was progradation in the south, leading to a relatively linear shelf margin in this interval. This may be attributable to partial erosion of the northwest region of the South Island, exposing the southern depocentre to higher sediment flux. Much of the Northern Graben had been infilled at this stage (Giba et al., 2010; Salazar et al., 2016), as extension migrated to the Central Graben area (Reilly et al., 2015).

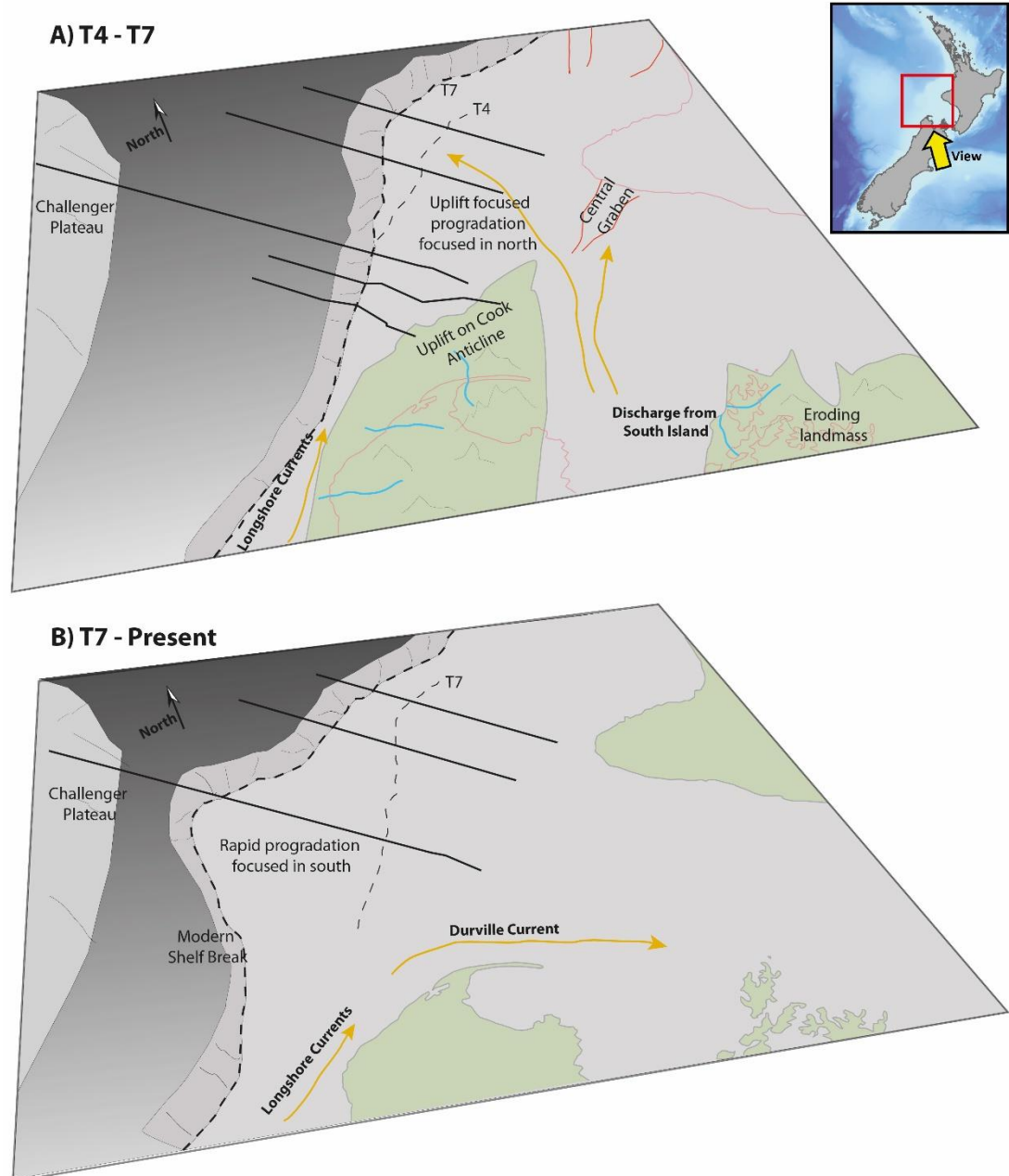


Figure 4.29 Schematic paleogeography for T4 to Present.

Perspective view looking northeast towards the Taranaki Basin showing the schematic evolution of the Western Stable Platform from T4 to present. Adapted from (Strogen, 2011).

Late in Unit C/early in Unit D, inversion on the Kahurangi and Wakamarara faults caused uplift (Figure 4.29A). This uplift had two consequences: 1) tilting of proximal topset strata on the Western Stable Platform and 2) focusing of discharge from South Island toward the northern depocentre of the WSP. This focused discharge allowed high progradation rates in the north from T4-T7, whilst effectively no progradation occurred in the south. Toward the top of Unit F, large conduits bypassing sediment from the Southern Alps are no longer observed in seismic data (although some smaller channels are evident up to T7

(see Unit F in Figure 5). The synchronous timing of these events may indicate a shift in the source to sink pathways from South Island.

From T7 to present, progradation was dominantly focused on the southern depocentre of the Western Stable Platform (Figure 4.29B). A notable incisional corridor between the northern and southern WSP was also established in this time period and continues to the present day. In the north, progradation continued at a slower rate with aggradation resulting in over-steepening and a large-scale collapse along the central and northern portions of the WSP.

4.6 Conclusions

This study identified and mapped nine seismic stratigraphic units spanning the entire temporal extent of the Giant Foresets Formation recording its progradation across the Western Stable Platform. The results demonstrate significant lateral variation as the GFF prograded through the Pliocene and Pleistocene. A composite chronostratigraphic framework has been constructed by integrating ages from biostratigraphic well data and correlation of sequence stratigraphic events to global eustatic fluctuations of known age (Chapter 5).

From approximately 5.33 Ma to 1.2 Ma, progradation was mainly focused in the northern area of the WSP between 5.33 to 1.2 Ma. From approximately 1.2 to 0 Ma, progradation was more strongly focused in the area of the WSP.

Clinofolds range from 0.5-1.3 km in height and are consistently smaller in the south of the WSP due to the bathymetric influence of the Challenger Plateau. Average progradation rates for the succession range from 16 to 22 m/kyr, with shorter term rates up to 77 m/kyr calculated in the south of the WSP from approximately 0.6 Ma to present. Based on context and scale, clinofolds in the GFF can be classified as continental margin scale clinofolds, but also retain many of the characteristics of shelf edge clinofolds, such as progradation rate and rollover depth.

Measurements of sediment wave geometries throughout the basin are consistent with parameters for fine-grained waves formed by turbidity currents. When imaged in 3D data, crests are aligned parallel to the shelf edge, suggesting that downslope processes dominated.

Observations of the slope stratigraphy on the WSP show that canyons migrated in a northerly direction through time, suggesting that a north directed current swept the slope. This observation is at odds with the sediment wave geometries consistent with a fine-grained turbidity current origin and wave crests aligned parallel to the margin.

Although the WSP remained tectonically quiescent throughout the deposition of the GFF, it is likely that tectonism on the inner shelf played a role in altering sediment routing from South Island, focusing sedimentation to the north until approximately 1.2 Ma. The lateral variations in architecture and progradation described here are attributed to uplift on inverted Cretaceous faults in the southern Taranaki Basin (the Kahurangi and Wakamarara faults) related to changes in subduction processes along the Hikurangi subduction zone. These changes are interpreted to have altered sediment routing from South Island sources.

Blank Page

Chapter 5

Mid-Pleistocene – Recent Evolution of the Egmont Terrace in the Southern Taranaki Basin.

5.1 Introduction

The Egmont Terrace (ET), lies off the northwest corner of New Zealand's South Island, making up a southerly deeper-water extension of the Western Stable Platform. The ET shelf edge is at 270 – 300 m water depth, whereas the Western Stable Platform to the north is in water depths of 150-170 m. This deeper water shelf is characterised by a smooth, unincised modern slope (Figure 5.2).

Previous work by Reilly et al. (2015) and Bull et al. (2015) have gone some way in describing the Plio - Pleistocene evolution of the Southern Taranaki Basin. Both studies, however, focus on the Eastern Mobile Belt (cf Figure 2.4 & Figure 2.11), and do not include the Egmont Terrace. Anell and Midtkandal (2017) utilised a sub-set of the dataset used in this chapter to quantify the geometric relationships and internal characteristics of the Giant Foresets Formation (GFF) on the Egmont Terrace, concluding in this part of the Taranaki Basin, the GFF clinothems are heavily degraded and chaotic with a low angle upward regressive trajectory averaging 0.19° to 0.33° , noting deep incisional patterns in topsets and foresets and evidence for large scale slope failures.

Building on the established regional seismic stratigraphy from Chapter 4, this chapter investigates in greater detail the stratigraphy between regional surface T7 and the modern seabed (Figure 5.1). On the Egmont Terrace, this portion of the stratigraphy is composed of a well-preserved succession of clinoforms prograding from southeast to northwest. Age equivalent stratigraphy in the northern depocenter displays a more chaotic and incised slope (Chapter 4), making detailed correlations difficult.

A higher quality seismic dataset across the Egmont Terrace (Figure 5.3), coupled with well preserved and non-chaotic stratigraphy have allowed a detailed sequence stratigraphic study of the clinoform succession in this part of the Taranaki Basin to be undertaken. This chapter aims to:

- Expand on the regional seismic stratigraphy of Chapter 4 by creating a detailed sequence stratigraphic interpretation of the Giant Foresets Formation on the Egmont Terrace.
- Investigate the controls on depositional architecture and sequence stratigraphy in the Southern Taranaki Basin.
- Investigate the nature of the cyclical seismic facies and make inferences on the timing and nature of deposits in the Southern Taranaki Basin.
- Compare and contrast the succession to analogous basin margins.

The studies undertaken in Chapter 4 and Chapter 5 are symbiotic and were developed iteratively side by side to better understand local and regional factors influencing how the Giant Foresets Formation prograded across the Western Stable Platform.

Epoch	NZ Stage	Seismic Stratigraphy (This Study)		Assigned Age	Age Source	
Pleistocene		Seabed		0 Ma	Seabed	
	Wq	T9	Unit I	0.191 Ma	Chapter 5	
	Wc	T8	Unit H	0.621 Ma	Chapter 5	
		T7	Unit G	1.2 Ma	Chapter 5	
		T6	Unit F	1.5 Ma	GNS N85 (Thrasher et al. 2018)	
	Wn	T5	Unit E	2.0Ma	GNS N82 (Thrasher et al. 2018)	
		T4	Unit D	2.4 Ma	GNS N80 (Thrasher et al. 2018)	
		Wm	T3	Unit C	3.0 Ma	Biostratigraphy (Crundwell, 2017 pers. comm)
			Wp	Unit B	4.3 Ma	Biostratigraphy (Kiwa-1)
	uWo					
Pliocene	lWo	T2	Unit A	5.33Ma	Biostratigraphy (All Wells)	
		T1				

Figure 5.1 Stratigraphic Framework

Regional seismic stratigraphic framework from Chapter 4 with the focus of Chapter 5 (this chapter) highlighted by a red dashed line.

5.2 Dataset and Methods

5.2.1 Data

This chapter utilises a subset of the main database introduced in Chapter 3, including approximately 14,000 line km of 2D seismic reflection data and one 3D seismic survey (Hector 3D) covering approximately 440 km² (Figure 5.3).

Only three wells are located within the area of interest for this chapter; Kiwa-1, Hector-1 and Hochstetter-1. Of these wells, only Kiwa-1 (Appendix 1) contains biostratigraphic data, petrophysical data and cuttings logs from a depth of 490 m (MDkb) of Plio-Pleistocene stratigraphy (i.e. below the interval of interest for this study). Hector-1 and Hochstetter-1 record petrophysical and cuttings data for only the bottom 250 m and 100 m of the Pliocene stratigraphy (approximately T1 – T3). The progradational nature of the Giant Foresets Formation coupled with sparse well data on the Egmont Terrace has resulted in poor age and lithological control on younger portions of the succession on the outer shelf.

5.2.2 Methods

To better understand the evolution of the Giant Foresets Formation a sequence stratigraphic approach was taken. The Accommodation-Succession methodology of Neal and Abreu (2009, 2016) was used to identify clinof orm stacking patterns and to interpret sequence boundaries. This approach was used iteratively across multiple dip and strike lines to identify and map regionally significant surfaces of sequence stratigraphic significance (i.e. sequence boundaries, transgressive and flooding surfaces).

Regional hemipelagic claystones, interpreted as flooding surfaces, typically form easily identifiable and correlatable timelines in outcrop and seismic surveys (e.g. Catuneanu et al., 2011; Flint et al., 2011; van der Merwe et al., 2010). On the Egmont Terrace, however, Anell & Mitkandell (2017) noted the succession is heavily degraded and chaotic with deep incisional patterns in the topsets, this topset incision, coupled with the 2D nature of the dataset makes correlating flooding surfaces difficult. The erosion and degradation features described by Anell & Mitkandell (2017) are interpreted here to represent sequence boundaries (sensu Van Wagoner et al. (1988) and split the succession into depositional sequences. This approach allowed for correlation of interpreted lowstand deposits to sequence boundary erosion surfaces updip.

Due to the complex progradational nature and stratal geometries of the GFF, sequence boundaries were selected as the main surfaces on which to define sequences (as opposed to genetic sequences bounded by flooding surfaces of Galloway (1989).

5.2.2.1 Seismic Facies & Depositional Environments

The remarkable cyclicity visible in seismic data on the Egmont Terrace allowed for identification of major surfaces of sequence stratigraphic significance and subsequent assignment of systems tracts to a given seismic facies.

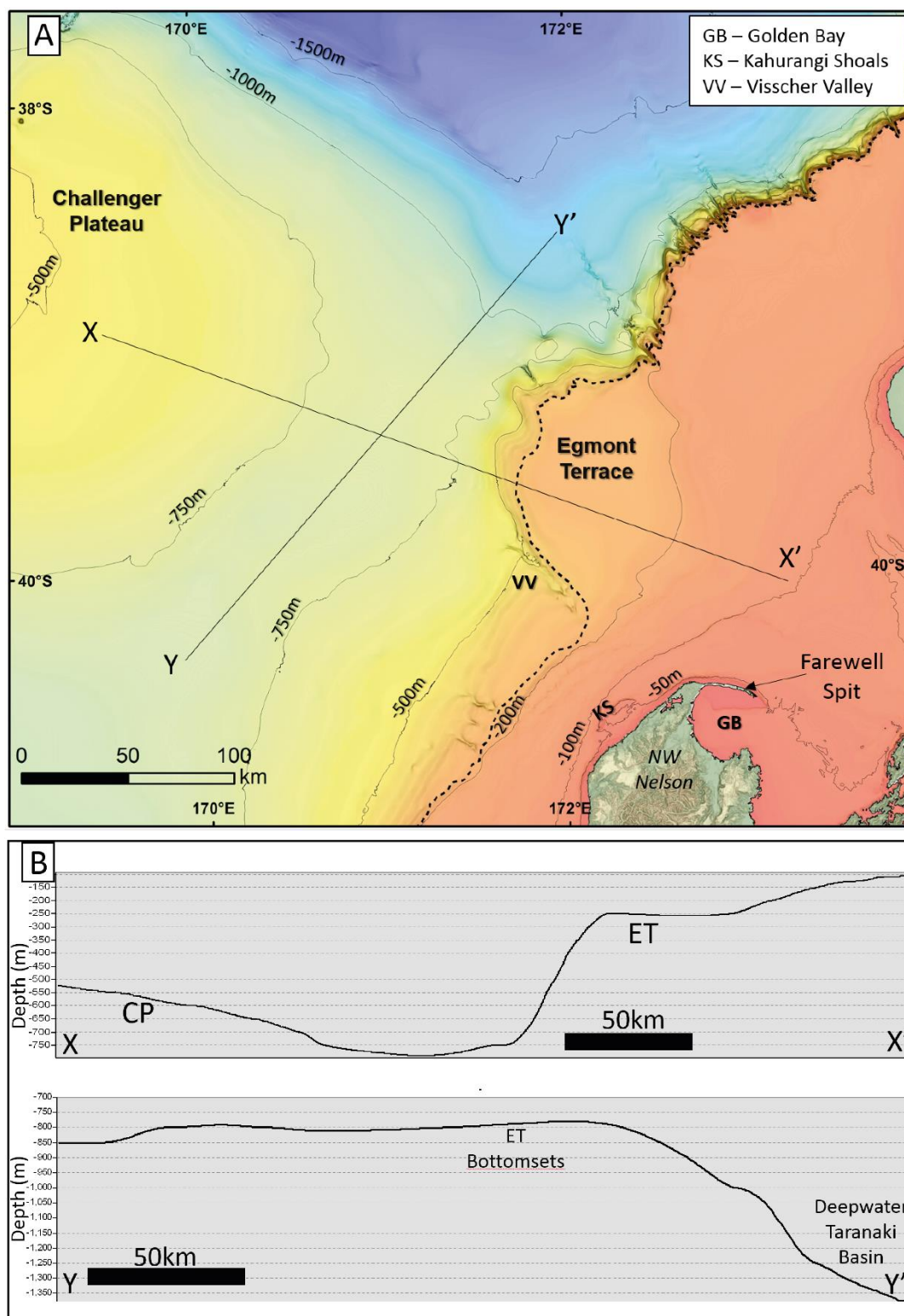


Figure 5.2 Bathymetry of the Southern Taranaki Basin.

A) Bathymetry showing physiography of the study area and locality names. B) Bathymetry profile extracted along line X-X' showing the relationship between the Egmont Terrace (ET) and Challenger Plateau (CP). C) Bathymetry profile extracted along line Y-Y' along the axis of the deepwater seaway between the Egmont Terrace and Challenger Plateau.

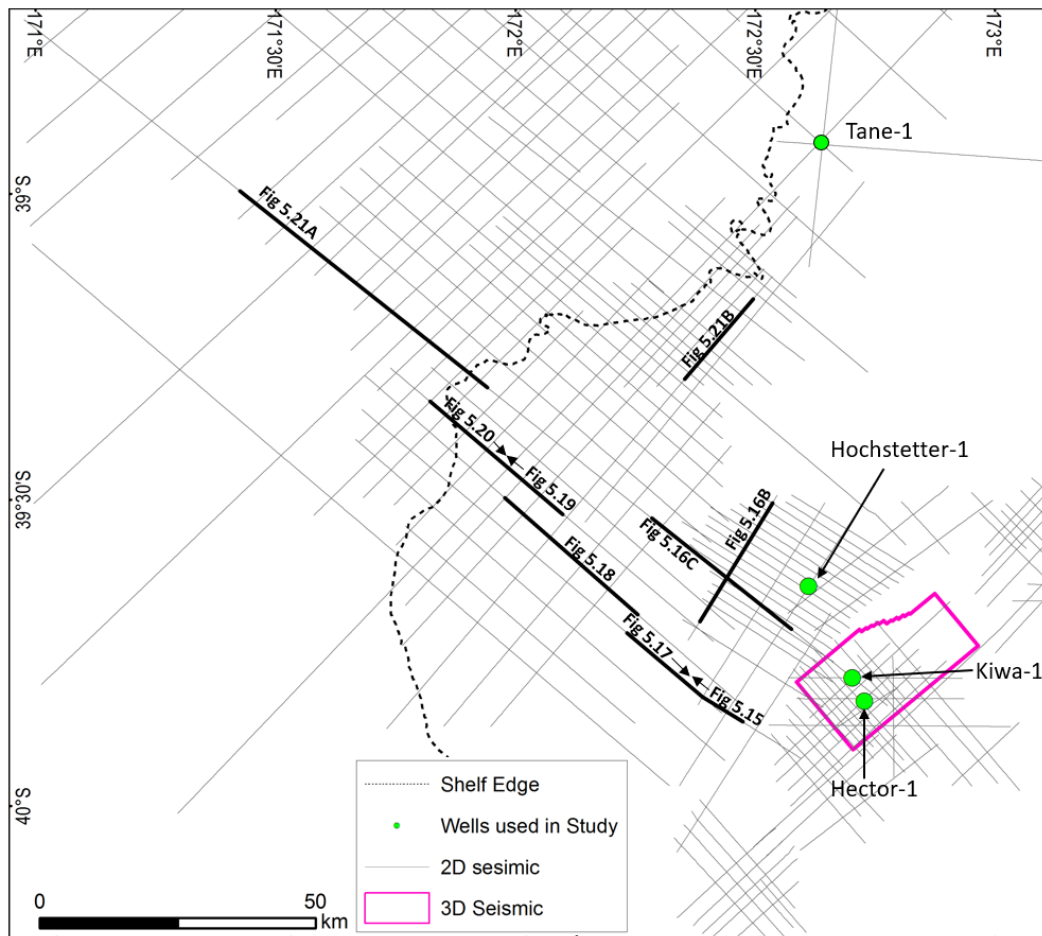


Figure 5.3 Data utilised in this chapter.

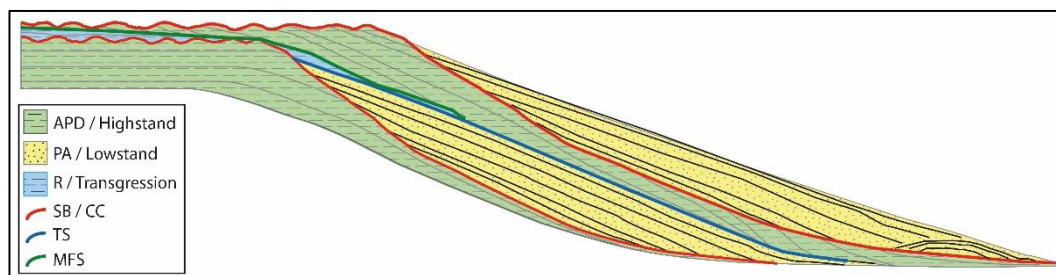
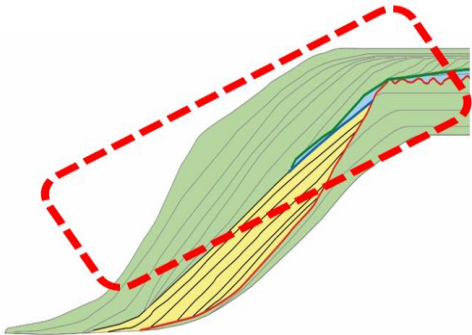
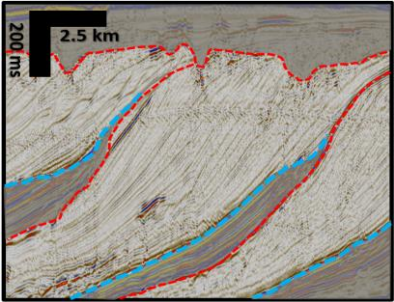
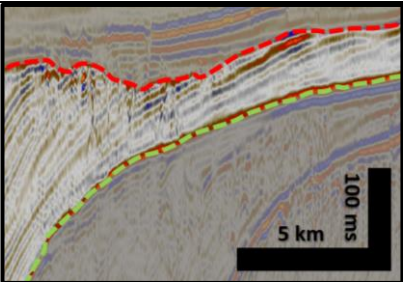


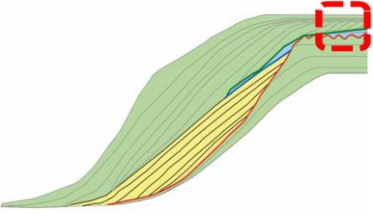
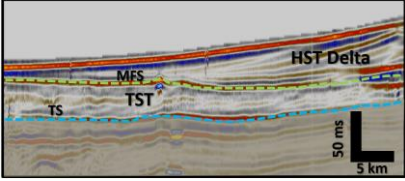
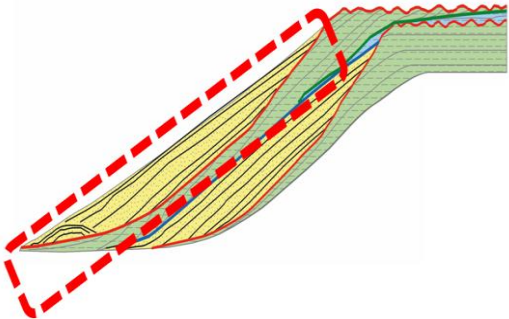
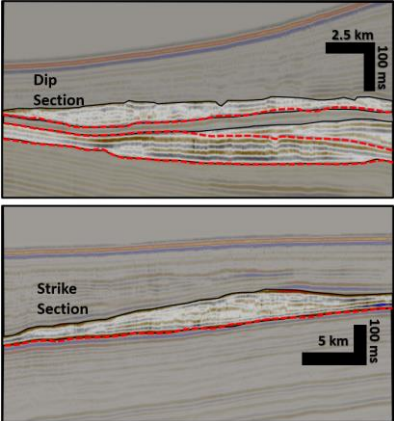
Figure 5.4 Egmont Terrace “slug”

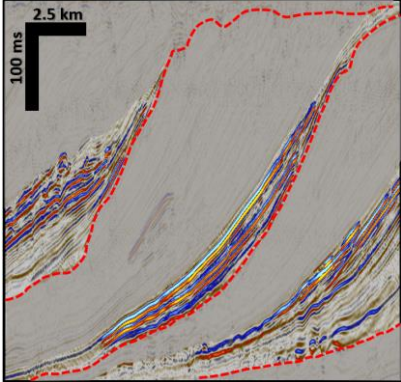
Typical depositional sequence architecture on the Egmont Terrace based on seismic interpretations for this chapter.

The typical sequence stratigraphic motif on the Egmont Terrace is given in Figure 5.4, with typical seismic facies and the interpreted depositional environment associated with each systems tract presented in Table 5.1.

Table 5.1 Examples of depositional systems tracts from the Egmont Terrace and their interpreted lithologies and environment of deposition.

Systems Tract	Reflection Geometries	Seismic Example from TB	Interpreted Lithology and Depositional Environment
<p style="writing-mode: vertical-rl; transform: rotate(180deg);">APD / Highstand</p>			<ul style="list-style-type: none"> • Typical HST/APD facies • Low amplitude semi-continuous reflectors. • Topsets commonly truncated sequence boundaries (red dash). • Downlaps onto flooding surface of slope fans (blue dash) • Flat to shallowly rising trajectory (trajectory not always evident due to later erosion). • Dominated by slope and basin floor deposits. • Interpreted to be dominated by silt and mud. • Deposited in 200 – 1000m water depth.
			<ul style="list-style-type: none"> • Shelf edge delta overlain by sequence boundaries (red dash). • Rarely preserved maximum flooding surface (MFS – green dash). • Deposited at shelf edge in water depths of 200 -250 m • Dominant lithology uncertain but may deliver coarse across the shelf break (e.g. Figure 5.18).

<p>R / TST</p>			<ul style="list-style-type: none"> • Rarely preserved example of a transgressive systems tract on the shelf which is overlain by delta during the current highstand. Transgressive deposits are often thin or absent in high supply settings (Cattaneo and Steel, 2003). • Transgressive surfaces typically interpreted when a landward shift in deposition occurs (transgressive facies are either not deposited or are below seismic resolution).
<p>PA - Lowstand</p>			<ul style="list-style-type: none"> • Base of slope fans sitting above sequence boundary/correlative conformity (red dash). • Rarely observed; most common in youngest sequences as turbidites pond against the topography of the Challenger Plateau. • Deposited at base of slope (800 – 1000 m) • Possibly composed of coarser sandy material and draped by muddy highstand deposits.

		 <p>The image is a geological cross-section showing a slope fan. The fan is composed of multiple layers of sediment, with a prominent high-amplitude continuous reflector (HAR) at the top. The HAR is shown as a thick, dark, wavy line that pinches out towards the top of the fan. Below the HAR, there are several layers of lower-amplitude, discontinuous reflectors. The fan is bounded by a sequence boundary at the base. A scale bar in the top left corner indicates a horizontal distance of 2.5 km and a vertical distance of 100 ms. The fan is shown in a perspective view, with the top of the fan on the right and the base on the left.</p>	<ul style="list-style-type: none">• Slope Fans sitting above sequence boundary / correlative conformity.• High amplitude continuous reflectors pinching out upslope and down slope.• Commonly observed in in the Egmont Terrace Stratigraphy.• Interpreted to be coarser sandy material. See chapters 5.3.2 and 5.4.2 for further discussion.• Interpreted to be overlain by a transgressive surface and subsequent muddy low amplitude discontinuous highstand reflectors.• Deposited between 200 – 800m water depth.
--	--	---	---

5.3 Results

The Giant Foresets Formation is spectacularly imaged on the Egmont Terrace; in this area, clinoforms are imaged as a NW prograding wedge of sediment with clear cyclical seismic facies observable. Clinoforms underpinning the modern shelf edge have a relief of approximately 500 m with a NW dipping foreset slope of 1.2 -2 degrees, becoming steeper and higher on north facing slopes toward the deepwater Taranaki Basin. These clinoforms downlap onto a submerged ridge between the Challenger Plateau and the continental margin, creating a saddle shaped geometry (Figure 5.2). Seismic data cover the portion of this saddle dipping gently to the northeast (i.e. toward the Taranaki Basin proper). In this area, bottomsets of the Egmont Terrace sit approximately 500m above the true basin floor of the Taranaki Basin.

This section will present results of detailed seismic stratigraphic mapping of the Egmont Terrace with creation of a sequence stratigraphic framework showing the evolution of the margin. Within this framework we will then examine a series of apparently cyclical high amplitude deposits present on the foreset slope of many of the clinoforms.

5.3.1 Sequence development

Following the mapping of regional surfaces T1 – T9 (Chapter 4), a more detailed analysis of the stratigraphy from T7 – T9 was undertaken on the Egmont Terrace. After T7, a marked change in the progradational style is observed (Figure 5.5) when the shelf margin changes from a northeast trending linear feature to that of a lobate geometry with progradation focused on the Egmont Terrace. The stratigraphy between T7 and the present-day seabed has been further subdivided by the recognition and mapping of 14 additional surfaces named, oldest to youngest, ET01 to ET14. Figure 5.5 to Figure 5.8 illustrate the overall evolution of the margin, followed by time structure maps of each sequence (Figure 5.9 to Figure 5.11) and thickness maps for each sequence (Figure 5.12 to Figure 5.14). A more detailed dissection of the sequence follows in section 5.3.1.1 of this chapter.

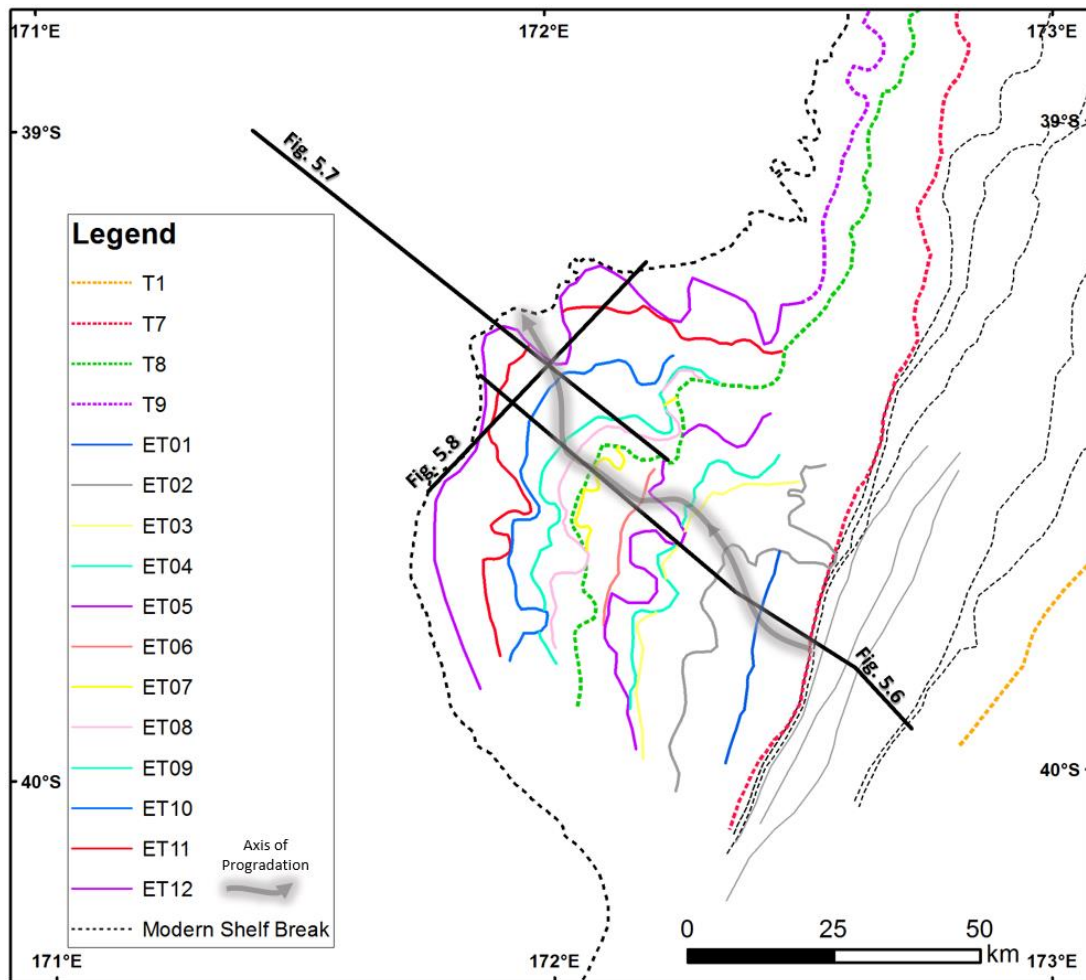


Figure 5.5 Shelf rollovers mapped in this study.

Mapped shelf breaks of sequences ET01 to ET14. Regional surfaces T1, T7, T8 & T9 from Chapter 4 are included for reference as dashed lines. The axis of progradation is marked as a grey arrow.

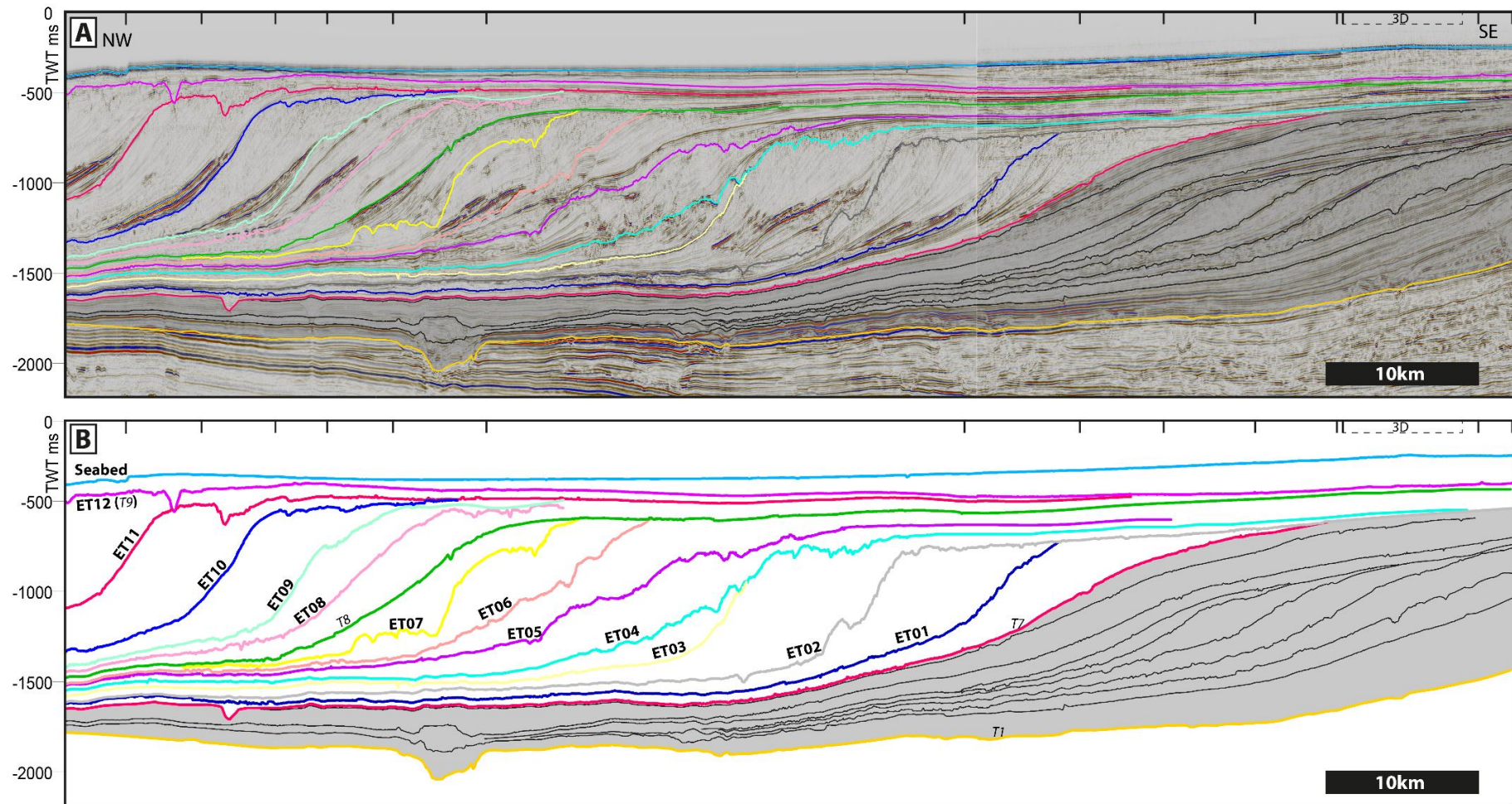


Figure 5.6 Composite dip section of DT08-042, K98-11 & T96-39.

Showing major sequence boundaries on the Egmont Terrace. Greyed out area is interpreted but not discussed in this chapter. Regional surfaces T1, T7, T8 and T9 are included for reference. Crossing line intersections are shown as ticks across the top of the image. See Figure 5.5 for location

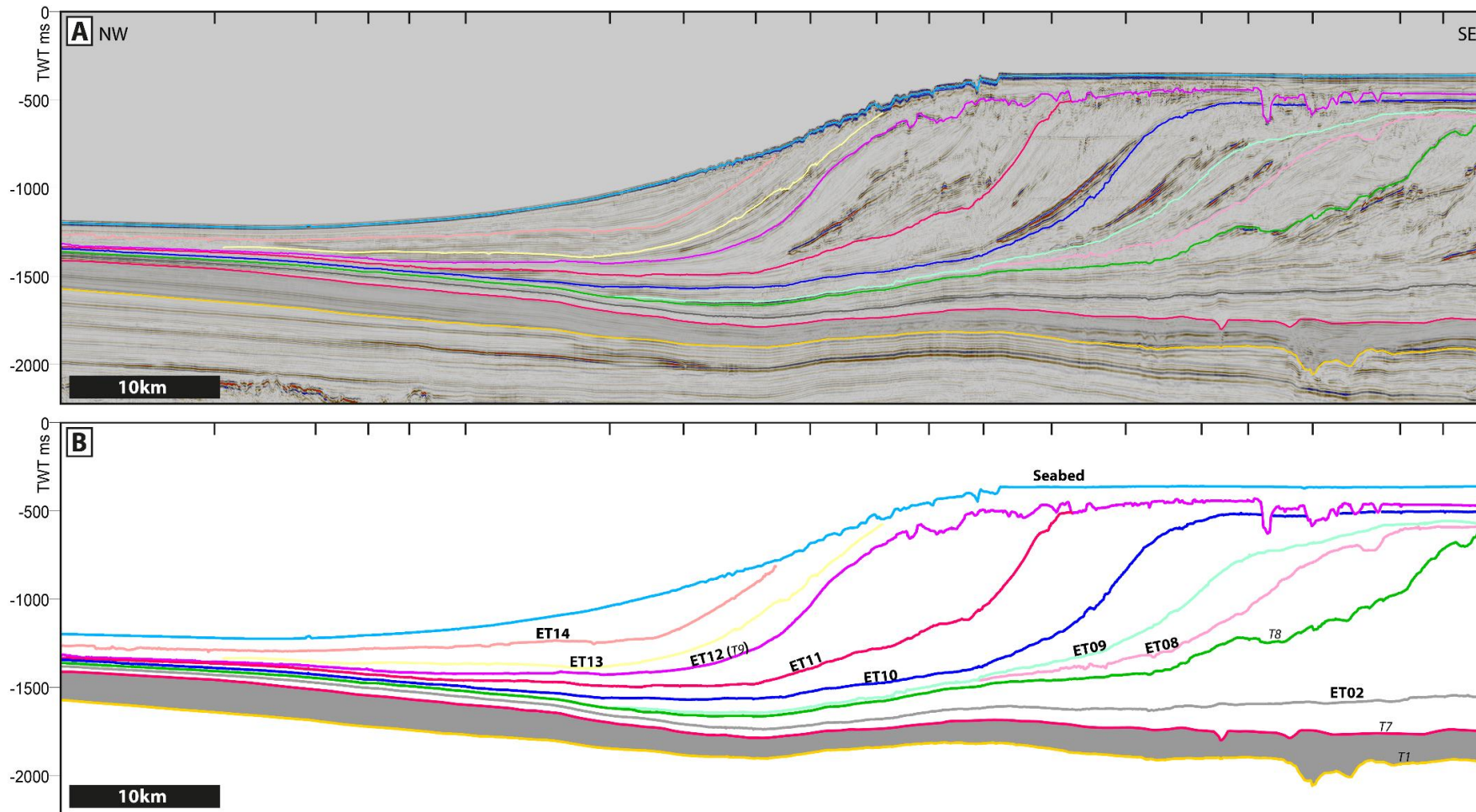


Figure 5.7 Dip section DTB01-31.

Showing major sequence boundaries on the Egmont Terrace. Greyed out area is interpreted but not discussed in this chapter. Regional surfaces T1, T7, T8 and T9 are included for reference. Crossing line intersections are shown as ticks across the top of the image. See Figure 5.5 for location

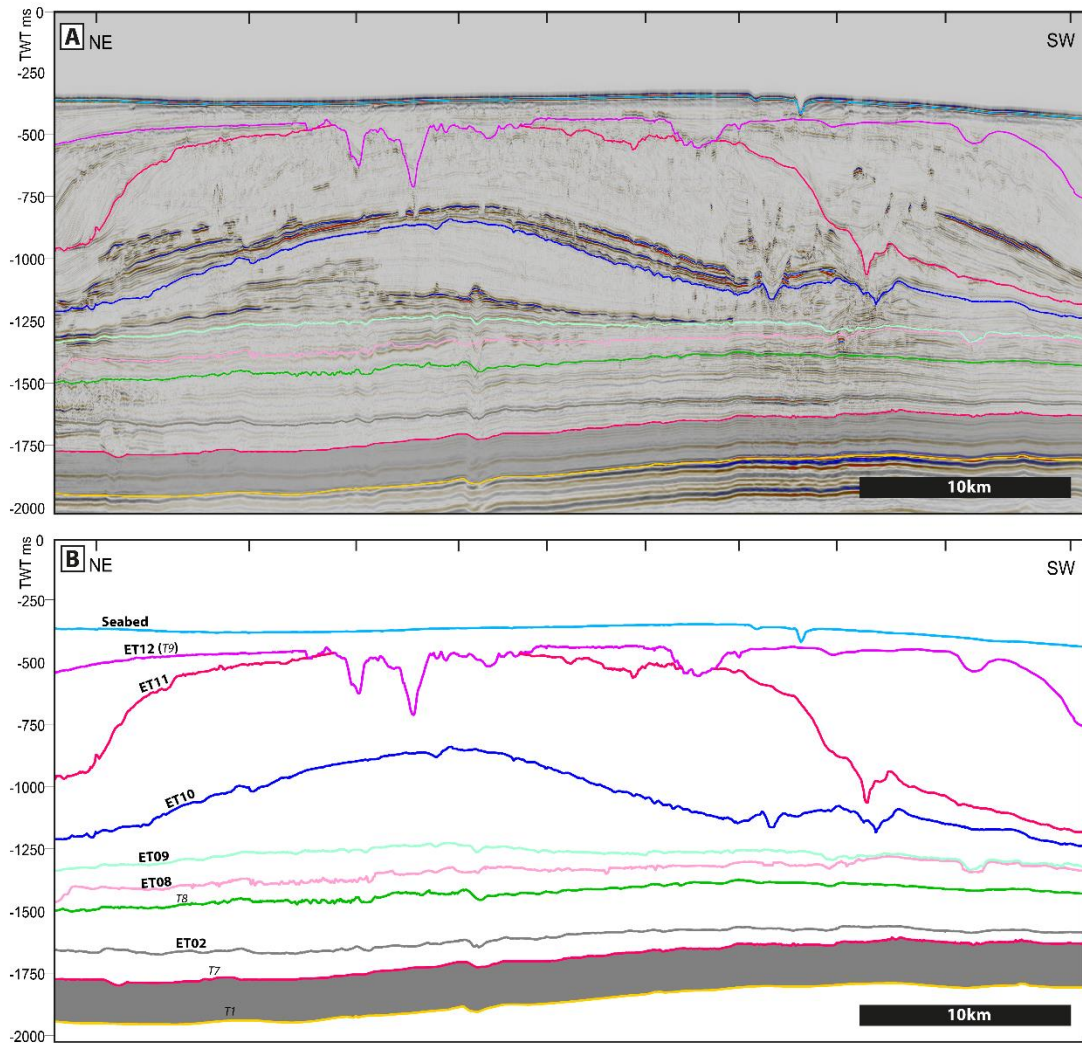


Figure 5.8 Strike section DTB08-132.

Showing major sequence boundaries on the Egmont Terrace. Greyed out area is interpreted but not discussed in this chapter. Regional surfaces T1, T7, T8 and T9 are included for reference. Crossing line intersections are shown as ticks across the top of the image. See Figure 5.5 for location.

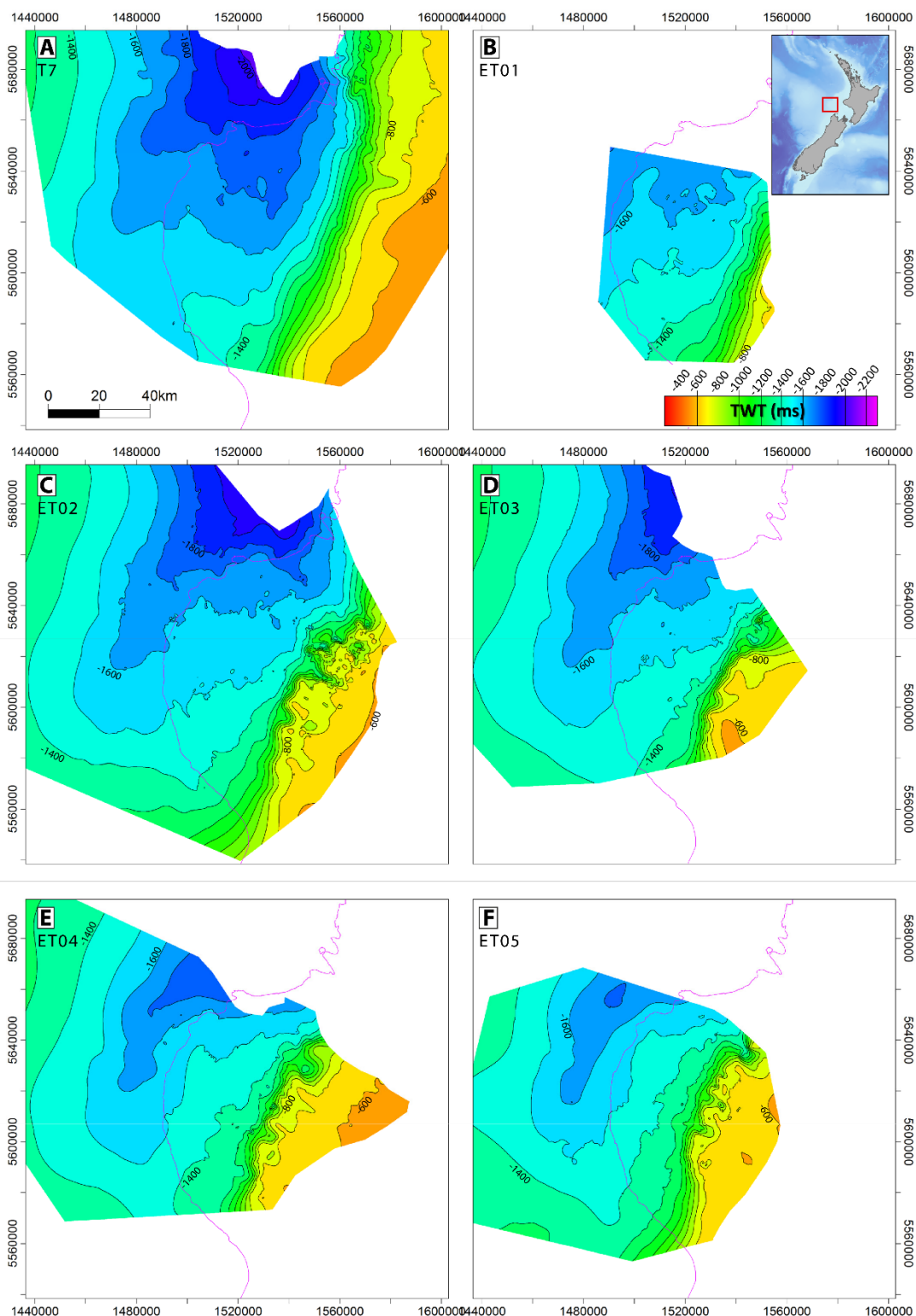


Figure 5.9 Time Structure Maps for T7 to ET05.

Time structure maps from Regional surface T7 to ET05. Modern shelf edge represented by dashed purple line. Location shown by inset map in panel B. In these panels the margin changes from a linear margin (A – B) to a more lobate geometry characterised by significant slope incisions (C – F), with extensive incision associated the ET02 sequence boundary (C). See Unit Descriptions for further discussion on about each surface.

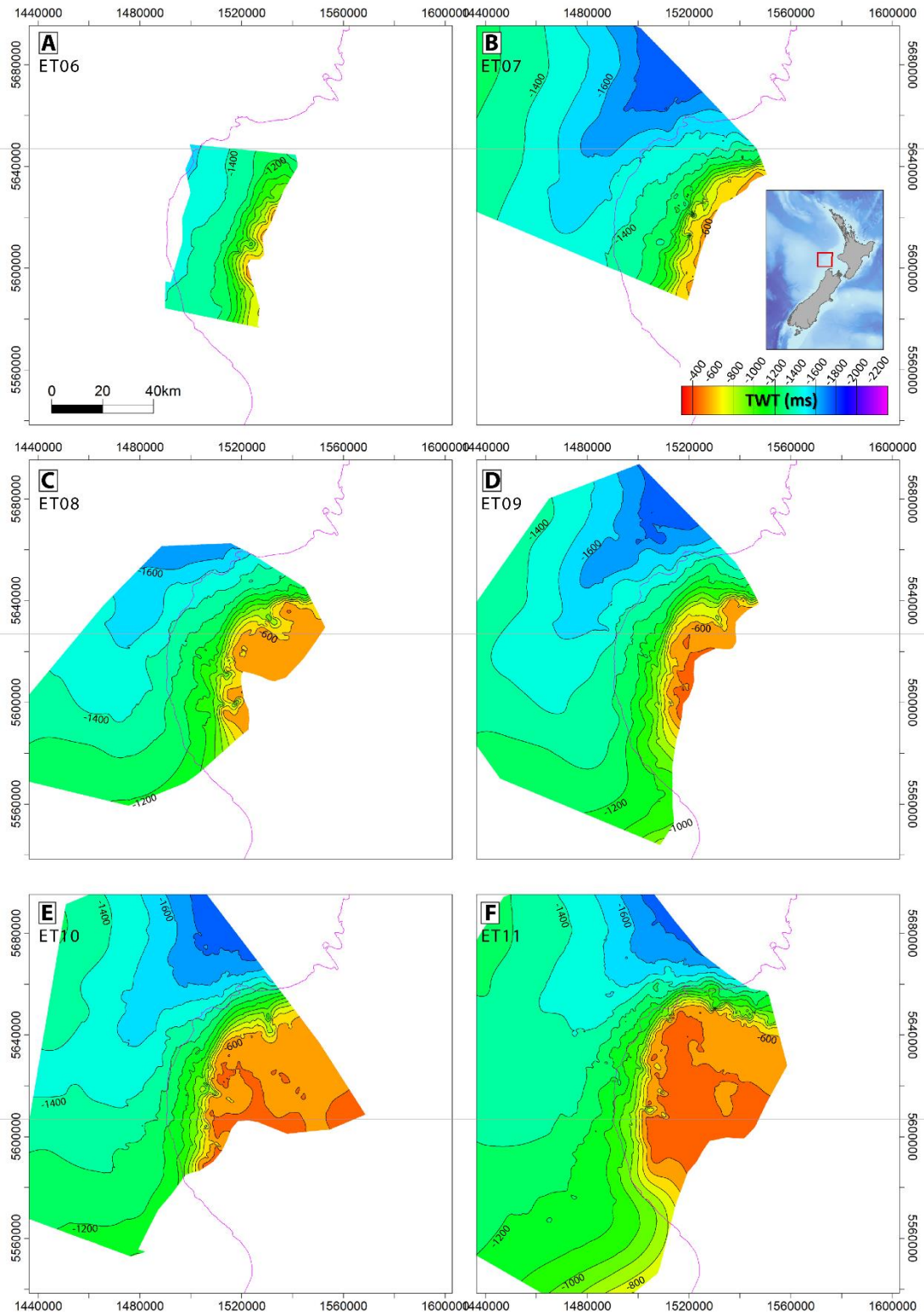


Figure 5.10 Time Structure Maps for ET06 to ET11.

Time structure maps for surfaces ET06 to ET11. Modern shelf edge represented by dashed purple line. Location shown by inset map in panel B. Maps in these panels record the progradation of the margin as it impinges upon the Challenger Plateau and interacts with accommodation in the Deepwater Taranaki Basin (Figure 5.2). See Unit Descriptions for further discussion about each surface.

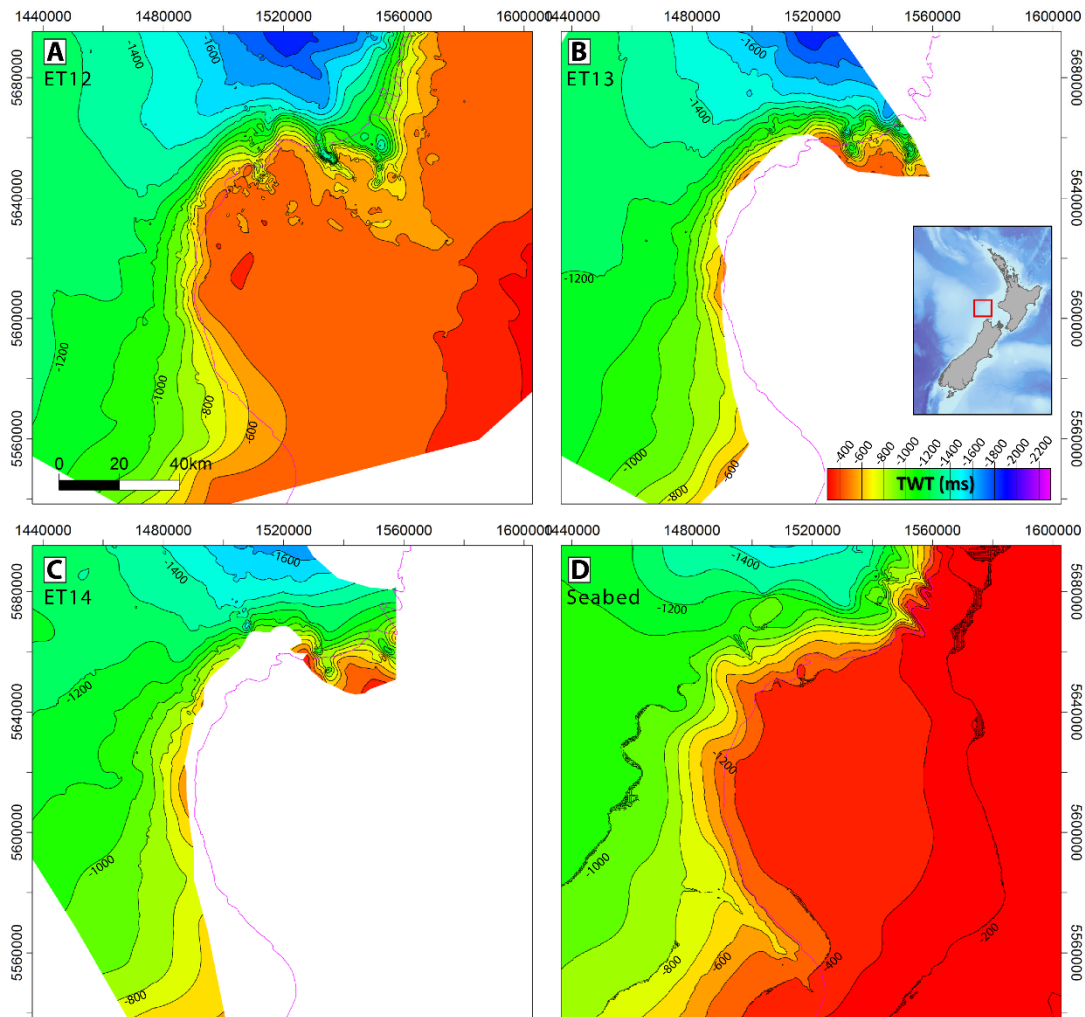


Figure 5.11 Time Structure Maps for ET12 to ET13

Time structure maps for surfaces ET12 to Seabed. Modern shelf edge represented by dashed purple line. Location shown by inset map in panel B. These panels show relatively smooth slope profiles on slopes facing the Challenger Plateau and a more heavily incised slope draining into the Deepwater Taranaki Basin. See Unit Descriptions for further discussion about each surface.

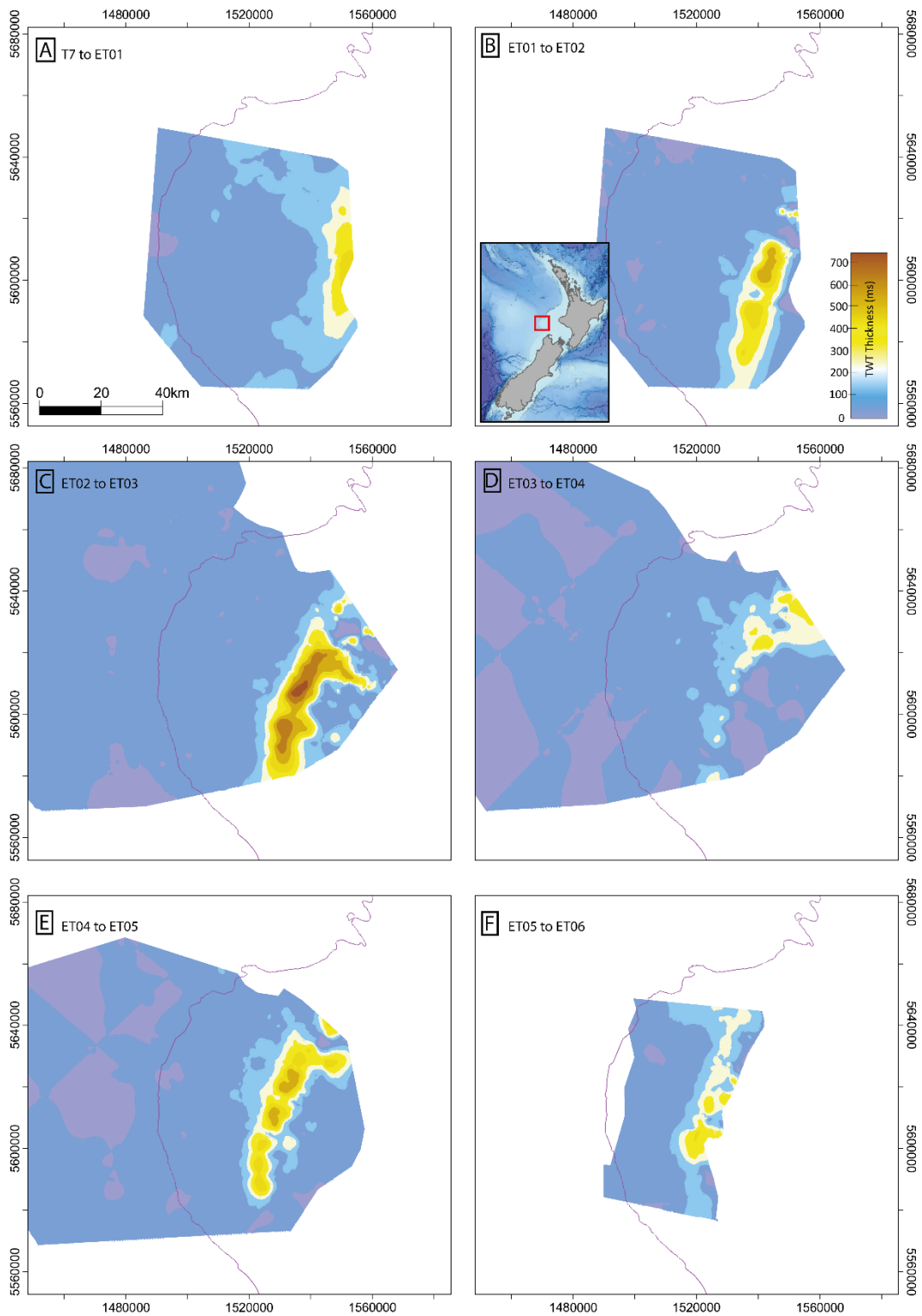


Figure 5.12 Time Thickness Maps for T7 to ET06

Time thickness maps for sequences T7 to ET06. Modern shelf edge represented by dashed purple line. Location shown by inset map in panel B. See Unit Descriptions for relevant discussion on about each surface.

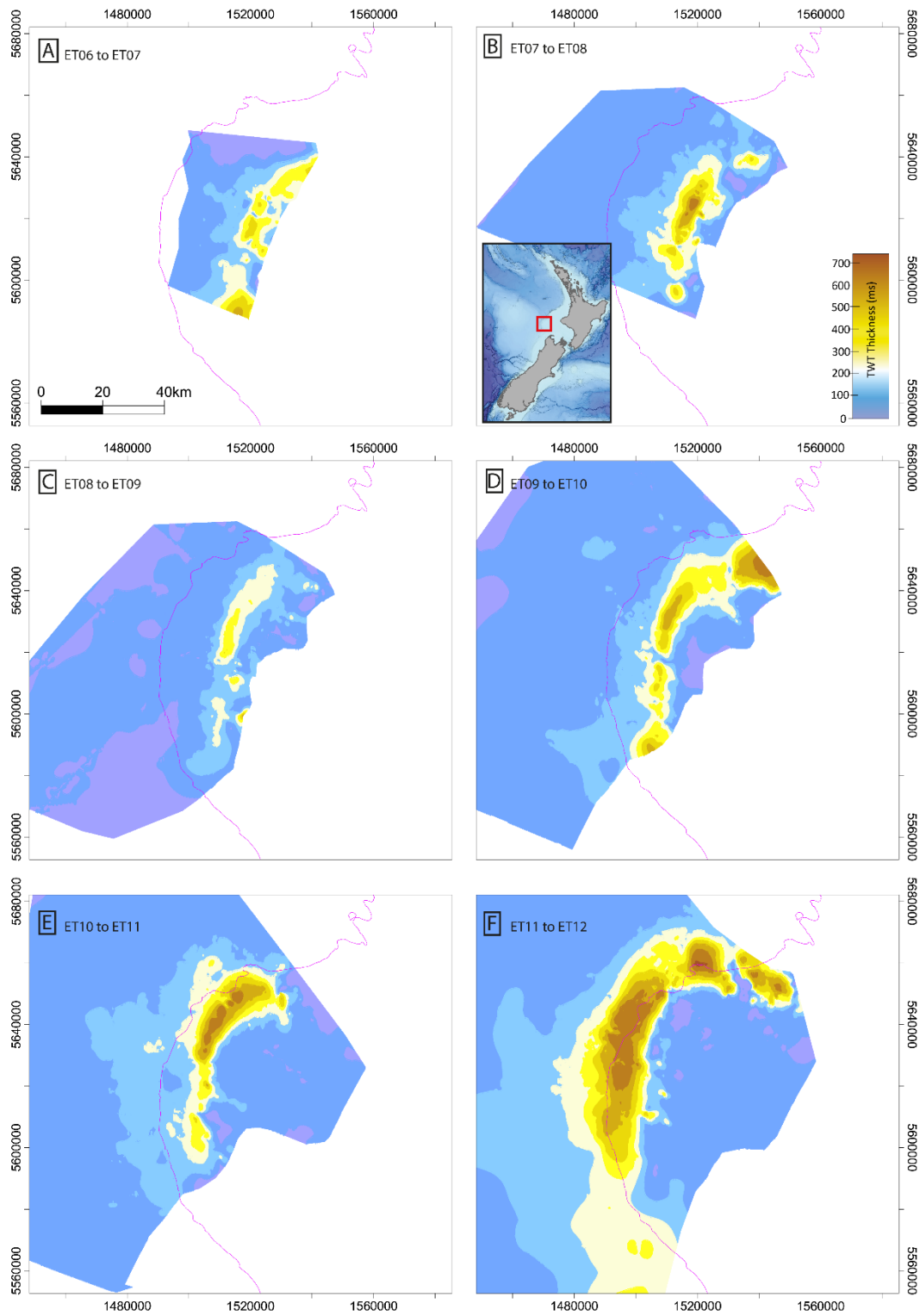


Figure 5.13 Time Thickness Maps for ET06 to ET12.

Time thickness maps for sequences ET06 to ET12. Modern shelf edge represented by dashed purple line. Location shown by inset map in panel B. See Unit Descriptions for relevant discussion about each map.

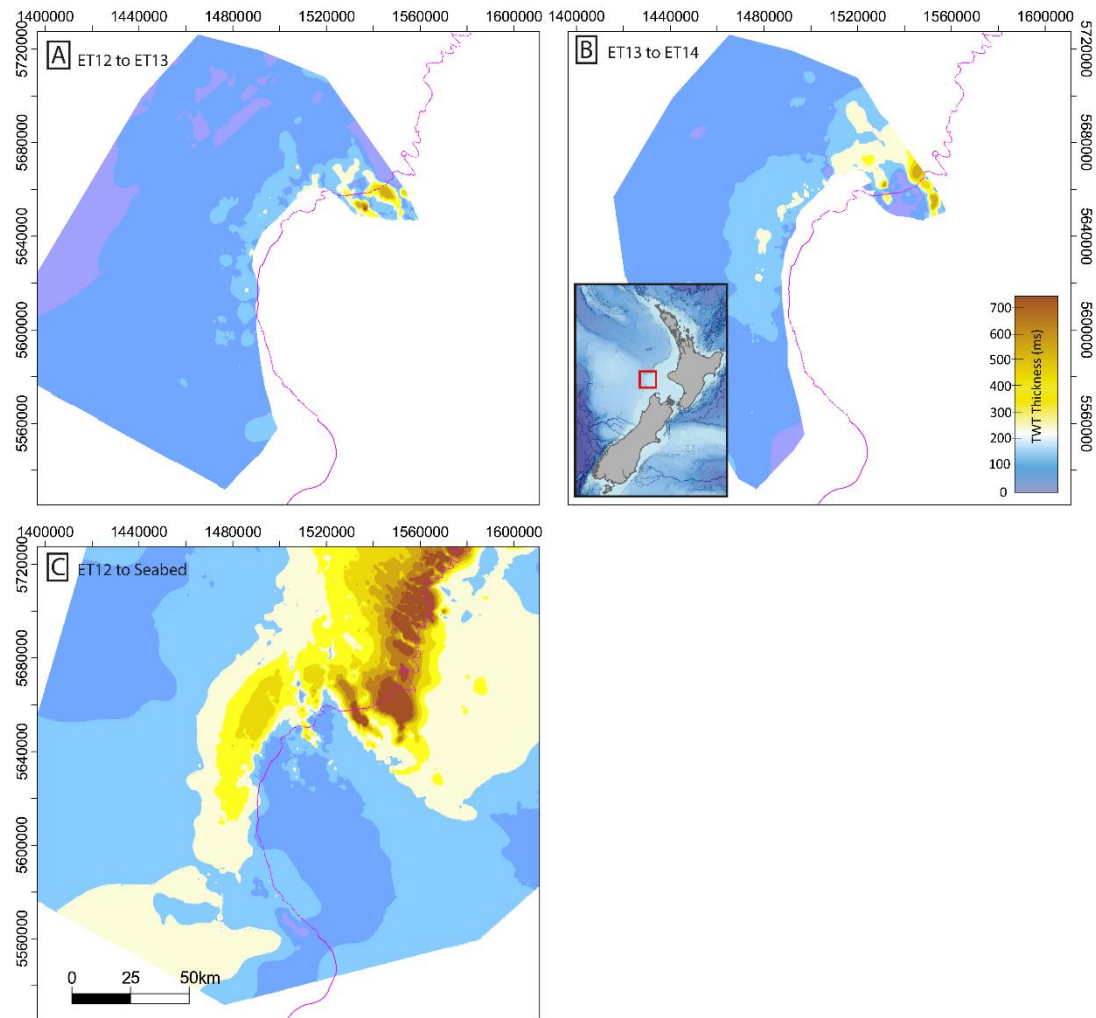


Figure 5.14 Time Thickness Maps from ET12 to Seabed.

Time thickness maps for sequences ET12 to seabed. Modern shelf edge represented by dashed purple line. Location shown by inset map in panel B. See Unit Descriptions for relevant discussion about each map. Thicknesses between ET12-seabed are also shown (Chapter 4).

5.3.1.1 Unit Descriptions

T7 to ET01 (Figure 5.9a & b and Figure 5.12a)

The stratigraphy between regional surface T7 and ET01 (Figure 5.15) is observed on only six seismic lines and much of the unit has been removed by post depositional erosion by ET02 (Figure 5.16b&c), particularly in the north of the Egmont Terrace region. Clinoforms offlap T7 at an oblique angle to the margin, in an approximately west-south-westerly direction (see Figure 5.16a&b), infilling accommodation in the south of the Western Stable Platform.

ET01 to ET02 (Figure 5.9b & c and Figure 5.12b)

Foresets of this unit are observed on only 6 seismic lines and have been modified by a later incision associated with ET02. In this time interval we see the first well developed slope fan in the Egmont Terrace succession.

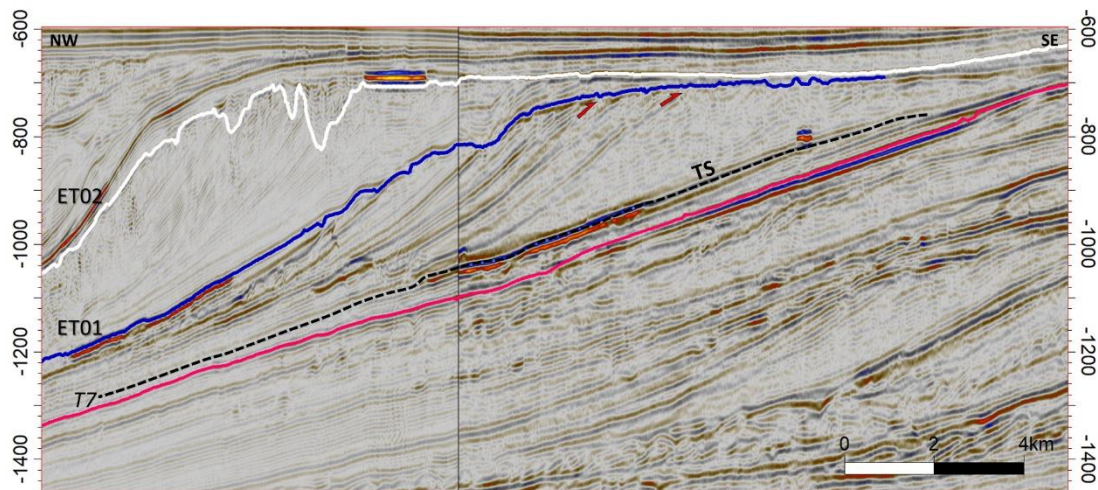


Figure 5.15 Composite seismic line of DTB08-44 & K98-9

Showing stratigraphy from T7 - ET02. Note extensive outer shelf incision associated with ET02. See Figure 5.3 for figure location.

ET01 incised and degraded the previous WSW offlapping highstand clinoforms, resulting in deposits being retained on the mid-lower slope as a slope fan. This is interpreted to represent a lowstand systems tract and is overlain by, low amplitude seismic facies interpreted to represent progradational highstand clinoforms downlapping onto a transgressive surface (dashed black line in Figure 5.17). Clinoforms between ET01-02 offlap in a WNW direction, marking a change in progradation of the GFF in this time period. This offlap direction shifts progressively towards the northwest resulting in the modern shelf break orientation. This shift in offlap direction may be related to a change in hinterland tectonics and sediment sources similar to those described in Chapter 4, where inversion related uplift along earlier cretaceous aged extensional faults is interpreted to have altered sediment pathways and diverted sediment to the northern depocenter.

ET02 to ET04 (Figure 5.9 c to e and Figure 5.12c & d)

ET02 is a strongly incisional event across the Egmont Terrace, affecting much of the underlying stratigraphy and complicating correlations (Figure 5.15 & Figure 5.16). Additionally, in the southern reaches of the Egmont Terrace there is a ~25 km section of dip lines with no cross-line control (see figures Figure 5.3 and Figure 5.6); this lack of cross line control is mitigated by the easily identifiable magnitude of incision on dip sections. A major change in offlap occurs across the ET02 boundary (Figure 5.16b), with clinoform offlap direction changing from a west south west direction to a northwest direction. A large canyon system approximately 8 km wide, 20 km long, with a depth of

550 ms (~550 metres) degraded the margin with creation of a highly incised shelf edge and generation of complex slope topography (see Figure 5.16a, Figure 5.17).

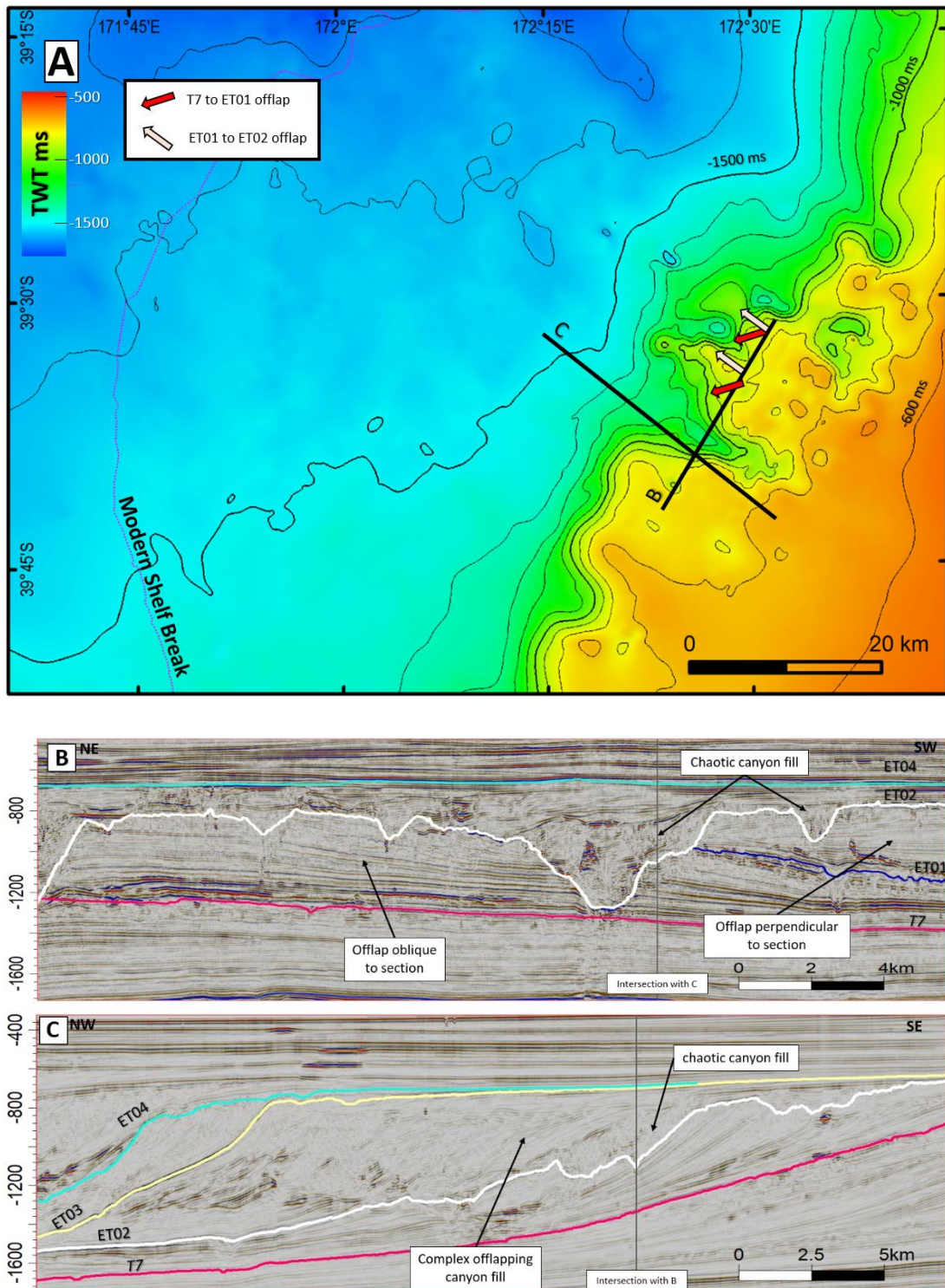


Figure 5.16 Change in offlap direction.

Map and seismic lines illustrating the change in clinoform offlap direction in pre & post ET01 stratigraphy. A) Time Structure map of surface ET02 with arrows illustrating the change in clinoform offlap direction from a west-south-westerly direction between regional surface T7 to ET01 (pink arrow) to a north-westerly direction in post ET01 stratigraphy (red arrow). B) Strike section K98-18 showing stratigraphy between regional surface T7 to ET04. Also note the change from oblique offlap to offlap

perpendicular to the seismic line across surface ET01. C) Dip section DTB01-31 showing significant incision of ET02 which has removed surface ET01. See A and Figure 5.3 for section locations.

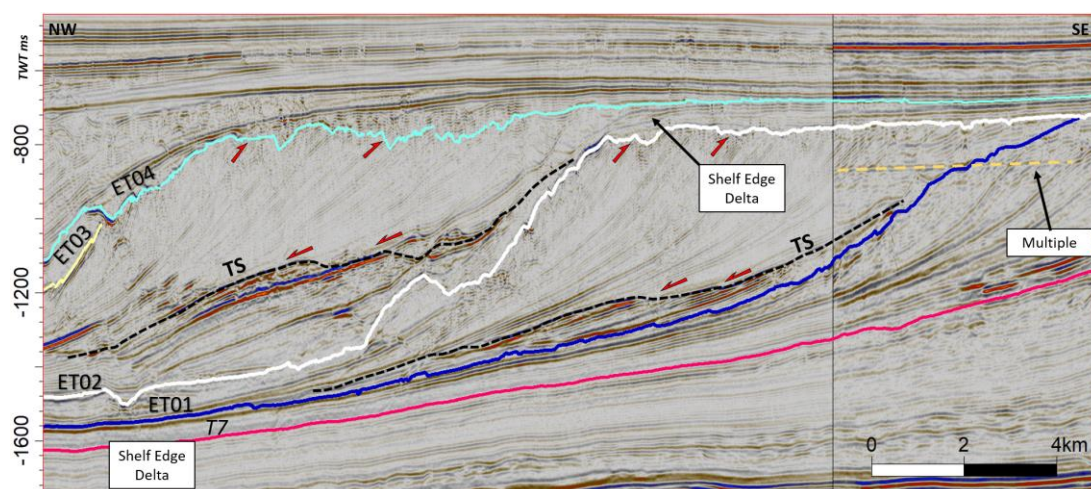


Figure 5.17 Composite seismic line of DTB08-42 & K98-11.

Showing stratigraphy from ET01 to ET04. Highstand reflectors are observed downlapping onto lowstand slope fan deposits above ET01 and ET02. See Figure 5.3 for figure location.

The basal portions of these canyons are filled with chaotic seismic facies, interpreted as a slump deposit. This chaotic facies is topped by complex offlapping and downlapping clinoforms as the canyon was filled and healed (Figure 5.16). In less incised areas of the Egmont Terrace a slope fan developed on the mid - lower slope, which is in turn overlain by low amplitude reflections arising from slope clinoforms sourced from a shelf edge delta downlapping onto the slope fan (Figure 5.17). Moving downslope, many of these low amplitude reflections pass to a higher amplitude facies.

Due to limitations in data quality from shallow gas and seismic coverage, it was not possible to map the sequence boundary of ET03 (e.g. Figure 5.16c). However, the interpreted transgressive surface/flooding surface was observable and correlated across numerous dip sections. This flooding surface subsequently underwent incision by the ET04 sequence boundary (Figure 5.17).

ET04 to ET06 (Figure 5.9e to Figure 5.10a and Figure 5.12 e & f)

Strata from ET04 to ET08 (Figure 5.18) represent the beginning of a more cyclical period of progradation on the Egmont Terrace. As with previous sequences, underlying highstand clinoforms are incised by the ET04 sequence boundary, to create a concave slope profile. This has been infilled and healed by a deposit characterized by high amplitude continuous reflections downlapping and onlapping into the concave slope topography. This deposit is interpreted as a slope fan. This slope fan was subsequently abandoned as transgression occurred, creating a transgressive surface at the top of the

slope fan. This is overlain by progressively steeper, low amplitude, semi-continuous reflections downlapping on to the transgressive surface; these are interpreted as highstand aggradation and progradation of the margin.

Progressive over steepening of these clinoforms resulted in margin degradation and formation of the ET05 sequence boundary and generation of a concave slope profile (Figure 5.18). Infilling this accommodation is a localised base of slope fan overlain by continuous medium to high amplitude reflectors interpreted as a slope fan. The slope fan is overlain by thin, locally developed transgressive deposits and a shelf edge delta; this delta passes from low-medium amplitude continuous reflectors on the upper slope to locally high amplitude reflectors on the mid to lower slope (Figure 5.18) indicating a potential pulse of coarser sediment delivery across the shelf edge in highstand.

ET06 to ET08 (Figure 5.10a to c and Figure 5.13 a to c)

The ET06 sequence boundary is locally developed and cryptic in some areas, merging to either a condensed sequence with the underlying highstand or to the top of the above-mentioned high amplitude body originating from the shelf edge delta (S.E.D). Only minor, localised incision and slope fan development is observed (Figure 5.19). Truncation of the slope fan and low amplitude semi continuous reflectors overlying ET06 along with a chaotic seismic facies is interpreted to represent localised mass wasting (Figure 5.18).

The ET07 sequence represents a complex incisional event with a deeply incised outer shelf margin. Accommodation generated in the degradation of the margin was highly variable, resulting in varied infill and healing slope fan thicknesses (compare Figure 5.18 and Figure 5.19). Lowstand deposits are overlain by regional surface T8. Although T8 represents a flooding surface, a large canyon (9 km across by 22 km long by 800 m (~800m) in depth) incises the shelf margin removing much of the underlying ET07 sequence at this location (Figure 5.7) Localised slumping is also observed in the overlying highstand clinoforms of low seismic amplitude (Figure 5.18).

The ET08 sequence boundary is comparatively less incised than other sequence boundaries on the Egmont Terrace; minor outer shelf degradation is observed but only subtle concave slope accommodation is generated from initiation of the sequence boundary (Figure 5.19). This has resulted in deposition of a thin slope fan overlain by a thick highstand clinoform succession characterised by low amplitude semi-continuous reflections above ET08.

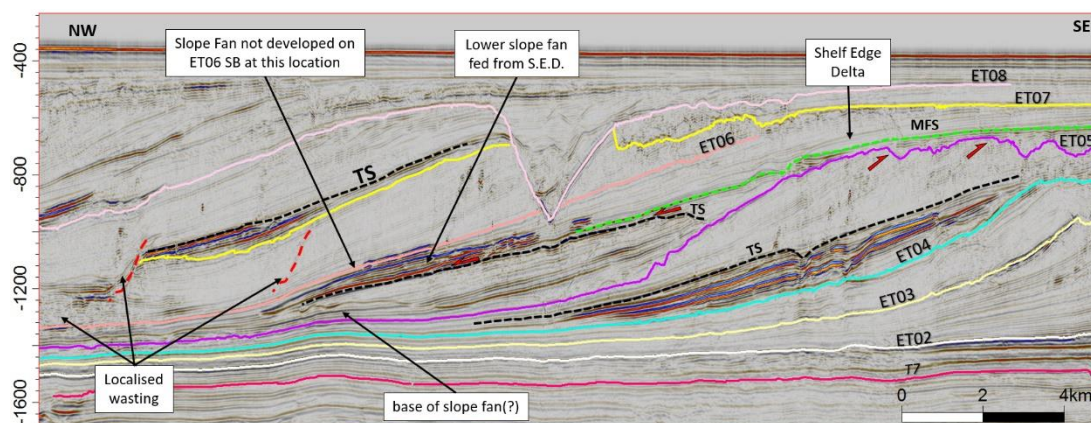


Figure 5.18 Seismic line DTB08-46 showing stratigraphy from ET03 to ET08.

In this location a shelf edge delta overlying ET05 passes to high amplitude deposits typically associated with lowstand seismic facies, suggesting delivery of coarse sediment to the lower slope. Note also that no slope fan is developed at this location in association with the ET06 sequence boundary. See Figure 5.3 for figure location.

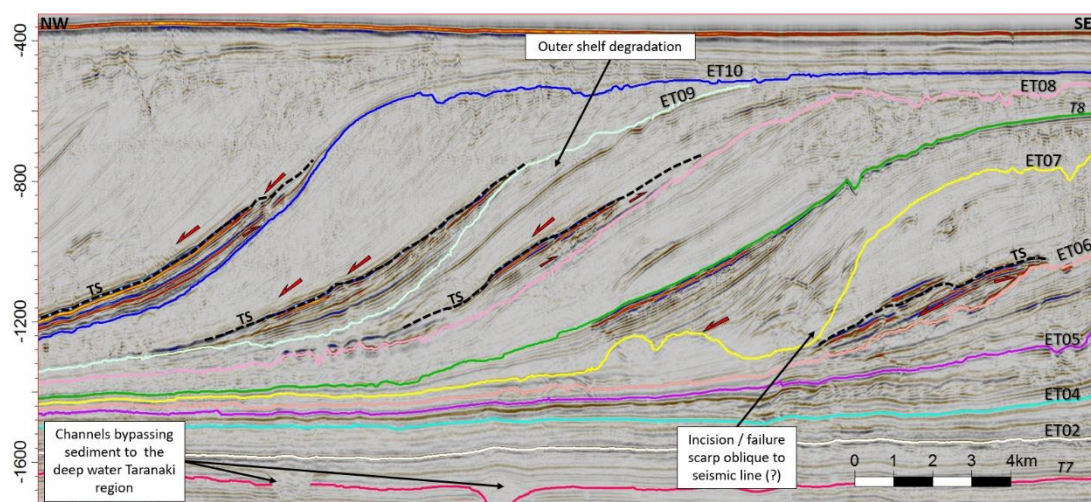


Figure 5.19 Seismic line DTB08-42 showing stratigraphy from ET06 to ET10.

Incision associated with ET07 has resulted in a complex package of reflections in this location, suggesting incision oblique to the line of section. Regional surface T8 is also observed on this section and represents a regional flooding surface. See Figure 5.3 for figure location.

ET09 to ET12 (Figure 5.10d to Figure 5.11a and Figure 5.13 d to f)

The ET09 sequence boundary is affected by outer shelf degradation, erosion of underlying highstand strata and generation of a concave slope profile, which was infilled by a slope fan characterized by high amplitude continuous reflections (Figure 5.19 and Figure 5.20). This is in turn overlain by low amplitude semi-continuous reflectors interpreted to represent highstand progradation.

A similar architecture is repeated for the ET10 sequence boundary but with less outer shelf incision into the underlying highstand clinofolds. On the lower slope to basin floor

transition, sediment waves are observed in association with the low amplitude highstand clinoforms (Figure 5.20). Sediment wave crests are oriented approximately parallel to the shelf margin (observations limited to 2D data).

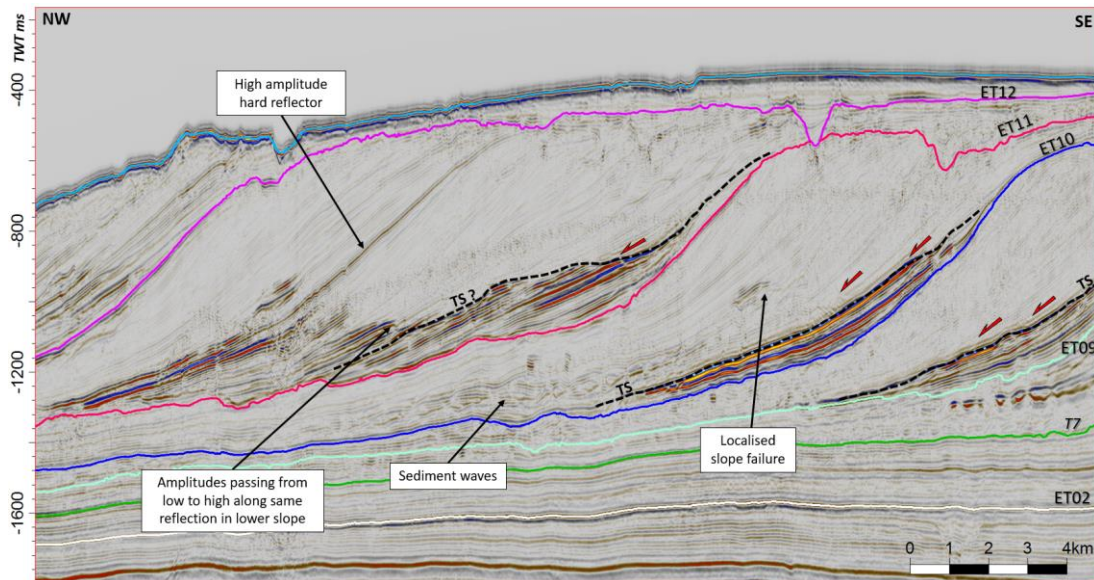


Figure 5.20 Seismic line DTB08-42 showing stratigraphy from ET09 to ET12.

Lowstand slope fans displaying high seismic amplitudes overlain by acoustically transparent, low amplitude reflectors typical of highstand facies. Some localised high amplitudes overlying the ET10 slope fan may be associated with coarse material from delivered over the shelf by a shelf edge delta. See Figure 5.3 for figure location.

As with earlier sequences, the ET11 sequence boundary incises low amplitude highstand clinoforms. The concave slope topography associated with ET11 degradation was highly incisional on the slope; the subsequent infill and healing of this topography has generated an undulatory topography. The low amplitude clinoforms typical in highstand progradation downlap onto the slope fan, later highstand clinoforms in the sequence appear to pass downslope from low to high amplitude in the lower slope (Figure 5.20). The base and top of this body is discussed further in section 5.3.2.

The highstand clinoforms between ET11 – ET12 are punctuated by a high amplitude ‘hard’ reflection (i.e. a downward increase in acoustic impedance) traceable across the Egmont Terrace (Figure 5.20). This horizon may represent a cemented condensed horizon. Overlying this high amplitude reflection are further low amplitude prograding clinoforms with isolated high amplitude bodies, interpreted to be sourced from delivery of coarser material over the shelf edge.

ET12 to ET14 (Figure 5.11a to d and Figure 5.14 a to c)

ET 12 – ET14 was initially mapped as one sequence (ET12 – Seabed) but was later subdivided into three units when attempting to extend interpretations to the northern depocentre. In the regional evolution of the basin (Chapter 4), a large slope failure was observed to the north of the Egmont Terrace. This failure generated a large MTD that ran out approximately 220 km into the deep-water regions of the basin. Additionally, it generated a significant amount of accommodation both in the northern depocentre and the heavily incised corridor separating north from south (see Unit H in the regional study). The accommodation generated by this event affected the regional progradation patterns, with sedimentation focused on the incised corridor separating north from south (Figure 5.21Figure 5.21B) and resulting in comparatively less stratigraphy preserved on the Egmont Terrace (Figure 5.21A). A basin floor fan can be observed abutting the challenger plateau, as with some underlying sequences ET10 and ET11 (Figure 5.21A).

5.3.1.2 Progradation Dynamics

The compiled stratigraphy described above is summarised in Figure 5.5 and seismic sections in Figure 5.6 to Figure 5.8. From Figure 5.5 we can observe that the axis of progradation has stepped gradually north as the margin has prograded (i.e. in the direction of accommodation in the deepwater Taranaki Basin). This sequential migration of the progradational axis is best observed in strike sections of Figure 5.8 and Figure 5.23, where autogenic compensational infill of accommodation is interpreted. An additional control on this northward migration of the progradational axis is the impingement of the Giant Foresets Formation on the Challenger Plateau.

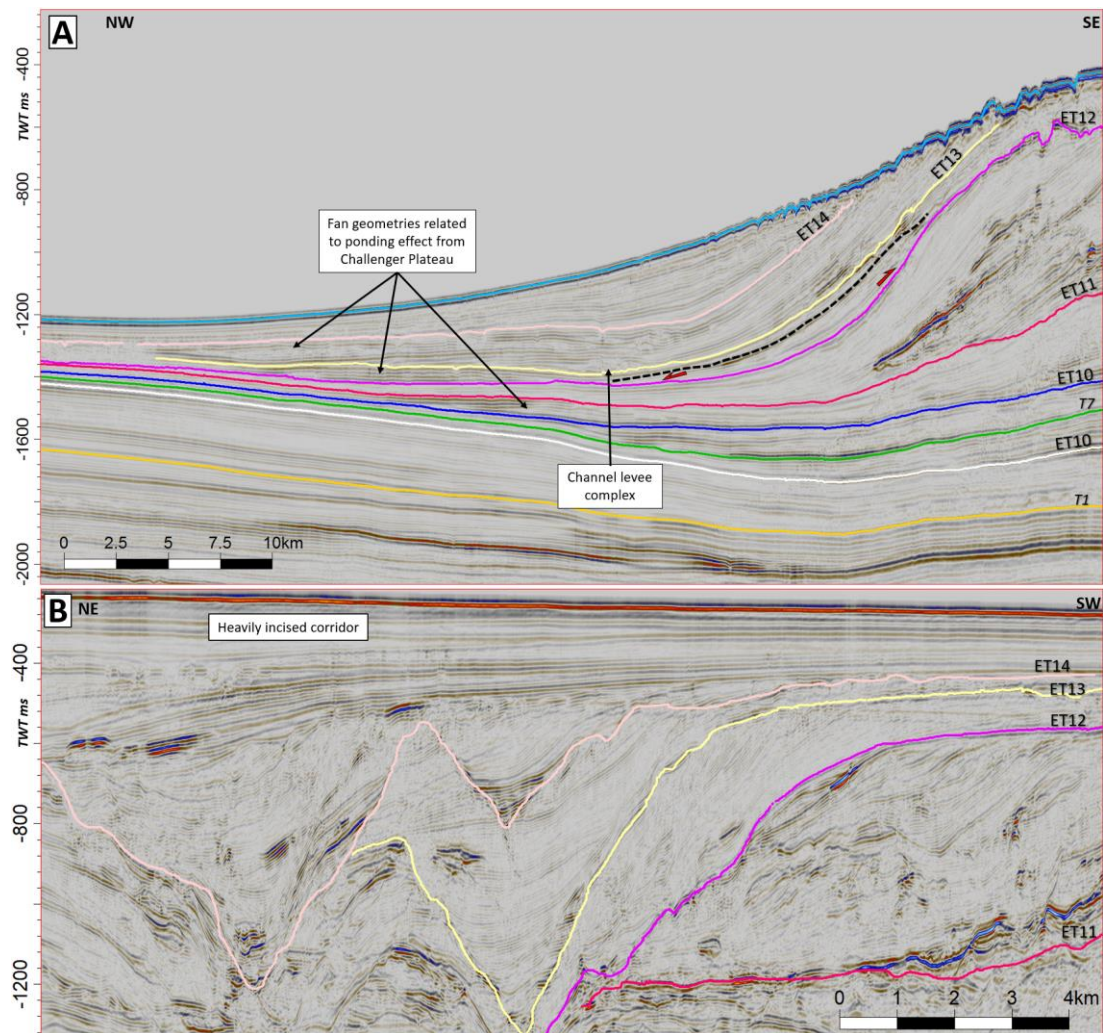


Figure 5.21 Stratigraphy from ET12 to Seabed.

A) Dip section DTB01-31 showing limited accumulations in the bottomsets and B) Strike section DTB08-129 showing units ET12-14 offlapping to the northeast into the incised corridor. See Figure 5.3 for figure location.

5.3.2 High amplitude deposits

High amplitude clinoform deposits have been described in the preceding section and occur cyclically (i.e. at regular time intervals) throughout the Giant Foreset stratigraphy of the Egmont Terrace. In this section these high amplitude bodies are described geologically and geophysically.

5.3.2.1 Geological Description

The basal surfaces display a concave upward geometry with steepest gradients near the shelf edge; they are interpreted here as out of grade or erosional margins (Hedberg, 1970; Prather, 2003; Prather et al., 2017, 1998; Ross et al., 1995, 1994). The regional erosional nature of these surfaces is consistent with their interpretation as sequence boundaries with the infilling slope fans interpreted as lowstand slope fan/apron deposits (Posamentier et al., 1988; Van Wagoner et al., 1988).

The slope fan deposits typically downlap and onlap concave upward accommodation on the slope. High amplitude seismic facies are mostly associated with slope fan geometries, however the full thickness occupied by the slope fans is not always anomalously high in amplitude (e.g. slope fan overlying ET05 in Figure 5.19). In the North Slope of Alaska, Ramon-Duenas et al. (2018) report that on average, out-of grade slopes show higher amplitude seismic facies which is likely related to sandier interbeds, due to downslope bypass via turbidites.

The geographic distribution of slope fans displaying anomalously high amplitudes is shown in Figure 5.22. Additionally, the anomalously high amplitudes are not exclusively confined to the slope fan; anomalously high amplitude reflections can often be observed downlapping on top of the slope fans; where this is observed these reflections often pass from low amplitude to high amplitude in the mid to lower slope region; for example, anomalous amplitudes overlying the slope fan associated with the ET05 sequence boundary are associated with a highstand shelf edge delta. Localised high amplitude bodies are also observed in the topsets of the Giant Foresets Formation (e.g. Figure 5.15).

Slope fans infill slope accommodation generated in the degradation phase of a depositional sequence. This degradation is likely caused by cyclical over-steeping and collapse of graded highstand clinoforms, resulting in an out of grade margin where sediment bypass was dominant in the shelf to upper slope (Hedberg, 1970; Prather, 2003; Prather et al., 2017, 1998; Ross et al., 1995, 1994). The degree of degradation and incision has resulted in variation in the basal surface of the slope fans (Figure 5.23). The base of ET10, for example, is smooth in both dip and strike sections, in stark contrast to the highly incisional and irregular base of the ET11 sequence boundary (Figure 5.23). This relationship is also observed on thickness maps in Figure 5.24.

Slope fans are developed as broadly linear northeast trending bodies up to ET07_HA, whilst fans from ET08 to present tend to be deposited as more arcuate deposits wrapping around the slope (Figure 5.22) with the thickest deposits typically on the northern flank of the Egmont Terrace (Figure 5.24) where the deepwater region of the Taranaki Basin provided additional accommodation.

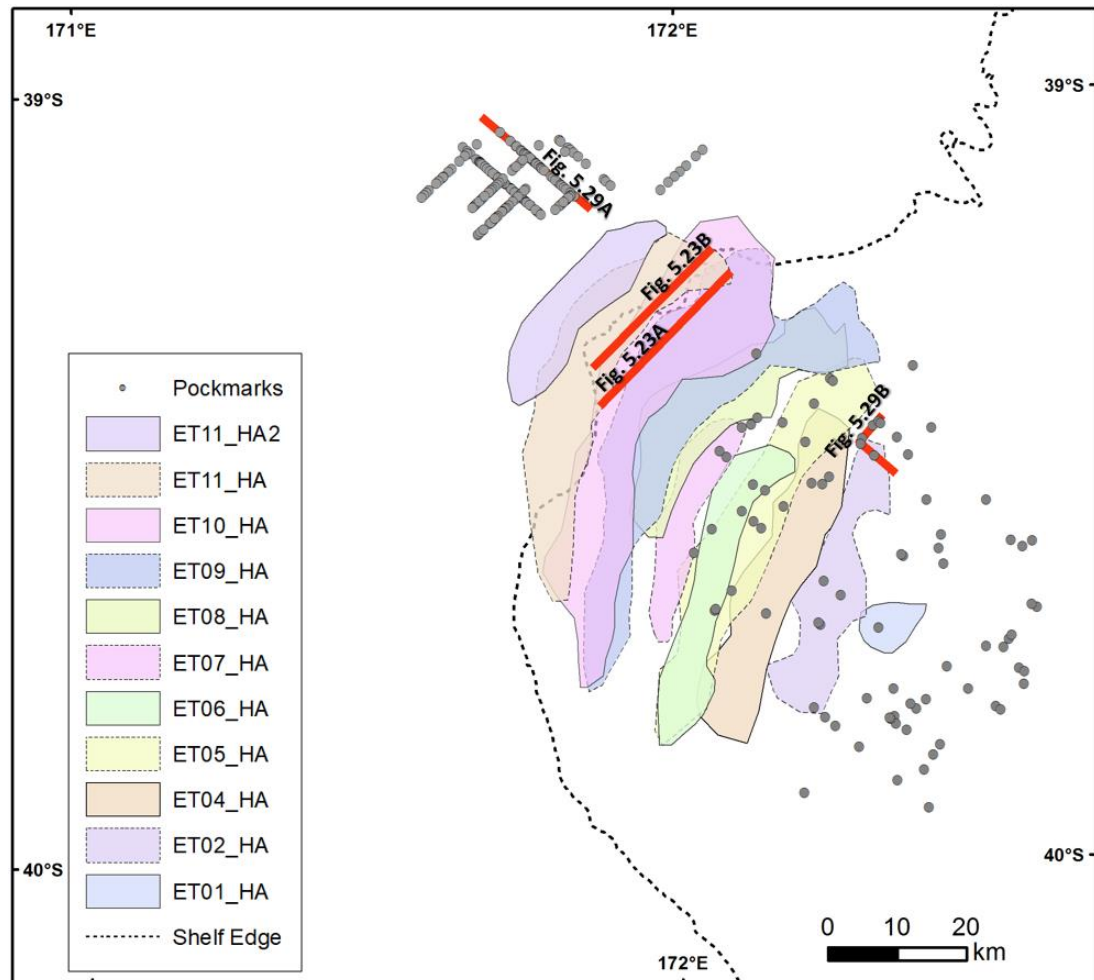


Figure 5.22 *Distribution of High-Amplitude (HA) Bodies on the Egmont Terrace.*

Nomenclature is such that each body is named after the basal bounding surface (e.g. ET10_HA is the high amplitude body overlying surface ET10). Outlines are alternately dashed / undashed to allow for easier identification of overlapping polygons. Pockmark locations are marked by grey circles and are not representative of the actual size of pockmarks.

A similar smooth vs. incised relationship is also observed for the top of the ET10 and ET11 slope fans whereby the top of ET10 is smooth and the top of ET11 is irregular and incised (Figure 5.8 & Figure 5.23). A possible explanation for this contrasting relationship is a rapid transgression and abandonment of slope deposition for the ET10 slope fan, resulting in a condensed, undisturbed transgressive surface at the top of the fan. Whereas the incision overlying the ET11 slope fan can be explained by the slope fan healing topography in a similar manner to the ET10 slope fan, however, in this case it was followed by a second base level fall shortly after transgression, inducing bypass and degradation of the existing slope fan (Figure 5.20 & Figure 5.23). Such a second base level fall is observed in Marine Isotope Stage 7 in correlations to the Global Eustatic Sea level curve in proceeding sections of this chapter.

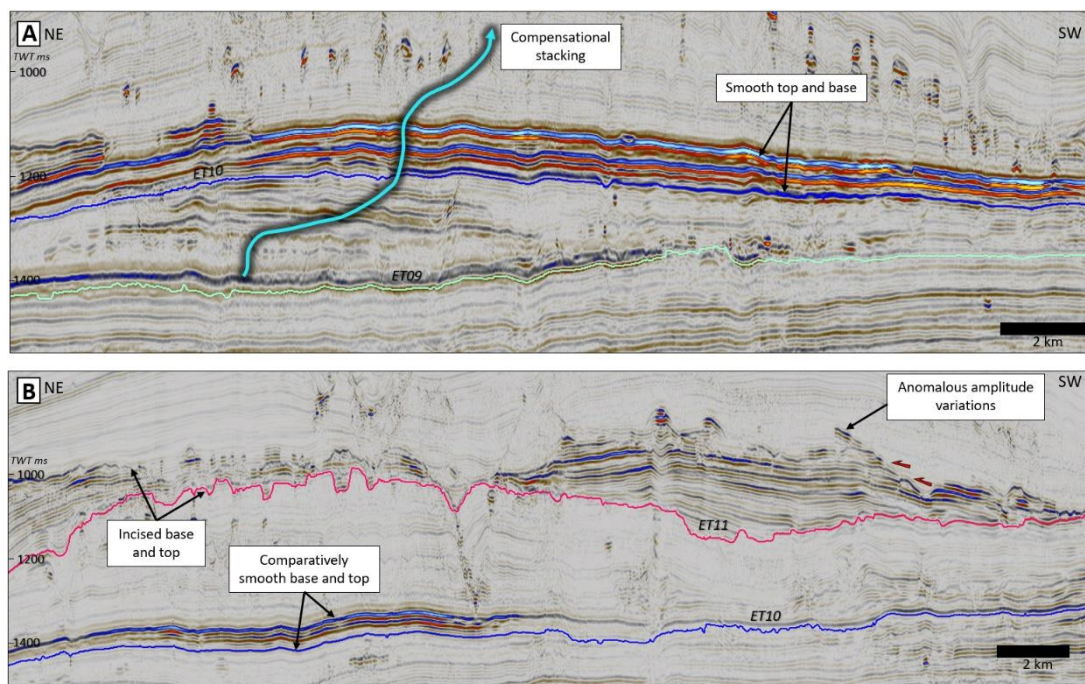


Figure 5.23 Variability in slope fan geometries.

A) Smooth top and base to slope fan overlying surface ET10 and B) Heavily incised base and top of slope fan overlying ET11 with low amplitude highstand deposits onlapping the slope fan. Also note compensational aggradation of deposits in A.

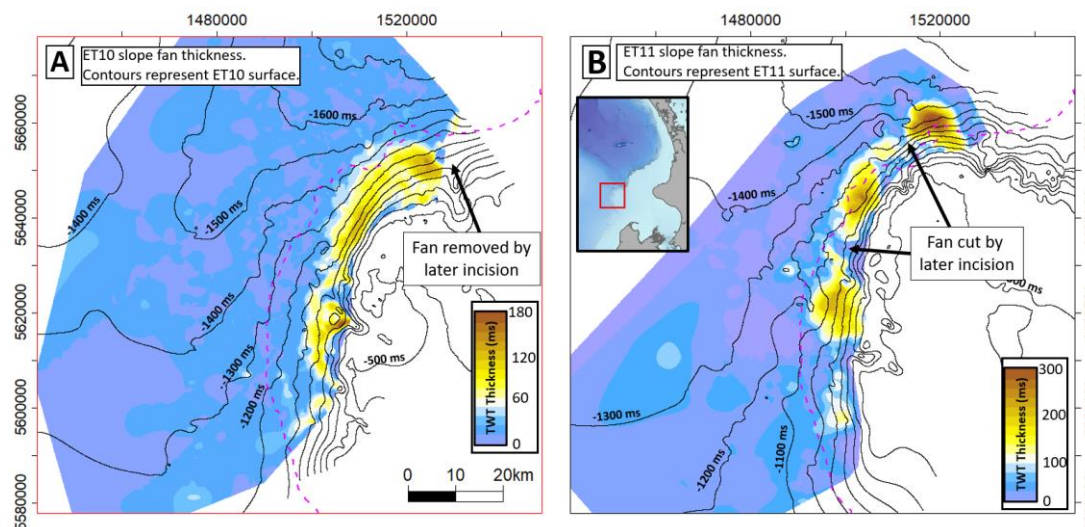


Figure 5.24 Time thickness maps of slope fans overlying A) ET10 and B) ET11.

Colours represent slope fan thickness whilst contours show the structure of the basal surfaces (i.e. sequence boundaries/correlative conformities). Location given by inset map in B. Slope fan overlying ET10 (A) forms a semi-continuous sheet along the slope whilst slope fan overlying ET11 (B) has been compartmentalised by later incision. In both instances, the most extensive deposition occurred on the northern flanks of the Egmont Terrace, likely due to accommodation of the deepwater Taranaki Basin.

5.3.2.2 Geophysical description of the high amplitude deposits.

The anomalous high amplitude reflections investigated in this section are consistently negative amplitude (blue in seismic amplitude colour bar) ‘soft’ topped anomalies (i.e. a downward decrease in acoustic impedance). The reflection coefficient of the soft

anomalies' acoustic impedance (A.I.) is quantitatively compared to that of the seabed overlying the anomaly as this reflection separates seawater and muddy substrate (i.e. another large impedance contrast) of relatively well constrained acoustic properties. By assuming standard muddy substrate properties at seabed and above the soft anomalies the acoustic impedance of the causative soft layer can be estimated. Investigation was carried out on zero phased seismic line DTB01-31 in IHS Kingdom 8.8 (Figure 5.25). The ET10 slope fan has an amplitude of approximately -39,000. To remove the possibility of the anomaly being caused by the bed being at or near the survey's tuning thickness this is detuned to a value of -27,850 (-39,000/1.4).

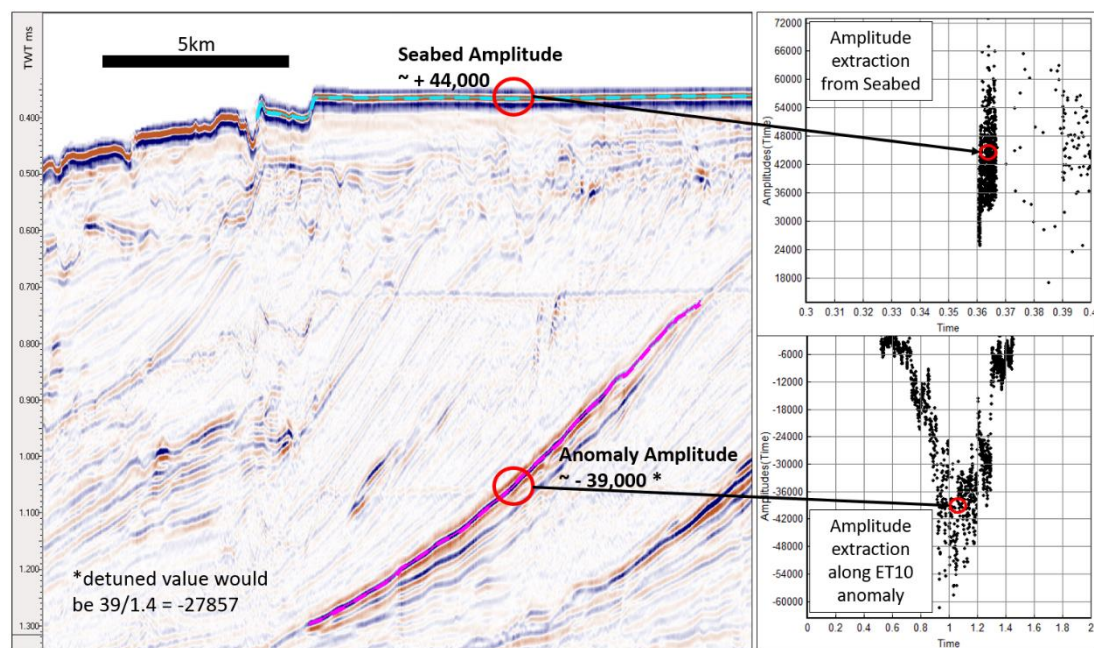


Figure 5.25 Amplitude extractions along DTB01-31

Comparing the magnitude of amplitude anomalies of the seabed against the soft topped anomaly of the ET10 slope fan.

- The acoustic impedance of seabed mudstones was calculated at approximately 3.4 using a seawater V_p of 1500 m/s and density of $1 \times 10^3 \text{ kg/m}^3$ and a shallow sediment density of $2 \times 10^3 \text{ kg/m}^3$ and V_p of 1700 m/s) using the equation:

$$\text{Acoustic Impedance} = V_p * \text{Density}$$

- From this the R_c of the seabed was derived as approximately 0.4 using the equation:

$$R_c \text{ Seabed} = \frac{(A.I. \text{ Seabed} - V_p \text{ seawater})}{(A.I. \text{ Seabed} + V_p \text{ seawater})}$$

- A background A.I. value of $5.28 \times 10^6 \text{ kg/m}^2\text{s}$ was then derived using Vp and density values of 2400 m/s and $2.2 \times 10^3 \text{ kg/m}^3$, respectively, from nearby well Kiwa-1 at a depth of approximately 1000 m.
- Using the RC of the seabed as a comparison, the RC of the slope fan anomaly is derived from the equation below giving a value of -0.25.

$$RC \text{ Anomaly} = \left(\frac{\text{Anomaly Amplitude}}{\text{Seabed Amplitude}} \right) * RC \text{ Seabed}$$

- From this, an acoustic impedance value of the ET10 slope fan amplitude anomaly of 3.168×10^6 was then derived by back calculating the equation:

$$RC \text{ Anomaly} = \frac{(\text{Anomaly A.I.} - \text{Background A.I.})}{(\text{Anomaly A.I.} + \text{Background A.I.})}$$

An AI of approximately 3.2 can be achieved by a combination of VP and density of e.g. 1600 m/s and 2000 kg/m^3 , equivalent to a low saturation gas sand.

5.4 Discussion

5.4.1 Age Model

The results above show, for the first time, a detailed progradational history of the Giant Foresets Formation on the Egmont Terrace; however, better age constraints would be beneficial to unravelling the mechanisms controlling progradation.

As discussed in Chapters 3 and 4, age constraints of the Giant Foresets Formation are sparse, particularly in Pleistocene strata of the Taranaki Basin. To overcome this lack of age control, stratal relationships and sequence boundaries have been correlated to fluctuations in global eustatic sea level (Lisiecki and Raymo, 2005; Miller et al., 2011). Correlations were carried out by counting back from a surface of known age (i.e. seabed = 0 ky) and matching sequence boundaries to the beginning of each glacial period (evenly numbered Marine Isotope Stages (MIS)). This method involves significant assumptions, uncertainties and errors in assigning precise MIS boundary ages to events in the depositional record; consequently, the ages derived from this correlation should only be used as first-pass approximate ages and not as a “golden spike” in the geological record. A similar cycle counting approach was used accurately in the neighbouring Wanganui Basin, with correlations also confirmed by a multiproxy approach integrating radiometric ages of interbedded rhyolitic tephtras, biostratigraphic data, paleomagnetic polarity

measurements, and cycle correlations with the oxygen isotope timescale (Naish et al., 1998). In using this cycle counting method, several assumptions and considerations must be made, as follows;

1. Eustatic sea level exerts the dominant control on accommodation and the generation of sequence boundaries in this part of the basin. On the Egmont Terrace there is no evidence of movement of major structural features to generate accommodation although, as the margin prograded and impinged on the Challenger Plateau we must consider the impact this had on stratal geometries.
2. Sediment supply to the Egmont Terrace did not fluctuate significantly through the study interval. This, and other source to sink considerations, are addressed further in Chapter 6.
3. One eustatic sea level cycle will result in deposition of one depositional sequence observable on a seismic scale.
4. The depositional system responded in a geologically fast manner to sea level changes.

Surfaces are correlated to the eustatic sea level curve of Miller et al. (2011) in Figure 5.26; from this correlation approximate horizon ages are listed in Table 5.2.

Counting back from the seabed, it is possible to correlate, with a modest degree of confidence, up to eleven sequences (ET14 – ET04); bringing interpretations to approximately 900,000 years (start of MIS 22). Correlation of stratigraphy from ET04 to T7 is more uncertain, although a notable change in the cyclicity and increased incision is observed. This change in cyclicity and incision correlates well to the Mid Pleistocene Transition (MPT); a period between approximately 1.2 million and 900,000 years in which the pacing of sea level fluctuations changed from obliquity paced, 41,000 year cycles to an average cyclicity of 100,000 years. This 100,000 year periodicity is commonly referred to as the eccentricity myth (Maslin and Ridgwell, 2005), and is likely a result of every second or third obliquity cycle (Huybers and Wunsch, 2005) or every fourth - fifth precessional cycle (Maslin and Brierley, 2015; Ridgwell et al., 1999) or, indeed a combination of the two (Huybers, 2011). In addition to a change in the duration of sea level cycles, the MPT represents a change in the magnitude of sea level fluctuations from general pre MPT fluctuations typically less than 60m, to post MPT fluctuations in excess of 100 m (Miller et al., 2011). The pacing and magnitude of eustatic sea level fluctuations

during the MPT itself do not follow a particular Milankovitch pacing. Due to the obscure cyclicity and increased amounts of incision (related to a fall in base level), the stratigraphy between T7 and ET04 is tentatively interpreted to represent the MPT.

In deep sea sediment cores around New Zealand, the MPT is recognisable after 0.87Ma with stable 100 kyr cycles only developed from approximately MIS 12 (Crundwell et al., 2008). Qualitatively examining the stratigraphy of the Egmont Terrace, a similar pattern may be recognised; in Figure 5.20, Figure 5.6 and Figure 5.7 the clearest cyclicity occurs from ET09 (correlated to MIS 12) onward.

In the neighbouring Whanganui Basin, a 2 km thick shallow marine basinal sequence spanning the entire Quaternary has been studied in detail and tied to Milankovitch cyclicity by magneto-stratigraphy, biostratigraphy and dating of interbedded tephra (Pillans, 2017). 47 unconformity bound shallow marine sequences were correlated by Carter and Naish, (1998) and Saul et al. (1999), from MIS 100 to MIS 3. Deposits consist mostly of shallow marine transgressive, highstand and regressive deposits truncated by a subaerial unconformity; in highstand the Taranaki and Whanganui Basins were linked by the same body of water with minor interfingering of deposits from the D'Urville Current (Gillespie et al., 1998; Gillespie and Nelson, 1996). In Lowstand, the two basins were separated by the Patea–Tongaporutu High and Farewell Rise (Figure 2.4). Correlations of lowstand deposits between the two basins have not been possible; Beggs (1990) and Abbott and Carter (1994) postulated that lowstand deposits missing from the Whanganui Basin were bypassed to the Giant Foresets Formation in the Taranaki Basin, however, no evidence linking the two basins at lowstand has been found (Nodder, 1995). It is more likely that Whanganui lowstand material was bypassed to the Cook Strait and Hikurangi Trough (Proust et al., 2005). Criteria for dating the succession in the Whanganui Basin can unfortunately not be applied to the Taranaki Basin as tephra deposits and shell beds used in the Whanganui are not observed in cuttings from industry hydrocarbon wells.

200 km to the north of this study, Hansen and Kamp (2002) tentatively suggest a 400 ky eustatic signal in a higher accommodation setting of the Taranaki Basin, with poorly defined clinoform geometries compared to the Egmont Terrace. Differences in interpretation may be explained by sparse age data and along margin variability in how the GFF prograded (Chapter 4) and highlights the uncertainties inherent in correlation of basin margin events to eustatic cycles (Miall, 1992).

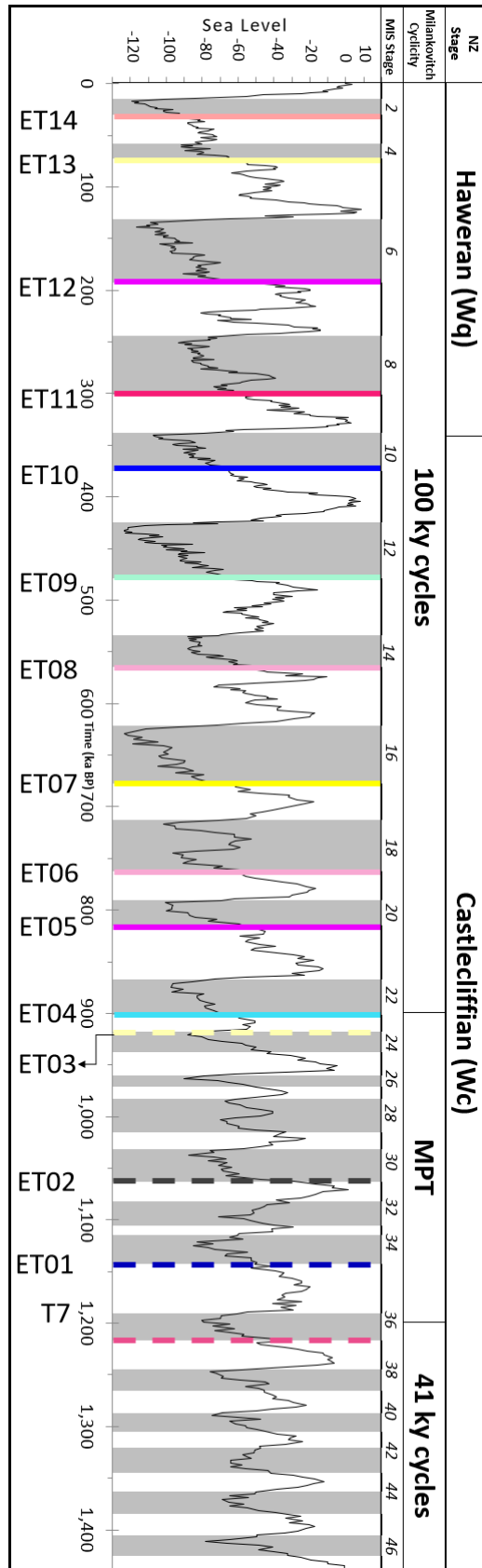


Figure 5.26 Sequence boundaries to sea level correlation.

Tentative correlation to SL curve using count back method to ET04, with possible correlations for ET03 to T7 represented as dashed lines.

Table 5.2 Horizon ages derived from correlation to the global eustatic sea level curve.

Horizon	MIS Stage	Approx. Age (kyrs)	Duration from previous SB (kyrs)
ET14	2	29	42
ET13	4	71	120
ET12	6	191	109
ET11	8	300	74
ET10	10	374	104
ET09	12	478	85
ET08	14	563	113
ET07	16	676	85
ET06	18	761	53
ET05	20	814	86
ET04	22	900	18
ET03 (FS)	end 24	918	144
ET02	30	1,062	79
ET01	34	1,141	74
T7	36	1,215	-

5.4.1.1 Alternative models for slope fan development

Whilst the generation of the slope fans and the cyclicity visible in the area has been attributed to Pleistocene eustatic sea level history, it is also important to consider alternative models for forming these patterns in the geological record. Depositional sequences are generated by the interplay of accommodation generation and destruction in time and space and sediment supply (Jervey, 1988; posamentier et al., 1988; Vail et al., 1977; van wagoner et al., 1988). Throughout the interval of interest, sediment discharge from the uplifting Southern Alps remained high throughout glacial and interglacial periods (Jiao et al., 2017). The dynamics of the sediment supply system from the Southern Alps are explored in greater detail in Chapter 6. Below, we discuss and evaluate alternative accommodation-based scenarios to explain the observed stratal geometries.

Accommodation is controlled by the interplay of subsidence and eustatic fluctuations. As stated earlier, by correlating the sequence boundaries of this study to falls in Pleistocene sea level, it is inferred that sea level was the main control on accommodation on the Egmont Terrace. Tectonic subsidence is not considered to have been the primary driver for generating sequences on the ET for the following reasons:

1. A tectonic driver would have to explain RSL rise as well as fall, therefore we would need high frequency cycles of relatively low subsidence rate (LST) and higher subsidence rate (TST/HST). There is no evidence of repeated fault movements on this timescale. Additionally, over area of the ET, a comprehensive seismic database shows no evidence of tectonics affecting the stratigraphy on the Western Stable Platform. King and Thrasher (1996) note that the WSP has been structurally quiescent since the Palaeocene.
2. Horizons of known age (seabed and regional surface T7) indicate a time span of approximately 1.5 million years for the packages discussed in this chapter to have been deposited. The frequency and cyclicity in the stratigraphy are considered unlikely to have developed from tectonic subsidence, which operate on longer time scales.

Whilst localised tectonics operating on a short timescale (10^3 to 10^4 ky) is not considered to have played a role in generating the observed cyclicity, it is feasible that it altered sediment routing in some way and hence affected sediment delivery to the basin, a model invoked in Chapter 4. In the ET sequences, however, there is no evidence for a similar event having occurred that would have led to the observed frequency and cyclicity of deposits in seismic data.

Another alternative model for generating slope accommodation is repeated phases of oversteepening and collapse, related to progradation of the margin into deep water followed by healing and continued progradation of the system. This model does not explain:

- The observed truncation of topset strata: In a continuous progradation scenario, degradation and erosion would be limited to the outer shelf and slope. However, we see truncated foreset reflectors and removal of topsets (e.g. ET09 truncated by ET10 in Figure 5.19), indicating significant base level fall rather than simple

collapse. In this model, the slope fans should correlate up dip to topset reflections, which they clearly do not.

- The contrast in seismic facies of the slope fans/healing phase reflectors with degraded low amplitude semi-continuous reflectors: In a continued progradation model, we could expect to see similar seismic facies in the pre degradation reflectors and reflectors healing the slope accommodation generated in collapse. Rather, we see a stark juxtaposition of high amplitude continuous reflectors against low amplitude semi-continuous reflectors. This juxtaposition invokes a possible difference in composition between the high and low amplitude deposits and hence potentially different provenance (as discussed in the proceeding section of this chapter and further elaborated upon in Chapter 6).
- The apparent basinward and landward movement of the depositional system interpreted in this study: Were continued progradation, oversteepening and collapse the sole driver of the observed cyclicity, we could expect to see the low amplitude discontinuous reflectors directly infilling the slope accommodation. Rather, we see high amplitude continuous slope fan reflectors onlapping the degradation surfaces (interpreted in this study as sequence boundaries) and evidence of sediment bypassing the outer shelf and slope incision and base of slope fans. Landward movement of the system is interpreted from infill of shelf incision by late lowstand and transgressive deposits overlain by a shelf edge delta.

5.4.2 Origin of the High Amplitude Deposits

The high amplitude deposits described in 5.3.2 are interpreted as lowstand slope fans deposited in concave up topography generated during progradation and degradation of the margin. Acoustically, the top of these deposits produces a soft kick with a reflection co-efficient of -0.25 and an acoustic impedance value of 3.168 (ET10). This soft kick is interpreted to be a fluid effect from the presence of gas trapped within pore space of sandstones within a lowstand slope fan.

Most oil and gas occurrences in the Taranaki Basin are thermogenic in nature and geochemically typed to Cretaceous – Palaeogene sources (King and Thrasher, 1996), however, on the Egmont Terrace is not underlain by a hydrocarbon source rock kitchen; this means thermogenic hydrocarbons would have had to undergo a tortuous migration pathway from either the Deepwater Taranaki Basin or the nearby Cretaceous sub basins to charge each slope fan individually.

A more likely scenario is that the anomalies are caused by locally generated biogenic gas as this removes the necessity of tortuous migration pathways and a widely available source. Biogenic gas accumulations form under specific conditions (Katz, 2011); an anoxic setting, high sedimentation rates, early trap formation and low temperatures. These conditions could have been available as a function of glacial-interglacial variations and the notion of biogenic gas thus ties well with the observed cyclicity.

The slope fan anomalies are buried to between 850-1500m depth (using a velocity of 2000 m/s); using a geothermal gradient of 30°C per km for this part of the Taranaki Basin (Funnell et al., 1996; Kroeger et al., 2013), a reservoir temperature of between 25.5 - 45°C is estimated. Peak microbial activity of methanogens occurs between 35 - 45°C (Katz, 2011), placing the slope fans in the optimal temperature window for biogenic gas generation.

When considering a source of carbonaceous material for generation of biogenic gas, two scenarios, or a combination thereof, are considered; 1) an increase in the amount of plant organic material delivered to the slope and, 2) an increase in the amount of coal debris to the slope. As the slope fans are considered lowstand deposits, we will consider the situation of a lower base level; this would have resulted in a narrower and shallower shelf, allowing increased transport efficiency of discharge from the North-West Nelson area across the Egmont Terrace to infill slope accommodation (Figure 5.28). NW Nelson is a present-day forested area but during the Last Glacial Maximum (LGM) (Figure 5.27A) was a mix of beech forest and shrubland (Alloway et al., 2007; Ryan et al., 2012). Highlands of NW Nelson region were also at a cooler temperature with localised glacial accumulations (Barrell, 2011; Shulmeister et al., 2003, 2001) (Figure 5.27B); seasonal meltwater discharge may have generated sufficiently large discharge events to create hyperpycnal flows capable of delivering entrained sediments and organic matter across the shelf edge where it was deposited within the slope fans. Additional biogenic material may have been sourced from plant material on the Farewell Rise (Figure 5.27A). The Farewell Rise was an exposed landmass in lowstands and was drained by northwest trending channels (Nodder, 1995) and was covered in scrubland/grassland with patches of beech and conifer trees during the LGM (Figure 5.29A; Newnham et al., 2013).

In addition to delivery of terrigenous organic matter across the shelf, it is also possible to have delivered detrital coal from outcrops of Eocene and Cretaceous outcrops located in NW Nelson (Figure 5.28). The Brunner and Papparoa coal seams (Figure 5.28) along the

Westland coast may have also provided sources of detrital coal which could have been carried north to the Egmont Terrace by a north directed littoral drift cell. Glacial lowstands are likely to have increased the efficiency of this transport through a combination of an intensified south-westerly wind driven swell on a decreased bathymetric profile (Payne et al., 2010). The dynamics of the LGM sediment delivery system are further elaborated upon in Chapter 6.

The biodegradation pathways for low grade coal and organic matter is the same, with methanogens converting organic matter to methane via three possible pathways, namely CO₂ reduction, acetate fermentation (Whiticar et al., 1986) or methylotrophic pathways (Strapoć et al., 2011, 2010). At the reservoir temperature of the Egmont Terrace slope fans, the most prolific of these is expected to be methanogenic CO₂ reduction (cf Strapoć et al., 2011).

Examples of microbial gas fields include the Barbara Field in the Adriatic sea (Ianniello et al., 1992), the Ballena and Riohacha fields in the Guajira Basin, Colombia (Rangel et al., 2003), western Nile Delta (Vandré et al., 2007) and the Cook Inlet Basin, Alaska (Strapoć et al., 2010).

The inferred gas charging of the slope fans is not observed in stratigraphy from ET12-14, however fluid escape structures (pockmarks) (Figure 5.29A) on the seabed may indicate early gas generation and escape due to lack of an overlying seal. Additional fluid escape structures are noted across the Egmont Terrace and may indicate leakage from the lobe fans and shallow gas accumulations on the shelf (Figure 5.22 and Figure 5.29B).

1. Progradation of highstand clinoforms into deep water resulting in an above grade margin.
2. Relative sea level fall resulting in degradation of the margin and long-term slope degradation processes such as mass wasting and canyon formation. This results in an out of grade margin with concave upward slope accommodation and shelf margin bypass.
3. The slope accommodation is then infilled by coarse material with entrained detrital coal and/or organic material, possibly derived from discharge from the NW Nelson area and west coast of South Island. The infill and healing of this slope accommodation results in a graded margin.

4. Transgression and subsequent progradation of highstand clinoforms then buried the slope fans forming an effective muddy seal across the deposits and creating anoxic burial conditions favourable to generation of biogenic gas.

Trap formation is also enhanced by the architecture of slope fans draping over early deposits (Figure 5.8 and Figure 5.23). Continued highstand progradation of results, once again in an unstable above grade margin and subsequent cyclical collapse of the margin in concert with global eustatic sea level fluctuations.

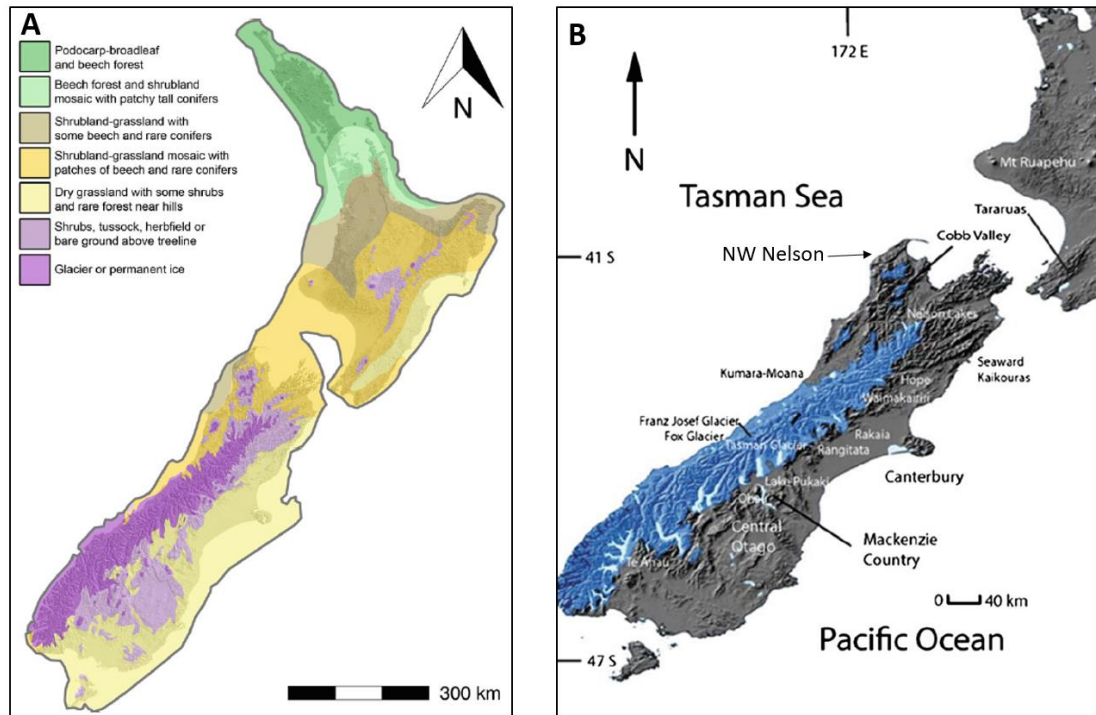


Figure 5.27 Ice extents and vegetation during the LGM.

A) Vegetation cover of New Zealand at the Last Glacial Maximum as reconstructed on the basis of pollen, macrofossil, beetle and geomorphic evidence (from Nevenham et al., 2013) B) Map showing the extent of ice cover in the Southern Alps during the LGM (from Schulmeister, 2017).

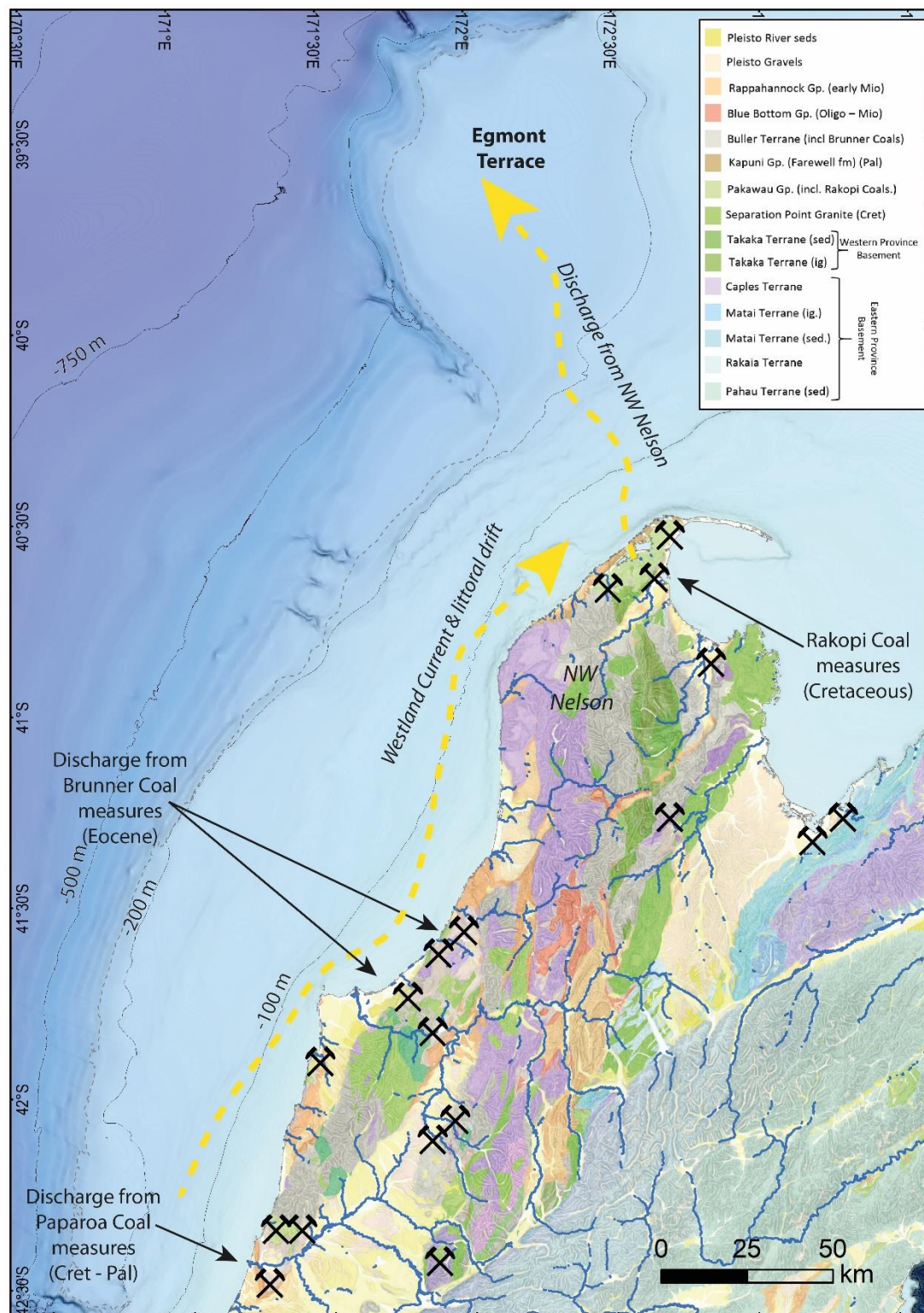


Figure 5.28 *Geology northwest South Island.*

Geological map, present day river drainage network and topography of the NW Nelson area including locations of active and closed coal mines. All data sourced from the New Zealand Petroleum and Minerals datapack.

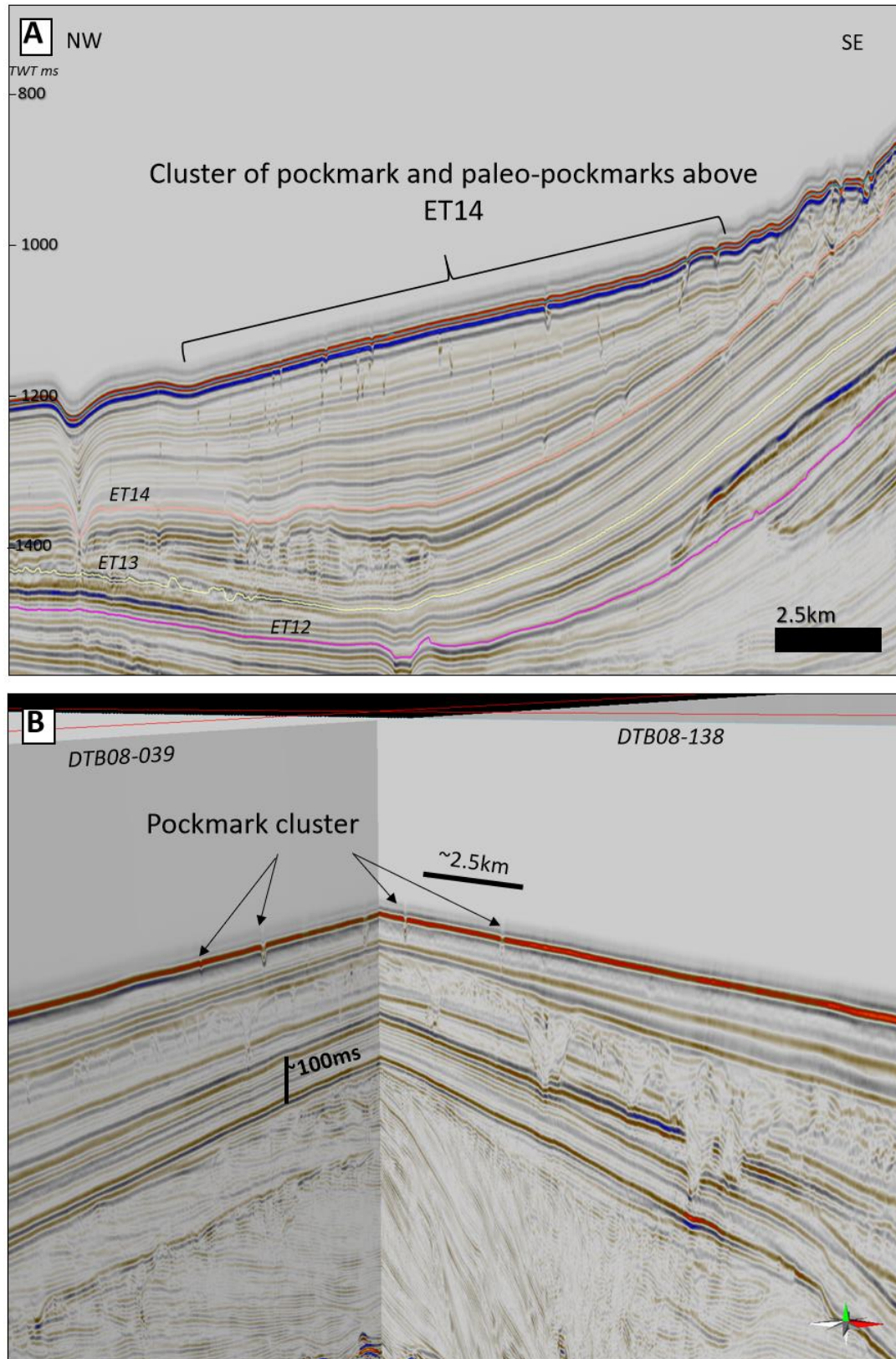


Figure 5.29 Pockmarks on the Egmont Terrace.

Pockmarks developed in the Egmont Terrace region, A) Pockmarks and paleo pockmarks developed above surface ET14 (most recent sequence) in the mid slope region. B) Clustered pockmarks developed on flat lying topsets. See Figure 5.22 for section locations.

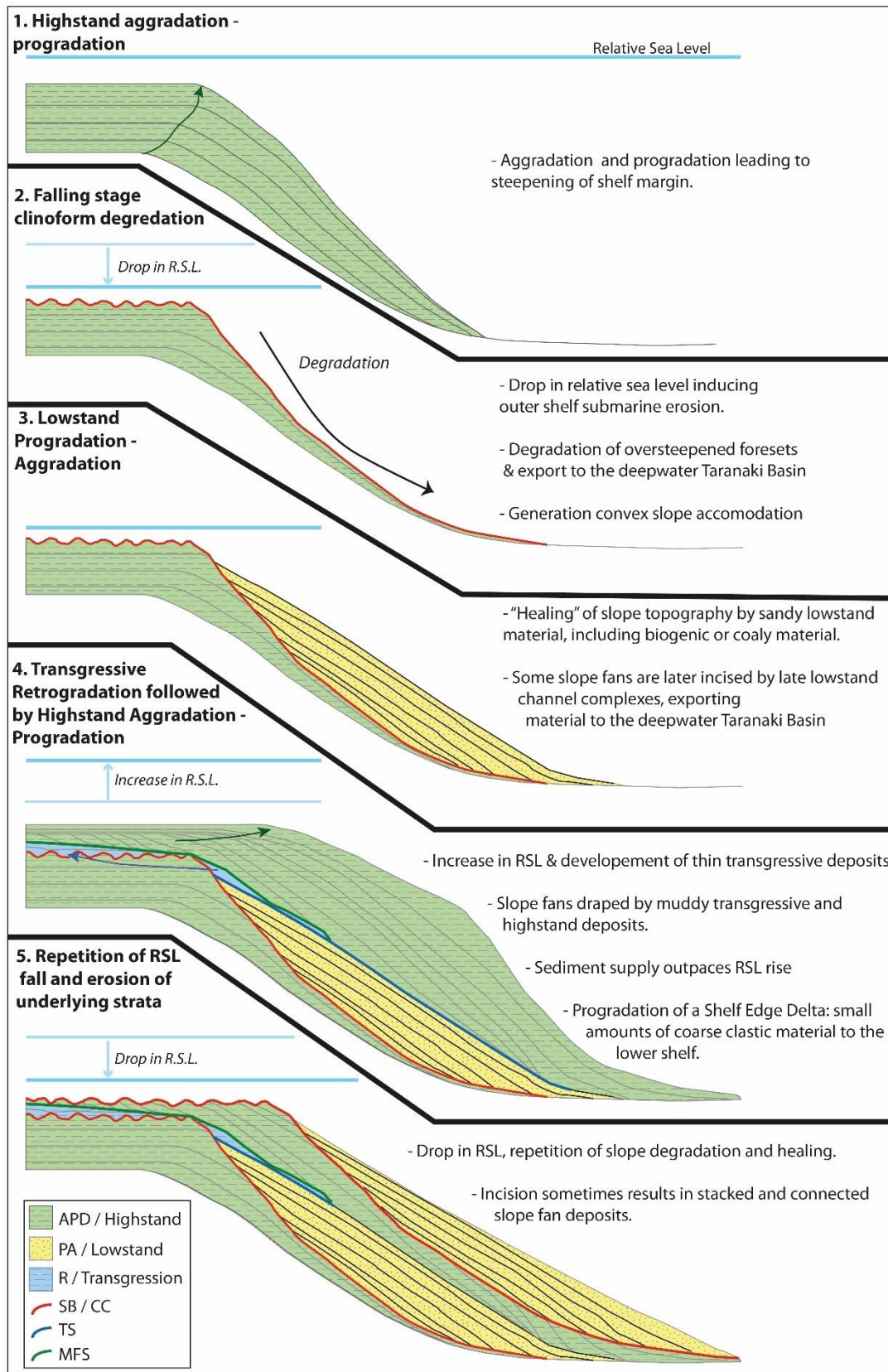


Figure 5.30 Idealised model of the formation of the high amplitude slope fans.

5.4.3 Comparison to other margins

Shelf margins can be defined by two end member geometries; 1) graded margins where erosion and deposition are broadly in equilibrium and 2) out of grade / ungraded where either erosion or deposition is dominant (Hedberg, 1970; Ross et al., 1994). As described above and in Figure 5.30, the Egmont Terrace has cyclically gone through phases of graded and out of grade morphologies throughout the Pleistocene.

Slope aprons/slope fans can be found on different types of slope resulting from varied processes and modes of formation. Prather (2000, 2003) and Prather et al. (2017) discuss in detail slope accommodation on graded and out of grade slopes on continental margins around the world. Much of this work is, however, related to mobile substrates on margins ~ 2,500 to 3,900 metres high (e.g. the Niger delta (Prather et al., 2012) & the Gulf of Mexico (Prather et al., 1998)) or active margins where tectonic modification of slope accommodation occurred (e.g. offshore Trinidad, Moscardelli et al., 2012 & offshore Brunei (ARTHUR and Blake, 2003)).

Hubbard et al. (2010) attribute the main controls on clinoform development as 1) basin margin relief, 2) factors affecting slope rugosity and 3) basin shape and sediment supply.

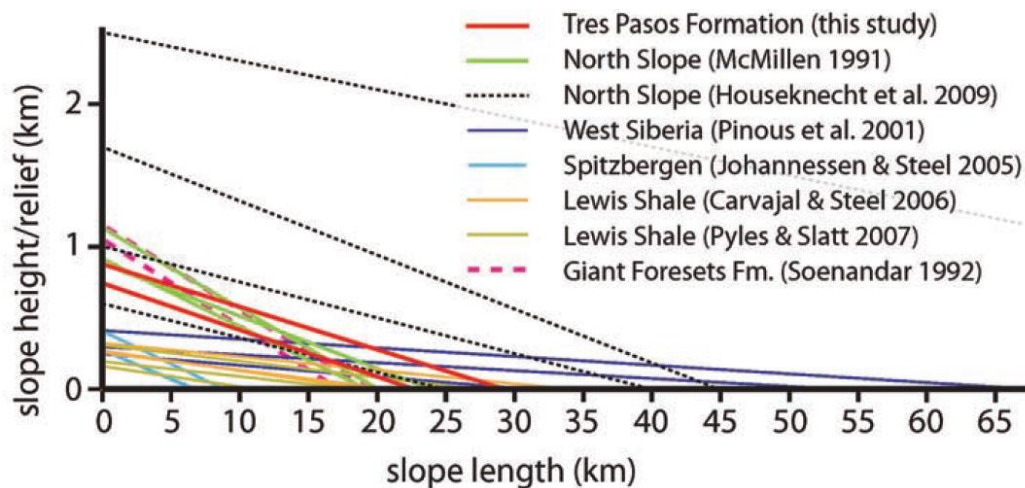


Figure 5.31 Comparison of clinoform lengths and heights from various slope systems from (Hubbard et al., 2010).

Basin Margin Relief

Relatively few examples of high relief margins (Figure 5.31) have been documented in detail (e.g. Cretaceous Tres Passos Fm (Hubbard et al., 2010) and North Slope of Alaska (Houseknecht et al., 2009)), with the geologic record biased towards the preservation of smaller examples such as the Eocene of Svalbard (e.g. Deibert et al., 2003; Mellere et al.,

2002) or the Permian Karoo Basin (Flint et al., 2011; Jones et al., 2015, 2013; Poyatos-Moré et al., 2016).

High relief margins such as Tres Pasos Formation (Hubbard et al., 2010; Romans et al., 2009) are prone to developing out of grade upper slopes that are prone to collapse, mass wasting and subsequent bypass on the upper slope, with thicker base of slope accumulations (McMillen, 1991; Pyles and Slatt, 2008). Contrasting this, however, the Giant Foresets Formation on the Egmont Terrace typically show accumulations in the lower and mid slope position with minimal lowstand accumulations at the base of slope. A likely reason for this is further bypass from the bottomset of the Egmont Terrace to the basin floor of the Deepwater Taranaki Basin (Figure 5.2, Chapter 6).

Slope Rugosity

Many high relief clinoforms are associated with mobile substrates such as salt or mud which result in the development of a rugose slope profile with ponded (e.g. Hodgson and Houghton, 2004; Prather and Pirmez, 2012; Sinclair and Tomasso, 2002) or stepped slope profiles (Brooks et al., 2018; Deptuck et al., 2012; Spychala et al., 2015). Well-ordered clinoform systems do not typically develop in these settings due to irregular slope surfaces and syn-depositional modification of the slope by substrate withdrawal (Hubbard et al., 2010). In the case of the Alaskan North Slope, Magallanes and Taranaki Basins, slopes are characterised by a low rugosity as they are not underlain by a mobile salt or mud substrate with slope accommodation typically healed by progradation of the margin.

Basin shape and sediment supply

High relief clinoforms such as the GFF are typically linked with a regular sediment supply sourced from active orogenic belts (Hubbard et al., 2010). Slope rugosity developed in clinoform systems can be healed depending on the sediment supply / accommodation ratio on the slope. In the Magallanes Basin, sediment input from the uplifting Andes was focused in a relatively narrow foreland trough approximately 50 – 100 km wide which was likely fed by numerous small mountainous rivers fed sediment over a narrow continental slope (Fildani et al., 2009; Hubbard et al., 2010). Likewise, clinoforms of the Lower Cretaceous Alaskan North Slope also prograded into a Foreland Trough 50 to 350 km wide (Bird and Molenaar, 1992). Both of these Cretaceous examples of high relief clinoforms were fed by fluvial systems derived from nearby orogenic belts. In the case of the Giant Foresets Formation, sediment was derived from the uplift and erosion of the

Southern Alps (Hansen and Kamp, 2002; Kamp et al., 2002). In contrast with the Magallanes and North Slope examples however, sediment is delivered to the Taranaki Basin via a combination of longshore drift and ocean currents where it is deposited along a 350 km wide basin margin. The dynamics of this transport system is explored further in Chapter 6. Despite the lack of direct fluvial connection and comparatively wide basin architecture, sediment delivery to the basin was sufficient to repeatedly infill out of grade/degraded slope profiles and efficiently prograde the margin.

Slope fans with high amplitudes have also been described in the Cretaceous North Slope Torok Formation (Figure 5.31; Houseknecht, 2019; Houseknecht et al., 2009) and are related to 400 k.y. Milankovitch cyclicity (Lease et al., 2017; Lease and Houseknecht, 2017). As on the Egmont Terrace, these fans are capped by sealing transgressive and highstand mudstones and shales. In contrast to the biogenic gas charged fans of the Egmont Terrace, however, these slope fans are charged by organic rich shale source rocks upon which they downlap and interfinger with (Houseknecht and Schenk, 2008; Houseknecht, 2019; Houseknecht et al., 2009). The Egmont Terrace slope fans also display a higher contrast seismic amplitude anomaly relative to the encapsulating muddy highstand deposits, possibly attributable to the higher fluid density contrast of a of gas saturated fan compared with that of an oil rich fan. This effect may be further enhanced by the shallow burial of the Giant Foresets Formation.

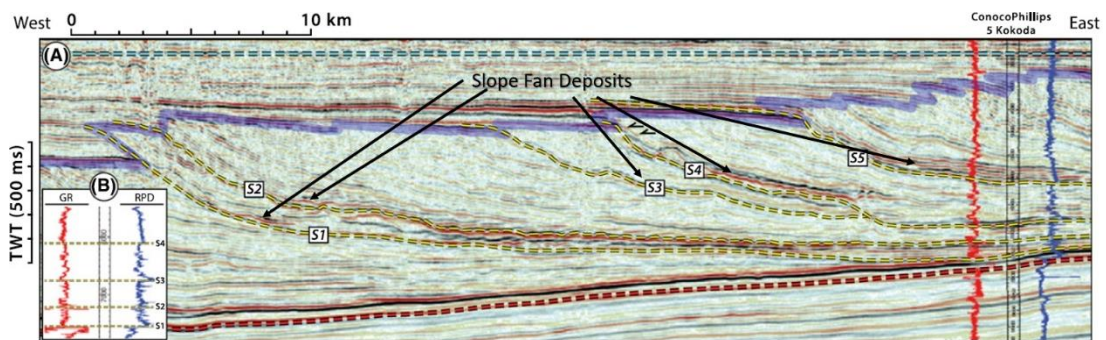


Figure 5.32 North Slope clinoforms.

Cretaceous slope fans overlying sequence boundaries S1-S5 in the Torok Formation on the North Slope of Alaska (from Houseknecht, 2019).

5.4.4 Lithology Control and Sediment Delivery

Control on the lithology and grain size of sediments comprising the Egmont Terrace is poor as no wells directly penetrate the studied packages. Well Kiwa-1 (Figure 5.3 & Appendix-1) acquired mud log and petrophysical data covering only the top ~40 m of topset stratigraphy discussed in this chapter; lithology is dominated by unconsolidated to

poorly consolidated interbedded silts, sands and bioclastic limestones with sandy intervals showing porosities up to 32% (Shell BP Todd Oil Services Ltd., 1982). Below this, thin horizons of coaly debris were also intersected although no further information was provided on the nature or origin of this coal.

Immediately northeast of the Egmont Terrace, exploration well Tane-1 drilled and logged a near complete succession of GFF of the same interval studied in this chapter (Appendix-1). This was dominated nearly entirely by thick units of unconsolidated light grey, silty micaceous calcareous mudstones and fine sandy argillaceous siltstones (Shell BP Todd Oil Services Ltd., 1976). Tane-1 lies on the north-eastern side of an incised corridor separating the Egmont Terrace from the rest of the Western Stable Platform. As shown in Chapter 4, the northern and southern depocentres of the WSP underwent different progradational histories, therefore information derived from Tane-1 may not be representative of sediments on the Egmont Terrace. Additionally, the Egmont Terrace sits in a more proximal location to sediment sourced from the Southern Alps so we may expect more proximal facies developed on the Egmont Terrace.

In a review of the surficial sediments around New Zealand, Bostock et al. (2018) compiled more than 30,000 surface sediment samples to generate a database of the nature of surficial sediments in New Zealand's Exclusive Economic Zone. Although coarse in nature, the grids presented in Figure 5.33 offer some insight into the modern seabed composition, which is likely to be representative of the seabed during interglacials in the time period covered in this chapter. The Egmont Terrace clinoforms are dominated by a mixture of mud with lesser amounts of sand and carbonate; shelf carbonates most likely represent shelly material and shell beds present across the shelf of the Taranaki Basin (King and Thrasher, 1996) whilst higher carbonate contents in deepwater regions are interpreted to represent deep sea oozes with limited to no siliciclastic input. Small amounts of gravel are recorded in the northern corner of the Egmont Terrace (Figure 5.33c) and are coincident with slope canyon systems draining towards the deepwater Taranaki Basin. Additional gravel deposits are observed at the northwest tip of South Island (NW Nelson) where this chapter hypothesises as a potential source for sediment for the Egmont Terrace (Figure 5.30).

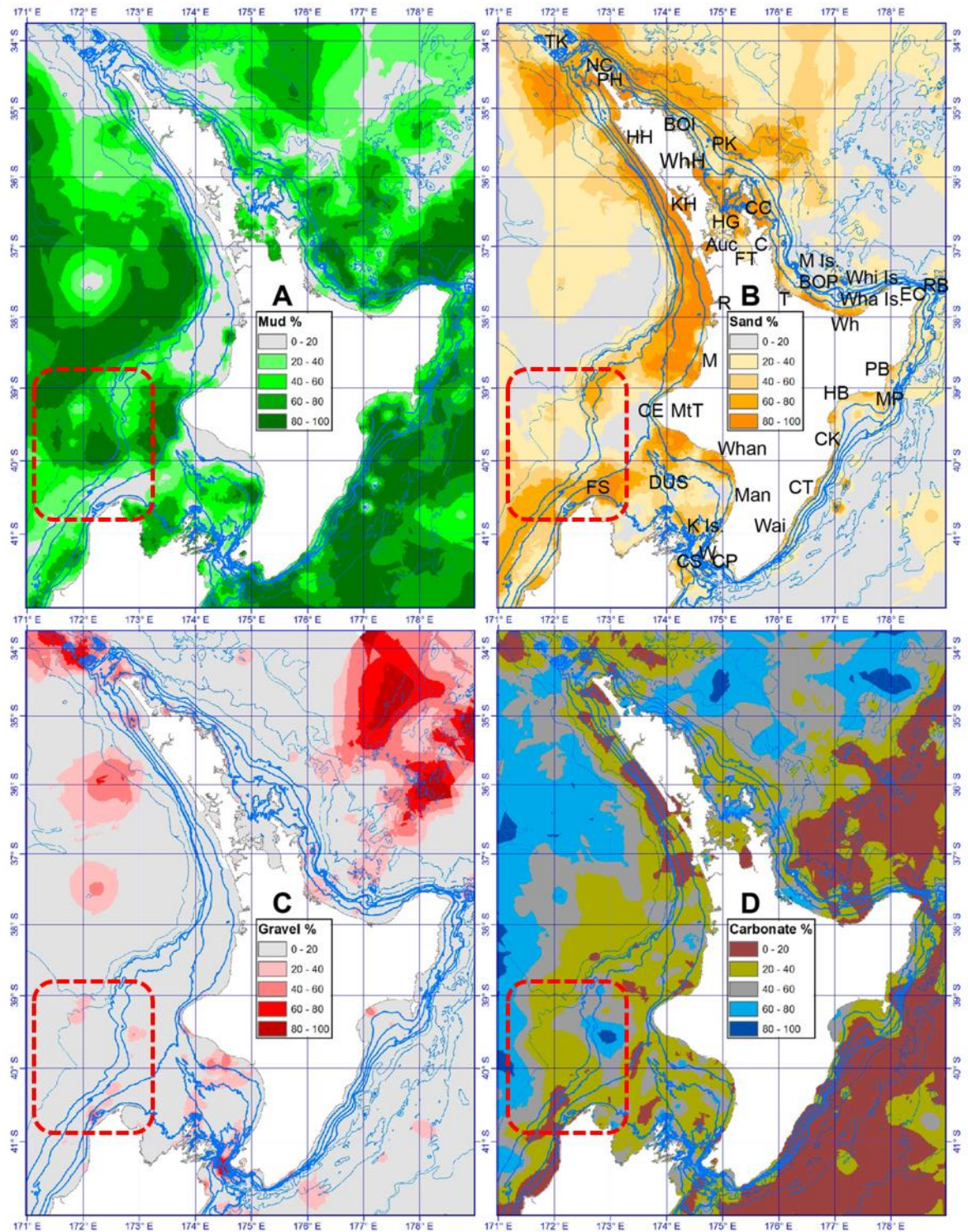


Figure 5.33 Map of the surficial sediments of the North Island continental shelf.

A) Mud %, B) Sand %, C) Gravel %; D) Carbonate %. The Egmont Terrace is highlighted by a red dashed box in each image. (from Bostock et al., 2018).

To supplement the poor control on the nature and grade of sediment in the subsurface of the Egmont Terrace, predictions were made based on sequence stratigraphic context and seismic facies, supported by analogues from other basins with additional core, well log or outcrop information.

5.4.4.1 *Highstand Deposits and Processes*

Highstand deposits on the Egmont Terrace are typified by a low amplitude to transparent and discontinuous seismic facies building basinward and are commonly related to shelf edge deltas traversing the shelf (e.g. Figure 5.17 & Figure 5.18). The transparent to low amplitude character of highstand reflections suggests these deposits are of relatively uniform acoustic properties (Posamentier and Kolla, 2003). Although there is some evidence of coarse sediment delivery across the shelf edge during highstands (e.g. Figure 5.20), highstand sedimentation was most likely dominated by silt and mud sized particles similar to the succession intersected 50 km northeast of the Egmont Terrace in well Tane-1 (Figure 5.3 & Appendix 1). Work in Chapter 6, suggests that modern highstand sedimentation is dominantly sourced from clay rich runoff from South Island which is carried north toward the Taranaki Basin via a combination of longshore drift, storm waves action and oceanic currents (Carter and Eade, 1980; Carter and Heath, 1975; Chiswell et al., 2015; Radford, 2012). This system transports sediment as far north as the Auckland coastline (Payne et al., 2010).

The observed delta scale clinoforms building out to form the shelf edge deltas do not appear to be related to a single river point source and in most cases their landward extent is not preserved. Although lacking in direct sedimentological evidence, the Egmont Terrace shelf is interpreted here to be dominated by storm and wave processes. Similar highstand occurrences of shelf edge deltas were postulated by Burgess and Hovius (1998) and documented in seismic, subsurface and outcrop data (Bullimore et al., 2005; Carvajal and Steel, 2006; Uroza and Steel, 2008 respectively). Highstand shelf edge deltas are most likely to develop in 1) areas of high and sustained sediment flux and/or 2) areas with narrow shelves (Uroza and Steel, 2008) and are most likely to be dominated by wave processes (Porebski and Steel, 2006; Uroza and Steel, 2008; Yoshida et al., 2007). Uroza and Steel (2008) note that in general highstand delta deposits are typically thick and store a large portion of their sediment budget on the shelf and coastal plain. Storm and wave-dominated deltas, however, typically deliver less sediment beyond the shelf-edge (Dixon et al., 2012; Johannessen and Steel, 2005) due to sediment being redistributed along the margin. Clinoforms on the Egmont Terrace however, show marked progradation with limited aggradation under the same process regime (Chapter 4), indicating that storm and wave action at the shelf edge was sufficient prograde a mud and silt dominated margin.

Shelf advance typically occurs where coarse grained material accretes on the outer shelf – upper slope in times of low topset accommodation and/or high sediment supply (e.g. Carvajal and Steel, 2009; Hubbard et al., 2010; Johannessen and Steel, 2005; Muto and Steel, 2002). Recent advances by Poyatos-Moré et al. (2016), however, highlight how significant basin margin progradation can also occur via mud rich gravity flows that underwent prolonged suspension by prevailing wave and/or storm conditions. Such a model is invoked here for highstand delivery of sediment across the Egmont Terrace, whereby the storm and wave action drives progradation during highstands.

5.4.4.2 Lowstand Deposits and Processes

Lowstands are typically considered favourable for deposition of submarine fan systems with coarser grain sizes (Posamentier and Vail, 1988; Van Wagoner et al., 1987). In the Egmont Terrace region, lowstands are dominated by slope fan deposits in a mid to lower slope position (e.g. Figure 5.34) and wrap around the margin as opposed to being confined to localised depocenters (Figure 5.24). Topset reflectors show extensive incision at the shelf edge as canyons erode landward (e.g. Figure 5.18 & Figure 5.20) and up to 100 m deep incisions of topsets 12 km landward of the rollover. These canyon systems do not link back to a cross shelf incised valley system that is resolvable in the 2D seismic dataset. This evidence, coupled with the water depth of the modern day (i.e. highstand) shelf edge in the Egmont Terrace (~ 270 - 300 m) and the amplitude of eustatic sea level falls in the interval of interest of approximately 120 m (Figure 5.28, Miller et al., 2011), suggest it is unlikely that the shelf edge rollover became subaerially exposed. Similar landward erosion of canyons without subaerial exposure or cross shelf incised valley connection is observed in the Plio-Pleistocene Ebro Delta (Kertznus et al., 2009).

Work in this chapter also suggests a possible difference in highstand and lowstand provenance of sediment delivered to the ET. This is further supported by work in Chapter 6 which shows ~ 3 km wide embayment draining the subaerially exposed Farewell Rise (Figure 5.29) onto the Egmont Terrace. It is envisaged that hyperpycnal discharge from the Farewell Rise and NW Nelson, combined with sediment delivered from further south by longshore drift and wave action, was delivered across the shelf and downslope as turbidity currents. Wave generated flows such as this have limited ability to incise the slope so remain unconfined and do not typically bypass the slope; consequently, flows tend to lose momentum and deposit their load as thin sheet sands (Carvajal et al., 2009; Dumas and Arnott, 2006). At odds with this, however, significant incision by large

canyon systems is evident on the Egmont Terrace slope (e.g. shelf rollover map in Figure 5.5, seismic lines in Figure 5.18 and Figure 5.20 and time structure maps in Figure 5.9 to Figure 5.11). These canyons bypass the Egmont Terrace slope and deliver sediment to the deepwater Taranaki Basin (Chapter 6) and in many cases appear to have been active across multiple eustatic cycles (e.g. Figure 5.21B).

The coexistence of both slope fans and canyons that bypassed the slope suggests that flows approached the shelf-edge rollover as multi-kilometre wide plumes of sediment as opposed to a single point source with some sediment cascading across the shelf rollover as unconfined turbidity currents to be deposited as slope fans, whilst other sediment was captured by canyon heads and bypassed to deepwater regions of the Taranaki Basin (e.g. Chapter 6). This model can also explain why the fans are localised on the slope and why basin floor fans are uncommon on the Egmont Terrace.

Further sub-seismic scale architecture and compositional control on the slope fan deposits can be gained by comparison to exhumed examples in the Permian Karoo Basin (Flint et al., 2011), where a relatively stable shelf to basin floor profile of a similar scale to the Egmont Terrace succession has been studied in detail (Figure 5.34A). In this example, geometries that would, on a seismic scale, typically be defined as a singular lowstand systems tract are more internally complex and comprised of three sequences separated by two claystone horizons to forming a lowstand sequence set. On the Egmont Terrace, however, the lowstand systems tract is inferred to represent one large singular lowstand deposit overlain by a clay/mud rich transgressive and highstand deposit. Consequently, a more homogenous lithology might be expected in the Egmont Terrace lowstand deposits when compared with the Karoo Basin. Sand prone slope deposits are most common in intra-slope lobe deposits and lowest in slope valley fills (Figueiredo et al., 2010).

5.4.4.3 Transgressive Deposits and Processes

Transgressive deposits in the Taranaki Basin are either rarely preserved or below seismic resolution. Transgression is typically inferred by a landward movement of the depositional system. During this transgressive phase, shelfal accommodation is generated which retains coarse sediment on the shelf. In the slope and basin floor environment this results in progressive sediment starvations recorded by deposition of progressively muddier turbidity currents and hemipelagic clays (e.g. Flint et al., 2011; Posamentier and Kolla, 2003; Posamentier and Walker, 2006).

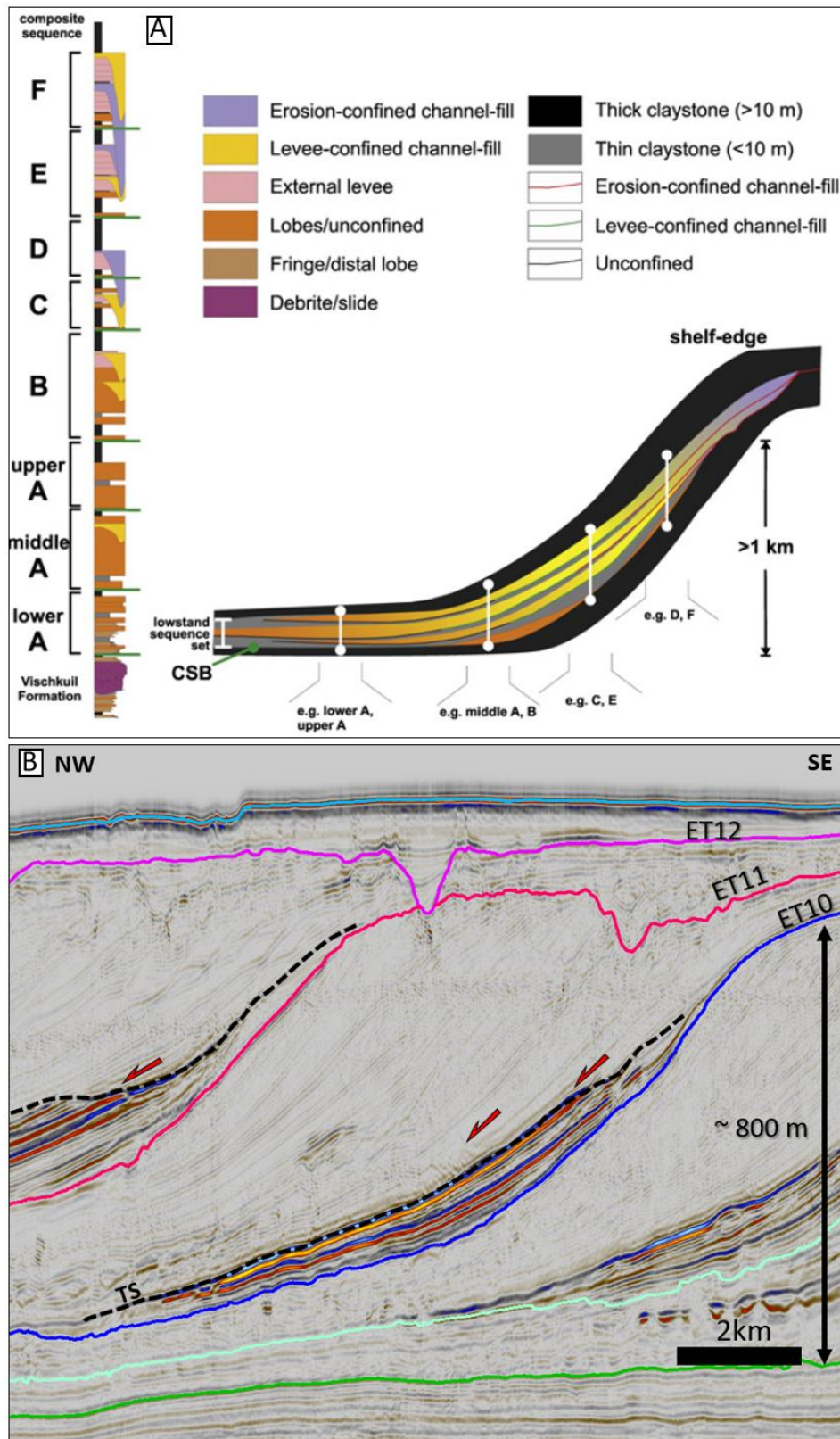


Figure 5.34 Comparison of outcrop and seismic lowstand slope succession.

A) Stratigraphic synthesis and lithologies of composite sequences mapped in outcrop in the Lainsburg basin floor and slope succession (Flint et al., 2011). B) Seismic section DTB08-042 (also see Figure 5.20) from this study showing comparative stratigraphy at a similar scale. Whilst the gross architecture observed in both A) and B) is similar, A) is composed of 34 depositional sequences whilst the slope succession overlying ET10, for example is most likely represents one depositional sequence.

It is also suggested that in the Taranaki Basin, a difference in the provenance of lowstand and highstand material is apparent and that different sedimentation patterns are recorded during different

stages of a eustatic cycle (Chapter 6). Consequently, a change in the nature of sediment and the sediment transport processes could be expected during transgression as the system switches from one sediment source to another.

5.5 Conclusions

Through detailed mapping of the 2D seismic data, this chapter developed a sequence stratigraphic model for the Giant Foresets Formation on the Egmont Terrace.

- 14 interpreted sequence boundaries were mapped and tentatively correlated to the global oxygen isotope curve (Lisiecki and Raymo, 2005; Miller et al., 2011) under the assumption that one depositional sequence correlates to one sea level cycle.
- Using this correlation, each depositional sequence is dated with some degree of confidence to approximately 900 kya, and more tentatively to ~1.2 Ma. This tentative period corresponds to the Mid Pleistocene Transition with the more certain ages relating to the establishment of low frequency, high magnitude global eustatic fluctuations.
- Slope deposits from approximately 900 kya are characterised by anomalously high amplitudes and are interpreted as lowstand slope fans within the established sequence architecture.
- The anomalously high amplitudes in lowstand slope fans are interpreted to be caused by some degree of gas saturation in sand rich slope deposits.
- This gas is likely the result of microbial degradation of biogenic and/or coaly material within each slope fan when it is buried beyond 850m.
- Biogenic and coaly material was likely sourced from the exposed lowstand Farewell Rise, NW Nelson and outcropping coal measures in the North Westland region.
- This material was delivered across the Egmont Terrace shelf via combination of fluvial discharge and longshore drift and deposited in concave slope accommodation generated during eustatic sea level falls.

Chapter 6

Late Pleistocene Sediment Pathways and Source to Sink considerations in the Taranaki Basin.

6.1 Introduction

Traditional sequence stratigraphic tools have long been focused on characterising and predicting the nature of infill in sedimentary basins. Typically, this has been carried out by solely examining the receiving sedimentary basins rich in data (i.e. seismic, wells and outcrops). Source to sink studies, on the other hand, focus on understanding all segments along the source to sink transect (Figure 6.1). This is done by treating the complete erosional area (source/catchment) and the complete depositional area (sink) as interlinked and equally important elements (Sømme et al., 2009). In addition to studying the individual elements highlighted in Figure 6.1, source to sink analysis aims to understand the “lost segments” of both the catchment and basin fill (Helland-Hansen et al., 2016), i.e. the areas in which sediment could be diverted to, which we do not see recorded in the sink.

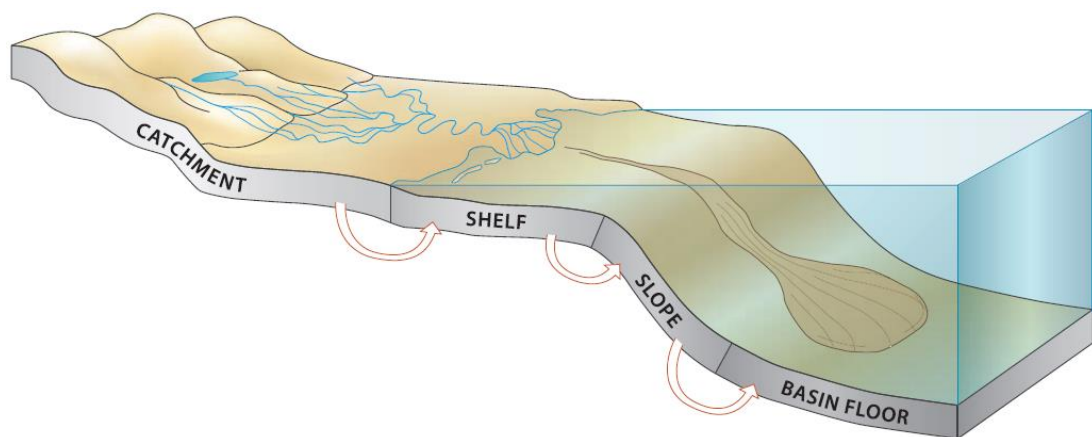


Figure 6.1 Elements of the source to sink system.

Source to sink studies aim to understand the interconnectivity of each of these segments in the depositional system. (from Helland-Hansen et al., 2016).

In the Late Pleistocene, the frequency and amplitude of global eustatic cycles changed from pre-mid-Pleistocene Transition (MPT) high frequency, low amplitude 41,000 year cycles to low frequency, high amplitude cycles averaging 100,000 years (Figure 6.2) (Lisiecki and Raymo, 2005; Miller et al., 2011). These eustatic fluctuations also significantly changed the shape of the New Zealand landmass in glacial – interglacial

cycles (Figure 6.4). The present day (i.e. highstand) geography of the New Zealand region is such that North and South Islands are separated by a shallow northeast – southwest trending submarine ridge known as the Farewell Rise (FR) (Figure 6.4)

(Lewis and Eade, 1974; Nodder, 1993). The FR dips gently northwest towards the Taranaki Basin and southeast towards the Wanganui Basin and tidally scoured Cook Straits. In highstand, the Wanganui and Taranaki Basins share a sediment budget delivered northward from the west coast of South Island by the Westland and d’Urville currents (Carter and Heath, 1975b; Chiswell et al., 2015; Gillespie et al., 1998; Lewis et al., 1994; Payne et al., 2010; Proust et al., 2005). During late Pleistocene lowstands, when sea level fluctuations exceeded 100 m (Figure 6.2), the Farewell Rise became subaerially exposed (Figure 6.4).

Chapter 5 of this thesis highlighted contrasting highstand and lowstand seismic facies and postulated that differing sediment sources in highstand and lowstand scenarios were responsible. In this chapter, bathymetric data and 3D seismic geomorphology are utilised to further investigate this hypothesis of different lowstand and highstand sediment sources and evaluate elements in the source to sink system for the latest Pleistocene. This is carried out by:

1. Utilising available 3D seismic data in the Taranaki Basin to examine sediment pathways on the shelf, slope and basin floor in endmember highstand and lowstand examples.
2. Reviewing sediment catchments for the Taranaki Basin.
3. Reviewing the dynamics of the sediment conveyor system from the catchment area to the Taranaki Basin.

6.2 Data and Methods

This chapter combines a library of 3D seismic data across the shelf, slope and basin floor with regional 2D data presented in Chapters 4 & 5.

Previous work by Nodder (1995, 1994, 1993) utilised a combination of high frequency shallow seismic data (3.5 kHz airgun), piston core and borehole data to identified four late Quaternary seismic and lithologic “couplets” on the Farewell Rise (Figure 6.3). These couplets comprise an acoustically transparent upper unit of silty sediment overlying a strongly reflective sandy unit with an erosive and channelised basal surface. Acoustically transparent silty units were interpreted as highstand deposits, whilst the erosive bases of

the sandy reflective facies are interpreted to represent sequence boundaries and lowstand systems tracts respectively (Nodder, 1995). Using sediments recovered from geotechnical borehole MP-2C (Figure 6.3), the couplets were dated by Nodder, (1994, 1993) using a combination of ^{14}C and calcareous nanoplankton and cyclo-stratigraphy and fall within MIS 9 to 1 (Figure 6.3).

Using industry standard 3D seismic surveys (Figure 6.4), seismic geomorphology of the “couplets” has been described and mapped to document sediment pathways across the Western Stable Platform during the late Pleistocene. When incorporating data from Nodder’s 3.5 kHz airgun and borehole studies with work from this study, it was not possible to directly correlate all ages and packages between surveys due the difference in resolution of industry standard 3D and 2D seismic datasets (typically 20 – 25 m vertical resolution) with the higher resolution 3.5 kHz airgun profiles (compare Figure 6.3A with 3C). Hydrocarbon exploration wells in the area do not record well log or chippings information in this uppermost portion of the stratigraphy so were of no use in this study.

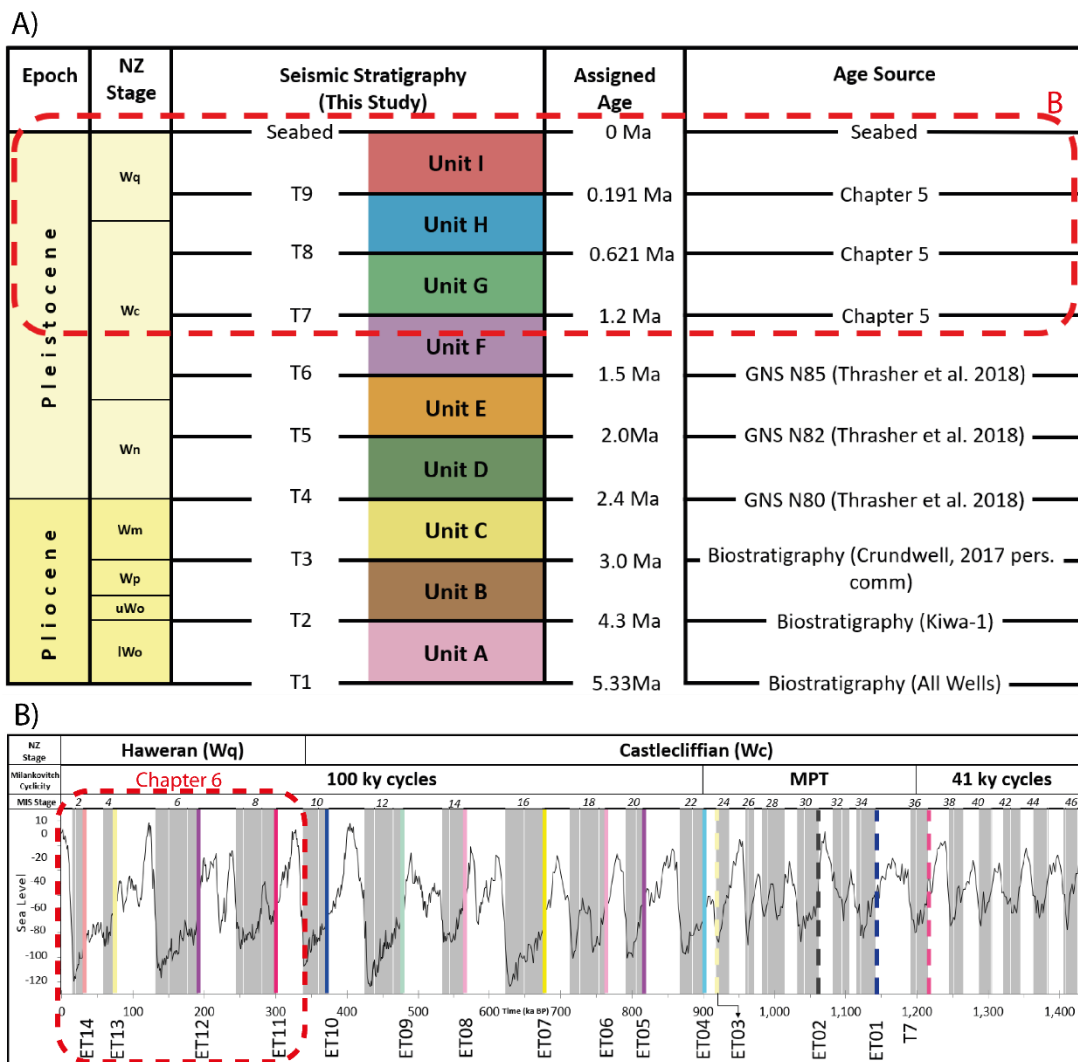


Figure 6.2 Stratigraphic Framework

Stratigraphy of the Giant Foresets Formation. A) Seismic stratigraphy established in Chapter 4 with the subset of stratigraphy studied in Chapter 5 highlighted by a red dashed box. B) Correlation of sequence boundaries from Chapter 5 to the eustatic curve of Miller et al. (2011). The portion of stratigraphy studied in this chapter (MIS 9 to present) is highlighted by a dashed red box.

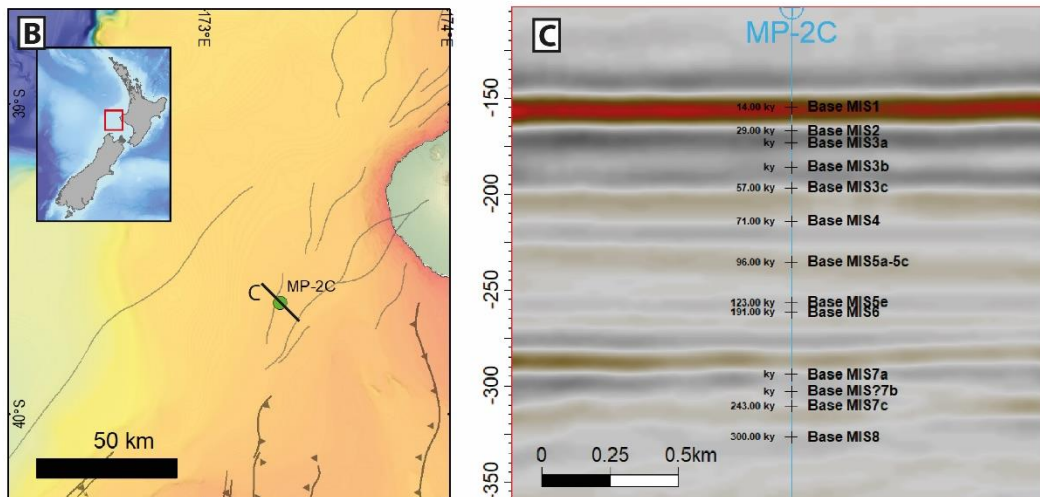
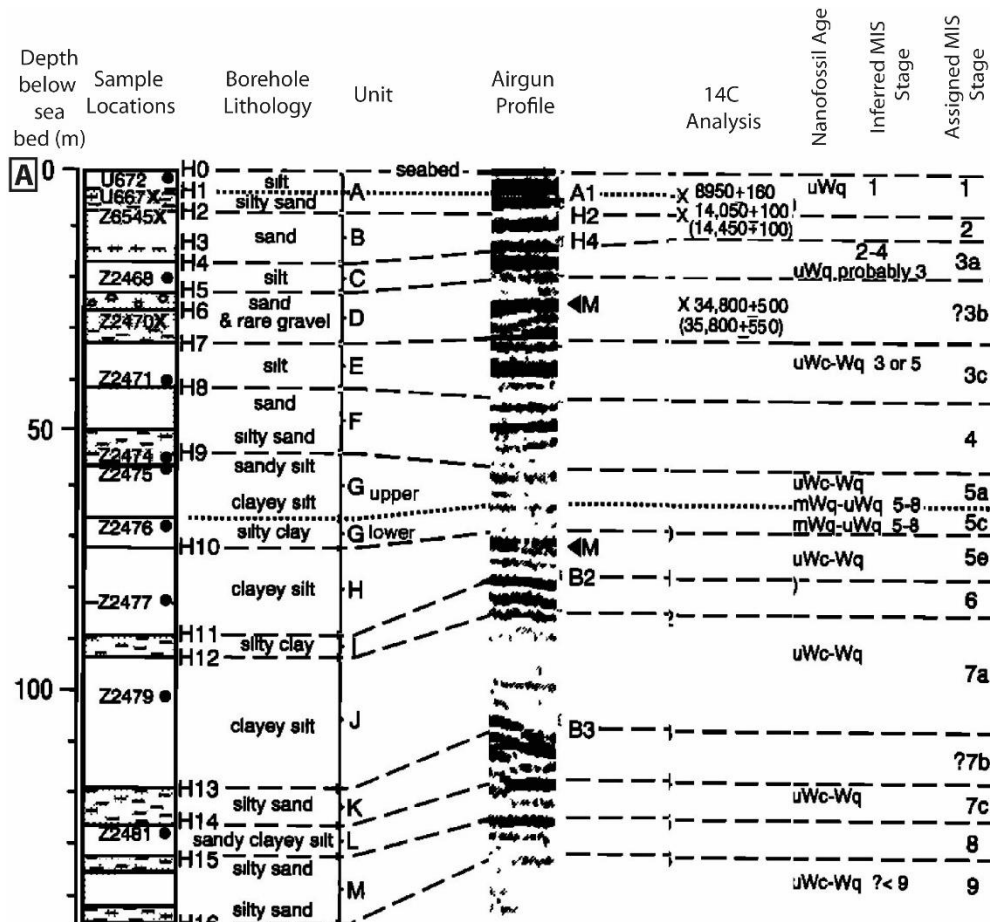


Figure 6.3 Late Quaternary ages from Nodder (1994).

A) Log of borehole MP-2C showing lithology, sample locations, correlation to an airgun profile, shallow carbon 14 ages dates, nanofossil ages and Marine Isotope Stage (MIS) assignments (modified from Nodder, 1994), B) Location of borehole MP-2C and location of seismic line C, C) Inline 296 from the Maui 4D survey showing sample locations from borehole MP-2C. Depth - TWT conversion of sample depths was carried out with a velocity of 1600 m/s for shallow, unconsolidated sediments as in Nodder (1994).

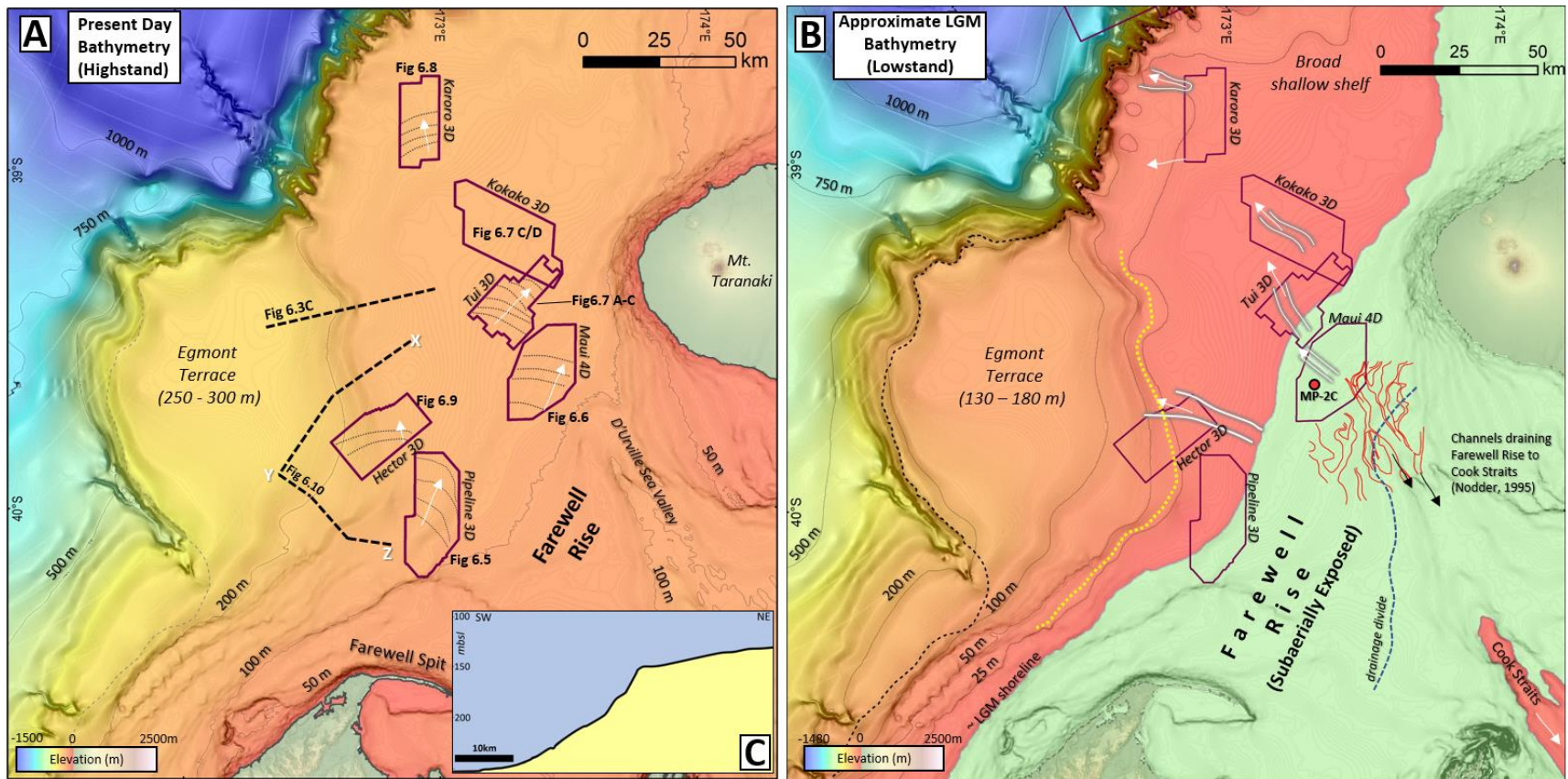


Figure 6.4 Data and bathymetry in the Taranaki Basin.

A) Present day (i.e. highstand) bathymetry in the Taranaki Basin with outlines of 3D surveys and schematic delta scale clinoform progradation fronts within 3D cubes. B) Approximate LGM bathymetry (~120m lower than present day) and the Farewell Rise land bridge with lowstand sediment pathways mapped in the subsurface from 3D seismic datasets and channels delineated by Nodder (1995) using shallow seismic profiles (red outlines). Rollover of the clinoform between the ET and northern WSP dashed in yellow C) bathymetric section showing clinoform rollover between the Western Stable Platform and Egmont Terrace. Bathymetry sourced from the New Zealand Petroleum and Minerals Petroleum Exploration data pack.

6.3 Cross Shelf Transport in the Taranaki Basin

Contrasting highstand and lowstand seismic facies on the Egmont Terrace were documented in Chapter 5 and hypothesised to be related to differing sediment sources. Pervious work has correlated progradational sections of the Giant Foresets Formation to uplift events in the Southern Alps (Hansen and Kamp, 2002; Salazar et al., 2016; Tippet and Kamp, 1995), with sediment transported north by a combination of ocean currents and a littoral drift cell as in the modern day (Payne, 2008). No work, however, has been undertaken to verify this linkage between uplift and progradation, and to document sediment transport pathways from the Southern Alps to the Taranaki Basin in the extensive subsurface dataset across the shelf.

In this section, 3D datasets are utilised to document geomorphic features in endmember highstand and lowstand systems tracts across shelf of the Taranaki Basin.

6.3.1 Highstand

Study of the acoustically transparent seismic facies identified in 3.5 kHz airgun data reveals more internal characteristics than previously reported by Nodder (1995). Multichannel 2D and 3D seismic data reveal outbuilding of delta scale clinofolds across the shelf of the Taranaki Basin (Figure 6.4). Foreset heights range from 20-45 m (using a velocity of 1600 m/s) in height with an average of 32 m. Foreset lengths range from 865 – 3685 m with an average length of 1970 m. Foreset gradients range from 0.6 to 2.3° with an average dip of 1.1°. Progradation rates were not calculated due to lack of well control and variability in resolution between surveys. Based on geometric characteristics of clinofolds set out by Patruno et al., 2015 and Patruno and Helland-Hansen (2018), these can be classified as sand prone sub-aqueous delta scale clinofolds. This classification is mainly based upon the calculated slope gradient as there is overlap between mud and sand prone geometric parameters for foreset height and length. Borehole calibrations to MP-2C show, however, that this seismic facies is dominated by pale grey-green micaceous silt with occasional shell fragments (Nodder, 1995, 1994, 1993).

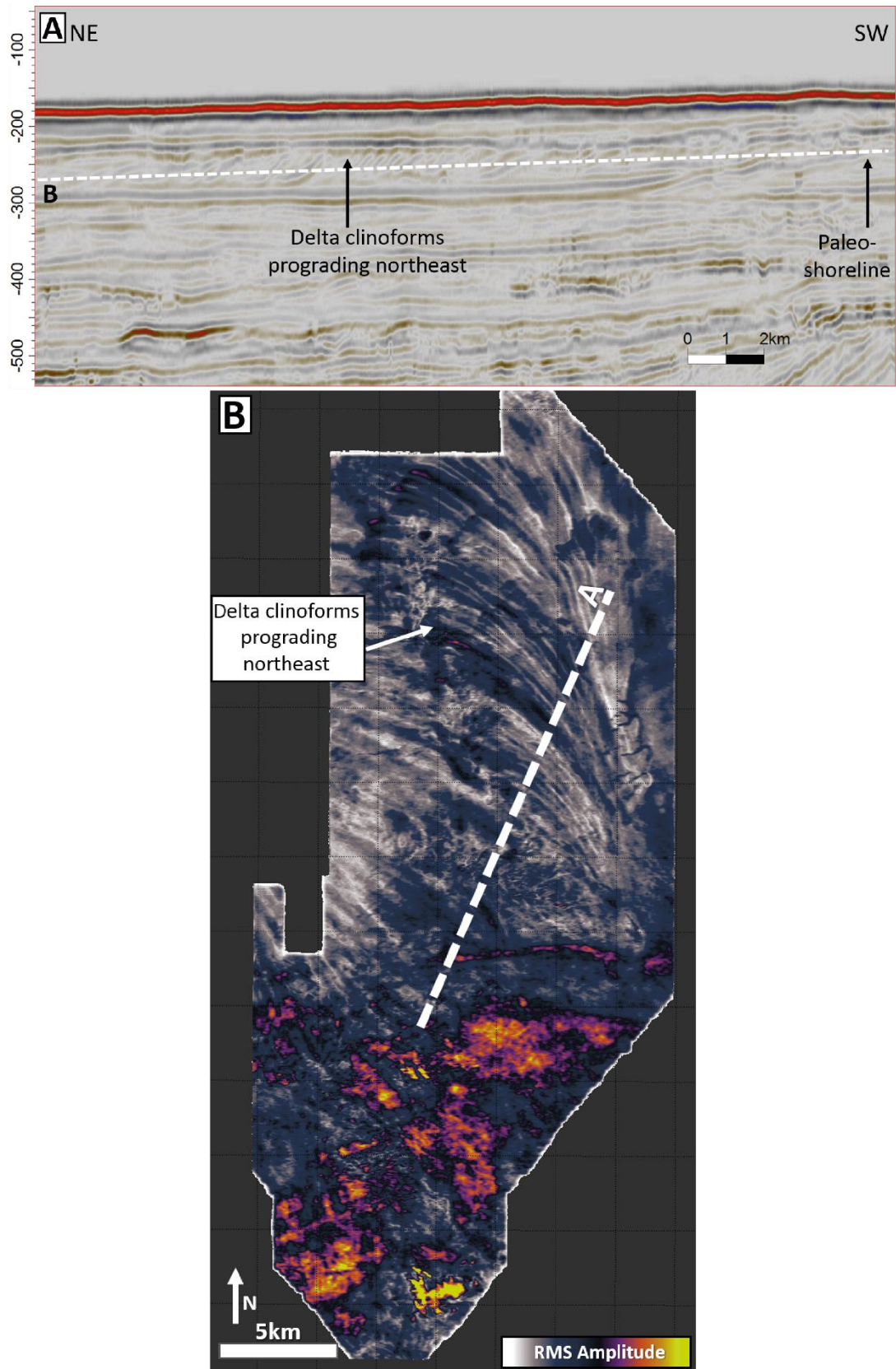


Figure 6.5 Delta scale clinofolds in the Pipeline 3D survey.

A) Line through the Pipeline 3D survey showing northeast progradation of highstand clinofolds. B) RMS stratal slice through delta scale clinofolds. Figure 6.4 for location.

The clinoforms prograde from approximately south to north, with local variations observed (Figure 6.4). In the south of the basin, the Pipeline 3D survey (Figure 6.5) images the delta scale clinoforms prograding from southwest to northeast, forming an arcuate progradational front; this geomorphology is attributed to interaction of the clinoforms as they impinge upon the topography of the Farewell Rise. To the northeast, the Maui 4D and Tui 3D surveys (Figure 6.6 and Figure 6.7A-C respectively) show a similar pattern of delta progradation toward the northeast. On the mid to outer shelf, the Karoro 3D survey shows a more northerly progradation of the delta front (Figure 6.8A).

The south to north progradation direction is attributed to the effects of the Westland Current and associated dominant wave and storm direction from the southwest. This current and its associated littoral drift cell is also considered responsible for the present day northeast trending Farewell Spit (Figure 6.4A; Tribe and Kennedy, 2010).

6.3.2 Lowstand

Within the seismic dataset, numerous channels are observed incising the highstand clinoforms discussed above (Figure 6.4B, Figure 6.9, Figure 6.6 and Figure 6.7). These channels are typically not traceable through the extensive network of 2D seismic data across the shelf due to poor image quality in the shallow subsurface and are best imaged in 3D datasets. The channels drain from approximately SE to NW and range from 2 to 7 km wide with typically less than 50 ms (approx. 80 m) of incision observed.

These broad, low angle SW-NE incisions erode the underlying northward prograding highstand delta clinoforms and delivered sediment onto the Western Stable Platform. They are interpreted to have formed as a result of sea level fall and subsequent subaerial exposure and erosion of the Farewell Rise (Figure 6.4B).

To the east of the 3D seismic survey used in this study, Nodder (1995) also identified and mapped a set of channels of similar dimensions using high resolution 3.5 kHz airgun data and interpreted them as fluvial or paralic channels draining the Farewell Rise (Figure 6.4B). Lithological correlation to borehole MP-2C (Figure 6.3) showed channel fills to contain well sorted, fine to medium grained quartz and feldspar rich sand, contrasting with the silt and clay rich micaceous highstand deposits (Nodder, 1995).

The Farewell Rise is a subtle 150 km long bathymetric high trending roughly NE-SW across which a drainage divide is traceable in the modern bathymetry dataset (Figure 6.4). It is dissected by the D'Urville Sea Valley, a NW – SE trending feature incising the Rise

by approximately 10 m, with the magnitude of incision increasing to the SE toward the Cook Straits. The FR dips gently to the west at 0.05° toward the Western Stable Platform and more steeply to the east at 0.15° into the D’Urville Sea Valley and subsequently to the Cook Straits (Figure 6.4). The channels mapped by Nodder (1995) are co-incident with the present day D’Urville Sea Valley on present day bathymetry.

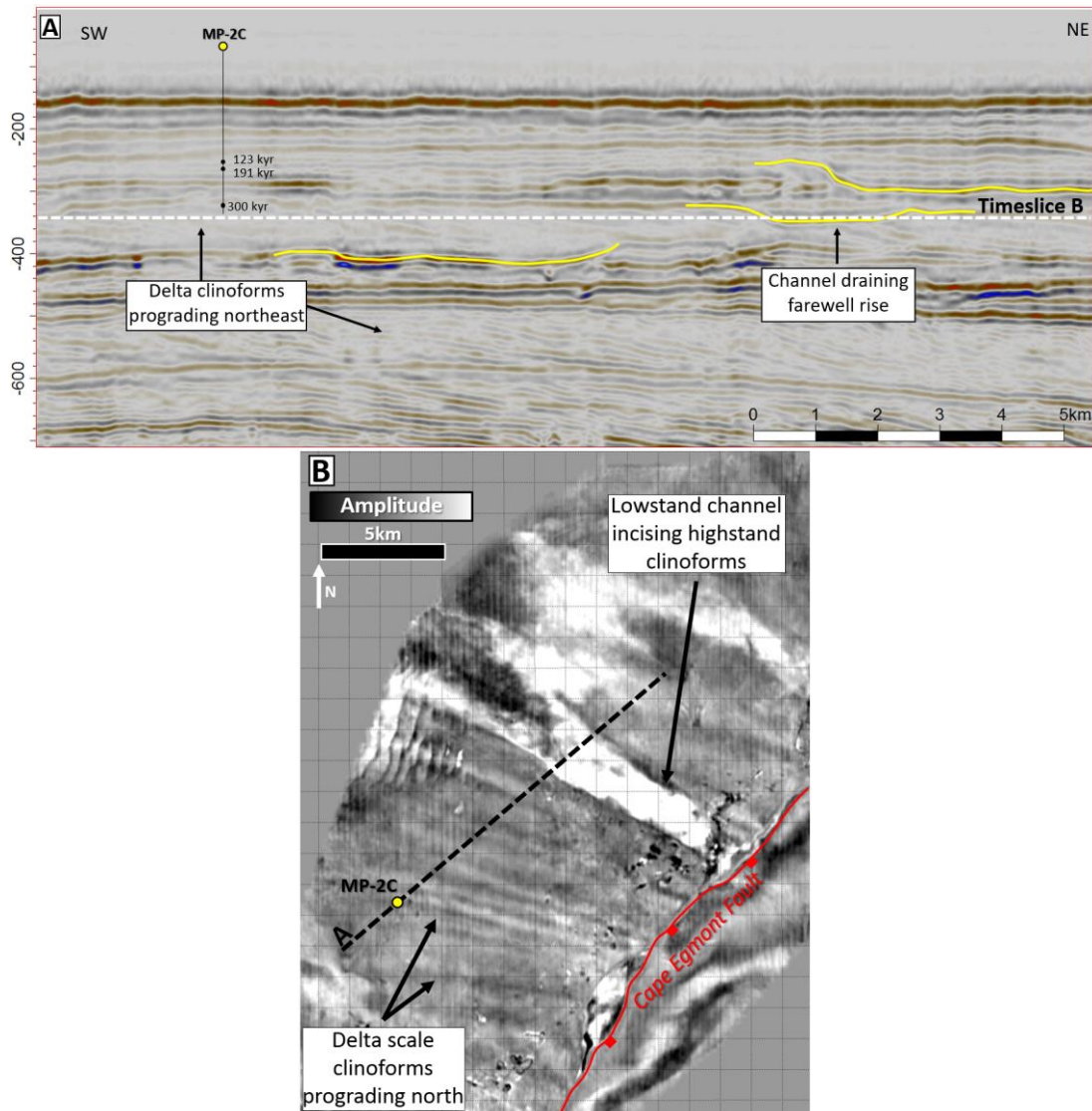


Figure 6.6 Geomorphology in the Maui 4D seismic survey.

A) NE – SW line through the Maui 4D survey with shallow borehole MP-2C with shallow age date estimates from Nodder (1995, 1994, 1993). Delta scale clinoforms are prograding to the northeast and are incised by an overlying broad low angle channel. Subtle lowstand incision is annotated in yellow. B) Amplitude time slice at -342 ms showing northeast prograding delta clinoforms and a northwest draining channel. See Figure 6.4 for location.

During the last glacial maximum, the Farewell Rise became subaerially exposed and was host to a mixture of shrubland and forests (Newnham et al., 2013). Contextually, the westward draining channels mapped in this chapter are thus interpreted to represent rivers draining the Farewell Rise toward the Taranaki Basin (Figure 6.4). These rivers

drained onto the Western Stable Platform, which during the LGM was a broad shallow shelf less than 50 m deep (Figure 6.4B).

Further south, in the Hector 3D survey, a broad southeast to northwest erosion surface up to 7 km, wide is mapped, incising underlying highstand clinoforms (Figure 6.9). When extrapolated beyond the 3D survey using regional 2D seismic lines, a northwest trending embayment –like feature is evident but limited data coverage make it impossible to characterise further.

On the mid to outer shelf, the Karoro 3D survey (Figure 6.8B) shows a dendritic drainage into a canyon associated with the T9/ET12 sequence boundary. This boundary is estimated to mark the start of MIS 6 (~191 kyr, see Figure 6.2) and shows incision into the shelf approximately 10 km shoreward from the rollover of the T9 surface. Figure 6.8C shows dendritic drainage in a westerly direction towards the incised corridor separating the north and south depocenters.

As discussed in Chapters 4 and 5, the Egmont Terrace, a southerly extension of the Western Stable Platform, sits approximately 120m deeper than the shelf to the north. The boundary between these two sections of the Western Stable Platform is defined by a clinoform striking approximately north – south, becoming northeast – southwest as it approaches the Farewell Rise (Figure 6.4). It has a relief of approximately 100 m (Figure 6.4 and Figure 6.10), rolls over at a present day water depth of approximately 150 m and downlaps onto the Egmont Terrace shelf at a present day depth of approximately 250m. The architecture of this clinoform is imaged on only a handful of seismic lines (Figure 6.10) but is well defined on seafloor bathymetry (Figure 6.4); from this data the clinoform has a foreset height of approximately 100 m, foreset length of 19.5 – 21 km and a dip of approximately 0.3°. These architectures are conspicuous when compared to the database of architectures of clinoform types and scales documented by Patruno et al., 2015 and Patruno and Helland-Hansen (2018). From its morphology, it can be classified as either a shelf edge clinoform or muddy subaqueous delta scale clinoform, sharing some characteristics of both scales (see Table 6.1 below) but with an anomalously long foreset length in either scenario.

The clinoform progrades approximately from east to west, in contrast to the dominant north – south trend identified in highstand clinoforms on the shelf. Additionally, this

clinoform is 70 m higher than delta scale clinoforms described in the previous section which were interpreted as highstand features.

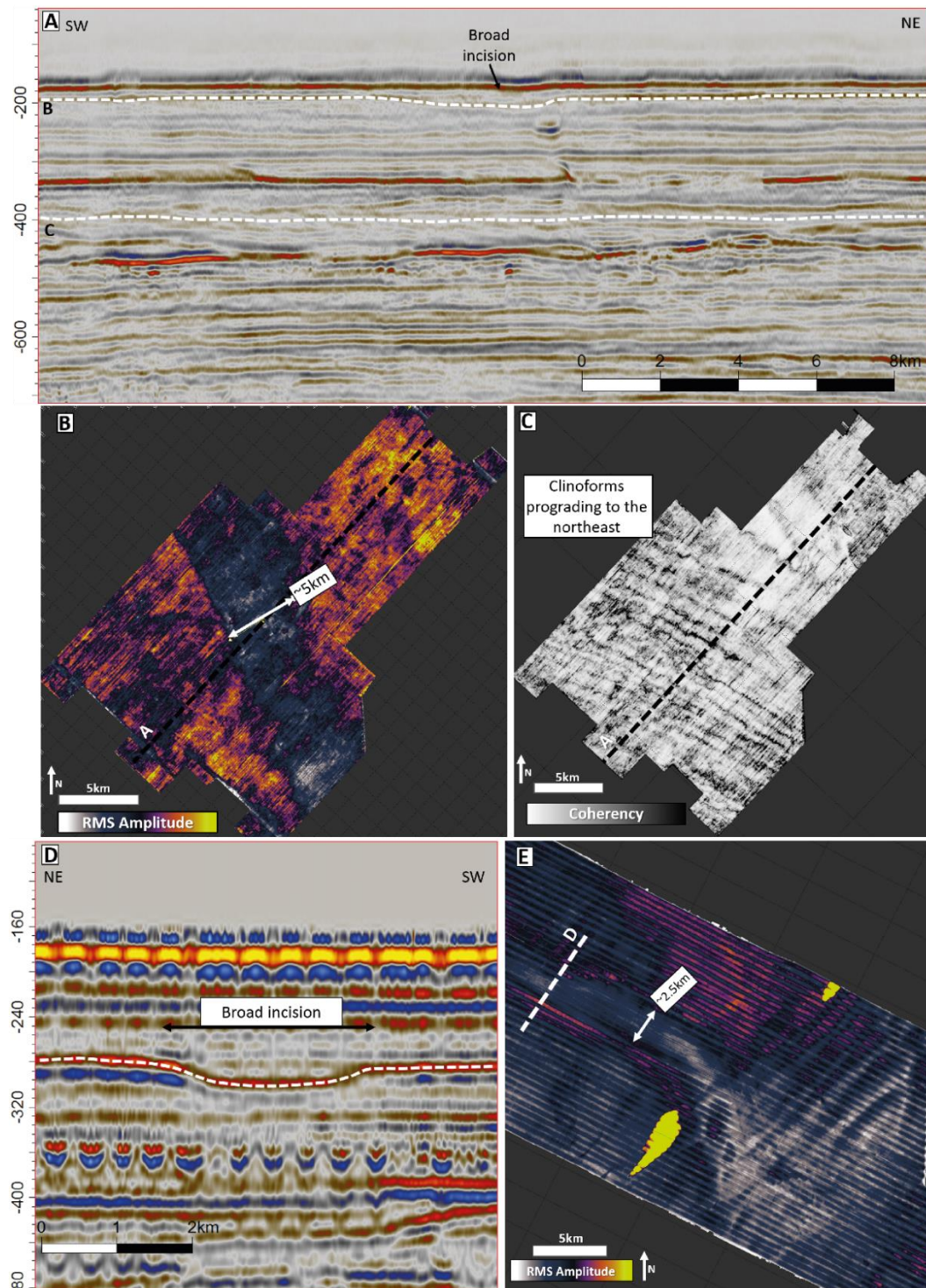


Figure 6.7 Seismic geomorphology of the Tui 3D survey.

A) inline 3813 from the Tui 3D survey showing broad, low angle incision draining to the northwest. B) RMS amplitude horizon extraction showing a 5 km wide low angle incision draining towards the northwest. C) Stratal slice through north prograding delta scale clinoforms (interpreted as highstand). D) Crossline through the Kokako 3D survey showing a northwest draining channel system as imaged in the RMS horizon extraction in E. See Figure 6.4 for location.

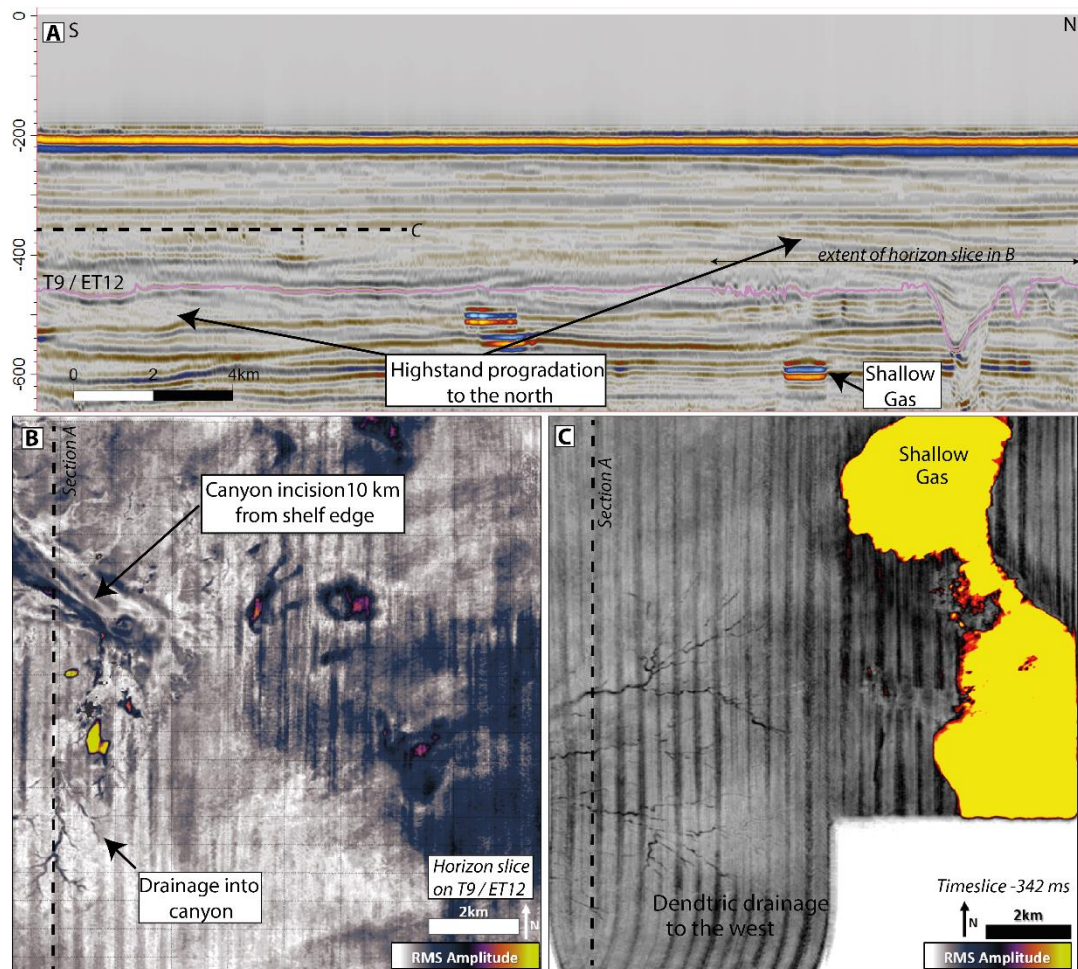


Figure 6.8 Seismic geomorphology of the Karoro 3D survey.

A) Inline 5049 from the Karoro 3D survey with regional horizon T9 (Chapter 4), B) RMS amplitude horizon slice along T9 showing dendritic drainage into a northeast trending canyon system set ~ 10 km back from the T9 shelf edge. C) RMS amplitude time slice (-342 ms) showing dendritic drainage across the shelf towards the west. See Figure 6.4 for location.

The contrasting progradation direction of this larger clinoform is interpreted to be associated with lowstand discharge from the Farewell Rise and North Island. Given the data coverage and quality, a link between channels draining the Farewell Rise and the clinoform separating the ET from the WSP is not apparent but would seem likely.

Table 6.1 Comparisons of clinoform geometries and types. Modified from (Patruño and Helland-Hansen, 2018).

	This clinoform	Shelf Edge Clinoforms	Muddy Subaqueous delta scale clinoforms
Rollover Depth	150 m (or 30 m in lowstand)	60 – 426 m	60 – 59 m
Foreset Height	100 – 110 m	97 – 300 m	3 - 46 m
Foreset Length	19.5 – 21 km	2.4 – 17.2 km	1 – 11.8 km
Foreset gradient	0.3 °	0.6 – 4.8°	0.1 – 0.9 °

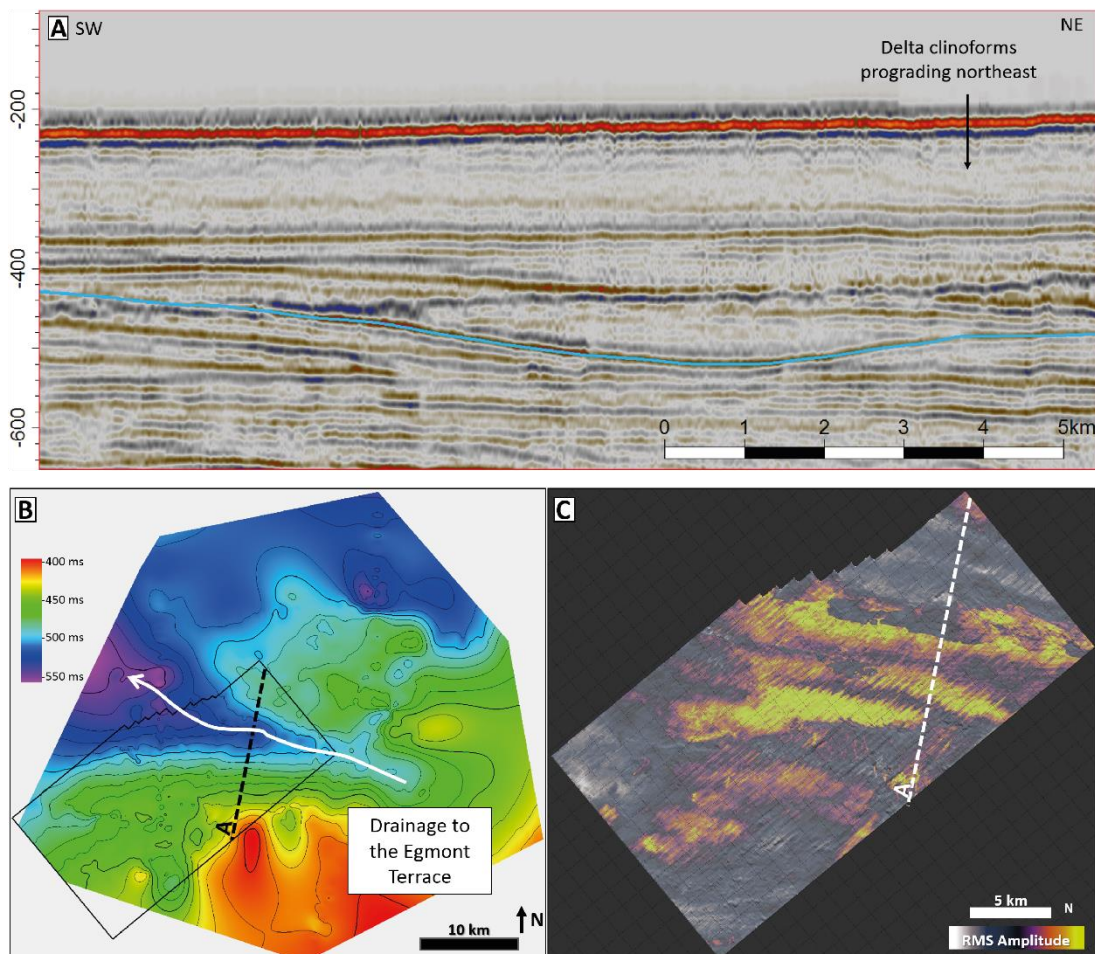


Figure 6.9 Embayment in the vicinity of the Hector 3D survey.

A) Large incision / depression (blue line) draining toward WNW from the Farewell Rise towards the Egmont Terrace. B) Time structure map of channel with outline of Hector 3D survey C) RMS Amplitude horizon slice of channel. See Figure 6.4 for location.

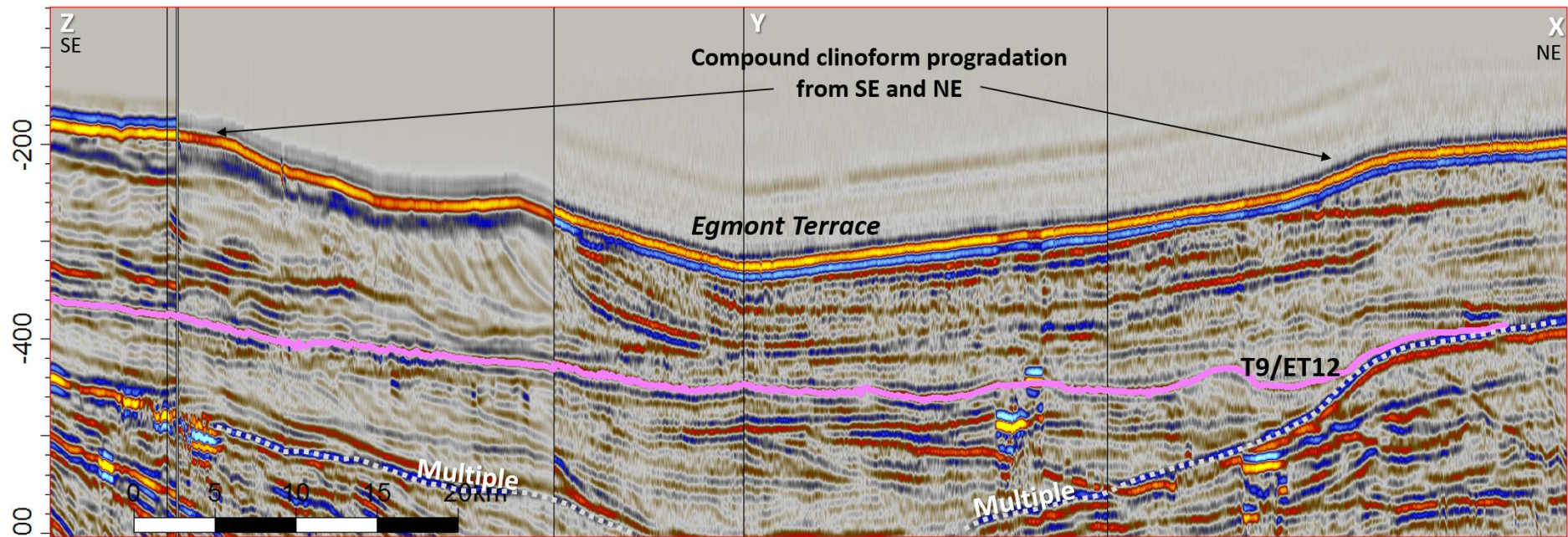


Figure 6.10 Composite section showing clinoforms downlapping on to Egmont Terrace. See Figure 6.1A for location.

6.4 Deepwater sediment pathways

This section examines the sediment pathways taken to deepwater regions of the basin once material was delivered across the shelf of the Taranaki Basin. Two main regions are considered; the Egmont Terrace/Challenger Plateau region and the true basin floor of the Taranaki Basin (Figure 6.11).

6.4.1 Egmont Terrace/Challenger Plateau Region

Bottomsets on the Egmont Terrace sit approximately 500 m above the basin floor of the Taranaki Basin proper, a feature attributed to the topographic elevation of the Challenger Plateau (CP). A drainage network mapped between regional 2D seismic lines and bathymetric data reveals canyons and channels flowing from south to north, from the Egmont Terrace bottomsets to the basin floor of the Taranaki Basin (Figure 6.11). This network comprises slope canyons linking directly from the shelf break to the Taranaki basin floor and a northeast trending channel (Figure 6.11A & B), unattached to the slope, draining the bottomsets of the Egmont Terrace to the Taranaki basin floor. On the basin floor, the Egmont Terrace drainage system converges with a northwest flowing deep-water channel system originating from the incised corridor separating the northern depocentre from the Egmont Terrace (Figure 6.11)

On the northeast flank of the Challenger Plateau, a northwest trending 110 km long channelised feature was identified on the seafloor and mapped on a network of 33 2D seismic lines with spacings ranging from 1.5 – 10 km (Figure 6.11).

The channel flows roughly perpendicular to the slope of the CP and is perched 100 – 150 m above the basin floor (Figure 6.12A). Initiation of the channel is observed at ~ 1300 metres below sea level (mbsl) and is mapped to a depth of 1700 mbsl, giving an average descent gradient of 0.2° along the trajectory of the channel (Figure 6.12 B). The channel is mapped to its maximum downstream extent using the available seismic data and is not resolved in the bathymetry data; it is unclear whether it continues beyond what is shown in Figure 6.11.

In cross section, sediment accumulation is asymmetric and consistently focused on the up-dip, southwestern (left) flank of the channel (Figure 6.12A). The geometry of this sediment accumulation is consistent with that of a plastered drift deposit (Rebesco et al., 2014), suggesting a possible oceanographic influence on deposits on the Challenger Plateau. Such a deposit could have formed from a combined influence of the Giant

Foresets Formation prograding onto the Challenger Plateau with a gentle current sweeping the plateau. Similar mounded geometries were also described in Unit A of Chapter 4.

The oceanography of the New Zealand region is well documented (Chiswell et al., 2015), however no currents have been identified at this depth in the Taranaki Basin (a factor attributed to the topography of the Challenger Plateau blocking currents from the south).

To further investigate the existence of an unreported water mass or bottom current, Current Temperature Depth (CTD) profiles of salinity and temperature were constructed using a publicly available data from the World Ocean Circulation Experiment (WOCE) (Figure 6.12C & D). No obvious water masses are observed on these sections at the depth of the channel / moat feature (although data is sparse on the northeast flank of the Challenger Plateau). This may indicate that the current causing the drift and moat features was a lowstand feature in the water column around New Zealand and the drift and moat are thus tentatively interpreted as relict lowstand features.

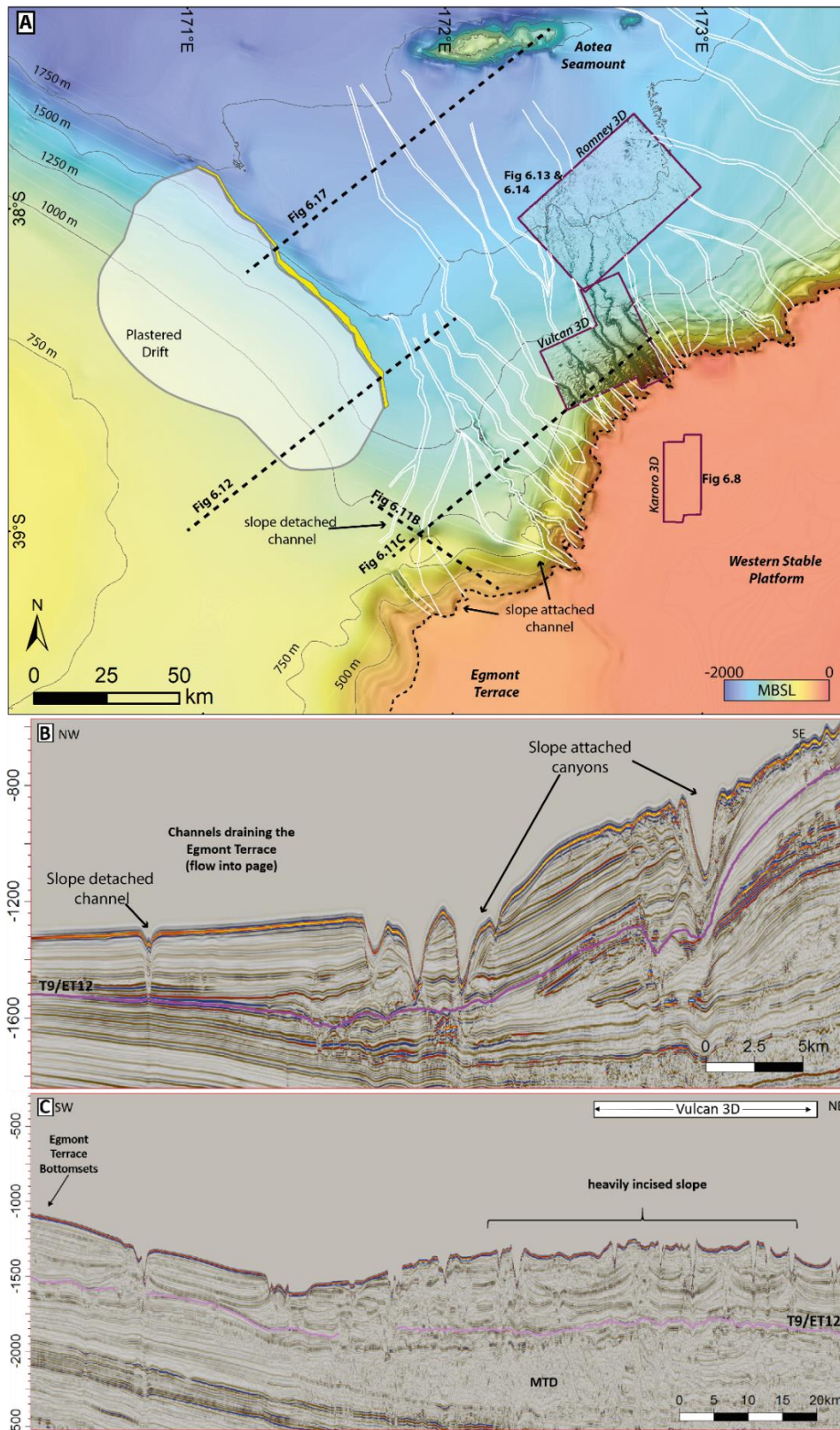


Figure 6.11 Sediment pathways from the Egmont Terrace to the Deepwater Taranaki Basin.

A) Bathymetry map showing subsequent figure locations and deep-water channels mapped on 2D seismic (not drawn to scale). B) 2D seismic line showing conduits draining the Egmont Terrace including canyons attached to the shelf edge and a channel initiating in the bottomsets of the Egmont Terrace. C) Regional 2D seismic line showing a heavily incised slope succession prograding over earlier MTDs (Chapter 4).

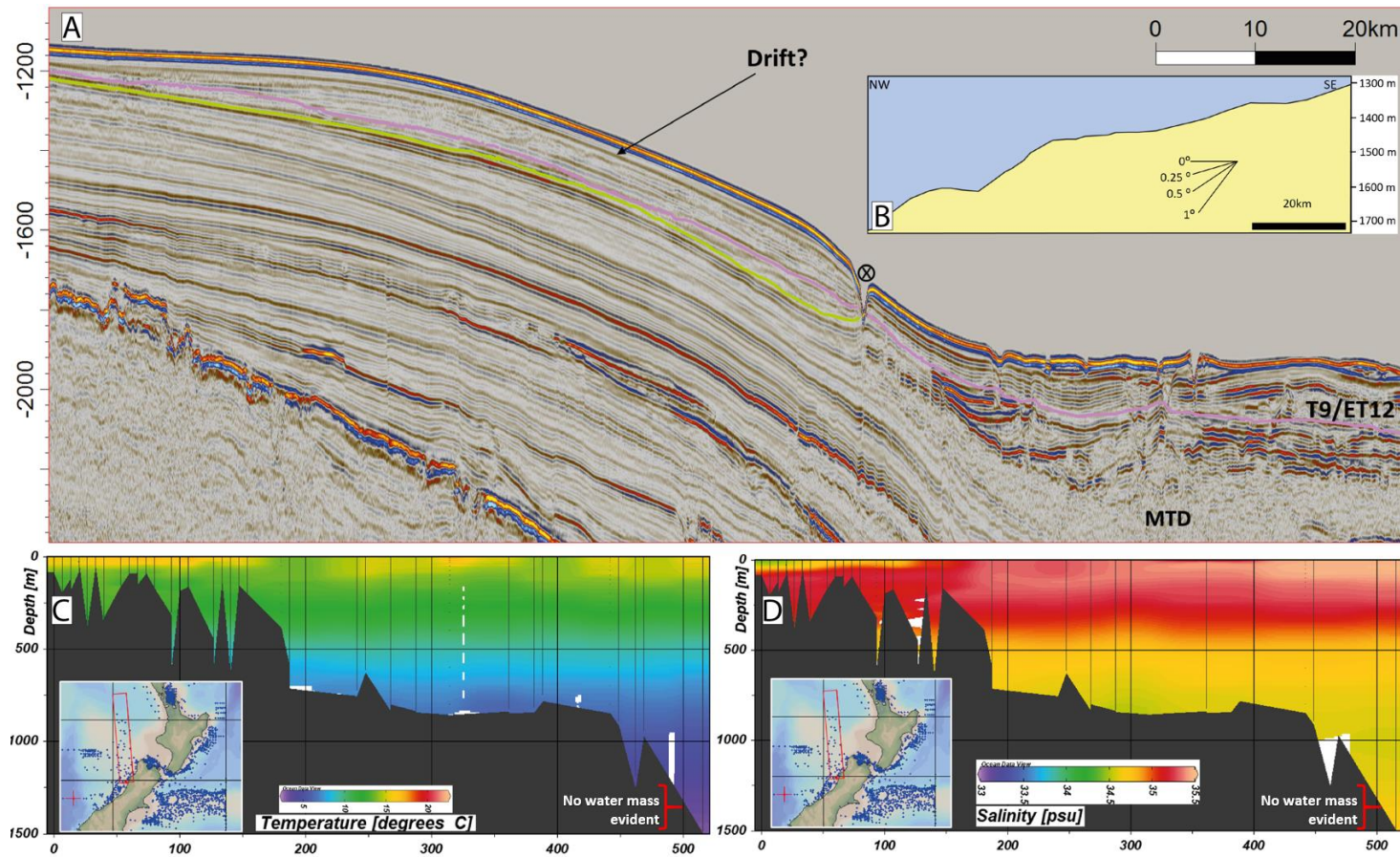


Figure 6.12 Contourite and moat.

A) Possible contourite and moat on seismic line DTB01-18 (See Figure 6.11 for location), circle with cross indicates flow direction into the page, B) Descent gradient along thalweg of moat/channel. C) & D) represent CTD Temperature and Salinity profiles respectively and show that no anomalous water body / contour current exists at the approximate location of the suspected moat. CTD data from the World Ocean Circulation Experiment (WOCE). Sections C and D were created with Ocean Data Viewer (Schlitzer, 2018).

6.4.2 Slope and Basin Floor of the Taranaki Basin.

In bathymetric data, the shelf rollover of the Western Stable Platform is dissected by numerous slope canyon systems that pass down dip into basin floor channels (Figure 6.11). Seven of these canyon / channel systems are imaged in detail by the Romney and Vulcan 3D seismic cubes (Figure 6.13 and Figure 6.14). These surveys image the depositional system from the shelf break at ~200 m, through the slope to the basin floor to a depth of 1600 metres below sea level (mbsl). This section utilises 3D seismic geomorphology of seabed and near seabed strata to investigate the processes in operation on the slope and in basin floor environments. Regional 2D seismic data are also utilised to map these channels beyond 3D control and image the ultimate sink for sediment to the Taranaki Basin.

In the area covered by the Vulcan and Romney surveys, the slope succession (~ 200 – 1200 mbsl) is incised by canyons up to 400 m deep, spaced at 3 to 6 km (with some merging down dip). Between the slope canyons, a rugose seabed is dominated by pockmarks, sediment waves and scours. Bland RMS amplitudes (Figure 6.14) suggest that the slope is comprised mostly of mud, which is also indicated in well logs from the Tane-1 exploration well (Shell BP Todd Oil Services Ltd., 1976)(see Appendix-1 for well log). Canyon and channel fills on the slope exhibit medium to high RMS amplitudes suggesting a coarser component to their fills (Figure 6.14).

Pockmarks are commonly observed on the mid to upper slope between 360 to 780 mbsl (Figure 6.13B). Kroeger et al., (2017) mapped a similar cluster of pockmarks on the slope 40 km to the southwest and attributed them to dissociation and escape of gas from microbial and thermogenic gas pockets. Such dissociation and escape can occur due to burial, increased seawater temperature or decreased water depth; these changes may be attributable to glacial-interglacial cycles. Assuming hydrate dissociation and fluid escape occurred following changes at the LGM, a tentative date of between 29 to 15 kyr can be suggested for their formation. This may infer that the slope has received little to no sedimentation since this date, that sedimentation is focused within the canyons, or that dissociation and pockmark formation is ongoing.

Sediment waves are observed throughout the slope and basin floor environments over a range of scales and settings (Figure 6.13 and Figure 6.15). Small scale, confined bedforms with a crescentic planform view and downslope asymmetric profile are observed in a base of slope setting (Figure 6.15D) with wavelengths of 240 – 450 m and wave heights of

approximately 2-3 m. Waves of this scale tend to be composed of medium sand to cobble sized sediment (Symons et al., 2016). Similar features have been documented in numerous localities around the globe, including the Monterey Canyon (Paull et al., 2011) and offshore La Réunion (Babonneau et al., 2013). Much debate still exists as to the processes these small scale bedforms represent. Three main hypothesis exist; 1) formation by internal tides (e.g. Xu et al., 2008), 2) by liquefaction and slumping of channel axis sediments (e.g. Paull et al., 2010) or 3) that these are cyclic steps caused by supercritical flow (Kostic and Parker, 2006; Taki and Parker, 2005).

Larger scale sediment waves are also observed in unconfined settings on the slope and basin floor, exhibiting wavelengths of 700 to 1500 metres and variable wave heights up to 45 metres. Waves of these dimensions tend to be composed of fine grained but mobile sediment (Symons et al., 2016; Russell B. Wynn and Stow, 2002). They are commonly observed in a setting immediately down dip of bends of canyons and channels on the slope and basin floor (Figure 6.15). They are interpreted to represent overbank deposits as turbidites overrun their containing walls at meander bends. They occasionally show moderate to high RMS amplitudes. Similar deposits have been reported in offshore eastern Borneo by Posamentier and Kolla (2003) and in the Shepard Meander of the Monterey Canyon, offshore California where they have been categorised as cyclic steps (Fildani et al., 2006). Additionally, sediment waves appear to initiate in regions overlying relict topography on the seafloor such as slump deposits (Figure 6.15E) with comparable examples in the Adriatic Sea (Cattaneo et al., 2004) and Orinoco slope (Ercilla et al., 2002).

In Figure 6.13 to Figure 6.15 scour trains are evident in the seafloor topography on the slope. Whilst these are erosional on the seabed, they show internal reflector continuity in the sub-seafloor at the resolution of the seismic dataset. Scours are net erosional crescentic to enclosed depressions that cut into the seafloor and commonly form linear trains of asymmetrical waveforms (Covault et al., 2017). Many seafloor scours may in fact be cyclic steps (Kostic, 2011); cyclic steps are long wave, upstream-migrating bedforms in regions where high gradients and slope breaks can induce an internal hydraulic jump in turbidity currents (Covault et al., 2017). Whilst they share characteristics of seafloor scours, cyclic steps are difficult to recognise on the basis of morphology and facies alone, so require either numerical modelling (e.g. Fildani et al., 2006) or direct monitoring of turbidity currents (e.g. Hughes Clarke, 2016). Similar features have also been imaged in the subsurface of the Nile Delta by Armitage et al. (2012) and offshore California in the

Santa Lucia channel system by Fildani et al. (2013) where they are interpreted to represent incipient channel features.

On the basin floor, channels pass from broadly linear features with long wavelength meanders to a highly sinuous channel network. These channels interact with underlying topography from mass transport deposits, infilling local topography (Figure 6.13, Figure 6.16, Figure 6.17). These fans are later incised by the channel as topography is healed and the channel continues basinward. The moderate to high RMS amplitudes associated with these channel and fans systems suggests that these channels were efficient conveyors of coarse material to the basin floor. Toward the north-western limits of the Romney 3D survey, the spacing between channels becomes narrower, and eventually merge down dip (outside of the 3D cube) into one larger conduit approximately 6km across (Figure 6.16); this is due to the effects of topography from underlying MTDs.

As channels pass basinward, they must infill a chaotic and undulating local topography; this process has resulted in generation of a patchwork of fans infilling local topography before channels proceed basinward (Figure 6.16 & Figure 6.17). Using the regional 2D seismic dataset of previous chapters, the channel systems have been mapped beyond the Vulcan and Romney 3D surveys where they terminate in the vicinity of the Aotea Seamount, approximately 160 km from the shelf edge (Figure 6.17 & Figure 6.18).

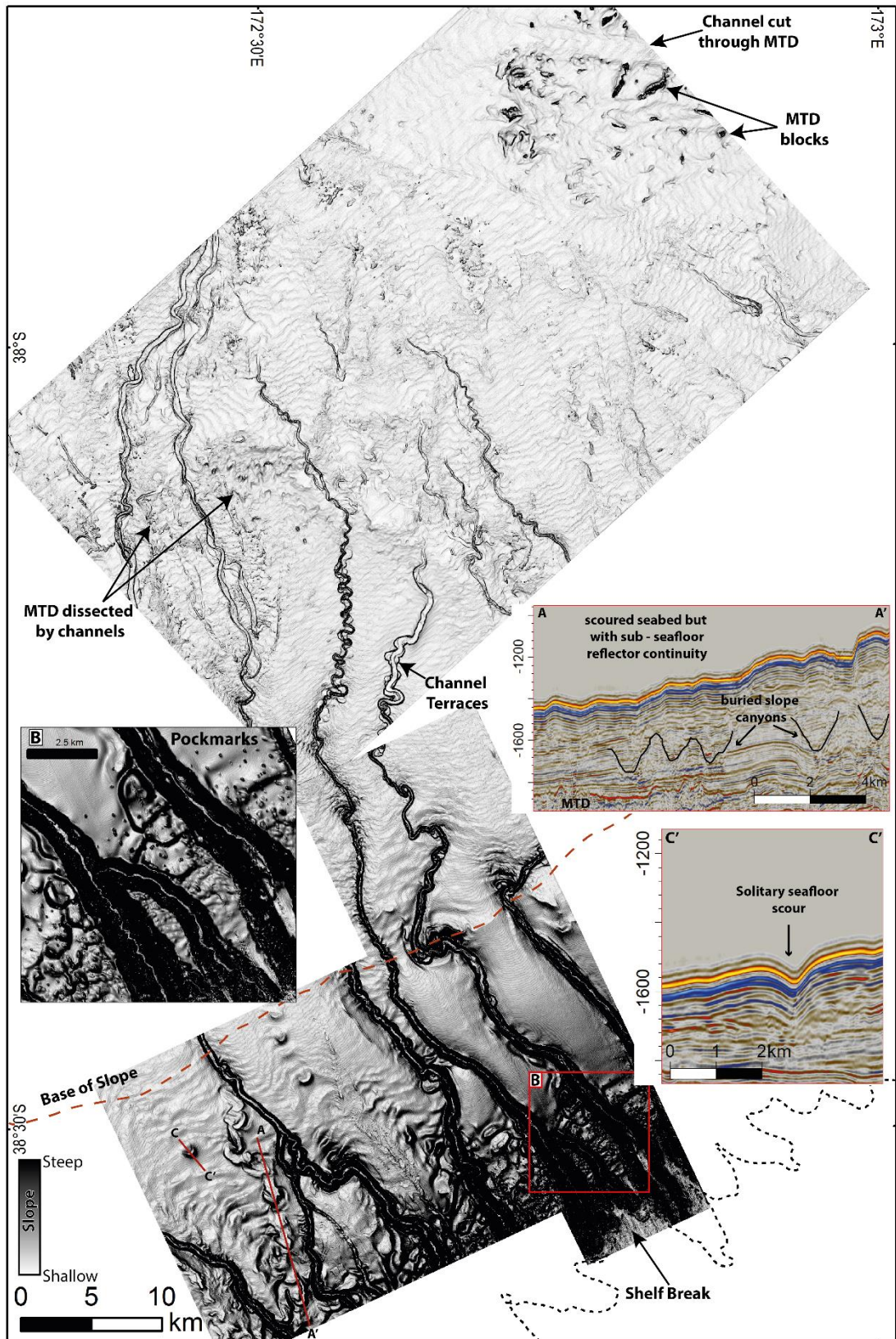


Figure 6.13 Seabed slope map from the Vulcan and Romney 3D seismic surveys Highlighting key depositional pathways from shelf to deep-water. See Figure 6.11 for location.

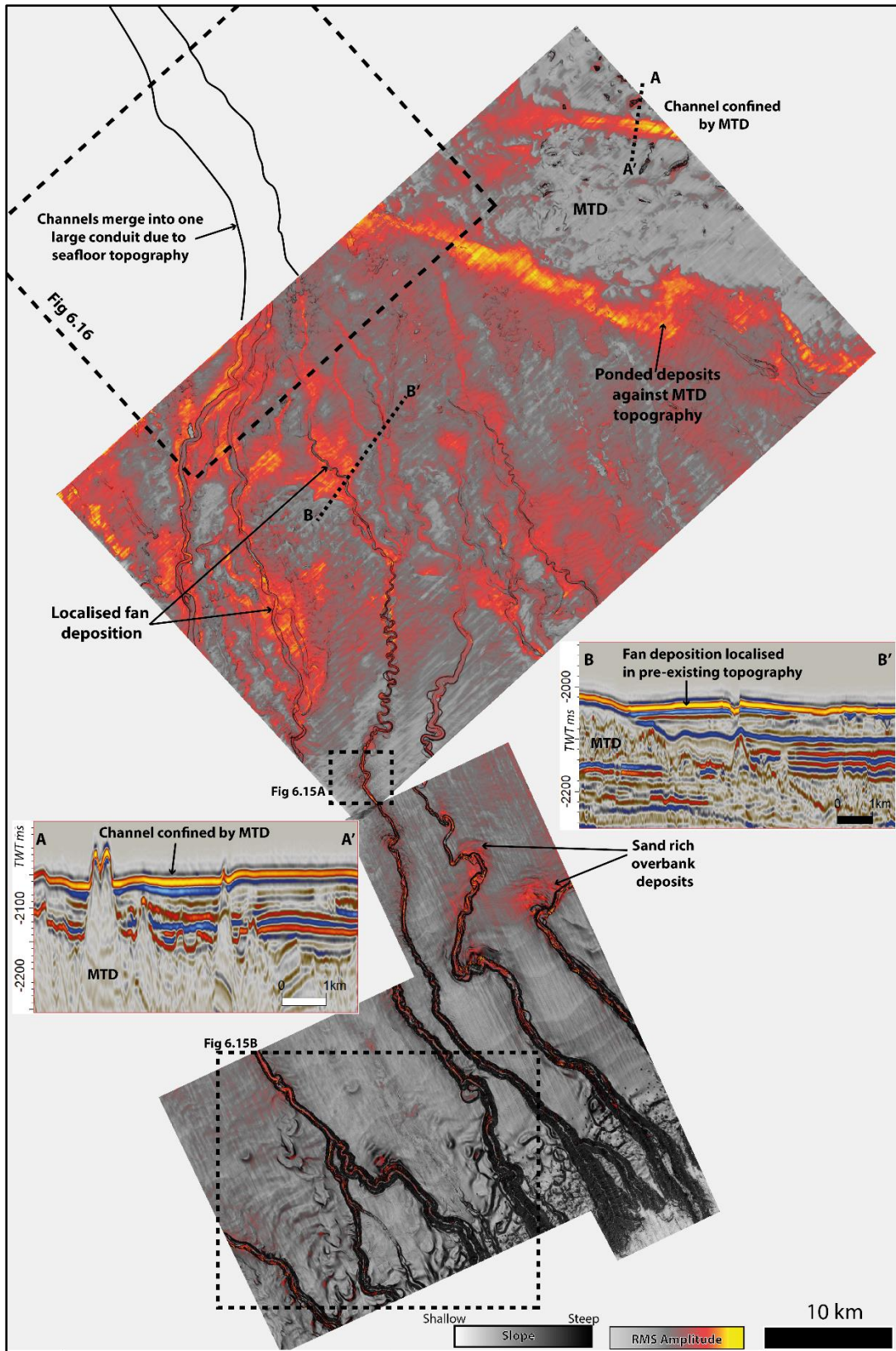


Figure 6.14 Co-rendered Slope and RMS Amplitude extraction with a sub sea floor window 25 ms on the Vulcan and Romney 3D surveys

Showing higher amplitudes are mostly confined to channels on the slope, with the exception of occasional overbank deposits. On the basin floor, amplitudes show local development of fan geometries infilling MTD topography. See Figure 6.11 for location

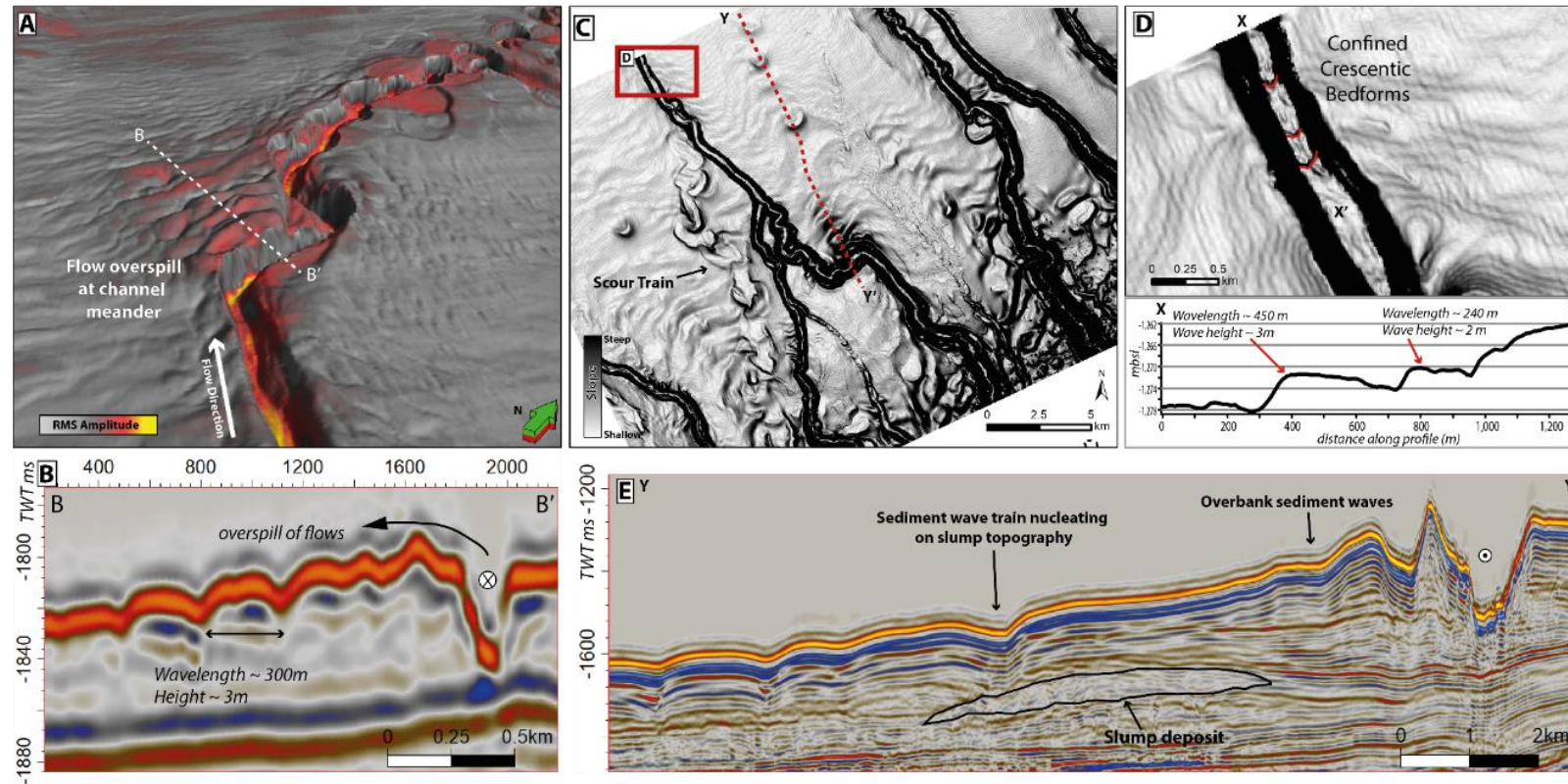


Figure 6.15 Sediment Waves in the Vulcan and Romney 3D surveys

A) RMS amplitude down-slope perspective view of the Romney 3D survey showing deposits related to overbank deposition on meanders. See for FIG location. B) Cross section showing overspill of flows and related sediment waves (circle with \times denotes flow into page). C) Slope magnitude map of the Vulcan 3D survey showing overbank sedimentation and seafloor scours. D) Close up slope magnitude map showing crescentic bedforms confined within a slope channel with profile X-X' showing cross sectional geometry. E) Cross section showing overbank sediment waves and sediment waves nucleating on pre-existing slump topography. Circle with dot denotes flow out of page (see C for section location).

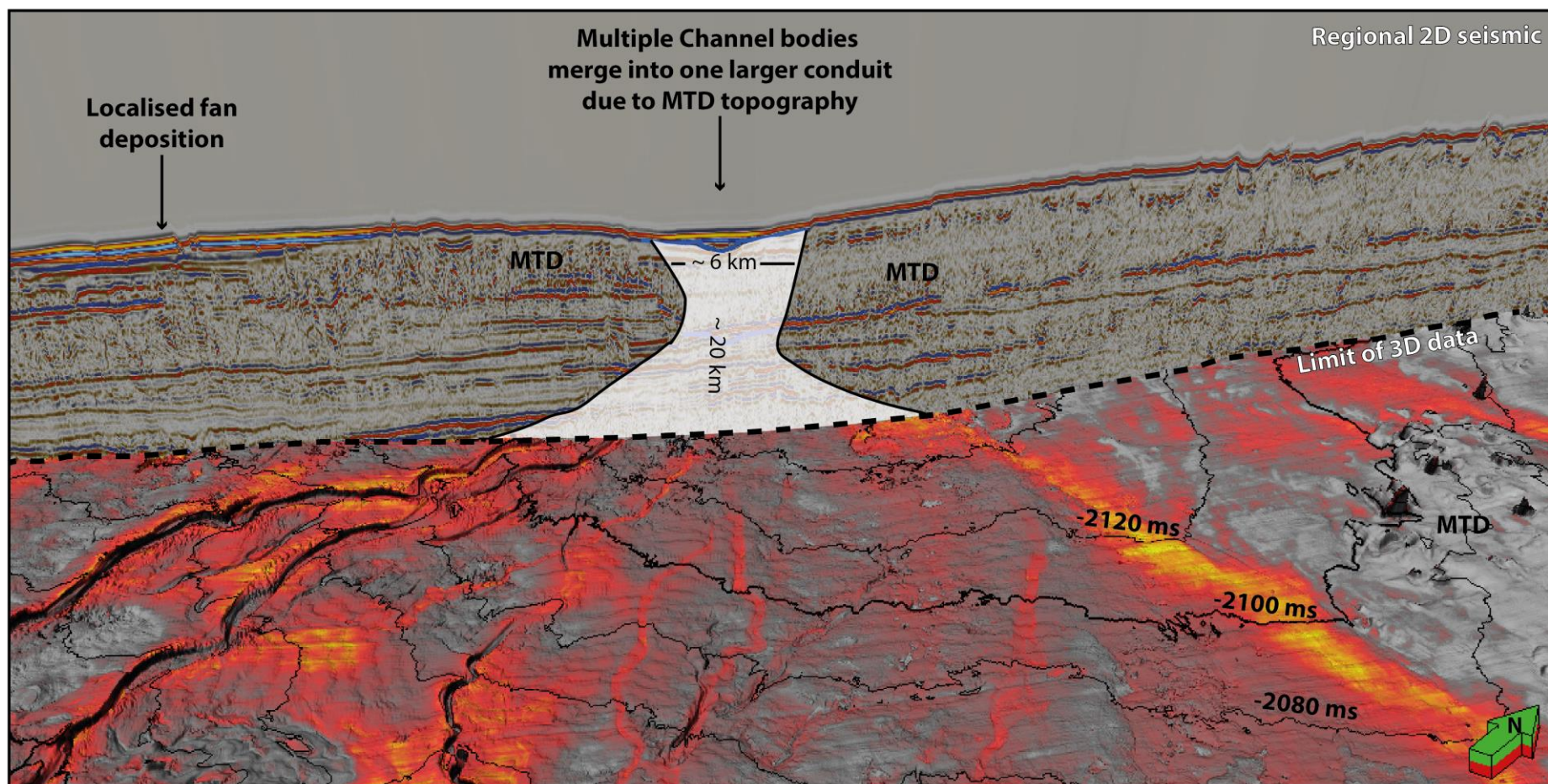


Figure 6.16 Channels, fans and MTDs.

Perspective view looking down slope: co-rendered RMS amplitude with slope magnitude showing multiple channels converging due to the effects of MTD topography with resulting localised fan deposition within topography. See for Figure 6.14 location.

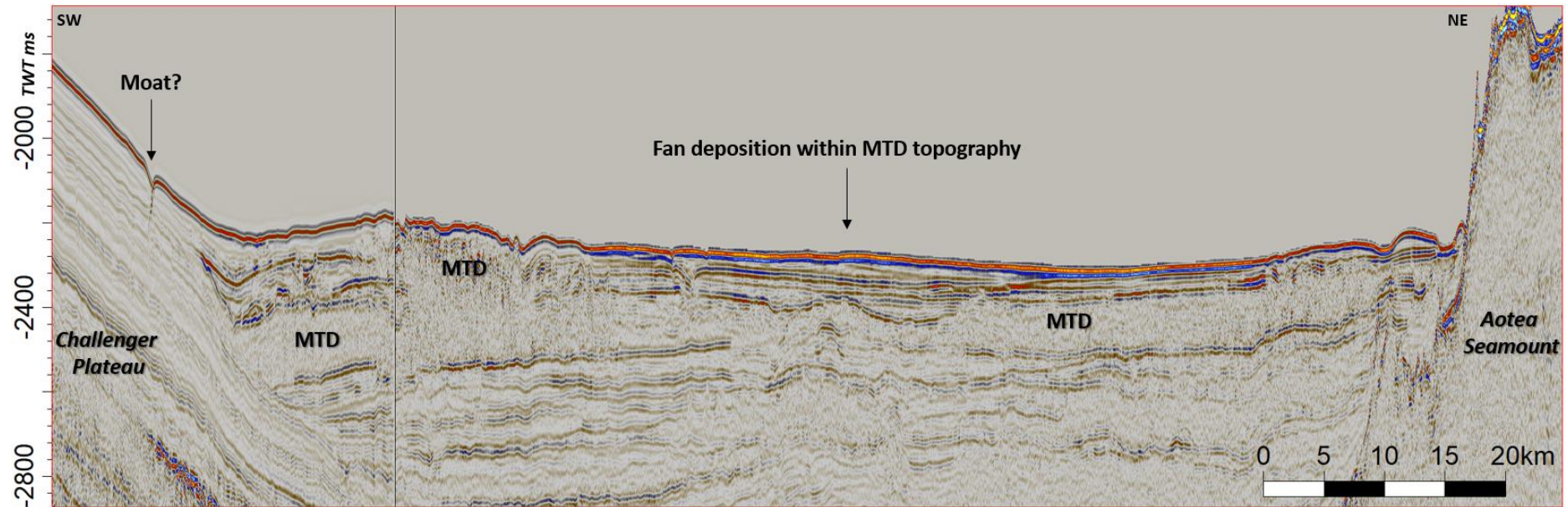


Figure 6.17 Composite seismic line DTB01-08 & ATB10-013

Showing fan deposition controlled by seafloor topography of MTDs, the Aotea Seamount and Challenger Plateau. See Figure 6.18 for location.

6.5 Synthesis of shelf, slope and basin floor conduits.

By synthesising sediment pathway data across the shelf, slope and basin floor, a picture of sand delivery to the deepwater Taranaki Basin and beyond emerges.

During sea level lowstands, a large part of the shelf was subaerially exposed, creating a land bridge between North and South Islands (i.e. the Farewell Rise). This land bridge was drained by channels flowing southeast toward the Wanganui Basin and Cook Straits (Nodder, 1995), and to the northwest toward the Western Stable Platform (this work). These channels discharged onto a shallow shelf less than 50 m deep, where surficial sediment samples compiled by Bostock et al. (2018a, 2018b) show a sand body approximately 85 km x 25 km (unknown thickness due to nature of the dataset) perched on the outer shelf of the Western Stable Platform (Figure 6.18). Moving northeast of the area examined in this chapter, the shelf is dominated by sandy material and the LGM shoreline came to within 5 km of the shelf edge rollover (Figure 6.18). In contrast, surficial sediments in the southern Taranaki Basin and Egmont terrace region are comparatively sand poor although the rollover of the Egmont Terrace still has up to 40 % sand (Figure 6.18).

Sand delivered to the outer shelf was captured by canyons incising the shelf edge. These canyons are spaced at 3 to 6 km and bypass the slope from approximately 200 to 1200 mbsl, where they pass into a sinuous network of basin floor channels. Turbidity currents were of sufficient size and velocity to frequently overflow the containing walls of the slope canyons and basin floor channel systems, resulting in common sediment wave fields developed across the slope and basin floor. Channel systems on the present day seabed can be traced in regional 2D seismic data up to 160 km from the shelf edge rollover; their paths are strongly influenced by an irregular bathymetry inherited from earlier MTD emplacement (Chapter 4), resulting in a patchwork development of basin floor fans that locally infilled bathymetric lows before prograding basinward once again. The present-day sink for sediment delivered by these channels sits in the vicinity of the Aotea Seamount between approximately 1600 to 1800 mbsl, where a large body of sand is evident in surficial sediments (Figure 6.18). This body of sand extends beyond seismic control where it merges with sediments sourced from the neighbouring Reinga - Northland Basins.

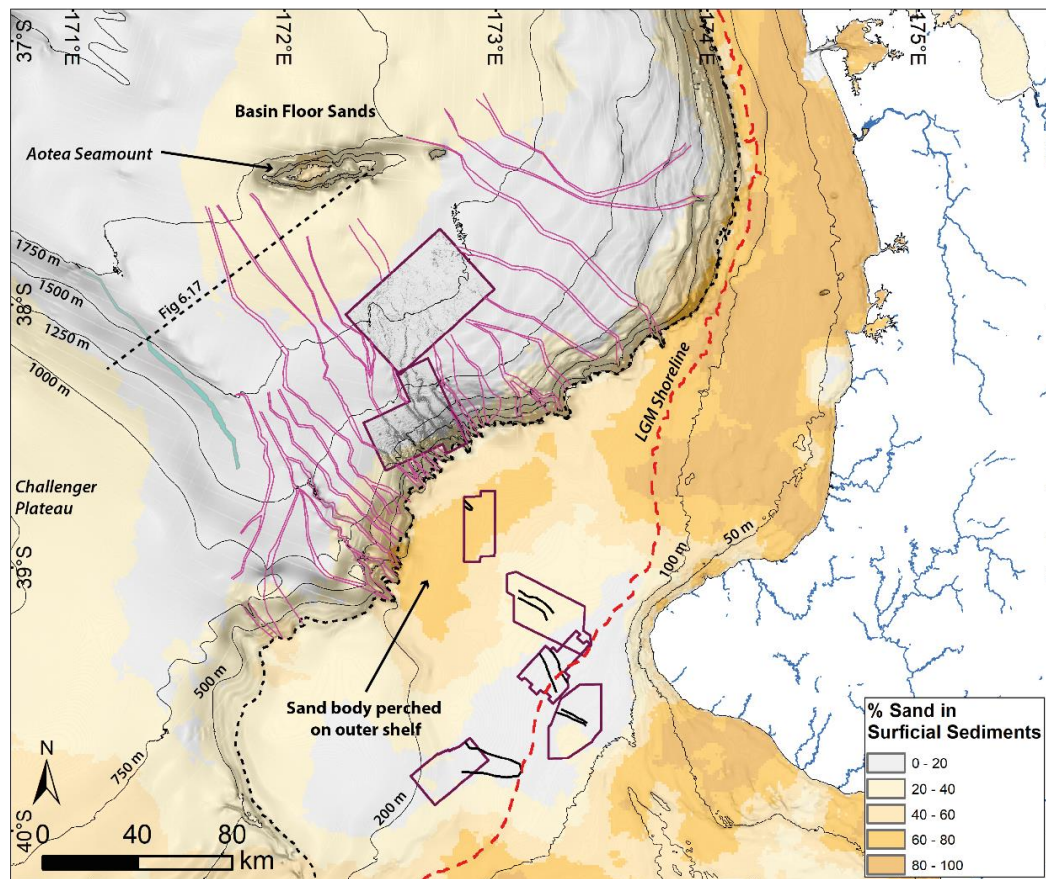


Figure 6.18 Surficial sand and sediment pathways.

Synthesis of sediment conduits (not to scale) mapped in this chapter on a base map of % sand in surficial sediments (after Bostock et al., 2018a, 2018b). Contours represent present day bathymetry.

On the shelf, highstand sedimentation patterns are dominated by delta scale clinoforms prograding from the southwest to northeast. This is attributed to the effects of a strong SW – NE littoral drift system combined with the effects of the Westland Current and is consistent with previous authors citing South Island as the sediment source for the Taranaki Basin (Hansen and Kamp, 2002; Kamp et al., 2004; Salazar et al., 2016). No geomorphic indicators in the 3D seismic datasets showed evidence for sediment contribution to the shelf edge from North Island during highstands. The northern portion of the basin, lying off the west coast of North Island is also subject to a strong north directed littoral transport system which disperses sediment along the shelf as far north as Auckland (Payne et al., 2010). It is unclear if this highstand sedimentation is currently contributing sediment to canyon heads, however there is evidence of deltas having reached the shelf edge repeatedly throughout the history of the Giant Foresets Formation (Chapter 4).

Contrasting highstand – lowstand activity at canyon heads has also been reported at along the Celtic-Armorican margin where canyon heads sit at a present-day water depth of

approximately 350 m and receive no terrigenous input. During the LGM however, canyon heads received terrigenous sediment from the “Fleuve Manche” (an amalgamation of some of Europe’s largest rivers (Bourillet et al., 2003) and discharge from the British Irish Ice Sheet (Bowen et al., 2002).

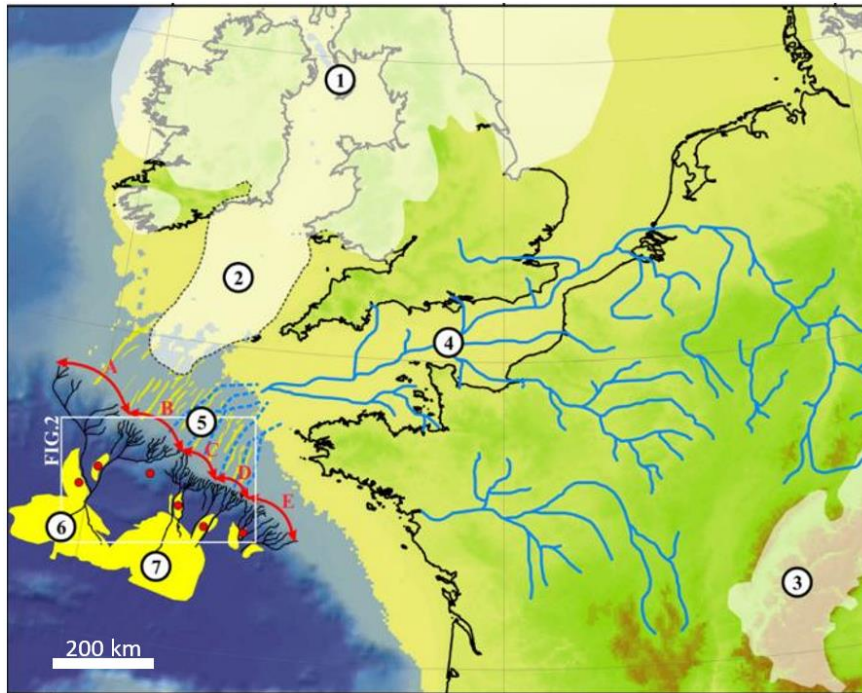


Figure 6.19 Celtic–Armorican margin during the Last Glacial Maximum (LGM).

Physiography of the Celtic–Armorican margin (north-western Europe) during the Last Glacial Maximum (LGM) showing discharge from the “Fleuve Manche” paleo river (4) and British Irish Ice Sheet (1 & 2) onto a shelf where they are captured by canyons (A-E) and deposited as fans (6&7). From Toucanne et al. (2008).

6.6 Taranaki Basin Catchments

The above work indicates contrasting sediment sources in highstand (South Island +/- North Island) and lowstand (Farewell Rise + North Island +/- South Island) scenarios for the Taranaki Basin. This section will classify catchment lithologies and present-day sediment budgets of each catchment and examine the dynamics of the sediment conveyor system.

6.6.1 South Island Catchments

New Zealand covers less than 0.2% of global land area, but despite this its rivers contribute ~1.7% towards the global suspended sediment yield to the world’s oceans (Hicks et al., 2011). The combined actions of tectonic uplift, steep terrain and high rainfall give rise to some of the highest erosion rates in the world (Larsen et al., 2014). The highest rates of uplift and erosion are focused along the west coast of South Island in the

Southern Alps (Figure 6.20C), with exhumation rates exceeding 5 km/Myr (Herman et al., 2013; Jiao et al., 2017; Koppes and Montgomery, 2009). Onset of Quaternary glaciations are likely to have caused increased relief in the Southern Alps, resulting in increased Quaternary erosion rates (Jiao et al., 2017). Since ~ 1 Ma, however, uplift, exhumation and erosion rates have equilibrated and remained at a steady state during glacial and interglacial periods (Batt et al., 2000; Herman et al., 2010). The present day configuration of South Island has a drainage divide running along the spine of the Southern Alps, with rivers draining to both east and west coasts (Figure 6.20). This section concentrates on rivers draining to the west coast of South Island. These rivers drain several small, steep and mountainous catchments ranging from ~ 500 to 6,400 km² (Hicks et al., 2011).

Geology

The geology of the west coast of South Island is dominated by pre-Cretaceous basement units divided into Western and Eastern provinces by the Alpine Fault (Figure 6.20). The Western Province is dominated by Early Palaeozoic rocks; in the area of interest the only outcrop in the region is of lower greenschist facies metamorphosed sandstone and mudstone turbidites deposited at the paleo-Pacific Gondwanan margin in the Early Ordovician (Laird, 1972; Rattenbury et al., 2010). Most rivers draining to the west coast are dominated by Eastern Province Terranes known as the Torlesse composite terrane and Alpine Schists (Radford, 2012). The Torlesse terrane is composed of Late Permian to Early Cretaceous greywacke dominated deep water fans sourced from a continental volcano-plutonic arc (Mortimer, 2004; Rattenbury et al., 2010; Roser and Korsch, 1986).

Large parts of this terrane were subjected to regional low-grade metamorphism, peaking during the Jurassic to Cretaceous, forming extensive schists approximately 12-25 km wide running sub parallel to the Alpine Fault (Mortimer, 2000; Vry et al., 2008). The metamorphic grade increases from east to west, from chlorite, biotite and garnet to an oligoclase zone at the Alpine Fault (Grapes, 1995; Vry et al., 2008). Schists are dominated by rocks with a fine grained, foliated matrix of quartz and muscovite with porphyroblasts ranging from ilmenite, titanite, chlorite, biotite, epidote, plagioclase, garnet, and amphiboles (Vry et al., 2008). In addition to metasedimentary rocks, small remnants of oceanic crust (serpentinite, gabbro and metabasites) of the Pounamu Ultramafic Group occur throughout the catchment draining to the west coast (Nathan et al., 2002).

Late Devonian to Early Carboniferous granitoids of the Karamea suite also outcrop within the catchment (Figure 6.20). These are dominated by muscovite – biotite granites, tonalites and orthogneisses intruding Western Province meta-sediments (Cox and Barrell, 2007; Nathan et al., 2002).

Sediment flux to the sea is highest from rivers in the South Westland district (Figure 6.20B), draining from South Island to the Tasman Sea (Hicks et al., 2011; Hicks and Shankar, 2003). This material is mainly sourced from the Arawata (7.2 Mt y^{-1}), Hokitika (6.2 Mt y^{-1}) and Haast (5.9 Mt y^{-1}) rivers, with additional input from other rivers in the region (Figure 6.22). In the North Westland region, sediment yields are much lower and mainly sourced from the Grey and Buller Rivers; 2.07 and 2.71 Mt y^{-1} respectively (Figure 6.20B and Figure 6.22). These lower sediment yields are likely due to the more indurated nature of bedrock within these catchments. Rivers in the Nelson region (Figure 6.20) contribute a comparatively small volume (totalling 0.82 Mt y^{-1}).

The geochemistry of surficial sediment transects across the Westland Shelf are dominated by Alpine Schist lithologies with a recycled orogen signature; localised contributions from other lithologies are rapidly diluted by Alpine Schist derived detritus (Radford, 2012).

During sea level lowstands, rivers giving the largest sediment contributions to the west coast (see above), bypassed directly from their terrestrial sources to deep-water regions offshore South Island (Radford, 2012), this would have resulted in up to 62.3 Mt y^{-1} less sediment available for delivery north to the Taranaki Basin (Figure 6.22).

6.6.2 North Island Catchments

In contrast to the dominance of Alpine Schist derived runoff from South Island, rivers draining toward the Taranaki Basin from New Zealand's North Island are dominated by quartz and feldspar rich sediments sourced from Quaternary volcanoclastic deposits associated with andesitic volcanism on the Taranaki Peninsula and Taupo Volcanic Zone in central North Island (Gillespie et al., 1998; Payne et al., 2010).

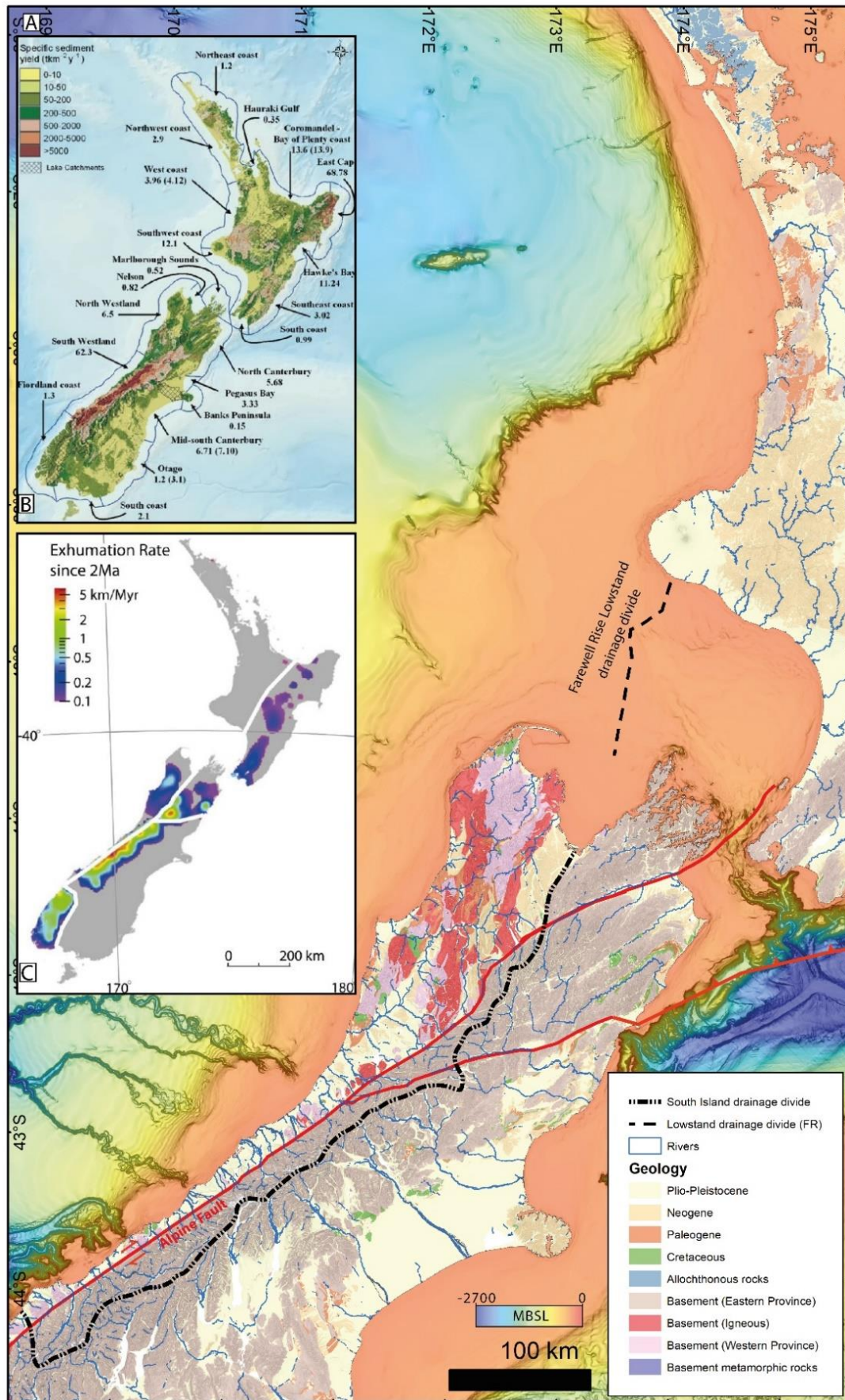


Figure 6.20 Generalised geology of New Zealand with exhumation rates and River sediment yields.

A) Geology of the New Zealand (modified from GNS QMAP) showing the drainage divide and rivers draining to New Zealand's west coast. B) Present day specific sediment yields of rivers to the coast from different regions of New Zealand (from Hicks et al. (2011) and C) Exhumation rates since 2Ma showing concentrated exhumation on in the Southern Alps along the Alpine Fault (from Jiao et al. (2017).

Present-day (i.e. highstand) runoff of rivers draining the west coast of North Island are comparatively low compared to those of New Zealand's South Island (4.12 vs. 68.8 Mt/y respectively) (Figure 6.20B), however these rivers are more proximal to the Taranaki Basin sink with less opportunity for sediment to be diverted from sinks in the Taranaki Basin. The comparatively lower runoff is attributed to lower rainfall values coupled with lower uplift and erosion rates on more competent indurated rocks (Bostock et al., 2018a; Hicks et al., 2011; Payne et al., 2010). Rivers on the southwest coast of North Island contribute 12.1 Mt y^{-1} to the sea (Hicks et al., 2011). In current highstand conditions this is mostly diverted south and east toward the Wanganui Basin and Cook Straits (Figure 6.4 & Figure 6.20) (Gillespie et al., 1998; Gillespie and Nelson, 1996).

During lowstand times when the Farewell Rise is exposed (Figure 6.4), these rivers would most likely have drained south and eastwards toward the Wanganui Basin and Cook Straits, with minor runoff toward the Taranaki Basin. Mapping in this chapter, however, showed a series of channels draining to the northwest toward the Taranaki Basin during lowstands, indicating runoff from the Farewell Rise. With the current quality and coverage of 2D and 3D seismic in the near sub-surface, it is unclear whether these channels merely drain the Farewell Rise land bridge or link to other mountainous upland sources on North or South Island.

6.6.3 Catchment Sizes & Productivity

When comparing catchment size vs productivity (Figure 6.21), individual rivers along New Zealand's west coast plot in the same regions as other rivers along small active margins around the world (Sømme et al., 2009). South Island rivers deliver significantly higher volumes of sediment to the marine environment than North Island rivers; a factor likely related to South Island's combination of steeper mountainous terrain, fissile protolith and active tectonics when compared to that of North Island.

Once sediment is in the marine environment, it is subject to lateral transport by littoral drift and ocean currents, thus combining the input of numerous rivers into one diverse and dynamic conveyor system (discussed in more detail below). Consequently, the catchment is dealt with from here on in terms of cumulative highstand and lowstand sizes.

Outlines of catchments feeding the area studied in this chapter (Figure 6.23) show that the combined area of the highstand catchments is approximately 20,000 km² smaller than combined lowstand catchments (~ 47,000 km² vs. ~ 67,000km² respectively). It is noteworthy, however, that approximately 28,000 km² of this additional lowstand catchment size is attributable to subaerial exposure of low gradient shelf areas which are not expected to contribute large amounts of sediment to the sink when compared to more mountainous sources.

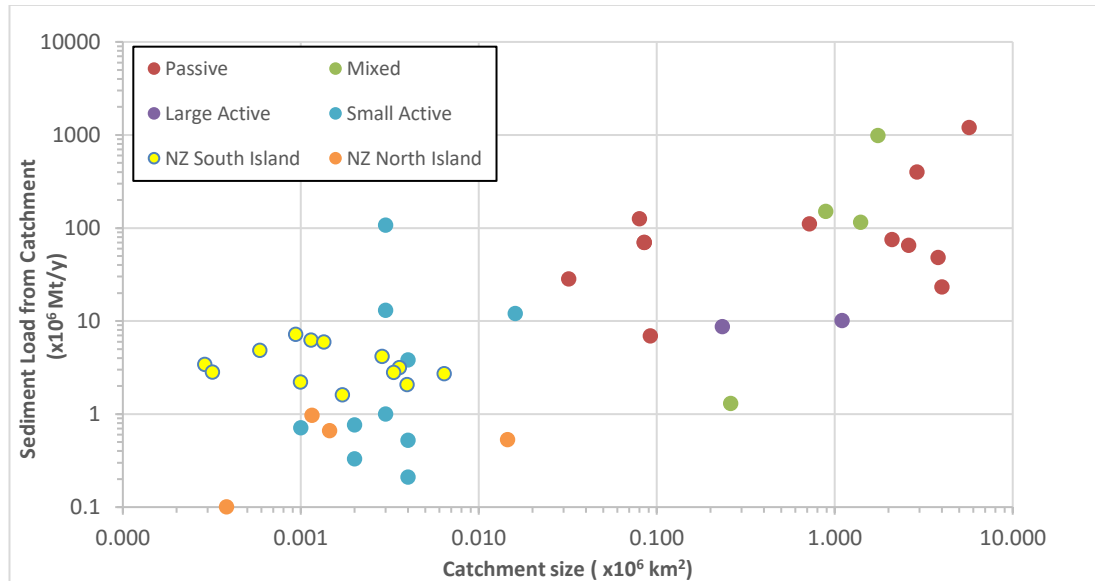


Figure 6.21 Catchment size vs Sediment Load.

Relationship between catchment size and sediment load from catchment for different margin types around the world. Data a combination of a global database synthesised by Somme et al. (2009) with additional datapoints for the New Zealand Margin from Hicks et al. (2011).

When comparing the “productivity” of highstand vs lowstand catchments (Figure 6.24), it is apparent that although South Island highstand catchments are cumulatively smaller in size, they deliver a much higher sediment supply to the marine environment. This is due to a combination of the fissile nature of Alpine Schist lithologies, steep terrain, high rainfall and tectonic activity (Hicks et al., 2011; Hicks and Shankar, 2003).

During lowstands, much of the upland regions of Northern South Island were glaciated (Shulmeister, 2017; Shulmeister et al., 2019, 2001), this would likely have increased the amount of sediment input from the North Westland region to the marine environment when compared with highstand sediment yields from non-glaciated terrains discussed above.

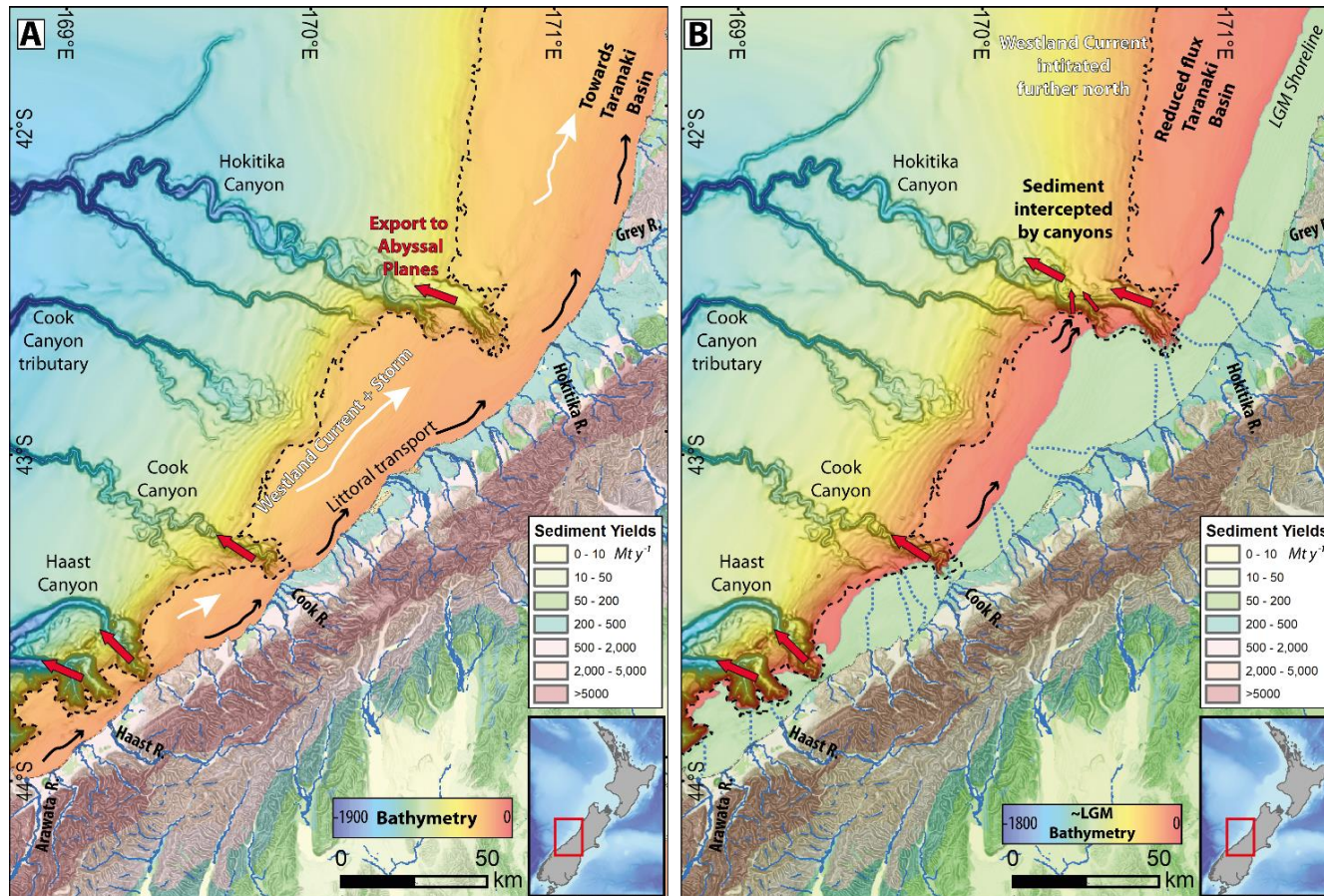


Figure 6.22 South Island sediment yield and drainage.

A) Present day (highstand) bathymetry and specific sediment yields from South Westland rivers, annotated sediment pathways. B) Approximate LGM bathymetry (~ -120m contour from present day) with annotated sediment pathways. Canyon heads linked back to their fluvial sources, exporting sediment to abyssal plains. The Westland Current had no effect on the area as it initiates further north. Compiled with data from Hayward et al. (2012), Hicks et al. (2011) and Radford (2012). Bathymetry sourced from the NZPAM petroleum exploration dataset

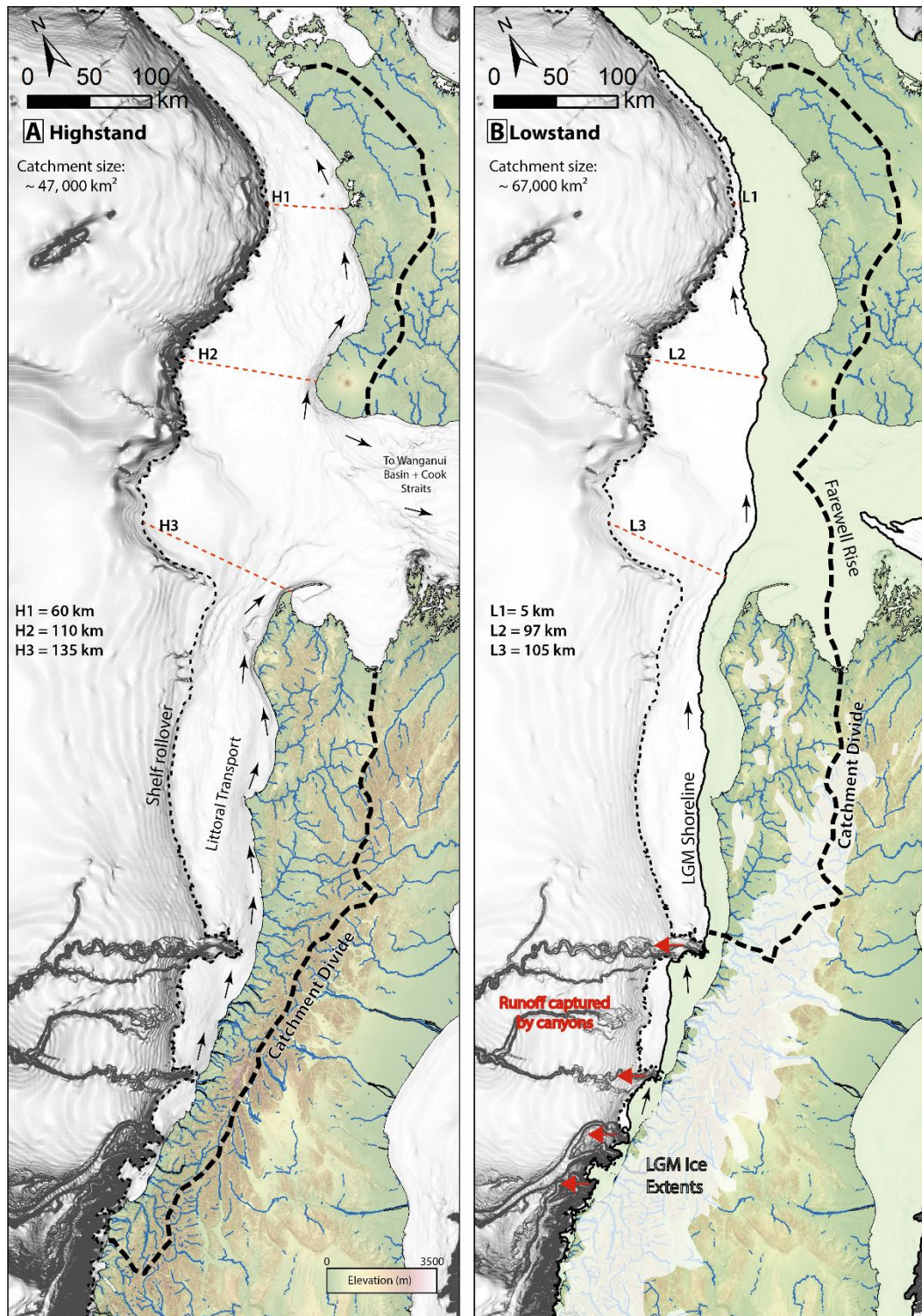


Figure 6.23 Highstand vs. Lowstand landmass.

A) Highstand showing combined input from west coast of North and South Islands and sediment transport toward the north and B) Lowstand Catchments with Ice extents (Shulmeister et al., 2019) showing a reduced South Island Catchment size as rivers connect to canyons, but increased catchment size from the exposed Farewell Rise and Taranaki Shelf. Profiles H1-3 & L1-3 represent shelf widths in highstand and lowstand respectively.

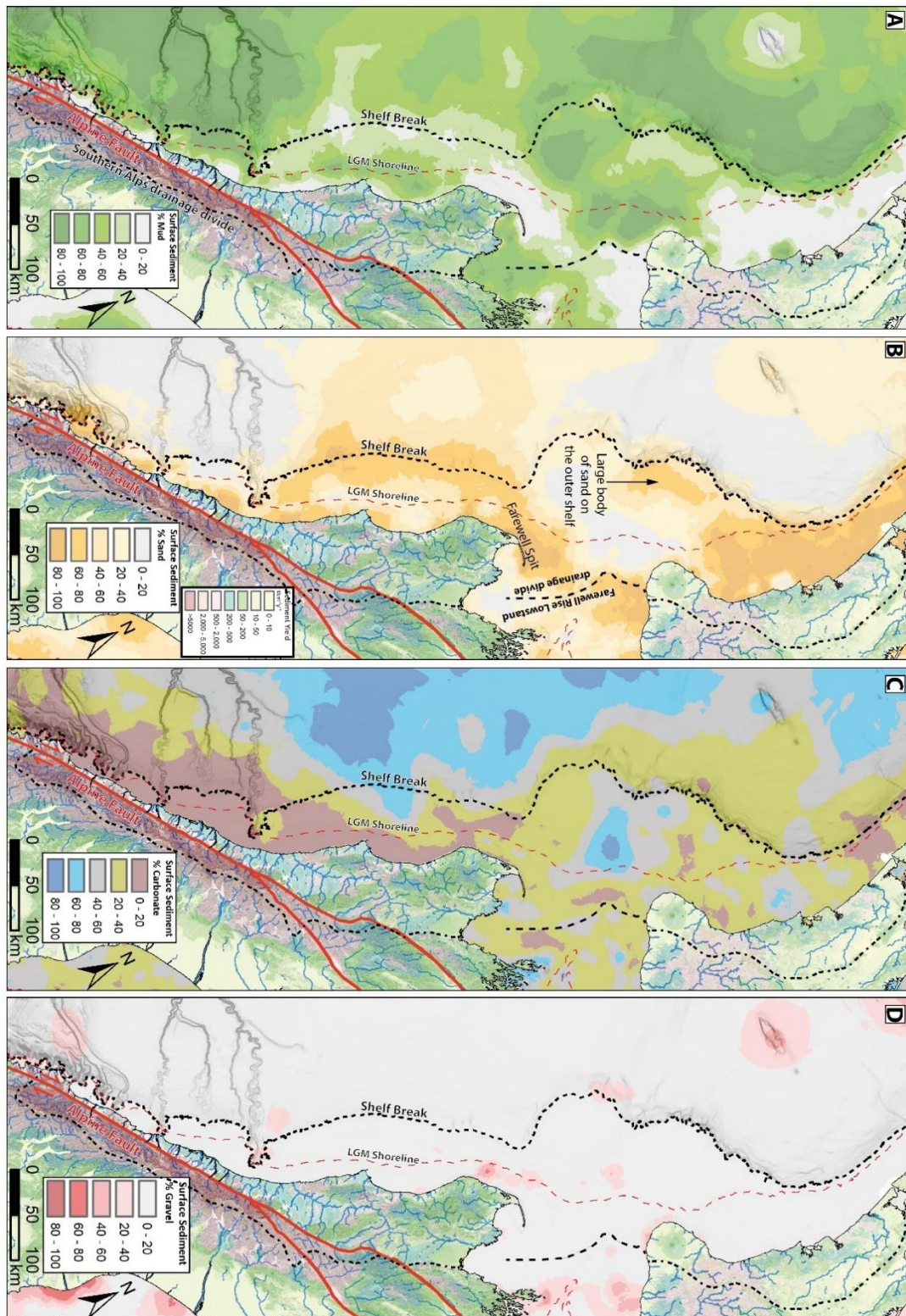


Figure 6.24 Sediment yields and surficial sediments.

Specific yield of river suspended sediment to New Zealand's West coast displayed alongside mapped seabed surficial sediment types. A) % Mud, B) % Sand C) % Carbonate and D) % Gravel. Compiled with data from Hicks et al. (2011) and (Bostock et al., 2018b, 2018a).

6.7 Sediment Conveyor to the Taranaki Basin

Once in the marine environment, net sediment transport along New Zealand's west coast is to the north via a combination of the Westland Current and littoral drift (Payne et al., 2010; Schofield, 1975). The system is at its highest efficiency during south-westerly storm conditions (Carter and Eade, 1980; Carter and Heath, 1975; Chiswell et al., 2015; Radford, 2012).

Zooming out to the scale of the SW Pacific, the Westland current is an offshoot of the Sub Tropical Front (STF), a zone delineated by large gradients in Sea Surface Temperature (SST) and salinity (Chiswell et al., 2015; Hamilton, 2006). Present day, the Sub Tropical Front crosses the Tasman Sea and meets the New Zealand land mass at approximately 43° South. From here it bifurcates into two separate flows; the north flowing Westland Current and the Southland Current; a bathymetrically locked current flowing around the southern tip of New Zealand and up its east coast (Brodie, 1960; Butler et al., 1992).

Through examining a suite of planktonic foraminiferal census data from around the SW Pacific, Hayward et al. (2012, 2008) suggested that the STF migrated by 3-5° north during post Mid Pleistocene Transition glacials (Figure 6.25). This northward migration of the STF also pushed the initiation zone of the Westland Current north, effectively removing up to 300 km of coastal sediment input available to be transported towards the Taranaki Basin during post MPT lowstands (Figure 6.22). In combination with many South Island rivers linking directly to canyon heads (see above), lowstand sediment flux from South Island was significantly lower than highstand.

Additional insight can be gained into the dynamics and efficiency of the sediment conveyor by examining the seabed surficial sediment composition, in particular that of sand (Figure 6.24B). On the Western Stable Platform, a conspicuous body of sand is evident on the outer shelf at a present-day water depth of 125 – 200 m. When combined with interpretations of channels identified in 3D seismic data on the shelf (Figure 6.4), it seems likely that this sand body is a relict lowstand feature fed by runoff from the Farewell Rise, whilst a large body of sand evident along the west coast of North Island is related to a combination of runoff from North Island rivers and the actions of a north directed littoral drift system.

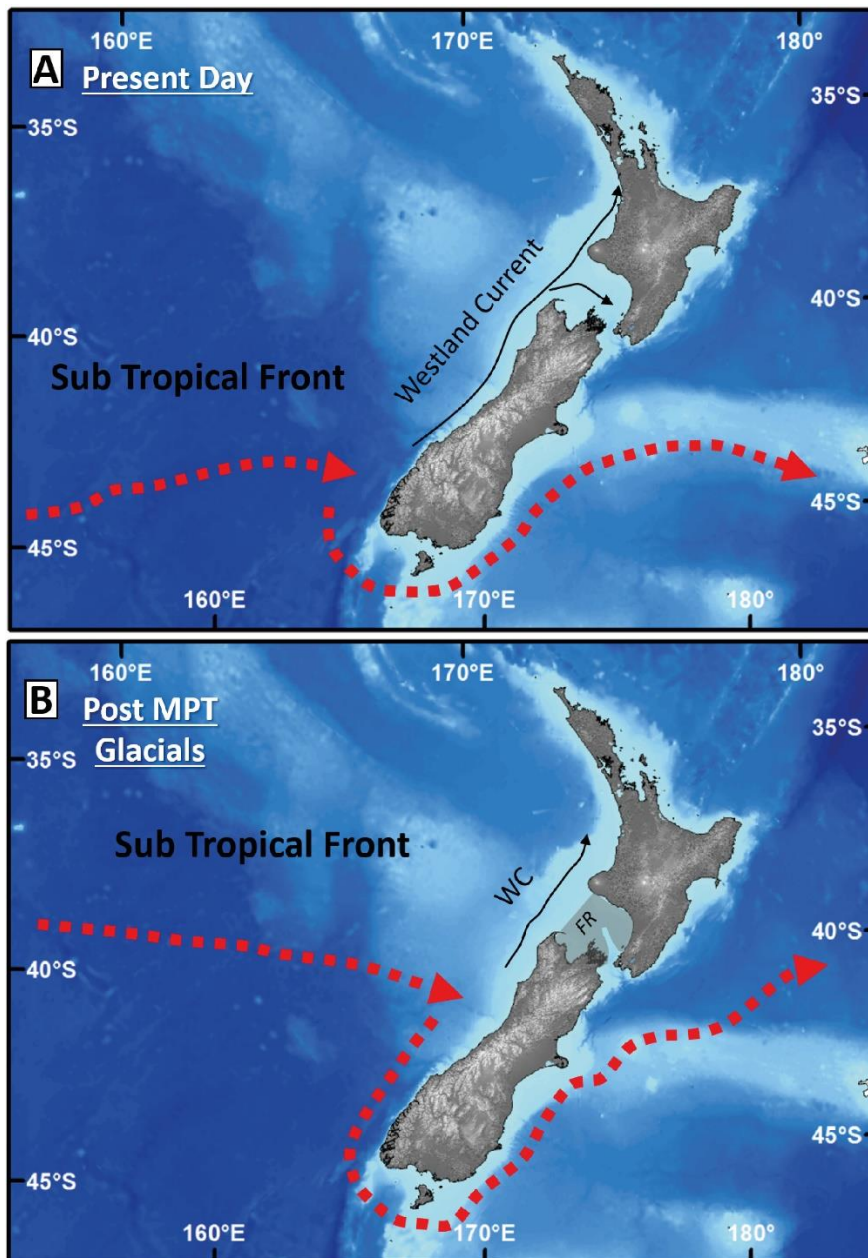


Figure 6.25 Sub Tropical Front variability.

Location of the Sub Tropical Front as it meets the New Zealand Landmass. A) The STF meets present day coastline at approximately 43°S, whilst in B), post Mid Pleistocene Transition Glacials, the STF meets the coastline between 39-40°S (after Hayward et al., 2012).

Along the west coast of South Island, several nearshore sand bodies are attributable to the north directed littoral transport system capturing runoff from South Island rivers. Additionally, these modern alongshore flows have formed the Farewell Spit by transporting fine sands to the northeast (Tribe and Kennedy, 2010). This pattern of sand distribution bares resemblance to highstand delta scale clinoforms identified in 3D seismic data (Figure 6.5).

Similar longshore transport has been documented on the east coast of Australia where longshore drift has transported sand over 1,500 km and formed Fraser Island (Roy and Thom, 1991), with onward bypass to the deepwater by interaction by a combination of estuarine ebb tidal flows and a change in margin orientation (Boyd et al., 2008). Additionally, significant volumes of sediment discharged from the Amazon river mouth is carried 1,100 km north by wind and waves, where it makes up 50% of the mud in the Orinoco delta (Warne et al., 2002).

Contrasting highstand and lowstand sediment pathways have also been documented in the Southern Californian borderlands (Covault et al., 2011, 2007; Covault and Fildani, 2014). In this system, highstand sediment discharged from several drainage basins is intercepted by the Oceanside littoral cell and carried south, where it is intercepted by the La Jolla Canyon and bypassed to the deepwater San Diego Trough and ultimately deposited in the La Jolla Fan (Covault et al., 2007). At sea level lowstands however, these rivers connected directly to canyon heads and diverted sediment directly to the deepwater, resulting in no lowstand growth in the La Jolla Fan (Figure 6.26).

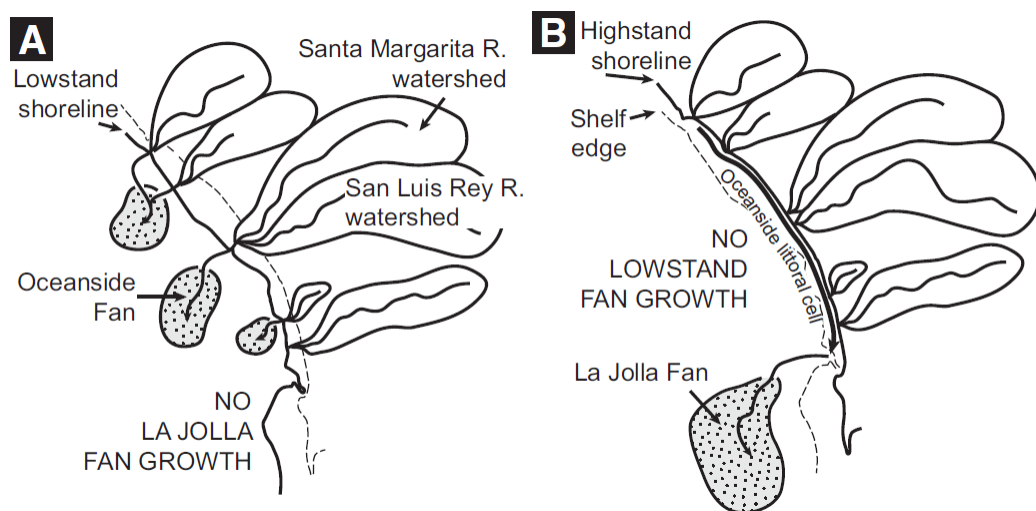


Figure 6.26 *Sediment routing from land to the deep sea in the Californian Borderlands.*

A) Sea level lowstand showing rivers connecting directly to canyons and B) sea level highstand where sediment is transported by the Oceanside littoral cell to the La Jolla Canyon, feeding highstand growth of the La Jolla Fan (from Covault et al., 2011).

6.8 Synthesis

Integrating observations from previous sections, schematic maps showing the factors affecting sediment delivery to depocentres in the Taranaki Basin were created for highstand and lowstand times (Figure 6.27 and Figure 6.28 respectively). These maps

collate features observed in stratigraphy interpreted to be represent the last 3 glacial-interglacial cycles (MIS 9 to present; ~337 – 0 kyrs). Interglacials are presented by the modern-day bathymetry whilst glacials are presented on approximated LGM bathymetry (modern minus 120 m); differences in the exact shoreline and shelf edge locations are expected, however these maps are sufficient to show schematic drainage patterns. Key parameters are shown in Table 6.2.

Table 6.2 Highstand and Lowstand Comparisons of the Taranaki Basin

	Highstand	Lowstand
Catchment Size	47,000 km ²	67,000 km ²
Dominant Source	Southern Alps (South Island)	North Island + Farewell Rise + Northern South Island (no alps)
Shelf Width	60 – 135 km	5 – 105 km
Rollover Depth	150 - 170 m (ET = 250 – 300m)	30 – 50 m (ET= 130 – 180 m)

6.8.1 Highstand

Seismic data consistently show northward progradation of delta scale (20 – 45 m high) clinoforms across the shelf, with minor northeast trending components attributed to the d'Urville Current. Sediment is interpreted to be dominantly sourced from uplift and erosion of meta-sediments in the Southern Alps although small amounts may also be sourced from North Island rivers. South Island rivers deliver high volumes of sediment dominated by fissile clay rich muds derived from Alpine Schists. Once in the marine environment, sediment may be either transported to canyon heads and hence abyssal depths or to the north towards the Taranaki Basin via a combination of the Westland Current, littoral transport and storm events. Exactly how this volume is partitioned between South Island canyons and northward transport is unclear. Seismic data show no evidence for major sediment pathways from North Island across the shelf in highstands although surficial sediment maps show a large body of sand on the inner shelf immediately north of the seismic data studied in this chapter. Under present day highstand conditions there is no evidence of the delta scale clinoforms reaching the shelf edge to contribute sediment to the slope and basin floor. However, work in Chapter 5 has shown

that these delta scale clinoforms reached the shelf edge throughout the evolution of the Giant Foresets Formation.

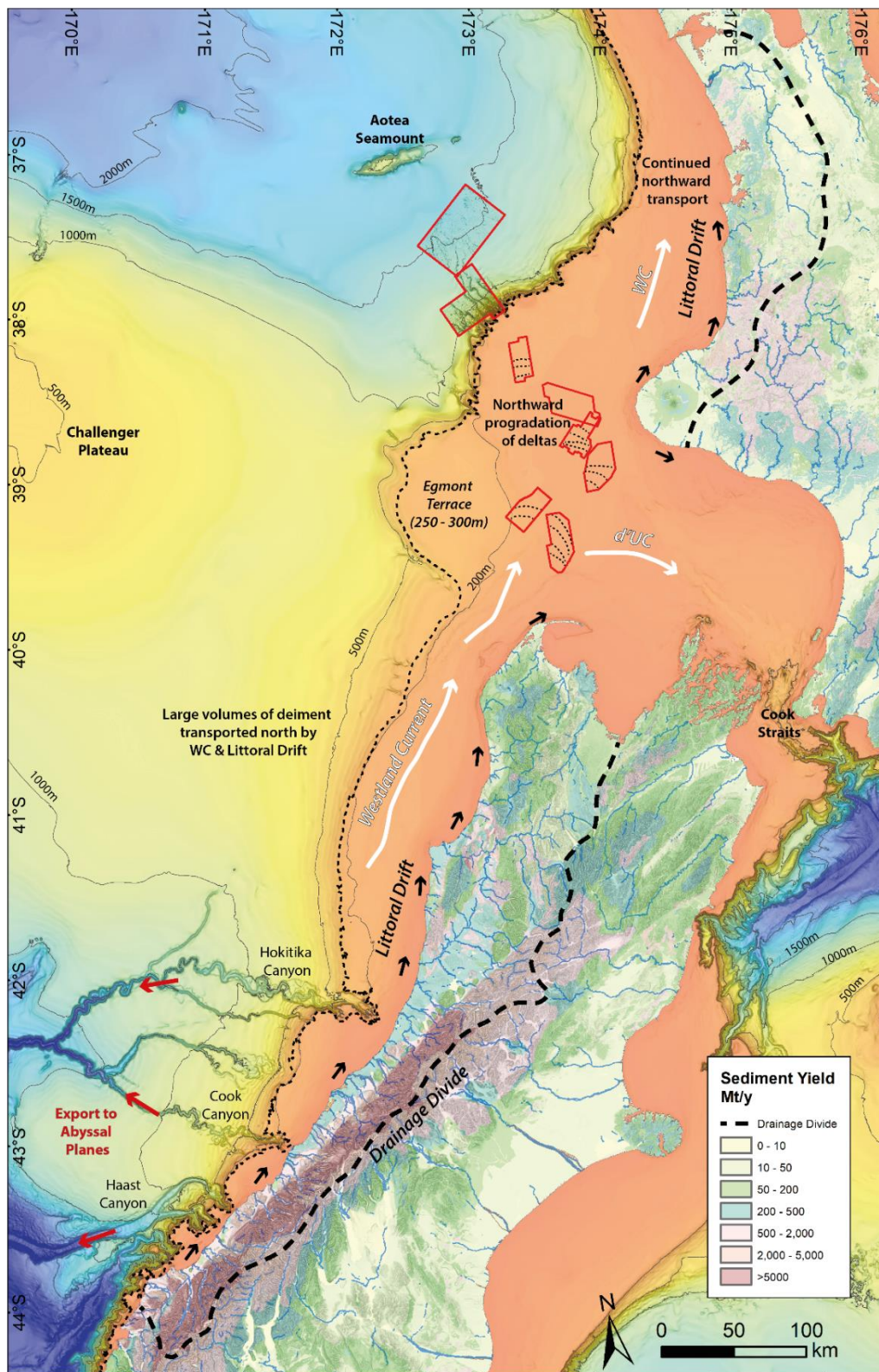


Figure 6.27 Highstand compilation

Compiled observations from this study integrated with data from Figure 6.22 to show regional sediment pathways in the Taranaki Basin in highstand/interglacials.

6.8.2 Lowstand

During the LGM, sea level was approximately 120 m lower than present day, exposing the Farewell Rise land bridge between New Zealand's North and South islands. Additionally, the narrow shelf in the South Westland region of South Island became subaerially exposed, linking submarine canyons directly to their fluvial source and exporting sediment directly to abyssal depths. Consequently, the volume of sediment available for delivery north toward the Taranaki Basin was significantly reduced during lowstands. A northward shift in the location of the STF, and consequently the Westland Current, is also reduced the volume of sediment transported north. It is envisaged, however, that the effects of decreased sediment volumes available for transport may have been partially offset by the Westland Current, littoral system and storms sweeping a shallower shelf, thereby increasing the transport efficiency. Any sediment arriving to the Taranaki Basin from the west coast of South Island was likely funnelled into the Egmont Terrace region, where they may be linked with lowstand slope fans with anomalously high seismic amplitudes discussed in Chapter 5.

Seismic data on the Farewell Rise and Western Stable Platform reveal a number of channels draining the subaerially exposed Farewell Rise, with possible links to North and South Islands. These channels drained onto the shallow shelf (<50 m) of the Western Stable Platform where modern day surficial sediment samples show a sand body approximately 85 x 25 km perched on the outer shelf; this is interpreted as a relict lowstand feature fed by channels draining the Farewell Rise and North Island. As in highstands, sediment on the shelf was swept by a north directed littoral drift system. During lowstands however, this would have been acting on a shallower bathymetry so is interpreted to have been more efficient. Sediment was captured by canyon heads spaced at 3 to 6 km along the margin of the WSP and subsequently transported to deepwater regions of the Taranaki Basin via a network of basin floor channels. Turbidity currents in these canyons and basin floor channels frequently overflowed their confining wall, resulting in a slope and basin floor with extensive sediment wave fields. Seismic data show that these channels were strongly influenced by seafloor topography related to underlying mass transport deposits, where channels locally infill topography before proceeding basinward. Present day, these channels deliver sediment to a body of sand evident in surficial sediment data in the vicinity of the Aotea Seamount, up to 160 km from the shelf edge.

On the Challenger Plateau, a possible plastered drift was mapped and is possibly a result of a mix of downslope and along slope processes as the Giant Foresets Formation encroached on the plateau. The presence of this drift suggests the action of a deep-water current sweeping the plateau from southeast to northwest. Such a current was likely focused through the broad saddle between South Island and the Challenger Plateau and is not observed in modern datasets, so may only be active during glacial periods.

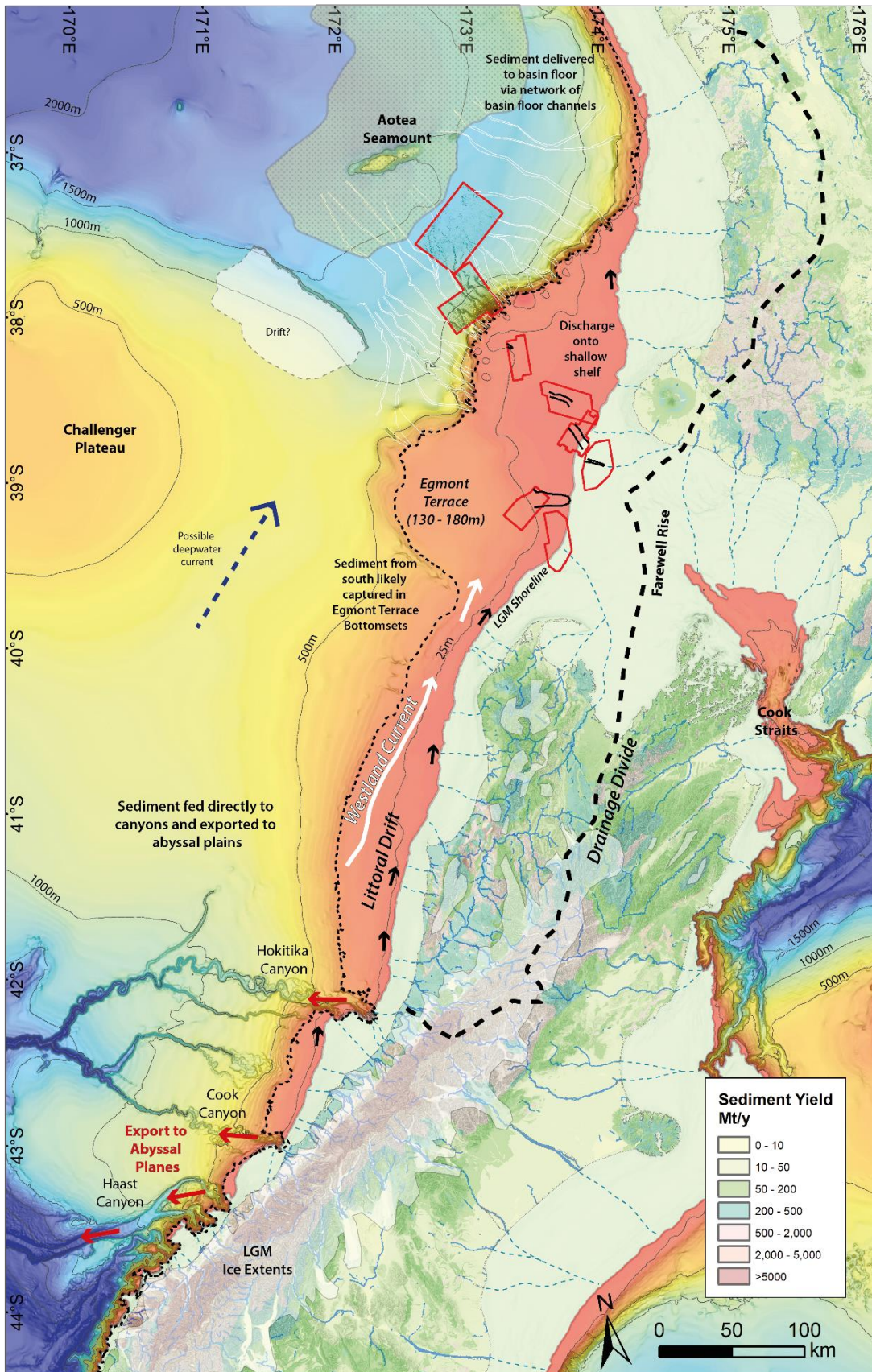


Figure 6.28 Lowstand compilation.

Compiled observations from this study integrated with data from Figure 6.22 to show regional sediment pathways in the Taranaki Basin in lowstands.

6.9 Conclusions

This chapter summarises the sediment sources and pathways in end member glacial and interglacial periods (highstand and lowstand systems tracts) of the latest Pleistocene with a source to sink approach. Comparisons are made with the present day highstand and with selected other examples worldwide. The main findings are summarised below:

- Highstand sediment transport along/across the shelf is consistently from southwest to northeast and is attributable to a combination of the Westland Current and littoral drift.
- Highstand sediment was dominantly sourced from runoff from the rapidly uplifting Southern Alps. No direct evidence was observed for significant contributions from North Island.
- In the available data, lowstand sediment transport across the shelf shows channels draining from southeast to northwest onto a shallow shelf less than 50 m deep and as close to 5 km from the shelf edge. These channels drain the Farewell Rise and possibly link to sources on North or South Island and delivered sand to the outer shelf.
- Sediment flux from South Island to the Taranaki Basin was likely lower during lowstands; the main South Westland rivers supplying sediment to the marine environment bypassed sediment to abyssal depths by canyons linking directly back to their source. This reduction in sediment from South Westland may have been partially offset by glaciated uplands in the North Westland region. Any sediment arriving from the south was likely diverted into the Egmont Terrace Region.
- In the Egmont Terrace and Challenger Plateau region, a possible moat and plastered drift may indicate the presence of a weak bottom current passing through the saddle between the Challenger Plateau and Egmont Terrace. No water mass is apparent in the sparse oceanographic data for this region, so this is inferred to be a lowstand feature.
- The Western Stable Platform is drained by canyon systems spaced at 3 – 6 km along the margin. These canyons pass to a network of sinuous channels which locally healed irregular seafloor topography from earlier MTDs. These channels have delivered sand to the region of the Aotea Seamount up to 160 km from the shelf edge. Canyons

and channels are inferred to now be inactive as there is no evidence of sediment transport at the modern shelf edge.

Chapter 7

Conclusions

7.1 Conclusions

The principal aim of this thesis is to unravel the controls on the evolution of the Giant Foresets Formation including tectonics, climate, eustasy, hinterland geology and sediment routing processes. The overarching objective was to establish a stratigraphic framework within which the Giant Foresets Formation (GFF) can be examined in a regional and global context. This chapter collates and summarises results from chapters 4, 5 and 6 in the context of objectives set out in Chapter 1 and discusses the relevance of this thesis to the study and understanding of other progradational shelf margin settings.

1. *To identify major changes in the stratigraphic architecture of the GFF and map these across the basin.*

Nine seismic sequences, bounded by regionally extensive sequence boundaries, were identified and mapped along approximately 200 km of the basin margin (Chapter 4). These seismic sequences document in detail, for the first time, the progradation of the GFF across the Western Stable Platform through the Pliocene to recent and reveal significant across strike variability through the succession; this is marked by contrasting progradation rates, clinoform heights and seismic facies.

Average progradation rates for the succession range from 16 to 22 m/kyr, with shorter term rates up to 77 m/kyr calculated in the south of the WSP from approximately 0.6 Ma to present. Based on clinoform heights (525 m to 1328 m), the GFF can be classified as continental margin scale clinoforms (*sensu* Patruno and Helland-Hansen, 2018), but also retain many of the characteristics of shelf edge clinoforms, such as progradation rate and rollover depth. Across strike variability in the succession is attributed to the effects of tectonic processes in the hinterland altering sediment pathways to focus supply on different parts of the WSP.

A more detailed sequence stratigraphic study identified and mapped 14 depositional sequences in the southern WSP. These are tentatively correlated to late Pleistocene eustatic sea level fluctuations of approximately 100 ky in the (Chapter 5). From this it is inferred that whilst tectonics played a key role in the focusing of sediment supply to the

basin, eustatic sea level was the dominant control on the depositional sequences in the southern Taranaki Basin during the Late Pleistocene.

This interpretation contrasts with interpretations by Hansen and Kamp (2002), who suggested a 400 ky eustatic signal is evident in a higher accommodation setting, 200 km further north in the basin (Figure 7.1). Salazar et al. (2016) also interpreted a eustatic component in their study of the Northern Graben, an active back arc rift within the basin. This is linked with the longer-term trend of an overall decrease in eustatic sea level since ~ 2.4 Ma (their SU3), rather than direct correlation of depositional sequences to eustatic cycles. Their work also identified an increase in sediment supply to the Northern Graben at from ~ 3 Ma, which they correlate to a broadly contemporaneous increase in uplift rates in the Southern Alps identified by Tippett and Kamp (1995). This may also be related to increased contraction and inversion along Cretaceous faults in the southern Taranaki Basin from ~ 3.7 Ma identified by Reilly et al. (2015). As shown in this thesis, such events are capable of altering sediment routing and influencing lateral variability in the progradation of the GFF.

2. *To date major architectural changes using existing biostratigraphy and, where lacking, investigate other methods of improving age control.*

Key events in the progradation of the GFF are marked by changes in clinoform architectures and stacking patterns along the basin margin (Chapters 4 and 5). Existing biostratigraphic census data (Morgans, 2006; Strong and Wilson, 2002) were compiled from limited well penetrations across the basin to identify bioevents of Raine et al. (2015) and Crundwell et al. (2004). Due to sampling density in wells, lack of age diagnostic fauna and sparse penetrations through the GFF, biostratigraphy alone was insufficient to bracket the progradations mapped in Chapters 4 and 5.

To address this, data from a published GNS study (Thrasher et al., 2018), an ongoing resampling study at GNS (Crundwell, pers. comm), shallow geotechnical boreholes (Nodder, 1995, 1994, 1993) and sequence stratigraphic correlations in Chapter 5 of this thesis are integrated to provide a workable age framework for the basin (Figure 7.2). The age model developed in this thesis evolved iteratively between Chapters 4 and 5, with observations in each chapter informing and complementing the other. This study particularly adds age constraint to the late Pleistocene succession in the southern region of the WSP.

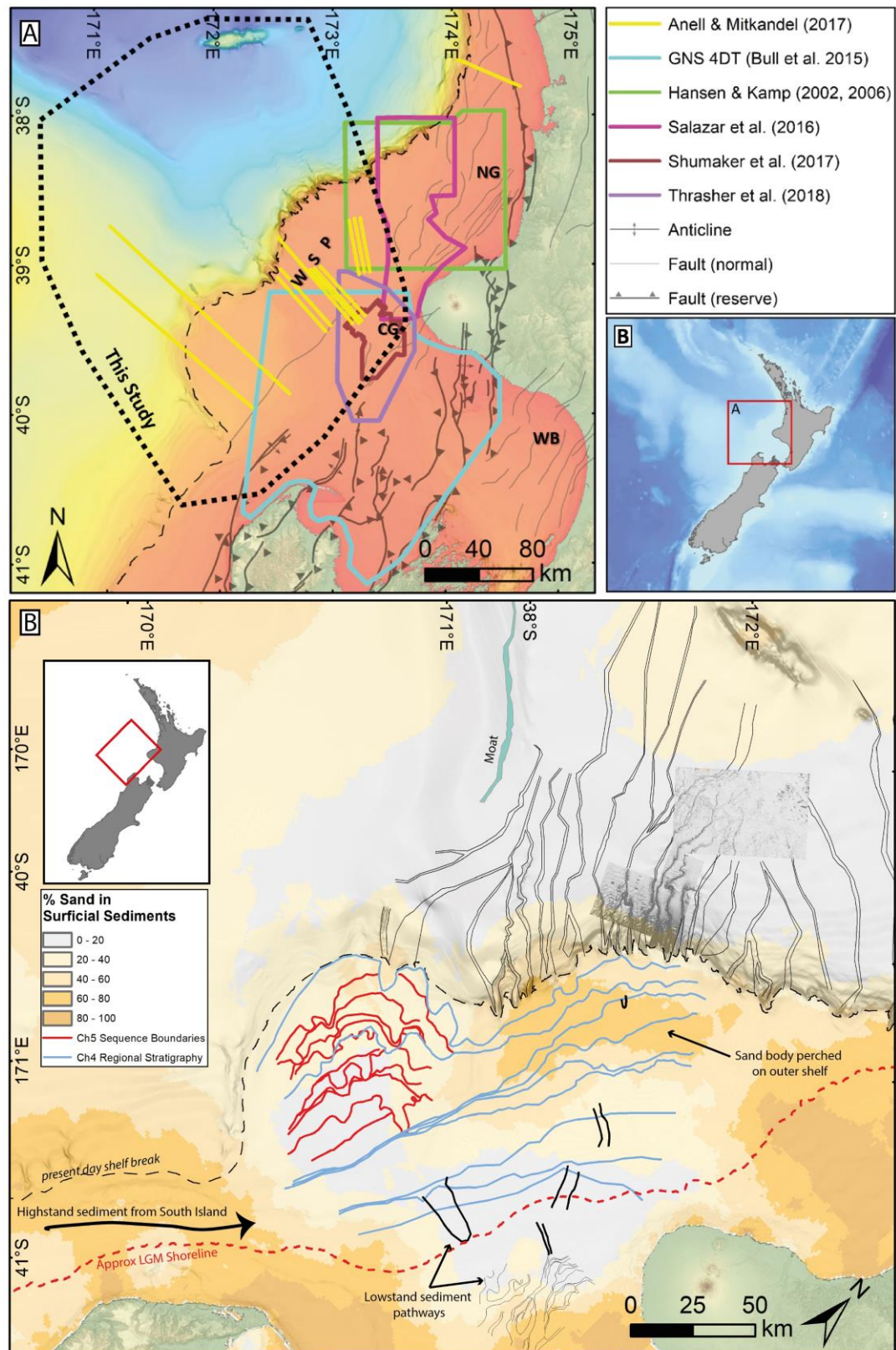


Figure 7.1 Overview of previous studies undertaken in this thesis.

A) Geographic area mapped by this study compared with previous studies in the Taranaki Basin and B) synthesis map showing regional seismic sequence boundaries (Ch4), depositional sequence boundaries (Ch5) and sediment pathways (Ch6) on a base map of % sand in surficial seabed samples. NG – Northern Graben, CG – Central Graben, WB – Wanganui Basin and WSP – Western Stable Platform.

Chapter 5 correlates mapped sequence boundaries to drops in global eustatic sea level established by Lisiecki and Raymo (2005) and Miller et al. (2011). Counting back sequences from the present-day seabed, the observed scale and cyclicity in the depositional record appears to follow that of major eustatic fluctuations. Using this correlation, each depositional sequence is dated with some degree of confidence back to approximately 0.9 Ma, and more tentatively to ~1.2 Ma. This tentative period corresponds to the Mid Pleistocene Transition with the more certain ages relating to the establishment of low frequency, high magnitude global eustatic fluctuations.

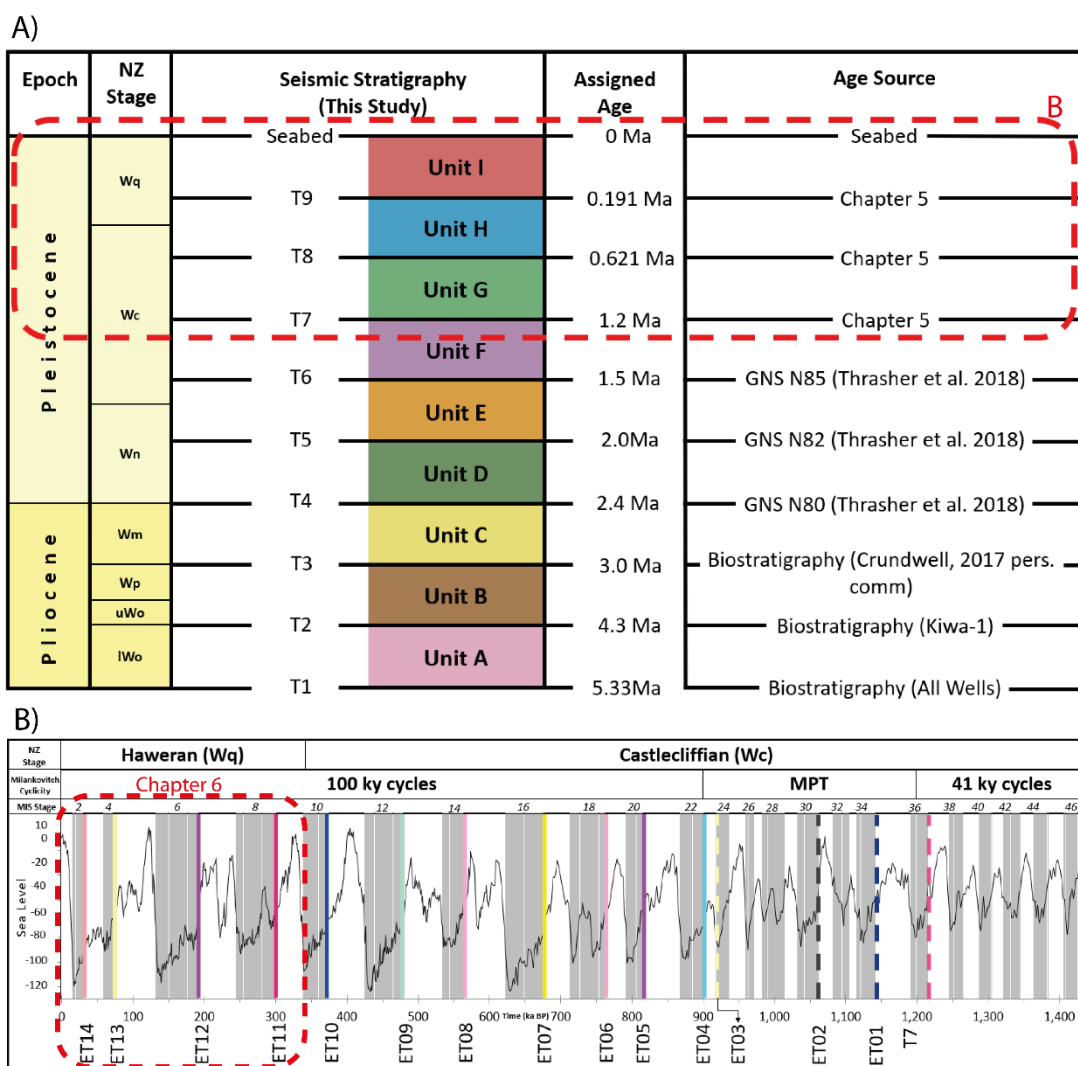


Figure 7.2 Stratigraphic Framework Stratigraphy of the Giant Foresets Formation.

A) Seismic stratigraphy established in Chapter 4 with the subset of stratigraphy studied in Chapter 5 highlighted by a red dashed box. B) Correlation of sequence boundaries from Chapter 5 to the eustatic curve of Miller et al. (2011).

As the model is built from multiple sources, each with their own degree of error (e.g. sampling density in biostratigraphy or matching eustatic cycles to observed events), the ages suggested should be considered best guess approximations rather than exact ages.

With regards to the correlation of sequence boundaries to eustatic events in Chapter 5; deposits in the neighbouring Wanganui Basin exhibit a eustatic signal in a stratigraphically correlative succession of 47 unconformity bound shallow marine sequences (Carter and Naish, 1998; Saul et al., 1999), the same signal may not be evident in the GFF and we may have incorrectly correlated events in the stratigraphy to eustatic events (e.g. Miall, 1992).

Any errors and inaccuracies in the age model will propagate into aggradation and progradation rate calculations of individual units mapped in Chapter 4, however, to avoid propagation of errors associated with this, average progradation rates for the entire succession are used in discussions.

3. *To search for and document pathways taken by sediment to the basin in glacial (lowstand) vs. interglacial (highstand) periods.*

The GFF is reported to be dominantly sourced from uplift and erosion of New Zealand's South Island (Beggs, 1990; Kamp et al., 2004; Payne et al., 2010), however no work has been undertaken to document sediment pathways and establish source to sink factors affecting sediment delivery to the basin. In the south of the basin, Chapter 5 identified lowstand slope deposits characterised by anomalously high seismic amplitudes when compared with low amplitude highstand reflectors; it is speculated that these contrasting seismic facies may indicate different highstand and lowstand sediment provenances.

To investigate these points, seismic and regional bathymetric data were used to map pathways taken by sediment across the shelf, down the slope and across the basin floor in the latest Pleistocene (Chapter 6).

During highstands, shelf sedimentation was focussed in the north and northeast of the study area via progradation of delta scale clinoforms. Sediment transport was driven by a combination of the north directed Westland Current and a littoral drift cell. This is consistent with sediment provenance studies of Payne et al. (2010), who tentatively correlated mineralogy of shelf sediments in the neighbouring Northland Basin to South Island sources. This suggests the littoral drift cell was capable of transporting sediment up to 1,000 km from South Island sources along the basin margin.

During lowstands, sediment flux from South Island to the basin was lower than during highstands, as the main rivers supplying sediment to the marine environment connected directly to canyon heads and exported sediment to abyssal depth offshore South Island. During lowstands, however, a large area of shelf became subaerially exposed and was drained by channels to the west and northwest; these channels discharged sediment onto a shallow shelf of less than 50 m deep where they were likely subject to wave reworking by prevailing south westerly swells and an littoral drift cell. Mapping of these channels, along with seabed sediment samples from Bostock et al. (2018) suggests that North Island and the Farewell Rise contributed sand to the outer shelf during lowstands. This was transported to deepwater regions of the basin by slope canyons spaced at 3 to 6 km along the WSP. These canyons and basin floor channels transported sediment up to 160 km from the shelf rollover and infilled irregular basin floor topography associated with earlier MTDs. Measurements of sediment waves on the slope and basin floor are consistent with parameters for fine-grained waves formed by turbidity currents (Chapters 4 & 6) and when imaged in 3D data, crests are aligned parallel to the shelf edge, suggesting downslope processes dominate. Any sediment arriving from South Island sources was likely diverted into the Egmont Terrace region during lowstands.

Additional climatic and oceanographic controls may also have influenced sedimentation in the basin with the efficiency of north directed sediment pathways inferred to have been linked with glacial – interglacial variations in the Sub Tropical Front (STF). The presence of a possible moat and plastered drift on the Challenger Plateau (Chapter 6) may indicate the presence of a north directed bottom current passing through the saddle between the Challenger Plateau and Egmont Terrace. This is further supported by observed northward migration of slope canyons along the WSP (Chapter 4) but is inconsistent with sediment wave crest orientations, suggesting that downslope rather than along slope processes were dominant. This may indicate that the Westland Current affected the slope stratigraphy below the shelf rollover or that an unidentified bottom current swept the margin. As no bottom currents have been identified in the literature or sparse present-day oceanographic dataset for the basin, the deposits identified in this study may have resulted from an ocean current in the lowstand water column.

To summarise, the main contributions this thesis has made are:

- Identification and mapping of nine regionally extensive seismic sequences along 200 km of the basin margin. Across strike variation as the margin prograded is

attributed to hinterland tectonics altering sediment supply pathways. Continuous mapping along the central and southern WSP was largely inexistent before this PhD (Figure 7.1).

- A more detailed sequence stratigraphic study in the southern WSP correlated depositional sequences to global eustatic fluctuations of approximately 100 ky duration, suggesting that eustatic sea level was the dominant control in generating depositional sequences in the southern Taranaki Basin during the Late Pleistocene.
- An age framework, integrating mapped seismic horizons with limited age information from biostratigraphy, shallow boreholes and sequence stratigraphic correlations is proposed; this requires further validation and biostratigraphic sampling.
- A possible bottom current flowing from south to north is suggested by canyon migration and a plastered moat and drift.

Sediment pathways were identified and mapped across the basin for the latest Pleistocene, showing for the first-time contrasting provenances of highstand supply from South Island and lowstand sediments from North Island and the Farewell Rise.

7.2 General Implications

Clinofolds occur on many scales and settings in basins around the world, and have been the subject of many investigations to classify them based on parameters such as structural setting, foreset height, rollover depths and progradation rate. The results of this thesis demonstrate that such classifications are not exhaustive, as characteristics of the GFF span the criteria of two separate scales in two schemes (Carvajal et al., 2009; Patruno and Helland-Hansen, 2018).

Basin margin evolution and lithology prediction have long been investigated on 2D dip oriented profiles (e.g. Covault et al., 2009; Helland-Hansen and Hampson, 2009; Houseknecht et al., 2009; Mountain and Proust, 2010), but has been shown by many authors to be a complex three dimensional problem, demonstrating major along-margin variations in process regime, subsidence, physiography and discharge rates (e.g. Jones et al., 2015; Madof et al., 2016; Poyatos-Moré et al., 2019). This has implications for understanding the nature of coarse sediment distribution along basin margins through

time and space, with applications to hydrocarbon exploration and Carbon capture/storage. This thesis provides a further case study on the importance of utilising regionally extensive datasets to reveal lateral variations not apparent on single 2D dip sections.

In a similar vein, utilising a regionally extensive dataset also revealed contrasting highstand and lowstand provenances associated with eustatic alteration of the margin physiography, affecting factors such as the nature and volume of sediment delivered to the basin. This highlights the value of understanding spatial and temporal variations in sediment routing systems and examining the basin in a source to sink context highlights that highstand and lowstand sediment flux to a basin can vary greatly.

Don't assume that sediment flux is the same in highstand and lowstand

Additionally, it is shown in this study that interpretation of sedimentary deposits along a basin margin may provide clues to glacial-interglacial variability in palaeoceanography and aid in paleoclimate studies.

7.3 Recommendations for Future Research

7.3.1 Refinement of Age Model

As summarised above, the resolution and reliability of the age model is a key limitation to work in this thesis. Future research should increase the density of sampling from the existing borehole catalogue; sample locations should be targeted and informed by seismic and sequence stratigraphic interpretations in order to maximise the value of results. This thesis provides a high-resolution framework in which to target future sampling.

7.3.2 Sediment Provenance Studies

To test and extend the results from Chapter 6, sediment provenance work should be carried out to determine the distribution patterns of present-day surficial sediment samples compiled in Bostock et al. (2018a, 2018b). Similar work carried out by Payne et al. (2010) further northwest of the Taranaki Basin, confirmed that a large volume of the sediment was likely from South Island sources. Additional analysis of sediment pathways in older Pliocene stratigraphy would also be beneficial, however much of the near shore and shelf stratigraphy has been removed by uplift and erosion on the Farewell Rise.

7.3.3 Embargoed Seismic Data

Additional 3D seismic data on the Egmont Terrace and in the vicinity of the Hector and Pipeline 3D surveys (Chapter 6) were acquired by PGS in 2017 but were unavailable to this project. Studies of these surveys would have contributed significantly to the outcomes of chapters 5 and 6. Further north, Schlumberger have also recently acquired a 3D multi-client survey covering large parts of the Western Stable Platform.

AVO data for the DTB 08 survey, covering the gas charged slope fans (Chapter 5) is also still under embargo. Access to these data would provide enhanced understanding of the anomalies. In the deep-water Taranaki and Aotea Basins, TGS have also acquired regional 2D seismic covering much of the northeast flanks of the Challenger Plateau. Investigation of this survey would enhance interpretations of the drift deposit straddling the Challenger Plateau.

7.3.4 IODP drilling

Many of the factors this thesis highlights as affecting the evolution of the Giant Foresets Formation contain an element of uncertainty due to sparse hard rock data. These could be addressed when the JOIDES Resolution is due to return to the SW Pacific in 2023. Some aims that such a drilling campaign would address are:

- Improved age constraints to accurately understand global vs regional processes.
- Better constrain the effects of glaciations on sediment supply and ocean currents.
- The retro-arc foreland (plus localised back arc) basin fill in the Taranaki Basin records the evolution of the Hikurangi subduction zone from its inception to present. Targeted drilling of the succession could further complement ongoing IODP projects along the Hikurangi Margin.

Blank Page

Bibliography

- Abbott, S., Carter, R.M., 1994. The sequence architecture of mid-Pleistocene (0.35–0.95 Ma) cyclothems from New Zealand: facies development during a period of known orbital control on sea-level cyclicity, in: de Boer, P.L., Smith, D.G. (Eds.), *Orbital Forcing and Cyclic Sequences Special Publication*. International Association of Sedimentologists, pp. 367–394.
- Abbott, S.T., Naish, T.R., Carter, R.M., Pillans, B.J., 2005. Sequence stratigraphy of the Nukumaruan Stratotype (Pliocene-Pleistocene, c. 2.08–1.63 Ma), Wanganui Basin, New Zealand. *J. R. Soc. New Zeal.* 35, 123–150. <https://doi.org/10.1080/03014223.2005.9517779>
- Adams, E.W., Schlager, W., 2000. Basic Types of Submarine Slope Curvature. *J. Sediment. Res.* 70, 814–828. <https://doi.org/10.1306/2DC4093A-0E47-11D7-8643000102C1865D>
- Ainsworth, R.B., Vakarelov, B.K., MacEachern, J.A., Rarity, F., Lane, T.I., Nanson, R.A., 2017. Anatomy of A Shoreline Regression: Implications For the High-Resolution Stratigraphic Architecture of Deltas. *J. Sediment. Res.* 87, 425–459. <https://doi.org/10.2110/jsr.2017.26>
- Alloway, B. V., Lowe, D.J., Barrell, D.J.A., Newnham, R.M., Almond, P.C., Augustinus, P.C., Bertler, N.A.N., Carter, L., Litchfield, N.J., McGlone, M.S., Shulmeister, J., Vandergoes, M.J., Williams, P.W., 2007. Towards a climate event stratigraphy for New Zealand over the past 30 000 years (NZ-INTIMATE project). *J. Quat. Sci.* 22, 9–35. <https://doi.org/10.1002/jqs.1079>
- Amorosi, A., Milli, S., 2001. Late Quaternary depositional architecture of Po and Tevere river deltas (Italy) and worldwide comparison with coeval deltaic successions. *Sediment. Geol.* 144, 357–375. [https://doi.org/10.1016/S0037-0738\(01\)00129-4](https://doi.org/10.1016/S0037-0738(01)00129-4)
- Anell, I., Midtkandal, I., 2017. The quantifiable clinothem - types, shapes and geometric relationships in the Plio-Pleistocene Giant Foresets Formation, Taranaki Basin, New Zealand. *Basin Res.* 29, 277–297. <https://doi.org/10.1111/bre.12149>
- Anell, I., Midtkandal, I., Braathen, A., 2014. Trajectory analysis and inferences on geometric relationships of an Early Triassic prograding clinoform succession on the northern Barents Shelf. *Mar. Pet. Geol.* 54, 167–179. <https://doi.org/10.1016/j.marpetgeo.2014.03.005>
- Anthonissen, D.E., Ogg, J.G., 2012. Appendix 3 - Cenozoic and Cretaceous Biochronology of Planktonic Foraminifera and Calcareous Nannofossils, The Geologic Time Scale. Elsevier. <https://doi.org/http://dx.doi.org/10.1016/B978-0-444-59425-9.15003-6>
- Armitage, D.A., McHargue, T., Fildani, A., Graham, S.A., 2012. Postavulsion channel evolution: Niger Delta continental slope. *Am. Assoc. Pet. Geol. Bull.* 96, 823–843. <https://doi.org/10.1306/09131110189>
- ARTHUR, S., Blake, G., 2003. Sequence Straigraphy and Syndepositional Tectonics of Upper Miocene and Pliocene Deltaic Sediments, Offshore Brunei Darussalam, in: *Tropical Deltas of Southeast Asia*. SEPM (Society for Sedimentary Geology), pp. 219–234. <https://doi.org/10.2110/pec.03.76.0219>
- Austin, J.A., Uchupi, E.J., 1982. Continental-Oceanic Crustal Transition Off Southwest Africa. *Am. Assoc. Pet. Geol. Bull.* 66, 1328–1347.

- <https://doi.org/10.1306/03B5A79B-16D1-11D7-8645000102C1865D>
- Babonneau, N., Delacourt, C., Cancouët, R., Sisavath, E., Bachèlery, P., Mazuel, A., Jorry, S.J., Deschamps, A., Ammann, J., Villeneuve, N., 2013. Direct sediment transfer from land to deep-sea: Insights into shallow multibeam bathymetry at La Réunion Island. *Mar. Geol.* 346, 47–57. <https://doi.org/10.1016/j.margeo.2013.08.006>
- Bache, F., Sutherland, R., King, P.R., 2014. Use of ancient wave-ravinement surfaces to determine palaeogeography and vertical crustal movements around New Zealand. *New Zeal. J. Geol. Geophys.* 57, 459–467. <https://doi.org/10.1080/00288306.2014.975254>
- Ballance, P.F., 1976. Evolution of the Upper Cenozoic Magmatic Arc and plate boundary in northern New Zealand. *Earth Planet. Sci. Lett.* 28, 356–370. [https://doi.org/10.1016/0012-821X\(76\)90197-7](https://doi.org/10.1016/0012-821X(76)90197-7)
- Barrell, D.J.A.J.A., 2011. Quaternary Glaciers of New Zealand, 1st ed, Developments in Quaternary Science. Elsevier Inc. <https://doi.org/10.1016/B978-0-444-53447-7.00075-1>
- Batt, G.E., Batt, G.E., Braun, J., Braun, J., Kohn, B.P., Kohn, B.P., McDougall, I., McDougall, I., 2000. Thermochronological analysis of the dynamics of the Southern Alps, New Zealand. *Geol. Soc. Am. Bull.* 112, 250–266. [https://doi.org/10.1130/0016-7606\(2000\)112<250:TAOTDO>2.0.CO;2](https://doi.org/10.1130/0016-7606(2000)112<250:TAOTDO>2.0.CO;2)
- Baur, J., Sutherland, R., Stern, T., 2014. Anomalous passive subsidence of deep-water sedimentary basins: A prearc basin example, southern New Caledonia Trough and Taranaki Basin, New Zealand. *Basin Res.* 26, 242–268. <https://doi.org/10.1111/bre.12030>
- Baur, J.R., 2012. Regional seismic attribute analysis and tectonstratigraphy of offshore south-western Taranaki Basin, New Zealand. Victoria University of Wellington.
- Beggs, J.M., 1990. Seismic Stratigraphy of the Plio-Pleistocene Giant Foresets, Western Platform, Taranaki Basin., in: 1989 New Zealand Oil Exploration Conference.
- Bird, K.J., Molenaar, C.M., 1992. The North Slope Foreland Basin, Alaska, in: Macqueen, R.W., Leckie, D.A. (Eds.), *Foreland Basins and Fold Belts*. American Association of Petroleum Geologists.
- Bland, K.J., Bache, F., Davy, B.W., Hill, M.G., Sahoo, T.R., Strogon, D.P., Bull, S., 2014. New Zealand National Seismic Framework : Reinga- Bounty Trough , and Pegasus-East Coast- Raukumara basins. GNS Science Consultancy Report 2013/254. Lower Hutt.
- Bostock, H., Jenkins, C., Mackay, K., Carter, L., Nodder, S., Orpin, A., Pallentin, A., Wysoczanski, R., 2018a. Distribution of surficial sediments in the ocean around New Zealand/Aotearoa. Part B: continental shelf. *New Zeal. J. Geol. Geophys.* 1–22. <https://doi.org/10.1080/00288306.2018.1523199>
- Bostock, H., Jenkins, C., Mackay, K., Carter, L., Nodder, S., Orpin, A., Pallentin, A., Wysoczanski, R., 2018b. Distribution of surficial sediments in the ocean around New Zealand/Aotearoa. Part A: continental slope and deep ocean. *New Zeal. J. Geol. Geophys.* 1–23. <https://doi.org/10.1080/00288306.2018.1523198>
- Bourillet, J.-F.J.-F., Reynaud, J.-Y., Baltzer, A.A., Zaragosi, S.S., 2003. The “Fleuve Manche”: the submarine sedimentary features from the outer shelf to the deep-sea fans. *J. Quat. Sci.* 18, 261–282. <https://doi.org/10.1002/jqs.757>

- Bowen, D.Q., Phillips, F.M., McCabe, A.M., Knutz, P.C., Sykes, G.A., 2002. New data for the Last Glacial Maximum in Great Britain and Ireland. *Quat. Sci. Rev.* 21, 89–101. [https://doi.org/10.1016/S0277-3791\(01\)00102-0](https://doi.org/10.1016/S0277-3791(01)00102-0)
- Boyd, R., Ruming, K., Goodwin, I., Sandstrom, M., Schröder-Adams, C., 2008. Highstand transport of coastal sand to the deep ocean: A case study from Fraser Island, southeast Australia. *Geology* 36, 15–18. <https://doi.org/10.1130/G24211A.1>
- Brodie, J.W., 1960. Coastal Surface Currents Around New Zealand. *New Zeal. J. Geol. Geophys.* 3, 235–252. <https://doi.org/10.1080/00288306.1960.10423596>
- Brooks, H.L., Hodgson, D.M., Brunt, R.L., Peakall, J., Poyatos-Moré, M., Flint, S.S., 2018. Disconnected submarine lobes as a record of stepped slope evolution over multiple sea-level cycles. *Geosphere* 14, 1753–1779. <https://doi.org/10.1130/GES01618.1>
- Bull, S., Hill, M., Arnot, M., Seebeck, H., Kroeger, K.F., Zhu, H., Reilly, C., 2015. Time structure and isochron maps from the southern Taranaki Basin (4D Taranaki Project) GNS Science Data Series 12B. Lower Hutt.
- Bullimore, S., Henriksen, S., Liestøl, F.M., Helland-Hansen, W., 2005. Clinof orm stacking patterns, shelf-edge trajectories and facies associations in Tertiary coastal deltas, offshore Norway: Implications for the prediction of lithology in prograding systems. *Nor. J. Geol. / Nor. Geol. Foren.* 85, 169–187.
- Burgess, P.M., Hovius, N., 1998. Rates of delta progradation during highstands: consequences for timing of deposition in deep-marine systems. *J. Geol. Soc. London.* 155, 217–222. <https://doi.org/10.1144/gsjgs.155.2.0217>
- Butler, E.C. V., Butt, J.A., Lindstrom, E.J., Teldesley, P.C., Pickmere, S., Vincent, W.F., 1992. Oceanography of the Subtropical Convergence Zone around southern New Zealand. *New Zeal. J. Mar. Freshw. Res.* 26, 131–154. <https://doi.org/10.1080/00288330.1992.9516509>
- Cahill, M.L., Middleton, J.H., Stanton, B.R., 1991. Coastal-Trapped Waves on the West Coast of South Island, New Zealand. *J. Phys. Oceanogr.* 21, 541–557. [https://doi.org/10.1175/1520-0485\(1991\)021<0541:CTWOTW>2.0.CO;2](https://doi.org/10.1175/1520-0485(1991)021<0541:CTWOTW>2.0.CO;2)
- Carter, L., Eade, J., 1980. Hauraki coastal sediments chart (1: 200 000).
- Carter, L., Heath, R.A., 1975. Role of mean circulation, tides, and waves in the transport of bottom sediment on the New Zealand continental shelf. *New Zeal. J. Mar. Freshw. Res.* 9, 423–448. <https://doi.org/10.1080/00288330.1975.9515579>
- Carter, R.M., Naish, T.R., 1998. A review of Wanganui Basin, New Zealand: Global reference section for shallow marine, Plio-Pleistocene (2.5-0 Ma) cyclostratigraphy. *Sediment. Geol.* 122, 37–52. [https://doi.org/10.1016/S0037-0738\(98\)00097-9](https://doi.org/10.1016/S0037-0738(98)00097-9)
- Carvajal, C., Steel, R., 2009. Shelf-Edge Architecture and Bypass of Sand to Deep Water: Influence of Shelf-Edge Processes, Sea Level, and Sediment Supply. *J. Sediment. Res.* 79, 652–672. <https://doi.org/10.2110/jsr.2009.074>
- Carvajal, C., Steel, R., Petter, A., 2009. Sediment supply: The main driver of shelf-margin growth. *Earth-Science Rev.* 96, 221–248. <https://doi.org/10.1016/j.earscirev.2009.06.008>
- Carvajal, C.R., Steel, R.J., 2006. Thick turbidite successions from supply-dominated shelves during sea-level highstand. *Geology* 34, 665. <https://doi.org/10.1130/G22505.1>
- Cattaneo, A., Correggiari, A., Langone, L., Trincardi, F., 2003. The late-Holocene

- Gargano subaqueous delta, Adriatic shelf: Sediment pathways and supply fluctuations. *Mar. Geol.* 193, 61–91. [https://doi.org/10.1016/S0025-3227\(02\)00614-X](https://doi.org/10.1016/S0025-3227(02)00614-X)
- Cattaneo, A., Correggiari, A., Marsset, T., Thomas, Y., Marsset, B., Trincardi, F., 2004. Seafloor undulation pattern on the Adriatic shelf and comparison to deep-water sediment waves. *Mar. Geol.* 213, 121–148. <https://doi.org/10.1016/j.margeo.2004.10.004>
- Cattaneo, A., Steel, R.J., 2003. Transgressive deposits: A review of their variability. *Earth-Science Rev.* 62, 187–228. [https://doi.org/10.1016/S0012-8252\(02\)00134-4](https://doi.org/10.1016/S0012-8252(02)00134-4)
- Cattaneo, A., Trincardi, F., Asioli, A., Correggiari, A., 2007. The Western Adriatic shelf clinof orm: energy-limited bottomset. *Cont. Shelf Res.* 27, 506–525. <https://doi.org/10.1016/J.CSR.2006.11.013>
- Catuneanu, O., 2006. Principles of sequence stratigraphy. Elsevier.
- Catuneanu, O., Abreu, V., Bhattacharya, J.P.P., Blum, M.D.D., Dalrymple, R.W.W., Eriksson, P.G.G., Fielding, C.R.R., Fisher, W.L.L., Galloway, W.E.E., Gibling, M.R.R., Giles, K.A. a., Holbrook, J.M.M., Jordan, R., Kendall, C.G.S.C.G.S.C., Macurda, B., Martinsen, O.J.J., Miall, A.D.D., Neal, J.E.E., Nummedal, D., Pomar, L., Posamentier, H.W.W., Pratt, B.R.R., Sarg, J.F.F., Shanley, K.W.W., Steel, R.J.J., Strasser, a., Tucker, M.E.E., Winker, C., 2009. Towards the standardization of sequence stratigraphy. *Earth-Science Rev.* 92, 1–33. <https://doi.org/10.1016/j.earscirev.2008.10.003>
- Catuneanu, O., Galloway, W.E., Kendall, C.G.S.C., Miall, A.D., Posamentier, H.W., Strasser, A., Tucker, M.E., St C Kendall, C.G., Miall, A.D., Posamentier, H.W., Strasser, A., Tucker, M.E., 2011. Sequence Stratigraphy: Methodology and Nomenclature. *Newsletters Stratigr.* 44, 173–245. <https://doi.org/10.1127/0078-0421/2011/0011>
- Chiswell, S.M., Bostock, H.C., Sutton, P.J., Williams, M.J., 2015. Physical oceanography of the deep seas around New Zealand: a review. *New Zeal. J. Mar. Freshw. Res.* 49, 286–317. <https://doi.org/10.1080/00288330.2014.992918>
- Cosgrove, G.I.E., Hodgson, D.M., Poyatos-Moré, M., Mountney, N.P., McCaffrey, W.D., 2018. Filter Or Conveyor? Establishing Relationships Between Clinof orm Rollover Trajectory, Sedimentary Process Regime, and Grain Character Within Intrashelf Clinothems, Offshore New Jersey, U.S.A. *J. Sediment. Res.* 88, 917–941. <https://doi.org/10.2110/jsr.2018.44>
- Covault, J.A., Fildani, A., 2014. Continental shelves as sediment capacitors or conveyors: Source-to-sink insights from the tectonically active Oceanside shelf, southern California, USA. *Geol. Soc. Mem.* 41, 315–326. <https://doi.org/10.1144/M41.23>
- Covault, J.A., Kostic, S., Paull, C.K., Sylvester, Z., Fildani, A., 2017. Cyclic steps and related supercritical bedforms: Building blocks of deep-water depositional systems, western North America. *Mar. Geol.* <https://doi.org/10.1016/j.margeo.2016.12.009>
- Covault, J.A., Normark, W.R., Romans, B.W., Graham, S.A., 2007. Highstand fans in the California borderland: The overlooked deep-water depositional systems. *Geology* 35, 783. <https://doi.org/10.1130/G23800A.1>
- Covault, J.A., Romans, B.W., Graham, S.A., 2009. Outcrop Expression of a Continental-Margin-Scale Shelf-Edge Delta from the Cretaceous Magallanes Basin, Chile. *J. Sediment. Res.* 79, 523–539. <https://doi.org/10.2110/jsr.2009.053>

- Covault, J.A., Romans, B.W., Graham, S.A., Fildani, A., Hilley, G.E., 2011. Terrestrial source to deep-sea sink sediment budgets at high and low sea levels: Insights from tectonically active Southern California. *Geology* 39, 619–622. <https://doi.org/10.1130/G31801.1>
- Cox, S., Barrell, D.J.A., 2007. *Geology of the Aoraki Area: 1:250 000 geological map* 15.
- Crundwell, M., Scott, G., Naish, T., Carter, L., 2008. Glacial–interglacial ocean climate variability from planktonic foraminifera during the Mid-Pleistocene transition in the temperate Southwest Pacific, ODP Site 1123. *Palaeogeogr. Palaeoclimatol. Palaeoecol.* 260, 202–229. <https://doi.org/10.1016/J.PALAEO.2007.08.023>
- Crundwell, M.P., Beu, A.G., Cooper, R.A., Morgans, H.E.G., Mildenhall, D.C., 2004a. Miocene (Pareora, Southland and Taranaki Series), in: Cooper, R.A. (Ed.), *The New Zealand Geological Timescale*. Institute of Geological & Nuclear Sciences, Lower Hutt, pp. 164–194.
- Crundwell, M.P., Beu, A.G., Morgans, H.E.G., Mildenhall, D.C., Wilson, G.S., 2004b. Chapter 12, Miocene, in: Cooper, R.A. (Ed.), *Ealand Geological Timescale*. Institute of Geological and Nuclear Sciences Monograph 22. Institute of Geological and Nuclear Sciences, p. 284.
- Damuth, J.E., 1994. Neogene gravity tectonics and depositional processes on the deep Niger Delta continental margin. *Mar. Pet. Geol.* 11, 320–346. [https://doi.org/10.1016/0264-8172\(94\)90053-1](https://doi.org/10.1016/0264-8172(94)90053-1)
- Daynac, N., Lacaze, S., Pauget, F., 2016. Interpretation of complex faulted deposits in the North Sea using the relative geological time model. *First Break* 34, 55–62. <https://doi.org/10.3997/1365-2397.2016006>
- Deibert, J.E., Benda, T., Løseth, T., Schellpeper, M., Steel, R.J., 2003. Eocene Clinoform Growth in Front of a {Storm-Wave-Dominated} Shelf, Central Basin, Spitsbergen: No Significant Sand Delivery to Deepwater Areas. *J. Sediment. Res.* 73, 546–558. <https://doi.org/10.1306/011703730546>
- Deptuck, M.E., Sylvester, Z., O’Byrne, C., 2012. Pleistocene Seascape Evolution Above A “Simple” Stepped Slope—Western Niger Delta, in: *Application of the Principles of Seismic Geomorphology to Continental-Slope and Base-of-Slope Systems: Case Studies from Seafloor and Near-Seafloor Analogues* SEPM Special Publication No. 99. SEPM, pp. 199–222.
- Dixon, J.F., Steel, R.J., Olariu, C., 2012. River-dominated, shelf-edge deltas: Delivery of sand across the shelf break in the absence of slope incision. *Sedimentology* 59, 1133–1157. <https://doi.org/10.1111/j.1365-3091.2011.01298.x>
- Dumas, S., Arnott, R.W.C., 2006. Origin of hummocky and swaley cross-stratification—The controlling influence of unidirectional current strength and aggradation rate. *Geology* 1073–1076. <https://doi.org/10.1130/G22930A.1>
- DUNBAR, G.B., BARRETT, P.J., 2005. Estimating palaeobathymetry of wave-graded continental shelves from sediment texture. *Sedimentology* 52, 253–269. <https://doi.org/10.1111/j.1365-3091.2004.00695.x>
- ENGE, H.D., HOWELL, J.A., BUCKLEY, S.J., 2010. Quantifying clinothem geometry in a forced-regressive river-dominated delta, Panther Tongue Member, Utah, USA. *Sedimentology* 57, 1750–1770. <https://doi.org/10.1111/j.1365-3091.2010.01164.x>
- Ercilla, G., Alonso, B., Wynn, R.B., Baraza, J., 2002. Turbidity current sediment waves

- on irregular slopes: Observations from the Orinoco sediment-wave field. *Mar. Geol.* 192, 171–187. [https://doi.org/10.1016/S0025-3227\(02\)00554-6](https://doi.org/10.1016/S0025-3227(02)00554-6)
- Fernández-Salas, L.M., Dabrio, C.J., Goy, J.L., Díaz del Río, V., Lobo, F.J., Sanz, J.L., Lario, J., 2009. Land–sea correlation between Late Holocene coastal and infralittoral deposits in the SE Iberian Peninsula (Western Mediterranean). *Geomorphology* 104, 4–11. <https://doi.org/10.1016/J.GEOMORPH.2008.05.013>
- Figueiredo, J.J.P., Hodgson, D.M., Flint, S.S., Kavanagh, J.P., 2010. Depositional Environments and Sequence Stratigraphy of an Exhumed Permian Mudstone-Dominated Submarine Slope Succession, Karoo Basin, South Africa. *J. Sediment. Res.* 80, 97–118. <https://doi.org/10.2110/jsr.2010.002>
- Fildani, A., Hubbard, S.M., Covault, J.A., Maier, K.L., Romans, B.W., Traer, M., Rowland, J.C., 2013. Erosion at inception of deep-sea channels. *Mar. Pet. Geol.* 41, 48–61. <https://doi.org/10.1016/j.marpetgeo.2012.03.006>
- Fildani, A., Hubbard, S.M., Romans, B.W., 2009. Stratigraphic evolution of deep-water architecture: Examples of controls and depositional styles from the Magallanes Basin, Chile: SEPM, Field Trip Guidebook. SEPM Society for Sedimentary Geology.
- Fildani, A., Normark, W.R., Kostic, S., Parker, G., 2006. Channel formation by flow stripping: large-scale scour features along the Monterey East Channel and their relation to sediment waves. *Sedimentology* 53, 1265–1287. <https://doi.org/10.1111/j.1365-3091.2006.00812.x>
- Flint, S.S., Hodgson, D.M., Sprague, A.R., Brunt, R.L., Van der Merwe, W.C., Figueiredo, J., Prélat, A., Box, D., Di Celma, C., Kavanagh, J.P., 2011. Depositional architecture and sequence stratigraphy of the Karoo basin floor to shelf edge succession, Laingsburg depocentre, South Africa. *Mar. Pet. Geol.* 28, 658–674. <https://doi.org/10.1016/J.MARPETGEO.2010.06.008>
- Fongngern, R., Olariu, C., Steel, R.J., Krézsek, C., 2015. Clinoform growth in a Miocene, Para-tethyan deep lake basin: thin topsets, irregular foresets and thick bottomsets. *Basin Res.* 28, 770–795. <https://doi.org/10.1111/bre.12132>
- Fulthorpe, C.S., Austin, J. a., 2008. Assessing the significance of along-strike variations of middle to late Miocene prograding clinoformal sequence geometries beneath the New Jersey continental shelf. *Basin Res.* 20, 269–283. <https://doi.org/10.1111/j.1365-2117.2008.00350.x>
- Funnell, R., Chapman, D., Allis, R., Armstrong, P., 1996. Thermal state of the Taranaki Basin, New Zealand. *J. Geophys. Res.* 101, 25197. <https://doi.org/10.1029/96JB01341>
- Galloway, W.E., 1989. Genetic stratigraphic sequences in basin analysis; I, Architecture and genesis of flooding-surface bounded depositional units. *Am. Assoc. Pet. Geol. Bull.* 73, 125–142. <https://doi.org/10.1306/703C9AF5-1707-11D7-8645000102C1865D>
- Gani, M.R., Bhattacharya, J.P., 2011. Lithostratigraphy versus Chronostratigraphy in Facies Correlations of Quaternary Deltas: Application of Bedding Correlation, in: *River Deltas-Concepts, Models, and Examples*. SEPM (Society for Sedimentary Geology), pp. 31–48. <https://doi.org/10.2110/pec.05.83.0031>
- Giba, M., Nicol, A., Walsh, J.J., 2010. Evolution of faulting and volcanism in a back-arc basin and its implications for subduction processes. *Tectonics* 29, 1–18.

- <https://doi.org/10.1029/2009TC002634>
- Giba, M., Walsh, J.J.J., Nicol, A., 2012. Segmentation and growth of an obliquely reactivated normal fault. *J. Struct. Geol.* 39, 253–267. <https://doi.org/10.1016/j.jsg.2012.01.004>
- Gillespie, J.L., Nelson, C.S., 1996. Distribution and control of mixed terrigenous-carbonate surficial sediment facies, Wanganui shelf, New Zealand. *New Zeal. J. Geol. Geophys.* 39, 533–549. <https://doi.org/10.1080/00288306.1996.9514731>
- Gillespie, J.L., Nelson, C.S., Nodder, S.D., 1998. Post-glacial sea-level control and sequence stratigraphy of carbonate–terrigenous sediments, Wanganui shelf, New Zealand. *Sediment. Geol.* 122, 245–266. [https://doi.org/10.1016/S0037-0738\(98\)00109-2](https://doi.org/10.1016/S0037-0738(98)00109-2)
- Gong, C., Steel, R.J., Wang, Y., Lin, C., Olariu, C., 2016. Shelf-margin architecture variability and its role in sediment-budget partitioning into deep-water areas. *Earth-Science Rev.* 154, 72–101. <https://doi.org/10.1016/j.earscirev.2015.12.003>
- Gong, C., Wang, Y., Pyles, D.R., 2015. Shelf-edge trajectories and stratal stacking patterns: Their significance and relation to styles of deep-water sedimentation and amount of deep-water sandstone 7, 1211–1243. <https://doi.org/10.1306/01311513229>
- Goodbred, S.L., Kuehl, S.A., 2000. Enormous Ganges-Brahmaputra sediment discharge during strengthened early Holocene monsoon. *Geology* 28, 1083. [https://doi.org/10.1130/0091-7613\(2000\)28<1083:EGSDDS>2.0.CO;2](https://doi.org/10.1130/0091-7613(2000)28<1083:EGSDDS>2.0.CO;2)
- Goodbred, S.L., Kuehl, S.A., 1999. Holocene and modern sediment budgets for the Ganges-Brahmaputra river system: Evidence for highstand dispersal to flood-plain, shelf, and deep-sea depocenters. *Geology* 27, 559. [https://doi.org/10.1130/0091-7613\(1999\)027<0559:HAMSBF>2.3.CO;2](https://doi.org/10.1130/0091-7613(1999)027<0559:HAMSBF>2.3.CO;2)
- Grahame, J., 2015. Deepwater Taranaki Basin, New Zealand—New Interpretation and Modelling Results for Large Scale Neogene Channel and Fan Systems: Implications for Hydrocarbon Prospectivity, in: International Conference and Exhibition, Melbourne, Australia 13-16 September 2015. Society of Exploration Geophysicists and American Association of Petroleum Geologists, pp. 518–518. <https://doi.org/10.1190/ice2015-2209985>
- Grapes, R.H., 1995. Uplift and exhumation of Alpine Schist, Southern Alps, New Zealand: Thermobarometric constraints. *New Zeal. J. Geol. Geophys.* 38, 525–533. <https://doi.org/10.1080/00288306.1995.9514679>
- Hamilton, L.J., 2006. Structure of the Subtropical Front in the Tasman Sea. *Deep. Res. Part I Oceanogr. Res. Pap.* 53, 1989–2009. <https://doi.org/10.1016/j.dsr.2006.08.013>
- Hampson, G.J., 2010. Sediment dispersal and quantitative stratigraphic architecture across an ancient shelf. *Sedimentology* 57, 96–141. <https://doi.org/10.1111/j.1365-3091.2009.01093.x>
- Hampson, G.J., 2000. Discontinuity Surfaces, Clinoforms, and Facies Architecture in a Wave-Dominated, Shoreface-Shelf Parasequence. *J. Sediment. Res.* 70, 325–340. <https://doi.org/10.1306/2DC40914-0E47-11D7-8643000102C1865D>
- Hampson, G.J., Rodriguez, A.B., Storms, J.E.A., Johnson, H.D., Meyer, C.T., 2008. Geomorphology and High-Resolution Stratigraphy of Progradational Wave-

- Dominated Shoreline Deposits: Impact on Reservoir-Scale Facies Architecture, in: Recent Advances in Models of Siliciclastic Shallow-Marine Stratigraphy. SEPM (Society for Sedimentary Geology), pp. 117–142. <https://doi.org/10.2110/pec.08.90.0117>
- Hansen, R.J., Kamp, P.J.J., 2008. New insights into the condensed nature and stratigraphic significance of the Late Neogene Ariki Formation , Taranaki Basin. New Zeal. Pet. Conf. Proc. 1–13.
- Hansen, Rochelle J., Kamp, P.J.J., 2006. An integrated biostratigraphy and seismic stratigraphy for the late neogene continental margin succession in northern taranaki basin, New Zealand. New Zeal. J. Geol. Geophys. 49, 39–56. <https://doi.org/10.1080/00288306.2006.9515146>
- Hansen, R J, Kamp, P.J.J., 2006. Sequence stratigraphy and architectural elements of the Giant Foresets Formation , northern Taranaki Basin, New Zealand, in: Proceedings of New Zealand Petroleum Conference 2006, 6-10 March. pp. 1–13.
- Hansen, R.J., Kamp, P.J.J., 2004. Late miocene to early pliocene stratigraphic record in northern taranaki basin: Condensed sedimentation ahead of northern graben extension and progradation of the modern continental margin. New Zeal. J. Geol. Geophys. 47, 645–662. <https://doi.org/10.1080/00288306.2004.9515081>
- Hansen, R.J., Kamp, P.J.J., 2002. Evolution of the Giant Foresets Formation, northern Taranaki Basin, New Zealand, in: Proceedings of New Zealand Petroleum Conference . Crown Minerals, Ministry of Economic Development, Wellington, pp. 419–449.
- Hansen, J.P. V., Rasmussen, E.S., 2008. Structural, Sedimentologic, and Sea-Level Controls on Sand Distribution in a Steep-Clinoform Asymmetric Wave-Influenced Delta: Miocene Billund Sand, Eastern Danish North Sea and Jylland. J. Sediment. Res. 78, 130–146. <https://doi.org/10.2110/jsr.2008.010>
- Hayward, B.W., Sabaa, A.T., Kolodziej, A., Crundwell, M.P., Steph, S., Scott, G.H., Neil, H.L., Bostock, H.C., Carter, L., Grenfell, H.R., 2012. Planktic foraminifera-based sea-surface temperature record in the Tasman Sea and history of the Subtropical Front around New Zealand, over the last one million years. Mar. Micropaleontol. 82–83, 13–27. <https://doi.org/10.1016/j.marmicro.2011.10.003>
- Hayward, B.W., Scott, G.H., Crundwell, M.P., Kennett, J.P., Carter, L., Neil, H.L., Sabaa, A.T., Wilson, K., Rodger, J.S., Schaefer, G., Grenfell, H.R., Li, Q., 2008. The effect of submerged plateaux on Pleistocene gyral circulation and sea-surface temperatures in the Southwest Pacific. Glob. Planet. Change 63, 309–316. <https://doi.org/10.1016/j.gloplacha.2008.07.003>
- Heath, R.A., 1985. A review of the physical oceanography of the seas around New Zealand — 1982. New Zeal. J. Mar. Freshw. Res. 19, 79–124. <https://doi.org/10.1080/00288330.1985.9516077>
- Heath, R.A., 1982. What drives the mean circulation on the New Zealand west coast continental shelf? New Zeal. J. Mar. Freshw. Res. 16, 215–226. <https://doi.org/10.1080/00288330.1982.9515964>
- Heath, R.A., 1972. The southland current. New Zeal. J. Mar. Freshw. Res. 6, 497–533. <https://doi.org/10.1080/00288330.1972.9515444>
- Hedberg, H.D., 1970. Continental margins from viewpoint of the petroleum geologist. AAPG Bull. 54, 3–43.

- Helland-Hansen, W., Gjelberg, H., 2012. Towards a Hierarchical Classification of Clinoforms, in: AAPG Annual Convention and Exhibition, April 22–25, 2012, Long Beach, California, U.S., Search and Discovery Article #90142.
- Helland-Hansen, W., Gjelberg, J.G., 1994. Conceptual basis and variability in sequence stratigraphy: a different perspective. *Sediment. Geol.* 92, 31–52. [https://doi.org/10.1016/0037-0738\(94\)90053-1](https://doi.org/10.1016/0037-0738(94)90053-1)
- Helland-Hansen, W., Hampson, G.J., 2009. Trajectory analysis: Concepts and applications. *Basin Res.* 21, 454–483. <https://doi.org/10.1111/j.1365-2117.2009.00425.x>
- Helland-Hansen, W., Martinsen, O.J., 1996. Shoreline trajectories and sequences; description of variable depositional-dip scenarios, *Journal of Sedimentary Research. GeoScienceWorld.* <https://doi.org/10.1306/D42683DD-2B26-11D7-8648000102C1865D>
- Helland-Hansen, W., Sømme, T.O., Martinsen, O.J., Lunt, I., Thurmond, J., 2016. Deciphering Earth's Natural Hourglasses: Perspectives On Source-To-Sink Analysis. *J. Sediment. Res.* 86, 1008–1033. <https://doi.org/10.2110/jsr.2016.56>
- Helland-Hansen, W., Steel, R.J., Somme, T.O., 2012. Shelf genesis revisited. *J. Sediment. Res.* 82, 133–148. <https://doi.org/10.2110/jsr.2012.15>
- Henriksen, S., Hampson, G.J., Helland-Hansen, W., Johannessen, E.P., Steel, R.J., 2009. Shelf edge and shoreline trajectories, a dynamic approach to stratigraphic analysis. *Basin Res.* 21, 445–453. <https://doi.org/10.1111/j.1365-2117.2009.00432.x>
- Henriksen, S., Helland-Hansen, W., Bullimore, S., 2011. Relationships between shelf-edge trajectories and sediment dispersal along depositional dip and strike: A different approach to sequence stratigraphy. *Basin Res.* 23, 3–21. <https://doi.org/10.1111/j.1365-2117.2010.00463.x>
- Herman, F., Rhodes, E.J., Braun, J., Heiniger, L., 2010. Uniform erosion rates and relief amplitude during glacial cycles in the Southern Alps of New Zealand, as revealed from OSL-thermochronology. *Earth Planet. Sci. Lett.* 297, 183–189. <https://doi.org/10.1016/j.epsl.2010.06.019>
- Herman, F., Seward, D., Valla, P.G., Carter, A., Kohn, B., Willett, S.D., Ehlers, T.A., 2013. Worldwide acceleration of mountain erosion under a cooling climate. *Nature* 504, 423–426. <https://doi.org/10.1038/nature12877>
- Hernandez-Molina, F.J., Fernandez-Salas, L.M., Lobo, F., Somoza, L., Diaz-del-Rio, V., Alveirinho Dias, J.M., 2000. The infralittoral prograding wedge: a new large-scale progradational sedimentary body in shallow marine environments. *Geo-Marine Lett.* 20, 109–117. <https://doi.org/10.1007/s003670000040>
- Hicks, D., Shankar, U., 2003. Sediment from New Zealand Rivers. NIWA Chart, Miscellaneous Series No. 79.
- Hicks, D., Shankar, U., McKerchar, A., Basher, L., Lynn, I., Page, M., Jessen, M., 2011. Suspended sediment yields from New Zealand rivers. *J. Hydrol. New Zeal.* 50, 81–142. <https://doi.org/10.1029/2006WR005570>
- Higgs, K.E., King, P.R., Raine, J.I., Sykes, R., Browne, G.H., Crouch, E.M., Baur, J.R., 2012. Sequence stratigraphy and controls on reservoir sandstone distribution in an Eocene marginal marine-coastal plain fairway, Taranaki Basin, New Zealand. *Mar. Pet. Geol.* 32, 110–137. <https://doi.org/10.1016/j.marpetgeo.2011.12.001>

- Hill, J.C., Driscoll, N.W., Weissel, J.K., Goff, J.A., 2004. Large-scale elongated gas blowouts along the U.S. Atlantic margin. *J. Geophys. Res. Solid Earth* 109, n/a-n/a. <https://doi.org/10.1029/2004JB002969>
- Hodgson, D.M., Houghton, P.D.W., 2004. Impact of syndepositional faulting on gravity current behaviour and deep-water stratigraphy: Tabernas-Sorbas Basin, SE Spain. *Geol. Soc. London, Spec. Publ.* 222, 135–158. <https://doi.org/10.1144/GSL.SP.2004.222.01.08>
- Holt, W.E., Stern, T. a., 1994. Subduction, platform subsidence, and foreland thrust loading: The late Tertiary development of Taranaki Basin, New Zealand. *Tectonics* 13, 1068. <https://doi.org/10.1029/94TC00454>
- Holt, W.E., Stern, T. a., 1991. Sediment loading on the Western Platform of the New Zealand continent: Implications for the strength of a continental margin. *Earth Planet. Sci. Lett.* 107, 523–538. [https://doi.org/10.1016/0012-821X\(91\)90098-3](https://doi.org/10.1016/0012-821X(91)90098-3)
- Houseknecht, D., Schenk, C.J., 2008. Outcrops of Turbidite-channel Facies in the Torok Formation: Reservoir Analogs for the Alaska North Slope, USA, in: Nilsen, T.H., Shew, R.D., Steffens, G.S., Studlick, J.R.J. (Eds.), *Atlas of Deep-Water Outcrops*. American Association of Petroleum Geologists, Oklahoma, U.S.A., pp. 373–377. <https://doi.org/10.1306/St561240>
- Houseknecht, D.W., 2019. Petroleum systems framework of significant new oil discoveries in a giant Cretaceous (Aptian–Cenomanian) clinothem in Arctic Alaska. *Am. Assoc. Pet. Geol. Bull.* 103, 619–652. <https://doi.org/10.1306/08151817281>
- Houseknecht, D.W., Bird, K.J., Schenk, C.J., 2009. Seismic analysis of clinoform depositional sequences and shelf-margin trajectories in Lower Cretaceous (Albian) strata, Alaska North Slope. *Basin Res.* 21, 644–654. <https://doi.org/10.1111/j.1365-2117.2008.00392.x>
- Hubbard, S.M., Fildani, A., Romans, B.W., Covault, J.A., McHargue, T.R., 2010. High-Relief Slope Clinoform Development: Insights from Outcrop, Magallanes Basin, Chile. *J. Sediment. Res.* 80, 357–375. <https://doi.org/10.2110/jsr.2010.042>
- Hughes Clarke, J.E., 2016. First wide-angle view of channelized turbidity currents links migrating cyclic steps to flow characteristics. *Nat. Commun.* 7, 1–13. <https://doi.org/10.1038/ncomms11896>
- Huybers, P., 2011. Combined obliquity and precession pacing of late Pleistocene deglaciations. *Nature* 480, 229–232. <https://doi.org/10.1038/nature10626>
- Huybers, P., Wunsch, C., 2005. Obliquity pacing of the late Pleistocene glacial terminations. *Nature* 434, 491–494. <https://doi.org/10.1038/nature03401>
- Ianniello, A., Bolelli, W., Di Scala, L., 1992. Barbara Field, Adriatic Sea, Offshore Italy - A Giant Gas Field Masked by Seismic Velocity Anomaly - A Subtle Trap.pdf, in: Halbouty, M. (Ed.), *Giant Oil and Gas Fields of the Decade 1978-1988*. AAPG Memoir 1992. AAPG, pp. 265–276.
- Jervey, M.T., 1988. Quantitative geological modeling of siliciclastic rock sequences and their seismic expression. *Sea-level Chang. an Integr. approach* 47–69. <https://doi.org/10.2110/pec.88.01.0047>
- Jiao, R., Herman, F., Seward, D., 2017. Late Cenozoic exhumation model of New Zealand: Impacts from tectonics and climate. *Earth-Science Rev.* 166, 286–298. <https://doi.org/10.1016/j.earscirev.2017.01.003>

- Johannessen, E.P., Steel, R.J., 2005. Shelf-margin clinoforms and prediction of deepwater sands. *Basin Res.* 17, 521–550. <https://doi.org/10.1111/j.1365-2117.2005.00278.x>
- Jol, H.M., Lawton, D.C., Smith, D.G., 2003. Ground penetrating radar: 2-D and 3-D subsurface imaging of a coastal barrier spit, Long Beach, WA, USA. *Geomorphology* 53, 165–181. [https://doi.org/10.1016/S0169-555X\(02\)00352-5](https://doi.org/10.1016/S0169-555X(02)00352-5)
- Jones, G.E.D., Hodgson, D.M., Flint, S.S., 2015. Lateral variability in clinoform trajectory, process regime, and sediment dispersal patterns beyond the shelf-edge rollover in exhumed basin margin-scale clinoforms. *Basin Res.* n/a-n/a. <https://doi.org/10.1111/bre.12092>
- Jones, G.E.D., Hodgson, D.M., Flint, S.S., 2013. Contrast in the process response of stacked clinoforms to the shelf-slope rollover. *Geosphere* 9, 299–316. <https://doi.org/10.1130/GES00796.1>
- Kamp, P.J.J., 1986. Late Cretaceous–Cenozoic tectonic development of the southwest Pacific region. *Tectonophysics* 121, 225–251. [https://doi.org/10.1016/0040-1951\(86\)90045-4](https://doi.org/10.1016/0040-1951(86)90045-4)
- Kamp, P.J.J., Vonk, A.J., Bland, K.J., Hansen, R.J., Hendy, A.J.W., McIntyre, A.P., Ngatai, M., Cartwright, S.J., Hayton, S., Nelson, C.S., 2004. Neogene stratigraphic architecture and tectonic evolution of Wanganui, King Country, and eastern Taranaki Basins, New Zealand. *New Zeal. J. Geol. Geophys.* 47, 625–644. <https://doi.org/10.1080/00288306.2004.9515080>
- Kamp, P.J.J., Vonk, A.J.A., Bland, K.K.J., Griffin, A., 2002. Megasequence architecture of Taranaki, Wanganui, and King Country basins and Neogene progradation of two continental margin wedges across western New Zealand. *New Zeal. Pet. Conf. Proc.* February, 464–481.
- Katz, B.J., 2011. Microbial Processes and Natural Gas Accumulations, *The Open Geology Journal*.
- Kear, D., 1994. A “least complex” dynamic model for late Cenozoic volcanism in the North Island, New Zealand. *New Zeal. J. Geol. Geophys.* 37, 223–236. <https://doi.org/10.1080/00288306.1994.9514617>
- Kertzus, V., Kneller, B., Petter, A.L., Kim, W., Muto, T., Steel, R.J., 2009. Clinoform quantification for assessing the effects of external forcing on continental margin development. *Basin Res.* 23, 118–121. <https://doi.org/10.1111/j.1365-2117.2010.00472.x>
- King, P.R., Boyes, A.F., Jones, C.M., Ogg, J., Lugowski, A., 2010. New Zealand Stratlink – Taranaki Basin chronostratigraphic transects. GNS Data Series 6a. Lower Hutt.
- King, P.R., Ilg, B.R., Arnot, M., Browne, G.H., Strachan, L.J., Crundwell, M.P., Helle, K., 2011. Outcrop and seismic examples of mass-transport deposits from a Late Miocene deep-water succession, Taranaki basin, New Zealand, SEPM Special Publication. <https://doi.org/>
- King, P.R., Thrasher, G.P., 1992. Post-Eocene Development of the Taranaki Basin, New Zealand: Convergent Overprint of a Massive Margin. *Geol. Geophys. Cont. Margins* 53, 93–118.
- King, R.R., Thrasher, G.P., 1996. Cretaceous–Cenozoic geology and petroleum systems of the Taranaki Basin, New Zealand, GNS Science Report.
- Klitgord, K.D., Hutchinson, D.R., Schouten, H., 1988. U.S. Atlantic continental margin;

- Structural and tectonic framework, in: *The Atlantic Continental Margin*. Geological Society of America, London, pp. 19–55. <https://doi.org/10.1130/DNAG-GNA-I2.19>
- Knox, G.J., 1982. Taranaki Basin, structural style and tectonic setting. *New Zeal. J. Geol. Geophys.* 25, 125–140. <https://doi.org/10.1080/00288306.1982.10421405>
- Koppes, M.N., Montgomery, D.R., 2009. The relative efficacy of fluvial and glacial erosion over modern to orogenic timescales. *Nat. Geosci.* 2, 644–647. <https://doi.org/10.1038/ngeo616>
- Kostic, S., 2011. Modeling of submarine cyclic steps: Controls on their formation, migration, and architecture. *Geosphere* 7, 294–304. <https://doi.org/10.1130/GES00601.1>
- Kostic, S., Parker, G., 2006. The response of turbidity currents to a canyon-fan transition: Internal hydraulic jumps and depositional signatures. *J. Hydraul. Res.* 44, 631–653. <https://doi.org/10.1080/00221686.2006.9521713>
- Kroeger, K.F., Crutchley, G.J., Hill, M.G., Pecher, I.A., 2017. Potential for gas hydrate formation at the northwest New Zealand shelf margin - New insights from seismic reflection data and petroleum systems modelling. *Mar. Pet. Geol.* 83, 215–230. <https://doi.org/10.1016/J.MARPETGEO.2017.02.025>
- Kroeger, K.F., Funnell, R.H., Nicol, A., Fohrmann, M., Bland, K.J., King, P.R., 2013. 3D crustal-scale heat-flow regimes at a developing active margin (Taranaki Basin, New Zealand). *Tectonophysics* 591, 175–193. <https://doi.org/10.1016/J.TECTO.2012.04.005>
- Kuchar, J., Milne, G., Wolstencroft, M., Love, R., Tarasov, L., Hijma, M., 2018. The Influence of Sediment Isostatic Adjustment on Sea Level Change and Land Motion Along the U.S. Gulf Coast. *J. Geophys. Res. Solid Earth* 123, 780–796. <https://doi.org/10.1002/2017JB014695>
- Kuehl, S.A., DeMaster, D.J., Nittrouer, C.A., 1986. Nature of sediment accumulation on the Amazon continental shelf. *Cont. Shelf Res.* 6, 209–225. [https://doi.org/10.1016/0278-4343\(86\)90061-0](https://doi.org/10.1016/0278-4343(86)90061-0)
- Kuehl, S.A., Levy, B.M., Moore, W.S., Allison, M.A., 1997. Subaqueous delta of the Ganges-Brahmaputra river system. *Mar. Geol.* 144, 81–96. [https://doi.org/10.1016/S0025-3227\(97\)00075-3](https://doi.org/10.1016/S0025-3227(97)00075-3)
- Laird, M.G., 1972. Sedimentology of the Greenland Group in the Paparoa Range, West Coast, South Island. *New Zeal. J. Geol. Geophys.* 15, 372–393. <https://doi.org/10.1080/00288306.1972.10422338>
- Larsen, I.J., Almond, P.C., Eger, A., Stone, J.O., Montgomery, D.R., Malcolm, B., 2014. Rapid soil production and weathering in the Southern Alps, New Zealand. *Science* 343, 637–40. <https://doi.org/10.1126/science.1244908>
- Leach, A.S., Wallace, M.W., 2001. Cenozoic Submarine Canyon Systems in Cool Water Carbonates from the Otway Basin, Victoria, Australia, in: *PESA East Australasian Basins Symposium*, Melbourne, Victoria, Australia. Petroleum Exploration Society of Australia (PESA), pp. 465–473.
- Lease, R.O., Houseknecht, D., 2017. Timing of Cretaceous Shelf Margins in the Colville Basin, Arctic Alaska, in: *AAPG Pacific Section Annual Meeting*. AAPG, Anchorage, Alaska.

- Lease, R.O., Houseknecht, D.W., Kylander-Clark, A.R.C., 2017. Rapid Progradation and 400 K.Y. Pacing of the World's Largest Foreland Clinotherm, Cretaceous Arctic Alaska. <https://doi.org/10.1130/abs/2017am-301048>
- Lewis, K., Eade, J., 1974. Sedimentation in the vicinity of the Maui gasfield. NZOI Oceanographic Summary 6.
- Lewis, K.B., Carter, L., Davey, F.J., 1994. The opening of Cook Strait: Interglacial tidal scour and aligning basins at a subduction to transform plate edge. *Mar. Geol.* 116, 293–312. [https://doi.org/10.1016/0025-3227\(94\)90047-7](https://doi.org/10.1016/0025-3227(94)90047-7)
- Li, J., Li, W., Alves, T.M., Rebesco, M., Zhan, W., Sun, J., Mitchell, N.C., Wu, S., 2019. Different origins of seafloor undulations in a submarine canyon system, northern South China Sea, based on their seismic character and relative location. *Mar. Geol.* 413, 99–111. <https://doi.org/10.1016/j.margeo.2019.04.007>
- Li, W., Alves, T.M., Wu, S., Rebesco, M., Zhao, F., Mi, L., Ma, B., 2016. A giant, submarine creep zone as a precursor of large-scale slope instability offshore the Dongsha Islands (South China Sea). *Earth Planet. Sci. Lett.* 451, 272–284. <https://doi.org/10.1016/j.epsl.2016.07.007>
- Lisiecki, L.E., Raymo, M.E., 2005. A Pliocene-Pleistocene stack of 57 globally distributed benthic $\delta^{18}O$ records. *Paleoceanography* 20, 1–17. <https://doi.org/10.1029/2004PA001071>
- Liu, J.P., Milliman, J.D., Gao, S., Cheng, P., 2004. Holocene development of the Yellow River's subaqueous delta, North Yellow Sea. *Mar. Geol.* 209, 45–67. <https://doi.org/10.1016/J.MARGE0.2004.06.009>
- Lobo, F.J., Fernández-Salas, L.M., Hernández-Molina, F.J., González, R., Dias, J.M.A., del Río, V.D., Somoza, L., 2005. Holocene highstand deposits in the Gulf of Cadiz, SW Iberian Peninsula: A high-resolution record of hierarchical environmental changes. *Mar. Geol.* 219, 109–131. <https://doi.org/10.1016/J.MARGE0.2005.06.005>
- López, C., Spence, G., Hyndman, R., Kelley, D., 2010. Frontal ridge slope failure at the northern Cascadia margin: Margin-normal fault and gas hydrate control. *Geology* 38, 967–970. <https://doi.org/10.1130/G31136.1>
- Madof, A.S., Harris, A.D., Connell, S.D., 2016. Nearshore along-strike variability: Is the concept of the systems tract unhinged? *Geology* 44, G37613.1. <https://doi.org/10.1130/G37613.1>
- Marin, D., Escalona, A., Sliwihska, K.K., Nøhr-Hansen, H., Mordasova, A., 2017. Sequence stratigraphy and lateral variability of Lower Cretaceous clinofolds in the southwestern Barents Sea. *Am. Assoc. Pet. Geol. Bull.* 101, 1487–1517. <https://doi.org/10.1306/10241616010>
- Martinsen, O.J., Helland-Hansen, W., 1995. Strike variability of clastic depositional systems: does it matter for sequence-stratigraphic analysis? *Geology* 23, 439–442. [https://doi.org/10.1130/0091-7613\(1995\)023<0439:SVOCDS>2.3.CO;2](https://doi.org/10.1130/0091-7613(1995)023<0439:SVOCDS>2.3.CO;2)
- Maslin, M.A., Brierley, C.M., 2015. The role of orbital forcing in the Early Middle Pleistocene Transition. *Quat. Int.* 389, 47–55. <https://doi.org/10.1016/j.quaint.2015.01.047>
- Maslin, M.A., Ridgwell, A.J., 2005. Mid-Pleistocene revolution and the 'eccentricity myth.' *Geol. Soc. London, Spec. Publ.* 247, 19–34.

- <https://doi.org/10.1144/GSL.SP.2005.247.01.02>
- McClymont, E.L., Elmore, A.C., Kender, S., Leng, M.J., Greaves, M., Elderfield, H., 2016. Pliocene-Pleistocene evolution of sea surface and intermediate water temperatures from the southwest Pacific. *Paleoceanography* 31, 895–913. <https://doi.org/10.1002/2016PA002954>. Received
- McMillen, K.J., 1991. Seismic Stratigraphy of Lower Cretaceous Foreland Basin Submarine Fans in the North Slope, Alaska. Springer, New York, NY, pp. 289–302. https://doi.org/10.1007/978-1-4684-8276-8_15
- Mellere, D., Steel, R., Plink-Bjorklund, P., 2002. Anatomy of shelf deltas at the edge of a prograding Eocene shelf margin, Spitsbergen. *Sedimentology* 49, 1181–1206. <https://doi.org/10.1046/j.1365-3091.2002.00484.x>
- Miall, A.D., 1992. Exxon global cycle chart: An event for every occasion? *Geology* 20, 787–790. [https://doi.org/10.1130/0091-7613\(1992\)020<0787:egccae>2.3.co;2](https://doi.org/10.1130/0091-7613(1992)020<0787:egccae>2.3.co;2)
- Michels, K., Kudrass, H., Hübscher, C., Suckow, A., Wiedicke, M., 1998. The submarine delta of the Ganges–Brahmaputra: cyclone-dominated sedimentation patterns. *Mar. Geol.* 149, 133–154. [https://doi.org/10.1016/S0025-3227\(98\)00021-8](https://doi.org/10.1016/S0025-3227(98)00021-8)
- Migeon, S., Savoye, B., Zanella, E., Mulder, T., Faugères, J.C., Weber, O., 2001. Detailed seismic-reflection and sedimentary study of turbidite sediment waves on the var sedimentary ridge (SE France): Significance for sediment transport and deposition and for the mechanisms of sediment-wave construction. *Mar. Pet. Geol.* 18, 179–208. [https://doi.org/10.1016/S0264-8172\(00\)00060-X](https://doi.org/10.1016/S0264-8172(00)00060-X)
- Miller, K.G., 2005. The Phanerozoic Record of Global Sea-Level Change. *Science* (80-.). 310, 1293–1298. <https://doi.org/10.1126/science.1116412>
- Miller, K.G., Mountain, G.S., Browning, J. V., Katz, M.E., Monteverde, D., Sugarman, P.J., Ando, H., Bassetti, M. a., Bjerrum, C.J., Hodgson, D., Hesselbo, S., Karakaya, S., Proust, J.N., Rabineau, M., 2013. Testing sequence stratigraphic models by drilling Miocene foresets on the New Jersey shallow shelf. *Geosphere* 9, 1236–1256. <https://doi.org/10.1130/GES00884.1>
- Miller, K.G., Mountain, G.S., Wright, J.D., Browning, J.V., 2011. Sea level and ice volume variations. *Oceanography* v, 40–53. <https://doi.org/10.5670/oceanog.2011.26.COPYRIGHT>
- Mitchum, R. M., Vail, P.R., Sangree, J.B., 1977a. Seismic stratigraphy and global changes of sea level, Part 6: stratigraphic interpretation of seismic reflection patterns in depositional sequences, in: Payton, C.E. (Ed.), *Seismic Stratigraphy: Applications to Hydrocarbon Exploration*. AAPG Memoir 26. AAPG, Tulsa, pp. 117–134. <https://doi.org/10.1038/272400a0>
- Mitchum, R.M., Vail, P.R., Thompson, S., 1977. Seismic stratigraphy and global changes in sealevel, part 2: The depositional sequence as a basic unit for stratigraphic analysis., in: Payton, C. (Ed.), *Seismic Stratigraphy: Application to Hydrocarbon Exploration*. AAPG-Memoir No. 26. AAPG, Tulsa, pp. 53–62.
- Mitchum, R. M., Vail, P.R., Thompson, S., 1977b. Seismic Stratigraphy and Global Changes of Sea Level, Part 2: The Depositional Sequence as a Basic Unit for Stratigraphic Analysis: Section 2. Application of Seismic Reflection Configuration to Stratigraphic Interpretation, in: Payton, C.E. (Ed.), *Seismic Stratigraphy: Applications to Hydrocarbon Exploration* AAPG Memoir 26. AAPG, Tulsa, pp. 53–62.

- Monteverde, D.H., Mountain, G.S., Miller, K.G., 2008. Early Miocene sequence development across the New Jersey margin. *Basin Res.* 20, 249–267. <https://doi.org/10.1111/j.1365-2117.2008.00351.x>
- Morgans, H., 2006. Foraminiferal Biostratigraphy of the Early Miocene to Pleistocene Sequences in Witiara-1, Taimana-1, Arawa-1 and Okoki-1. GNS SCIENCE REPORT 2006/37.
- Mortimer, N., 2004. New Zealand's Geological Foundations. *Gondwana Res.* 7, 261–272. [https://doi.org/10.1016/S1342-937X\(05\)70324-5](https://doi.org/10.1016/S1342-937X(05)70324-5)
- Mortimer, N., 2000. Metamorphic discontinuities in orogenic belts: example of the garnet-biotite-albite zone in the Otago Schist, New Zealand. *Int. J. Earth Sci.* 89, 295–306. <https://doi.org/10.1007/s005310000086>
- Moscardelli, L., Wood, L.J., Dunlap, D.B., 2012. Shelf-edge deltas along structurally complex margins: A case study from eastern offshore Trinidad. *Am. Assoc. Pet. Geol. Bull.* 96, 1483–1522. <https://doi.org/10.1306/01241211046>
- Mountain, G., Proust, J.N., 2010. The New Jersey margin scientific drilling project (IODP expedition 313): Untangling the record of global and local sea-level changes. *Sci. Drill.* 26–34. <https://doi.org/10.2204/iodp.sd.10.03.2010>
- Mountjoy, J.J., Pecher, I., Henrys, S., Crutchley, G., Barnes, P.M., Plaza-Faverola, A., 2014. Shallow methane hydrate system controls ongoing, downslope sediment transport in a low-velocity active submarine landslide complex, Hikurangi Margin, New Zealand. *Geochemistry, Geophys. Geosystems* 15, 4137–4156. <https://doi.org/10.1002/2014GC005379>
- Muto, T., Steel, R.J., 2002. In Defense of Shelf-Edge Delta Development during Falling and Lowstand of Relative Sea Level. *J. Geol.* 110, 421–436. <https://doi.org/10.1086/340631>
- Naish, T., Kamp, P.J.J., 1997. Sequence stratigraphy of sixth-order (41 k.y.) Pliocene-Pleistocene cyclothems, Wanganui basin, New Zealand: A case for the regressive systems tract. *Bull. Geol. Soc. Am.* 109, 978–999. [https://doi.org/10.1130/0016-7606\(1997\)109<0978:SSOSOK>2.3.CO;2](https://doi.org/10.1130/0016-7606(1997)109<0978:SSOSOK>2.3.CO;2)
- Naish, T.R., Abbott, S.T., Alloway, V., Beu, A.G., Carter, R.M., Edwards, A.R., Journeaux, T.D., Kamp, P.J., Pillans, B.J., Saul, G., Woolfe, K.J., 1998. Astronomical calibration of a southern hemisphere Plio-Pleistocene reference section, Wanganui Basin, New Zealand. *Quat. Sci. Rev.* 17, 695–710. [https://doi.org/10.1016/S0277-3791\(97\)00075-9](https://doi.org/10.1016/S0277-3791(97)00075-9)
- Naish, T.R., Field, B.D., Zhu, H., Melhuish, a., Carter, R.M., Abbott, S.T., Edwards, S., Alloway, B. V., Wilson, G.S., Niessen, F., Barker, a., Browne, G.H., Maslen, G., 2005. Integrated outcrop, drill core, borehole and seismic stratigraphic architecture of a cyclothem, shallow-marine depositional system, Wanganui Basin, New Zealand. *J. R. Soc. New Zeal.* 35, 91–122. <https://doi.org/10.1080/03014223.2005.9517778>
- Nathan, S., Rattenbury, M.S., Suggate, R.P., 2002. *Geology of the Greymouth Area: 1:250 000 geological map* 12.
- Neal, J., Abreu, V., 2009. Sequence stratigraphy hierarchy and the accommodation succession method. *Geology* 37, 779–782. <https://doi.org/10.1130/G25722A.1>
- Neal, J.E., Abreu, V., Bohacs, K.M., Feldman, H.R., Pederson, K.H., 2016.

- Accommodation succession ($\delta A / \delta S$) sequence stratigraphy: observational method, utility and insights into sequence boundary formation. *J. Geol. Soc. London.* 173, 803–816. <https://doi.org/10.1144/jgs2015-165>
- Newnham, R., McGlone, M., Moar, N., Wilmshurst, J., Vandergoes, M., 2013. The vegetation cover of New Zealand at the Last Glacial Maximum. *Quat. Sci. Rev.* 74, 202–214. <https://doi.org/10.1016/J.QUASCIREV.2012.08.022>
- Nicol, A., Mazengarb, C., Chanier, F., Rait, G., Uruski, C., Wallace, L., 2007. Tectonic evolution of the active Hikurangi subduction margin, New Zealand, since the Oligocene. *Tectonics* 26, 1–24. <https://doi.org/10.1029/2006TC002090>
- Nicol, A., Seebeck, H., Wallace, L., 2017. Quaternary Tectonics of New Zealand, in: *Landscape and Quaternary Environmental Change in New Zealand*. pp. 1–34. https://doi.org/10.2991/978-94-6239-237-3_1
- Nodder, S.D., 1995. Late quaternary transgressive/regressive sequences from Taranaki continental shelf, western New Zealand. *Mar. Geol.* 123, 187–214. [https://doi.org/10.1016/0025-3227\(95\)00004-I](https://doi.org/10.1016/0025-3227(95)00004-I)
- Nodder, S.D., 1994. Characterizing potential offshore seismic sources using high-resolution geophysical and seafloor sampling programs: An example from Cape Egmont fault zone, Taranaki shelf, New Zealand. *Tectonics* 13, 641–658. <https://doi.org/10.1029/94TC00296>
- Nodder, S.D., 1993. Neotectonics of the offshore cape egmont fault zone, Taranaki Basin, New Zealand. *New Zeal. J. Geol. Geophys.* 36, 167–184. <https://doi.org/10.1080/00288306.1993.9514566>
- Norris, R.J., Toy, V.G., 2014. Continental transforms: A view from the Alpine Fault. *J. Struct. Geol.* <https://doi.org/10.1016/j.jsg.2014.03.003>
- NZP&M, 2014. *New Zealand Petroleum Basins*.
- O'Grady, D., Syvitski, J., Pratson, L.F., Sarg, J.F., 2000. Categorizing the morphologic variability of siliciclastic passive continental margins. *Geology* 28, 207–210. [https://doi.org/10.1130/0091-7613\(2000\)28<207:CTMVOS>2.0.CO;2](https://doi.org/10.1130/0091-7613(2000)28<207:CTMVOS>2.0.CO;2)
- Olariu, C., Steel, R.J., 2009. Influence of point-source sediment-supply on modern shelf-slope morphology: implications for interpretation of ancient shelf margins. *Basin Res.* 21, 484–501. <https://doi.org/10.1111/j.1365-2117.2009.00420.x>
- Omeru, T., 2014. *Mass transport deposits: implications for reservoir seals*. Cardiff University.
- Omeru, T., Cartwright, J.A., Bull, S., 2016a. Kinematics of Submarine Slope Failures in the Deepwater Taranaki Basin, New Zealand. Springer, Cham, pp. 61–70. https://doi.org/10.1007/978-3-319-20979-1_6
- Omeru, T., Cartwright, J.A., Bull, S., 2016b. Submarine Mass Movements and their Consequences 41, 61–70. <https://doi.org/10.1007/978-3-319-20979-1>
- Ottesen, D., Rise, L., Andersen, E.S., Bugge, T., Eidvin, T., 2009. Geological evolution of the Norwegian continental shelf between 61°N and 68°N during the last 3 million years. *Nor. J. Geol.* 89, 251–265.
- Patrino, S., Hampson, G.J., Jackson, C.A.-L., Whipp, P.S., 2014. Quantitative progradation dynamics and stratigraphic architecture of ancient shallow-marine clinoform sets: a new method and its application to the Upper Jurassic Sognefjord

- Formation, Troll Field, offshore Norway. *Basin Res.* 27, 412–452. <https://doi.org/10.1111/bre.12081>
- Patruno, S., Hampson, G.J., Jackson, C.A.L., 2015a. Quantitative characterisation of deltaic and subaqueous clinoforms. *Earth-Science Rev.* 142, 79–119. <https://doi.org/10.1016/j.earscirev.2015.01.004>
- Patruno, S., Hampson, G.J., Jackson, C.A.L., Dreyer, T., 2015b. Clinoform geometry, geomorphology, facies character and stratigraphic architecture of a sand-rich subaqueous delta: Jurassic Sognefjord Formation, offshore Norway. *Sedimentology* 62, 350–388. <https://doi.org/10.1111/sed.12153>
- Patruno, S., Helland-Hansen, W., 2018. Clinoforms and clinoform systems: Review and dynamic classification scheme for shorelines, subaqueous deltas, shelf edges and continental margins. *Earth-Science Rev.* 185, 202–233. <https://doi.org/10.1016/j.earscirev.2018.05.016>
- Pauget, F., Lacaze, S., Valding, T., 2009. A global approach in seismic interpretation based on cost function minimization, in: SEG Technical Program Expanded Abstracts 2009. Society of Exploration Geophysicists, pp. 2592–2596. <https://doi.org/10.1190/1.3255384>
- Paull, C.K., Caress, D.W., Ussler, W., Lundsten, E., Meiner-Johnson, M., 2011. High-resolution bathymetry of the axial channels within Monterey and Soquel submarine canyons, offshore central California. *Geosphere* 7, 1077–1101. <https://doi.org/10.1130/GES00636.1>
- Paull, C.K., Ussler, W., Caress, D.W., Lundsten, E., Covault, J.A., Maier, K.L., Xu, J., Augenstein, S., 2010. Origins of large crescent-shaped bedforms within the axial channel of Monterey Canyon, Offshore California. *Geosphere* 6, 755–774. <https://doi.org/10.1130/GES00527.1>
- Paumard, V., Bourget, J., Payenberg, T., Ainsworth, R.B., George, A.D., Lang, S., Posamentier, H.W., Peyrot, D., 2018. Controls on shelf-margin architecture and sediment partitioning during a syn-rift to post-rift transition: Insights from the Barrow Group (Northern Carnarvon Basin, North West Shelf, Australia). *Earth-Science Rev.* 177, 643–677. <https://doi.org/10.1016/j.earscirev.2017.11.026>
- Payne, D., Nelson, C., Hood, S., 2010. Mixed glauconitic-carbonate-siliciclastic surficial sediments on the north Kaipara continental margin, northwestern North Island, New Zealand. *New Zeal. J. Geol. Geophys.* 53, 307–326. <https://doi.org/10.1080/00288306.2010.498782>
- Payne, D.S., 2008. Shelf-To-Slope Sedimentation on the North Kaipara Continental Margin, Northwestern North Island, New Zealand 1994.
- Pellegrini, C., Asioli, A., Bohacs, K.M., Drexler, T.M., Feldman, H.R., Sweet, M.L., Maselli, V., Rovere, M., Gamberi, F., Valle, G.D., Trincardi, F., 2018. The Late Pleistocene Po River lowstand wedge in the Adriatic Sea: Controls on architecture variability and sediment partitioning. *Mar. Pet. Geol.* 96, 16–50. <https://doi.org/10.1016/J.MARPETGEO.2018.03.002>
- Pilaar, W.F.H., Wakefield, L.L., 1978. Structural and Stratigraphic Evolution of the Taranaki Basin, Offshore North Island, New Zealand. *APPEA J.* 18, 93. <https://doi.org/10.1071/aj77011>
- Pillans, B., 2017. Quaternary Stratigraphy of Whanganui Basin—A Globally Significant Archive, in: *Landscape and Quaternary Environmental Change in New Zealand*.

- Atlantis Press, Paris, pp. 141–170. https://doi.org/10.2991/978-94-6239-237-3_4
- Pinous, O. V., Levchuk, M.A., Sahagian, D.L., 2001. Regional synthesis of the productive neocomian complex of West Siberia: Sequence stratigraphic framework. *Am. Assoc. Pet. Geol. Bull.* 85, 1713–1730. <https://doi.org/10.1306/8626d04f-173b-11d7-8645000102c1865d>
- Porebski, S.J., Steel, R.J., 2006. Deltas and Sea-Level Change. *J. Sediment. Res.* 76, 390–403. <https://doi.org/10.2110/jsr.2006.034>
- Posamentier, H.W., 2004. Seismic Geomorphology: Imaging Elements of Depositional Systems from Shelf to Deep Basin Using 3D Seismic Data: Implications for Exploration and Development. *Geol. Soc. London, Mem.* 29, 11–24. <https://doi.org/10.1144/GSL.MEM.2004.029.01.02>
- Posamentier, H.W., Allen, G.P., 1999. Siliciclastic Sequence Stratigraphy - Concepts and Applications, *Concepts in Sedimentology and Paleontology*. SEPM, Tulsa.
- Posamentier, H.W., Davies, R.J., Cartwright, J.A., Wood, L.J., 2007. Seismic geomorphology - an overview, in: Davies, R.J., Posamentier, H.W., Wood, L.J., Cartwright, J.A. (Eds.), *Seismic Geomorphology: Applications to Hydrocarbon Exploration and Production*. Geological Society, Special Publications, London, pp. 1–14.
- Posamentier, H.W., Jervey, M.T., Vail, P.R., 1988. Eustatic Controls on Clastic Deposition I - Conceptual Framework, in: Wilgus, C.K. (Ed.), *Sea-Level Changes: An Integrated Approach*. Paleontologists and Mineralogists Special Publication, pp. 125–154.
- Posamentier, H.W., Jervey, M.T., Vail, P.R., 1981. Eustatic Controls on Clastic Deposition I-Conceptual Framework. *Spec. Publ. SEPM* 109–124. <https://doi.org/10.2110/pec.88.01.0109>
- Posamentier, H.W., Kolla, V., 2003. Seismic Geomorphology and Stratigraphy of Depositional Elements in Deep-Water Settings. *J. Sediment. Res.* 73, 367–388. <https://doi.org/10.1306/111302730367>
- Posamentier, H.W., Vail, P.R., 1988. Eustatic controls on clastic deposition II—Sequence and systems tract models, in: Wilgus, C. (Ed.), *Sea-Level Changes: An Integrated Approach*. Society of Economic Paleontologists and Mineralogists Special Publication, pp. 47–69.
- Posamentier, H.W., Walker, R.G., 2006. Facies models revisited, in: SEPM Special Publication. (CD), Vol. 84. Society for Sedimentary Geology, pp. 399–520.
- Poyatos-Moré, M., Jones, G.D., Brunt, R.L., Hodgson, D.M., Wild, R.J., Flint, S.S., 2016. Mud-Dominated Basin-Margin Progradation: Processes and Implications. *J. Sediment. Res.* 86, 863–878. <https://doi.org/10.2110/jsr.2016.57>
- Poyatos-Moré, M., Jones, G.D., Brunt, R.L., Tek, D.E., Hodgson, D.M., Flint, S.S., 2019. Clinoform architecture and along-strike facies variability through an exhumed erosional to accretionary basin margin transition. *Basin Res.* bre.12351. <https://doi.org/10.1111/bre.12351>
- Prather, B., 2000. Calibration and visualization of depositional process models for above-grade slopes: a case study from the Gulf of Mexico. *Mar. Pet. Geol.* 17, 619–638. [https://doi.org/10.1016/S0264-8172\(00\)00015-5](https://doi.org/10.1016/S0264-8172(00)00015-5)
- Prather, B.E., 2003. Controls on reservoir distribution, architecture and stratigraphic

- trapping in slope settings. *Mar. Pet. Geol.* 20, 529–545. <https://doi.org/10.1016/J.MARPETGEO.2003.03.009>
- Prather, B.E., Booth, J., Steffans, G., Craig, P., 1998. Classification, Lithologic Calibration, and Stratigraphic Succession of Seismic Facies of Intraslope Basins, Deep-Water Gulf of Mexico. *Am. Assoc. Pet. Geol. Bull.* 82, 701–728.
- Prather, B.E., O’Byrne, C., Pirmez, C., Sylvester, Z., 2017. Sediment partitioning, continental slopes and base-of-slope systems. *Basin Res.* 29, 394–416. <https://doi.org/10.1111/bre.12190>
- Prather, B.E., Pirmez, C., 2012. Stratigraphy of Linked Intraslope Basins: Brazos–Trinity System Western Gulf of Mexico, in: *Application of the Principles of Seismic Geomorphology to Continental-Slope and Base-of-Slope Systems: Case Studies from Seafloor and Near-Seafloor Analogues*. pp. 83–109.
- Prather, B.E., Pirmez, C., Sylvester, Z., Prather, D.S., 2012. Stratigraphic Response to Evolving Geomorphology in a Submarine Apron Perched On the Upper Niger Delta Slope, in: *Application of the Principles of Seismic Geomorphology to Continental-Slope and Base-of-Slope Systems: Case Studies from Seafloor and Near-Seafloor Analogues* SEPM Special Publication No. 99. SEPM, pp. 145–161.
- Proust, J.-N.N., Lamarche, G., Nodder, S., Kamp, P.J.J.J., 2005. Sedimentary architecture of a Plio-Pleistocene proto-back-arc basin: Wanganui Basin, New Zealand. *Sediment. Geol.* 181, 107–145. <https://doi.org/10.1016/j.sedgeo.2005.06.010>
- Pyles, D.R., Slatt, R.M., 2008. Stratigraphy of the Lewis Shale, Wyoming, USA: Applications to Understanding Shelf-edge to Base-of-slope changes in Stratigraphic Architecture of Prograding Basin Margins, in: Nilsen, T.H., Shew, R.D., Steffans, G.S., Studlick, J.R.J. (Eds.), *Atlas of Deep-Water Outcrops*. American Association of Petroleum Geologists, Oklahoma, U.S.A. <https://doi.org/10.1306/St561240>
- Radford, J., 2012. Shelf-To-Canyon Sedimentation on the South Westland Continental Margin, Westland, New Zealand. University of Canterbury.
- Raine, J., Beu, A., Boyes, A., Campbell, H., Cooper, R., Crampton, J., Crundwell, M., Hollis, C., Morgans, H., Mortimer, N., 2015. New Zealand Geological Timescale NZGT 2015/1. *New Zeal. J. Geol. Geophys.* 8306, 1–6. <https://doi.org/10.1080/00288306.2015.1086391>
- Raine, J.I., Beu, A.G., Boyes, A.F., Campbell, H.J., Cooper, R.A., Crampton, J.S., Crundwell, M.P., Hollis, C.J., Morgans, H.E.G., 2015. Revised calibration of the New Zealand Geological timescale: NSGT2015/1. GNS Science Report 2012/39. Lower Hutt.
- Rait, G., Chanier, F., Waters, D.W., 1991. Landward- and seaward-directed thrusting accompanying the onset of subduction beneath New Zealand. *Geology* 19, 230–233. [https://doi.org/10.1130/0091-7613\(1991\)019<0230:LASDTA>2.3.CO;2](https://doi.org/10.1130/0091-7613(1991)019<0230:LASDTA>2.3.CO;2)
- Ramon-Duenas, C., Rudolph, K.W., Emmet, P.A., Wellner, J.S., 2018. Quantitative analysis of siliciclastic clinoforms: An example from the North Slope, Alaska. *Mar. Pet. Geol.* 93, 127–134. <https://doi.org/10.1016/j.marpetgeo.2018.02.013>
- Rangel, A., Katz, B., Ramirez, V., Vaz dos Santos Neto, E., 2003. Alternative interpretations as to the origin of the hydrocarbons of the Guajira Basin, Colombia. *Mar. Pet. Geol.* 20, 129–139. [https://doi.org/10.1016/S0264-8172\(03\)00061-8](https://doi.org/10.1016/S0264-8172(03)00061-8)
- Rasmussen, E.S., 1994. The relationship between submarine canyon fill and sea-level

- change: an example from Middle Miocene offshore Gabon, West Africa. *Sediment. Geol.* 90, 61–75. [https://doi.org/10.1016/0037-0738\(94\)90017-5](https://doi.org/10.1016/0037-0738(94)90017-5)
- Rattenbury, M.S., Jongens, R., Cox, S., 2010. *Geology of the Haast Area: 1:250 000 geological map 14.*
- Rebesco, M., Hernández-Molina, F.J., Van Rooij, D., Wåhlin, A., 2014. Contourites and associated sediments controlled by deep-water circulation processes: State-of-the-art and future considerations. *Mar. Geol.* 352, 111–154. <https://doi.org/10.1016/j.margeo.2014.03.011>
- Rebesco, M., Neagu, R.C., Cuppari, A., Muto, F., Accettella, D., Dominici, R., Cova, A., Romano, C., Caburlotto, A., 2009. Morphobathymetric analysis and evidence of submarine mass movements in the western Gulf of Taranto (Calabria margin, Ionian Sea). *Int. J. Earth Sci.* 98, 791–805. <https://doi.org/10.1007/s00531-009-0429-1>
- Reilly, C., Nicol, A., Walsh, J.J., Kroeger, K.F., 2016. Temporal changes of fault seal and early charge of the Maui Gas-condensate field, Taranaki Basin, New Zealand. *Mar. Pet. Geol.* 70, 237–250. <https://doi.org/10.1016/j.marpetgeo.2015.11.018>
- Reilly, C., Nicol, A., Walsh, J.J., Seebeck, H., 2015. Evolution of faulting and plate boundary deformation in the Southern Taranaki Basin, New Zealand. *Tectonophysics* 651, 1–18. <https://doi.org/10.1016/j.tecto.2015.02.009>
- Ribó, M., Puig, P., Urgeles, R., Van Rooij, D., Muñoz, A., 2016. Spatio-temporal evolution of sediment waves developed on the Gulf of Valencia margin (NW Mediterranean) during the Plio-Quaternary. *Mar. Geol.* 378, 276–291. <https://doi.org/10.1016/j.margeo.2015.11.011>
- Rich, J.L., 1951. Three Critical Environments of Deposition, and Criteria For Recognition Of Rocks Deposited In Each Of Them THREE CRITICAL ENVIRONMENTS OF DEPOSITION, AND CRITERIA FOR RECOGNITION OF ROCKS DEPOSITED IN EACH OF THEM. *Geol. Soc. Am. Bull.* 62, 1–20.
- Ridgwell, A.J., Watson, A.J., Raymo, M.E., 1999. Is the spectral signature of the 100 kyr glacial cycle consistent with a Milankovitch origin? *Paleoceanography* 14, 437–440. <https://doi.org/10.1029/1999PA900018>
- Roberts, H.H., Sydow, J., 2003. Late Quaternary Stratigraphy and Sedimentology of the Offshore Mahakam Delta, East Kalimantan (Indonesia), in: *Tropical Deltas of Southeast Asia - Sedimentology, Stratigraphy and Petroleum Geology*. SEPM Special Publication No. 76. Special Publications of SEPM, pp. 125–145.
- Romans, B.W., Hubbard, S.M., Graham, S.A., 2009. Stratigraphic evolution of an outcropping continental slope system, Tres Pasos Formation at Cerro Divisadero, Chile. *Sedimentology* 56, 737–764. <https://doi.org/10.1111/j.1365-3091.2008.00995.x>
- Roser, B.P., Korsch, R.J., 1986. Determination of Tectonic Setting of Sandstone-Mudstone Suites Using SiO₂ Content and K₂O/Na₂O Ratio. *J. Geol.* 94, 635–650. <https://doi.org/10.1086/629071>
- Ross, W.C., Halliwell, B. a., May, J. a., Watts, D.E., Syvitski, J.P.M.P.M., 1994. Slope readjustment: a new model for the development of submarine fans and aprons. *Geology* 22, 511–514. [https://doi.org/10.1130/0091-7613\(1994\)022<0511:SRANMF>2.3.CO](https://doi.org/10.1130/0091-7613(1994)022<0511:SRANMF>2.3.CO)
- Ross, W.C., Watts, D.E., May, J.A., 1995. Insights from Stratigraphic Modeling: Mud-

- Limited Versus Sand-Limited Depositional Systems. *Am. Assoc. Pet. Geol. Bull.* 79, 231–258.
- Roy, P.S., Thom, B.G., 1991. Cainozoic shelf sedimentation model for the Tasman Sea margin of southeastern Australia, in: Williams, M.A.J., De Dekker, P., Kershaw, A.P. (Eds.), *The Cainozoic in Australia: A Reappraisal of the Evidence: Geological Society of Australia Special Publication 18*, Geological Society of Australia, pp. 119–136.
- Ryan, M., Newnham, R., Dunbar, G., Vandergoes, M., Neil, H., Bostock, H., 2012. Mid-Late Quaternary vegetation and climate change reconstructed from palynology of marine cores off southwestern New Zealand. *Quat. Int.* 279–280.
- Ryan, M.C., Helland-Hansen, W., Johannessen, E.P., Steel, R.J., 2009. Erosional vs. accretionary shelf margins: The influence of margin type on deepwater sedimentation: An example from the Porcupine Basin, offshore western Ireland. *Basin Res.* 21, 676–703. <https://doi.org/10.1111/j.1365-2117.2009.00424.x>
- Salazar, M., Moscardelli, L., Wood, L., 2016. Utilising clinoform architecture to understand the drivers of basin margin evolution: a case study in the Taranaki Basin, New Zealand. *Basin Res.* 28, 840–865. <https://doi.org/10.1111/bre.12138>
- Saller, A., Blake, G., 2003. Sequence Stratigraphy and Syndepositional Tectonics of Upper Miocene and Pliocene Deltaic Sediments, Offshore Brunei Darussalam, in: Sidi, F.H., Nummedal, D., Imbert, P., Darman, H., Posamentier, H.W. (Eds.), *Tropical Deltas of Southeast Asia*. SEPM (Society for Sedimentary Geology), pp. 219–234. <https://doi.org/10.2110/pec.03.76.0219>
- Sanchez, C.M., Fulthorpe, C.S., Steel, R.J., 2012. Miocene shelf-edge deltas and their impact on deepwater slope progradation and morphology, Northwest Shelf of Australia. *Basin Res.* 24, 683–698. <https://doi.org/10.1111/j.1365-2117.2012.00545.x>
- Saul, G., Naish, T.R., Abbott, S.T., Carter, R.M., 1999. Sedimentary cyclicity in the marine Pliocene-Pleistocene of the Wanganui basin (New Zealand): Sequence stratigraphic motifs characteristic of the past 2.5 m.y. *Geol. Soc. Am. Bull.* 111, 524–537. [https://doi.org/10.1130/0016-7606\(1999\)111<0524:SCITMP>2.3.CO;2](https://doi.org/10.1130/0016-7606(1999)111<0524:SCITMP>2.3.CO;2)
- Schlee, J.S., Dillon, W.P., Grow, J.A., 1979. Structure of the continental slope off the eastern United States. *Geol. Cont. slopes* 95–117. <https://doi.org/10.2110/pec.79.27.0095>
- Schlitzer, R., 2018. Ocean Data View [WWW Document]. URL <https://odv.awi.de/>
- Schofield, J.C., 1975. Sea-level fluctuations cause periodic, post-glacial progradation, South Kaipara Barrier, North Island, New Zealand. *New Zeal. J. Geol. Geophys.* 18, 295–316. <https://doi.org/10.1080/00288306.1975.10418201>
- Seebeck, H., Nicol, A., Giba, M., Pettinga, J., Walsh, J., 2014. Geometry of the subducting Pacific plate since 20 Ma, Hikurangi margin, New Zealand. *J. Geol. Soc. London.* 171, 131–143. <https://doi.org/10.1144/jgs2012-145>
- Shell BP Todd Oil Services Ltd., 1986. Well Resume Te Ranga-1, Ppl 38107 Taranaki New Plymouth. Ministry of Economic Development unpublished petroleum report 1197.
- Shell BP Todd Oil Services Ltd., 1982. PR880: Well Resume Kiwa-1. New Plymouth.
- Shell BP Todd Oil Services Ltd., 1976. Well Resume Tane-1 (Offshore). Ministry of

- Economic Development, New Zealand. Unpublished Petroleum Report PR698.
- Shepard, F.P., Marshall, N.F., McLoughlin, P.A., 1974. "Internal Waves" Advancing along Submarine Canyons. *Science* (80-). 183, 195–198. <https://doi.org/10.1126/science.183.4121.195>
- Sherwood, A.M., Lindqvist, J.K., Newman, J., Sykes, R., 1992. Controls on the Distribution and Quality of Cretaceous Coals, Geological Society of America Special Papers, Geological Society of America Special Papers. Geological Society of America. <https://doi.org/10.1130/SPE267>
- Shillington, D.J., Seeber, L., Sorlien, C.C., Steckler, M.S., Kurt, H., Dondurur, D., Çifçi, G., Imren, C., Cormier, M.H., McHugh, C.M.G., Gürçay, S., Poyraz, D., Okay, S., Atgin, O., Diebold, J.B., 2012. Evidence for widespread creep on the flanks of the sea of Marmara transform basin from marine geophysical data. *Geology* 40, 439–442. <https://doi.org/10.1130/G32652.1>
- Short, K.C., Stauble, A.J., 1967. Outline of Geology of Niger Delta. *Am. Assoc. Pet. Geol. Bull.* 51, 761–779.
- Shulmeister, J., 2017. Landscape and Quaternary Environmental Change in New Zealand. <https://doi.org/10.2991/978-94-6239-237-3>
- Shulmeister, J., McKay, R., Singer, C., Mclea, W., 2001. Glacial geology of the Cobb valley. *New Zeal. J. Geol. Geophys.* 44, 47–54. <https://doi.org/10.1080/00288306.2001.9514921>
- Shulmeister, J., McLea, W.L., Singer, C., McKay, R.M., Hosie, C., 2003. Late Quaternary pollen records from the Lower Cobb Valley and adjacent areas, North-West Nelson, New Zealand. *New Zeal. J. Bot.* 41, 503–533. <https://doi.org/10.1080/0028825X.2003.9512867>
- Shulmeister, J., Thackray, G.D., Rittenour, T.M., Fink, D., Patton, N.R., 2019. The timing and nature of the last glacial cycle in New Zealand. *Quat. Sci. Rev.* <https://doi.org/10.1016/j.quascirev.2018.12.020>
- Shumaker, L.E., Jobe, Z.R., Graham, S.A., 2017. Evolution of submarine gullies on a prograding slope: Insights from 3D seismic reflection data. *Mar. Geol.* 393, 35–46. <https://doi.org/10.1016/j.margeo.2016.06.006>
- Shumaker, L.E., Sharman, G.R., King, P.R., Graham, S.A., 2018. The source is in the sink: Deep-water deposition by a submarine volcanic arc, Taranaki Basin, New Zealand. *Sedimentology*. <https://doi.org/10.1111/sed.12475>
- Sinclair, H.D., Tomasso, M., 2002. Depositional Evolution of Confined Turbidite Basins. *J. Sediment. Res.* 72, 451–456. <https://doi.org/10.1306/111501720451>
- Smith, R.O., Vennell, R., Bostock, H.C., Williams, M.J.M., 2013. Interaction of the subtropical front with topography around southern New Zealand. *Deep. Res. Part I Oceanogr. Res. Pap.* 76, 13–26. <https://doi.org/10.1016/j.dsr.2013.02.007>
- Sømme, T.O., Helland-Hansen, W., Martinsen, O.J., Thurmond, J.B., Sømme, T.O., Helland-Hansen, W., Martinsen, O.J., Thurmond, J.B., 2009. Relationships between morphological and sedimentological parameters in source-to-sink systems: A basis for predicting semi-quantitative characteristics in subsurface systems. *Basin Res.* 21, 361–387. <https://doi.org/10.1111/j.1365-2117.2009.00397.x>
- Spychala, Y.T., Hodgson, D.M., Flint, S.S., Mountney, N.P., 2015. Constraining the sedimentology and stratigraphy of submarine intraslope lobe deposits using

- exhumed examples from the Karoo Basin, South Africa. *Sediment. Geol.* 322, 67–81. <https://doi.org/10.1016/J.SEDGEO.2015.03.013>
- Stagpoole, V., Nicol, a., 2008. Regional structure and kinematic history of a large subduction back thrust: Taranaki Fault, New Zealand. *J. Geophys. Res. Solid Earth* 113, 1–19. <https://doi.org/10.1029/2007JB005170>
- Steckler, M.S., Mountain, G.S., Miller, K.G., Christie-Blick, N., 1999. Reconstruction of Tertiary progradation and clinoform development on the New Jersey passive margin by 2-D backstripping. *Mar. Geol.* 154, 399–420. [https://doi.org/10.1016/S0025-3227\(98\)00126-1](https://doi.org/10.1016/S0025-3227(98)00126-1)
- Steel, R., Olsen, T., 2002. Clinoforms, clinoform trajectory and deepwater sands, in: Armentrout, J.M., Rosen, N.C. (Eds.), *Sequence Stratigraphic Models for Exploration and Production: Evolving Methodology, Emerging Models and Application Histories*, GCS-SEPM Special Publication. pp. 367–381.
- Steel, R., Porebski, S.J., Plink-Bjorklund, P., Mellere, D., Schellpeper, M., 2003. Shelf-edge delta types and their sequence-stratigraphic relationships. *Shelf Margin Deltas Linked Down Slope Pet. Syst.* 205–230.
- Steel, R.J., Olsen, T., 2002. Clinoforms, clinoform trajectories and deepwater sands., in: Armentrout, J.M., Rosen, N.C. (Eds.), *Sequence Stratigraphic Models for Exploration and Production: Evolving Methodology, Emerging Models and Application Histories*, 22rd Annual Bob F. Perkins Research Conference. GCS-SEPM Special Publication, Houston, pp. 367–381.
- Stern, T. a., 1987. Asymmetric back-arc spreading, heat flux and structure associated with the Central Volcanic Region of New Zealand. *Earth Planet. Sci. Lett.* 85, 265–276. [https://doi.org/10.1016/0012-821X\(87\)90037-9](https://doi.org/10.1016/0012-821X(87)90037-9)
- Stern, T. a., Davey, F.J., 1990. Deep seismic expression of a foreland basin: Taranaki Basin, New Zealand. *Geology* 18, 979–982. [https://doi.org/10.1130/0091-7613\(1990\)018<0979:DSEOAF>2.3.CO;2](https://doi.org/10.1130/0091-7613(1990)018<0979:DSEOAF>2.3.CO;2)
- Stern, T. a, Holt, W.E., 1994. Platform subsidence behind an active subduction zone. *Nature* 368, 233–236. <https://doi.org/10.1038/368233a0>
- Stern, T. a, Stratford, W.R., Salmon, M.L., 2006. Subduction Evolution and Mantle Dynamics At a Continental Margin : Central North Island , New Zealand. *Rev. Geophys.* 44, 1–36. <https://doi.org/10.1029/2005RG000171.1.INTRODUCTION>
- Strapoć, D., Ashby, M., Wood, L., Levinson, R., Huizinga, B., 2010. How Specific Microbial Communities Benefit the Oil Industry: Significant Contribution of Methyl/Methanol-Utilising Methanogenic Pathway in a Subsurface Biogas Environment, in: *Applied Microbiology and Molecular Biology in Oilfield Systems*. Springer Netherlands, Dordrecht, pp. 211–216. https://doi.org/10.1007/978-90-481-9252-6_25
- Strapoć, D., Mastalerz, M., Dawson, K., Macalady, J., Callaghan, A. V., Wawrik, B., Turich, C., Ashby, M., 2011. Biogeochemistry of Microbial Coal-Bed Methane. *Annu. Rev. Earth Planet. Sci.* 39, 617–656. <https://doi.org/10.1146/annurev-earth-040610-133343>
- Stride, A.H., Tucker, M.J., 1960. Internal waves and waves of sand. *Nature* 188, 933. <https://doi.org/10.1038/188933a0>

- Strogen, 2014. Regional seismic transects of selected lines from Taranaki Basin. GNS Data Ser. 7b 0–1.
- Strogen, D.P., 2011. Updated paleogeographic maps for the Taranaki Basin and surrounds. GNS Science Report 2010/53. Lower Hutt.
- Strogen, D P, Bland, K.J., Bull, S., Fohrmann, M.F., Scott, G.P.L., Zhu, H., 2014. Regional seismic transects of selected lines from Taranaki Basin, GNS Data Series 7b.
- Strogen, Dominic P, Bland, K.J., Nicol, A., King, P.R., 2014. Paleogeography of the Taranaki Basin region during the latest Eocene–Early Miocene and implications for the ‘total drowning’ of Zealandia. *New Zeal. J. Geol. Geophys.* 57, 110–127. <https://doi.org/10.1080/00288306.2014.901231>
- Strong, C.P., Wilson, G.J., 2002. Biostratigraphic reassessment (foraminiferal & palynology) of key western platform drillholes, Taranaki Basin. Lower Hutt.
- Sultan, N., Cochonat, P., Cayocca, F., Bourillet, J.F., Colliat, J.L., 2004. Analysis of submarine slumping in the Gabon continental slope. *Am. Assoc. Pet. Geol. Bull.* 88, 781–799. <https://doi.org/10.1306/01260403086>
- Sutherland, R., Collot, J., Lafoy, Y., Logan, G. a., Hackney, R., Stagpoole, V., Uruski, C., Hashimoto, T., Higgins, K., Herzer, R.H., Wood, R., Mortimer, N., Rollet, N., 2010. Lithosphere delamination with foundering of lower crust and mantle caused permanent subsidence of New Caledonia Trough and transient uplift of Lord Howe Rise during Eocene and Oligocene initiation of Tonga-Kermadec subduction, western Pacific. *Tectonics* 29, 1–16. <https://doi.org/10.1029/2009TC002476>
- Sutton, P.J.H., 2003. The Southland Current: A subantarctic current. *New Zeal. J. Mar. Freshw. Res.* 37, 645–652. <https://doi.org/10.1080/00288330.2003.9517195>
- Sydow, J.C., Finneran, J., Bowman, A.P., 2003. Stacked Shelf-Edge Delta Reservoirs of the Columbus Basin, Trinidad, West Indies, in: *Shelf Margin Deltas and Linked Down Slope Petroleum Systems: 23rd Annual. SOCIETY OF ECONOMIC PALEONTOLOGISTS AND MINERALOGISTS*, pp. 441–464. <https://doi.org/10.5724/gcs.03.23.0441>
- Sykes, R., 2001. Depositional and Rank Controls on the Petroleum Potential of Coaly Source Rocks, in: Hill, K.C., Bernecker, T. (Eds.), 2001 PESA Eastern Australian Basins Symposium Proceedings. Petroleum Exploration Society of Australia Special Publication, Carlton, Victoria, Australia, The Australasian Institute of Mining and Metallurgy, Melbourne, pp. 591–601.
- Sykes, R., Volk, H., George, S.C., Ahmed, M., Higgs, K.E., Johansen, P.E., Snowdon, L.R., 2014. Marine influence helps preserve the oil potential of coaly source rocks: Eocene Mangahewa Formation, Taranaki Basin, New Zealand. *Org. Geochem.* 66, 140–163. <https://doi.org/10.1016/j.orggeochem.2013.11.005>
- Symons, W.O., Sumner, E.J., Talling, P.J., Cartigny, M.J.B., Clare, M.A., 2016. Large-scale sediment waves and scours on the modern seafloor and their implications for the prevalence of supercritical flows. *Mar. Geol.* 371, 130–148. <https://doi.org/10.1016/j.margeo.2015.11.009>
- Taki, K., Parker, G., 2005. Transportational cyclic steps created by flow over an erodible bed. Part 1. Experiments. *J. Hydraul. Res.* 43, 488–501. <https://doi.org/10.1080/00221680509500147>

- Tesson, M., Gensous, B., Allen, G.P., Ravenne, C., 1990. Late Quaternary deltaic lowstand wedges on the Rhône continental shelf, France. *Mar. Geol.* 91, 325–332. [https://doi.org/10.1016/0025-3227\(90\)90053-M](https://doi.org/10.1016/0025-3227(90)90053-M)
- Thrasher, G., Seebeck, H., Vistokovic, P., Bull, S., Sarma, K., Kroeger, K., 2018. Time structure grids for the greater Maui-Maari-Tui region, Taranaki Basin, New Zealand, GNS Science Data Series 25a.
- Tippett, J.M., Kamp, P.J.J.P., 1995. Geomorphic evolution of the Southern Alps, New Zealand. *Earth Surf. Process. Landforms* 20, 177–192. <https://doi.org/10.1002/esp.3290200207>
- Toucanne, S., Zaragosi, S., Bourillet, J.F., Naughton, F., Cremer, M., Eynaud, F., Dennielou, B., 2008. Activity of the turbidite levees of the Celtic-Armorican margin (Bay of Biscay) during the last 30,000 years: Imprints of the last European deglaciation and Heinrich events. *Mar. Geol.* 247, 84–103. <https://doi.org/10.1016/j.margeo.2007.08.006>
- Tribe, H.M., Kennedy, D.M., 2010. The geomorphology and evolution of a large barrier spit: Farewell Spit, New Zealand. *Earth Surf. Process. Landforms* 35, 1751–1762. <https://doi.org/10.1002/esp.2009>
- Tulloch, A.J., Kimbrough, D.L., 1989. rocks include Ordovician turbidites, Paleozoic and Cretaceous. *Tectonics* 8, 1217–1234.
- Uroza, C.A., Steel, R.J., 2008. A highstand shelf-margin delta system from the Eocene of West Spitsbergen, Norway. *Sediment. Geol.* 203, 229–245. <https://doi.org/10.1016/J.SEDGEO.2007.12.003>
- Uruski, C., Wood, R., 1991. A new look at the New Caledonia Basin, an extension of the Taranaki Basin, offshore North Island, New Zealand. *Mar. Pet. Geol.* 8, 379–391. [https://doi.org/10.1016/0264-8172\(91\)90061-5](https://doi.org/10.1016/0264-8172(91)90061-5)
- Vail, P.R., 1987. Seismic Stratigraphy Interpretation Using Sequence Stratigraphy Part I : Seismic Stratigraphy Interpretation Procedure, in: Bally, A.W. (Ed.), *AAPG Studies in Geology #27*, Volume 1: Atlas of Seismic Stratigraphy. pp. 1–10.
- Vail, P.R., Mitchum, R.M., Thompson, S., 1977. Seismic Stratigraphy and Global Change in Sea Level, Part 3: Relative Change of Sea Level from Coastal Onlap. Payton, C.E. *Seism. Stratigr. – Appl. to Hydrocarb. Explor. Am. Assoc. Pet. Geol.*
- van der Merwe, W.C., Flint, S.S., Hodgson, D.M., 2010. Sequence stratigraphy of an argillaceous, deepwater basin-plain succession: Vischkuil Formation (Permian), Karoo Basin, South Africa. *Mar. Pet. Geol.* 27, 321–333. <https://doi.org/10.1016/J.MARPETGEO.2009.10.007>
- Van Wagoner, J., Posamentier, H.W., Mitchum, R.M., Vail, P.R., Sarg, J.F., Loutit, T.S., Hardenbol, J., 1988. An overview of the fundamentals of sequence stratigraphy and key definitions. *Sea-level Chang. An Integr. approach*, SEPM Spec. Publ. 42 39–45. <https://doi.org/10.2110/pec.88.01.0039>
- Van Wagoner, J.C., Mitchum, R.M., Posamentier, H.W., Vail, P.R., 1987. Seismic stratigraphy interpretation using sequence stratigraphy: Part 2, Key definitions of sequence stratigraphy, in: Bally, A.W. (Ed.), *AAPG Studies in Geology #27*, Volume 1: Atlas of Seismic Stratigraphy. AAPG, pp. 11–14.
- Vandré, C., Cramer, B., Gerling, P., Winsemann, J., 2007. Natural gas formation in the western Nile delta (Eastern Mediterranean): Thermogenic versus microbial. *Org.*

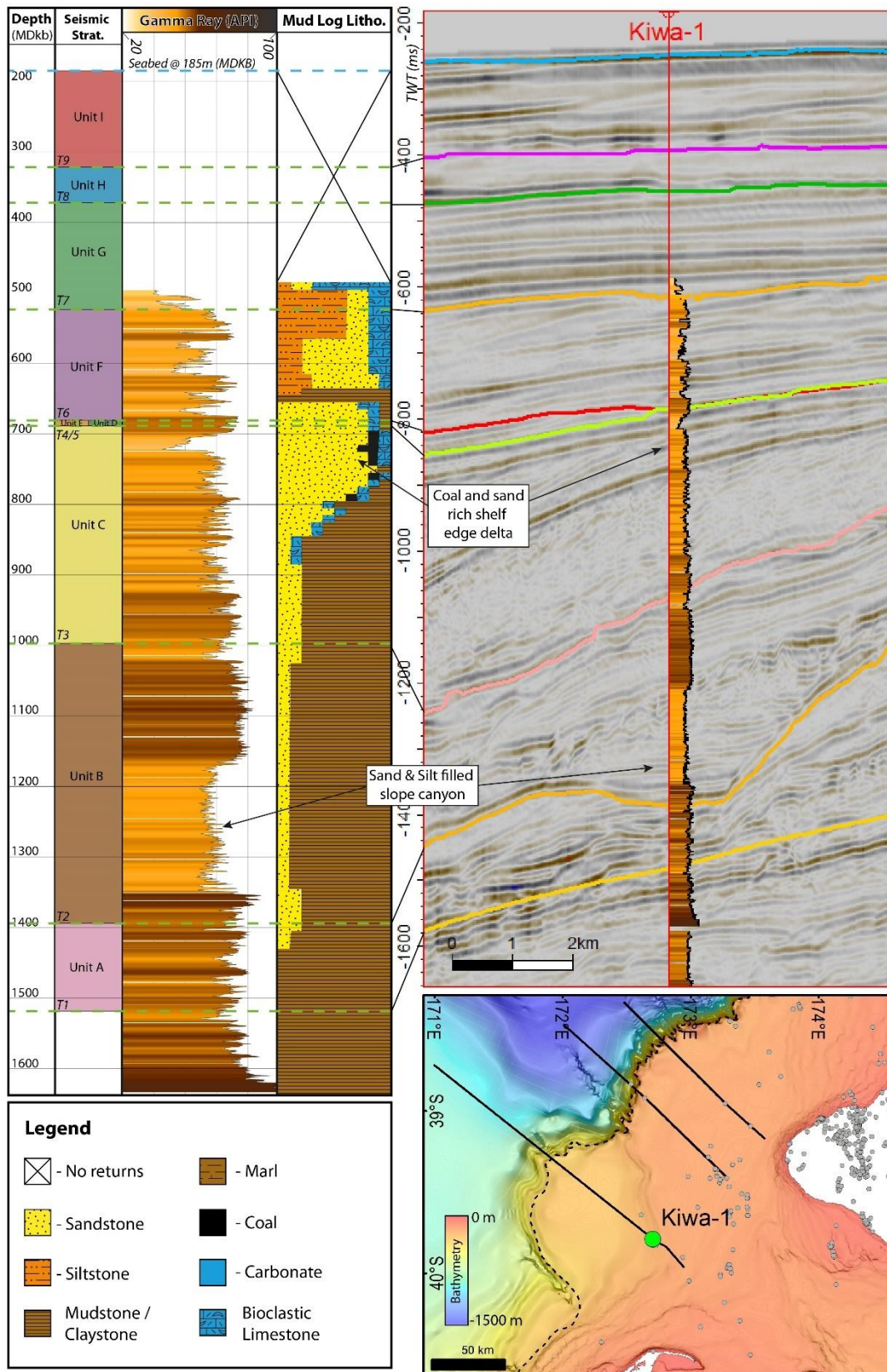
- Geochem. 38, 523–539. <https://doi.org/10.1016/j.orggeochem.2006.12.006>
- Viana, A.R., Faugeres, J.C., Kowsmann, R.O., Lima, J.A.M., Caddah, L.F.G., Rizzo, J.G., 1998. Hydrology, morphology and sedimentology of the Campos continental margin, offshore Brazil. *Sediment. Geol.* 115, 133–157. [https://doi.org/10.1016/S0037-0738\(97\)00090-0](https://doi.org/10.1016/S0037-0738(97)00090-0)
- Viana, A.R., Hercos, C.M., de Almeida Jr., W., Magalhaes, J.L.C., de Andrade, S.B., 2002. Evidence of bottom current influence on the Neogene to Quaternary sedimentation along the northern Campos Slope, SW Atlantic margin. *Deep. Contourite Syst. Mod. Drifts Anc. Ser. Seism. Sediment. Charact.* 22, 249–259. <https://doi.org/10.1144/gsl.mem.2002.022.01.18>
- Viana, A.R., Jr., W.A., Machado, L.C., 1999. Different Styles Of Canyon Infill Related To Gravity And Bottom Current Processes : Examples From The Upper Slope Of The Se Brazilian Margin cp-215-00190. <https://doi.org/10.3997/2214-4609-PDB.215.SBGF014>
- Vry, J.K., Powell, R., Williams, J., 2008. Establishing the P-T path for Alpine Schist, Southern Alps near Hokitika, New Zealand. *J. Metamorph. Geol.* 26, 81–97. <https://doi.org/10.1111/j.1525-1314.2007.00746.x>
- Walsh, J., Nittrouer, C., 2003. Contrasting styles of off-shelf sediment accumulation in New Guinea. *Mar. Geol.* 196, 105–125. [https://doi.org/10.1016/S0025-3227\(03\)00069-0](https://doi.org/10.1016/S0025-3227(03)00069-0)
- Warne, A.G., Meade, R.H., White, W.A., Guevara, E.H., Gibeaut, J., Smyth, R.C., Aslan, A., Tremblay, T., 2002. Regional controls on geomorphology, hydrology, and ecosystem integrity in the Orinoco Delta, Venezuela. *Geomorphology* 44, 273–307. [https://doi.org/10.1016/S0169-555X\(01\)00179-9](https://doi.org/10.1016/S0169-555X(01)00179-9)
- Wehr, F.L. (Exxon P. research company), 1993. Effects of variations in subsidence and sediment supply on parasequence stacking patterns, in: Weimer, P., Posamentier, H. (Eds.), *Siliciclastic Sequence Stratigraphy: Recent Developments and Applications: American Association of Petroleum Geologists Memoir 58*. American Association of Petroleum Geologists, Houston, pp. 369–379.
- Whiticar, M., Faber, E., Schoell, M., 1986. Biogenic methane formation in marine and freshwater environments: CO₂ reduction vs. acetate fermentation—Isotope evidence. *Geochim. Cosmochim. Acta* 50, 693–709. [https://doi.org/10.1016/0016-7037\(86\)90346-7](https://doi.org/10.1016/0016-7037(86)90346-7)
- Wizevich, M.C., Thrasher, G.P., Bussell, M.R., Wilson, G.J., Collen, J.D., 1992. Evidence for marine deposition in the Late Cretaceous Pakawau group, northwest Nelson. *New Zeal. J. Geol. Geophys.* 35, 363–369. <https://doi.org/10.1080/00288306.1992.9514529>
- Wolinsky, M. a., Pratson, L.F., 2007. Overpressure and slope stability in prograding clinoforms: Implications for marine morphodynamics. *J. Geophys. Res. Earth Surf.* 112, 1–20. <https://doi.org/10.1029/2007JF000770>
- Wood, R., Woodward, D., 2002. Sediment thickness and crustal structure of offshore western New Zealand from 3D gravity modelling. *New Zeal. J. Geol. Geophys.* 45, 243–255. <https://doi.org/10.1080/00288306.2002.9514971>
- Wynn, Russell B., Stow, D. a V, 2002. Classification and characterisation of deep-water sediment waves. *Mar. Geol.* 192, 7–22. [https://doi.org/10.1016/S0025-3227\(02\)00547-9](https://doi.org/10.1016/S0025-3227(02)00547-9)

- Wynn, R.B., Stow, D.A. V., 2002. Classification and characterisation of deep-water sediment waves. *Mar. Geol.* 192, 7–22.
- Wynn, R.B., Weaver, P.P.E., Ercilla, G., Stow, D.A. V., Masson, D.G., 2000. Sedimentary processes in the Selvage sediment-wave field, NE Atlantic: new insights into the formation of sediment waves by turbidity currents. *Sedimentology* 47, 1181–1197. <https://doi.org/10.1046/j.1365-3091.2000.00348.x>
- Xu, J.P., Wong, F.L., Kvitek, R., Smith, D.P., Paull, C.K., 2008. Sandwave migration in Monterey Submarine Canyon, Central California. *Mar. Geol.* 248, 193–212. <https://doi.org/10.1016/j.margeo.2007.11.005>
- Yoshida, S., Steel, R.J., Dalrymple, R.W., 2007. Changes in Depositional Processes--An Ingredient in a New Generation of Sequence-Stratigraphic Models. *J. Sediment. Res.* 77, 447–460. <https://doi.org/10.2110/jsr.2007.048>
- Zhu, M., Graham, S., Pang, X., McHargue, T., 2010. Characteristics of migrating submarine canyons from the middle Miocene to present: Implications for paleoceanographic circulation, northern South China Sea. *Mar. Pet. Geol.* 27, 307–319. <https://doi.org/10.1016/j.marpetgeo.2009.05.005>

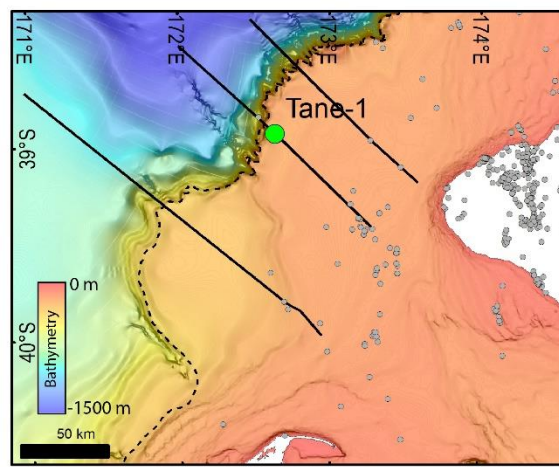
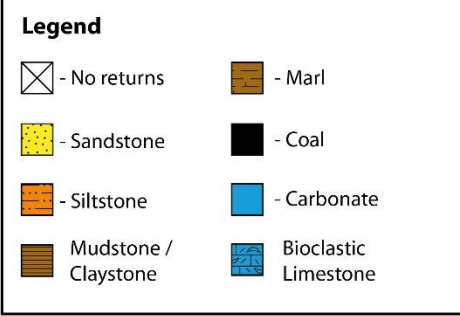
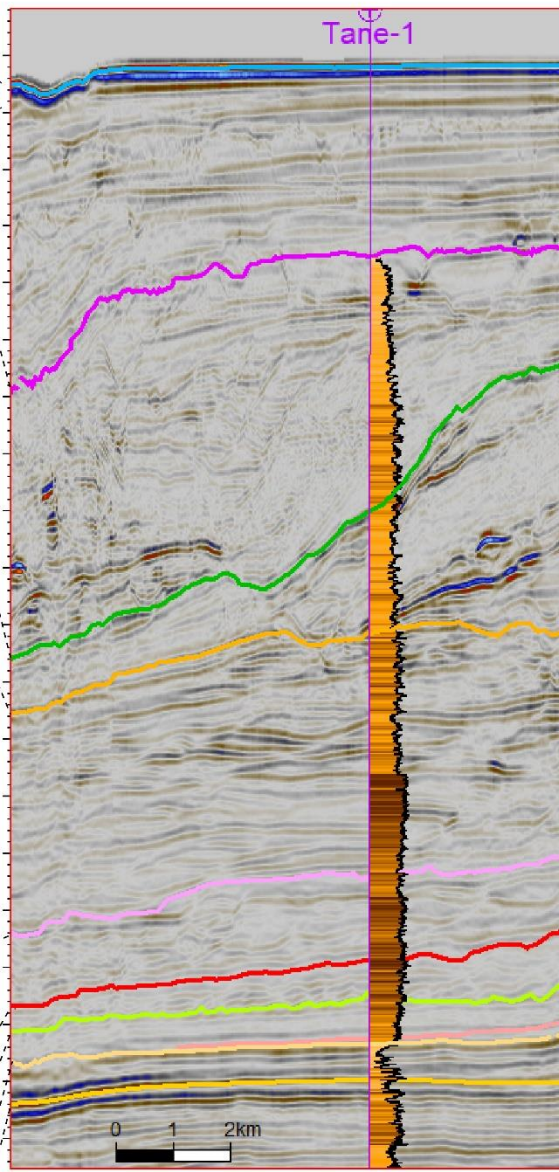
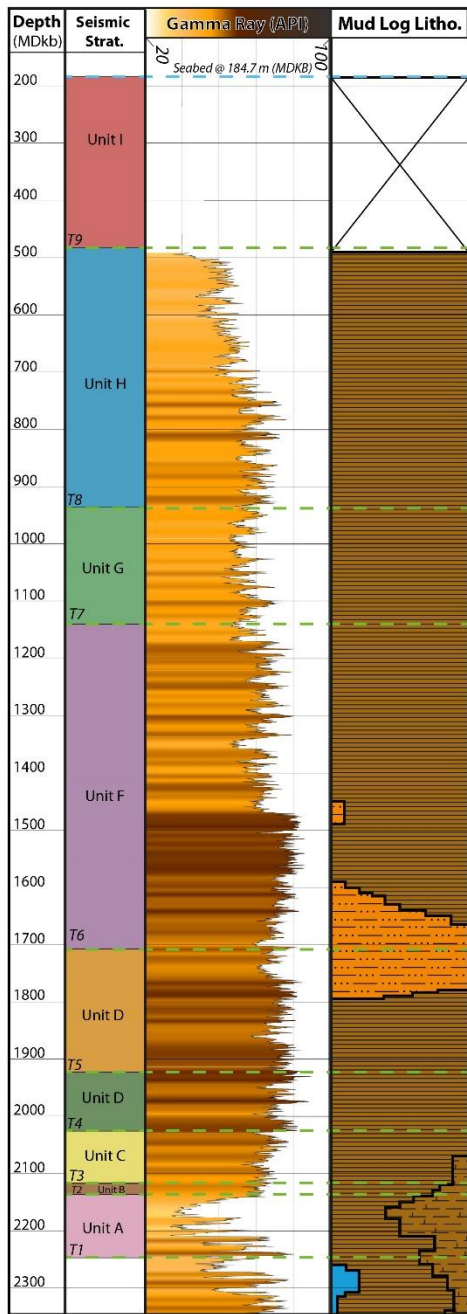
Blank Page

Appendix 1 – Well Logs

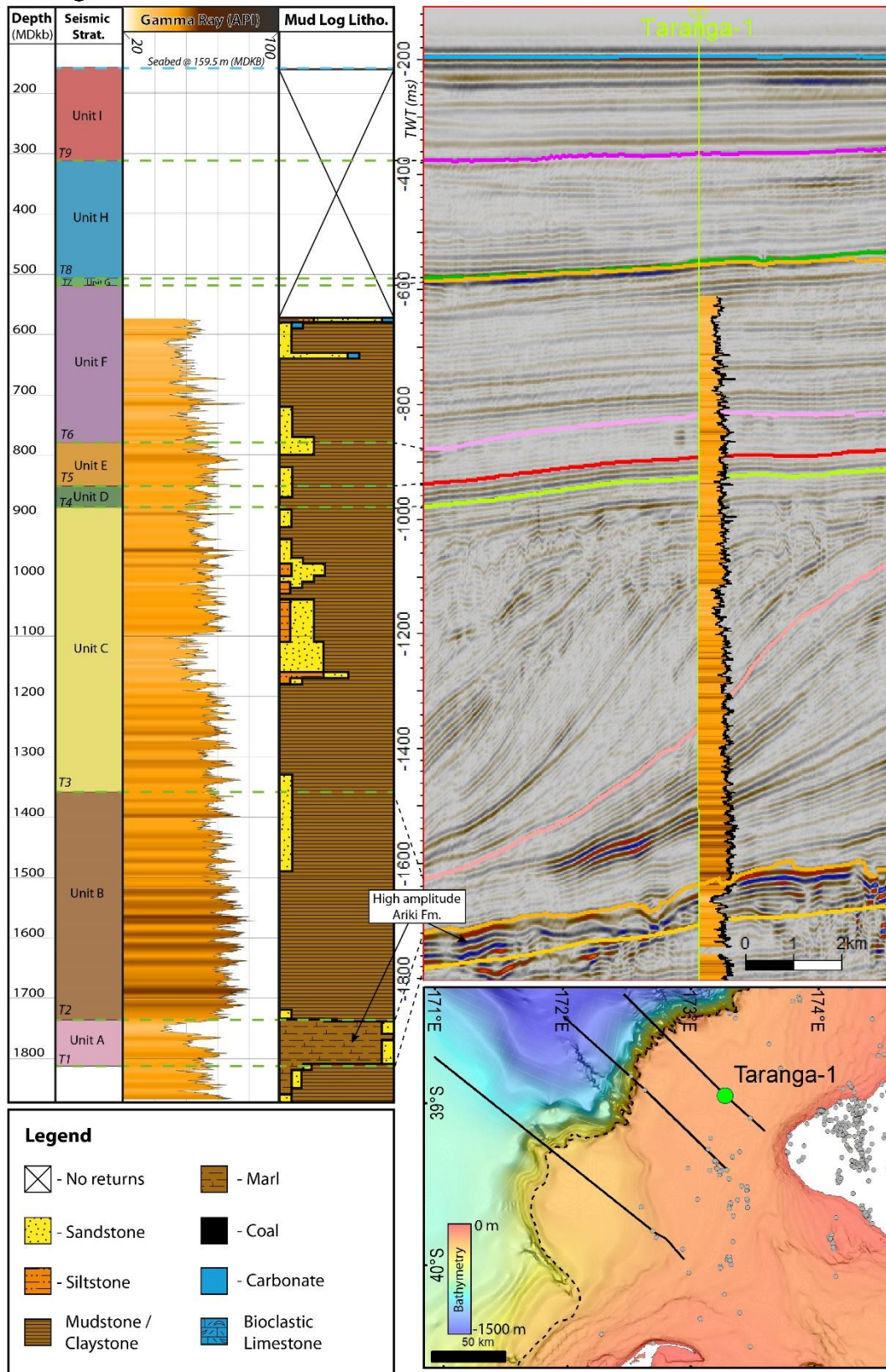
Kiwa-1



Tane-1



Taranga-1



Appendix 2 – Biostratigraphy

Epoch	NZ Stage Name (abbreviation)	Adopted Age	Primary Criteria (Raine et al., 2015) ¹	Secondary Criteria (Crundwell et al., 2004) ²	Kiwa-1 (Strong & Wilson, 2002)	Tane-1 (Strong & Wilson, 2002)	Taranga-1 (Strong & Wilson, 2002)	Witiora-1 (Morgans, 2006)
					Top Sample @ 500 m	Top Sample @ 490 m	Top Sample @ 590 m	Top Sample @ 220 m
Pleistocene	Base Haweran (Wq)	0.34	Base Rangitawa Tephra		NO	NO	NO	NO
	Base Castlecliffian (Wq)	1.63	Base Ototoka Tephra		NO	NO	NO	NO
	Base Nukumaruan (Wn)	2.4	LO Truncorotalia crassula and top upper dextral Truncorotalia oceanica	Top dextral Globorotalia crassaformis	940 ²	1310 ¹	1190 ²	700 ²
Pliocene	Base Mangapanian (Wm)	3.04	Base dextral Truncorotalia crassaformis	FDHA <i>Cibicides molestus</i>	1100 ²	NO	1700 ¹	1000 ²
	Base Waipipian (Wp)	3.7	HO Reticulofenestra psuedoumbilica (Calcareous Nanoplankton)	Not Defined	NO	NO	NO	NO
	Base Upper Opoitian (uWo)	4.3	LO Globorotalia inflatata	FDHA Globorotalia pliozea	1360 ¹ (1440 ²)	2000 ¹ (2090 ²)	1790 ²	1060 ²
	Base Opoitian (Top Mio) (lWo)	5.33	LO Globoconella puncticulata	FDHA Globorotalia sphericomiozea	1500 ¹	2170 ¹ (2190 ²)	1850 ¹	1220 ²
Miocene	Base upper Kapitean	5.6	LO Globoconella sphericomiozea	Top Dextral Globorotalia conomiozea	1600 ²	2200 ¹	1890 ²	1320 ²

Table 10.1 Biostratigraphy and well intercepts.

Biostratigraphic criteria established by Raine et al. (2015)¹ and Crundwell et al. (2004)² plotted with depths of intersection observed in foraminiferal census reports of Strong & Wilson (2002) and Morgans (2006). HO – Highest Occurrence, LO – Lowest Occurrence, FDHA – First Downhole Appearance.